Structural and Functional Characterization of Metallothioneins in Plants and Fungi

Dissertation*

zur

Erlangung der naturwissenschaftlichen Doktorwürde

(Dr. sc. nat.)

vorgelegt der

Mathematisch-naturwissenschaftlichen Fakultät

der

Universität Zürich

Von

Jens Loebus

von/aus

Jena / Deutschland

Promotionskomitee

Prof. Dr. Eva Freisinger (Vorsitz und Leitung der Dissertation)

Prof. Dr. Roland K. O. Sigel

Prof. Dr. Oliver Zerbe

Zürich, 2012

Acknowledgements

This work is a truly collaborative effort. I am deeply grateful to all that participated, as supervisors, colleagues and friends. Since they are so many, who I am sure, all know that they contributed I won't name them. Nevertheless, I would like to express my honest gratitude to all that fostered and nourished my curiosity in science, because admittedly, I really like it.

TABLE OF CONTENT

Abbreviations

Methods:

AAS	**a**tomic **a**bsorption **s**pectroscopy
CD	**c**ircular **d**ichroism
CE	**c**apillary **e**lectrophoresis
MCD	**m**agnetic **c**ircular **d**ichroism
MS	**m**ass **s**pectrometry
NMR	**n**uclear **m**agnetic **r**esonance
SAXS	**s**mall **a**ngle **X**-ray **s**cattering
SDS-PAGE	**s**odium-**d**odecyl**s**ulfat-**p**oly**a**crylamide **g**el **e**lectrophoresis
SEC	**s**ize **e**xclusion **c**hromatography
UVvis	**u**ltra-**v**iolet, **vis**ible
TD-PAC	**t**ime-**d**ependent **p**erturbed **a**ngular **c**orrelation

NMR:

HMBC	**h**eteronuclear **m**ultiple-**b**ond **c**orrelation
HSQC	**h**eteronuclear **s**ingle **q**uantum **c**oherence
NOESY	homonuclear (proton-proton) **n**uclear **o**verhauser **e**ffect
TOCSY	homonuclear (proton-proton) **to**tal **c**orrelation
^{15}N-(^{1}H)-NOE	steady state **n**uclear **o**verhauser **e**nhancement

Spectroscopy:

LMCT	**l**igand to **m**etal **c**harge **t**ransfer
ε / M^{-1} cm^{-1}	molar extinction coefficient
θ / deg dmol^{-1} cm^{2}	molar ellipticity coefficient
θ_M / deg dmol^{-1} cm^{2} T^{-1}	molar magnetic ellipticity coefficient

Chemicals:

APS	**a**mmonium **p**er**s**ulfate
DTT	**di**thio**t**hreitol
EDTA	**e**thylen**d**iamine**t**etra**a**cetic acid

γEC	**γ**-glutamyl-**c**ysteine
GHOST	**G**ST **H**ydr**o**gel **S**ys**t**em
GSH	**g**lutathione
GST	**g**lutathione-***S***-**t**ransferase
IPTG	**i**so**p**ropyl β-D-1-**t**hio**g**alactopyranoside
mBBr	**m**onobromo**b**imane (3,7-dimethyl1-4 bromethyl-6-methyl-octa-3,6-dien-2,8-dion)
MT	**m**etallo**t**hionein
PBS	**p**hosphate **b**uffered **s**aline
PC	**p**hyto**c**helatin
2-PDS	**2**'2-dithiodi**p**yridine
ROS	**r**adical **o**xygen **s**pecies
-S$^-$	thiolate
TEMED	N,N,N`,N`-**te**tra**m**ethylen**e**thylene**d**iamine
TFA	**t**ri**f**luoro**a**cetic acid
Tricine	N-(**tri(**hydroxymethyl)methyl)gly**cine**
TRIS	**tris-**(hydroxymethyl)-aminomethane

Summary

Metallothioneins (MTs) are small (2-10 kDa), Cysteine-rich (20-35%) proteins, coordinating various metal ions, including Zn^{II} and Cd^{II}. The highly stable metal centers are evidenced to be mostly metal clusters but also single metal binding sites have been recently observed. So far it is not completely understood, how exactly these metal centers are formed and what constitutes the basis of their exceptional stability, rendering MTs particularly interesting from a structural and chemical point of view. The MT E_c-1 from wheat (*Triticum aestivum*) and more particular the sub-domain γ-E_c-1 is an excellent target to elucidate both, the molecular structure and the chemical mechanisms of metallation of plant MTs. E_c-1 is a zinc associated protein described in the wheat grain consisting of two domains, the β_E-domain, which was already investigated in depth in the group of Prof. Freisinger, and the γ-E_c-1 domain, a 25 amino acid, two d^{10} metal ions coordinating polypeptide. The 3D structure of the γ-domain was solved as Zn_2- and Cd_2-form using multidimensional NMR, including ^{113}Cd-NMR for resolving the embedded binuclear tetrahedral tetrathiolate $M^{II}{}_2Cys_6$ metal cluster. In conjecture, the metal binding properties were investigated in depth applying a multitude of spectroscopic techniques i.e. F-AA(S), UVvis, CD, MCD and EXAF(S) spectroscopy revealing tighter Cd^{II} ($pK_a = 3.95 \pm 0.06$) than Zn^{II} ($pK_a = 4.79 \pm 0.06$) binding along with a non-cooperative metallation pathway. Moreover we probed fundamental aspects of d^{10} M^{II} (M^{II}: Zn^{II} and Cd^{II}) metal ion binding to tetrahedral tetrathiolate ligands in order to gain a more thorough understanding of the chiral and magnetically induced chiral features of the M^{II}-S-Cys (M^{II}: Zn^{II} and Cd^{II}) bond as well as the electronic absorption properties. Here, especially the character of the absorption band, which was proposed to originate from ligand to metal charge transfer (LMCT) transitions, was investigated regarding the contribution of terminal (one metal ion bound) versus bridging (two metal ions bound) cysteines. We especially applied Zn^{II}/Cd^{II} substitution experiments to understand the metallation process and the spectroscopical data adhering to. In this regard NMR has proven to be a very valuable tool owing to the development of a new sample preparation method termed GHOST, which enables fast, cheap and reliable sample preparation in combination with, at least for γ-E_c-1, a superb NMR spectra resolution along with the opportunity to stabilize otherwise non observable metallated states – in our case the ZnCd-form of γ-E_c-1. We validated this technique by comparing the Cd^{II} substitution of Zn_2γ-E_c-1 as isolated γ-domain and as gelated GST fusion protein, which actually is the key feature of GHOST, by applying mass

spectrometry, UVvis- and NMR spectroscopy and by comparing the resulting 3D solution structures.

To increase the complexity from the simplest binuclear Zn_2- and Cd_2-cluster ($M^{II}_2Cys_6$) to a slightly more sophisticated system we choose Neclu_MT1, the first exclusively Cd^{II} inducible metallothionein from an aquatic fungus, which potentially provides eight cysteines and one histidine for metal ion binding. In response to Cd^{II} ions MT Neclu_MT1 is expressed in *Heliscus lugdunensis* - an aquatic hyphomycetes - inhabiting a spring in a closed down mining area in the Mansfelder Land area, Germany. First, we tested the metal ion specificity of the recombinant protein, confirming the Cd^{II} preference on the molecular level by witnessing a stoichiometrically different metal ion binding (Cd_3 and Zn_2) at physiological relevant protein concentration. We also evidenced a concentration dependent Zn^{II} Neclu_MT1 metallation either forming a Zn_2- or at higher protein concentration a Zn_3-cluster with Zn_3 Neclu_MT1 strongly coordinating the metal ions ($pK_a = 4.56 \pm 0.03$) in contrast to the weaker associated Zn_2-cluster ($pK_a = 4.87 \pm 0.03$). In a next step we embarked on a more in-depth investigation of the metallation pathway along with the analysis of the resulting metal ion cluster formed. Relying on the methodology developed for γ-E_c-1, we propose a so far unprecedented $M^{II}_3Cys_8His$ (M^{II}: Zn^{II} and Cd^{II}) cluster, which is topologically similar to the well-known β-cluster ($M^{II}_3Cys_9$) in mammalian MTs. In addition we believe to have encountered a second cluster type in Neclu_MT1 a $M^{II}_3Cys_8$ (M^{II}: Zn^{II} and Cd^{II}) cluster, which is unparalleled in biological and biomimetic systems. A key experiment in the process of identifying these cluster architectures was to photo-spectroscopically follow the thiol to thiolate transition along with the formation of disulfide bridges at different Neclu_MT1 concentrations and metal ion loads. We suggest this thiolate titration experiment to be introduced to the standard experimental portfolio for elucidating the structure and function of thiol containing metalloproteins.

Zusammenfassung

Metallothioneine (MT) sind kleine (2-10 kDa), cysteinreiche (20-35%) Proteine, die verschiedene Metallionen koordinieren, wie z.B. Zn^{II} oder Cd^{II}. Die im Protein eingelagerten sehr stabilen Metallzentren treten entweder als Metallcluster oder als einzelne Metallbindungsstellen auf. Zum jetzigen Zeitpunkt ist es nicht vollständig bekannt, wie genau diese Metallzentren sich ausbilden, noch was die Basis ihrer Stabilität darstellt. Diese Fragen bilden die Grundlage unseres Interesses an Metallothioneinen, im Besonderen an ihrer Struktur. Das Weizen (*Triticum aestivum*) Metallothionein E_c-1, speziell die Subdomäne γ-E_c-1 stellt ein ausgezeichnetes Modell für Pflanzen MTs zu strukturellen und molekular mechanistischen Untersuchungen der Metallierung dar. E_c-1 ist ein Zink bindendes Protein, welches im Weizenkorn beschrieben wurde. Es besteht aus zwei Domänen, der β_E-Domäne, die bereits intensiv in der Arbeitsgruppe von Prof. Freisinger untersucht wurde und der γ-E_c-1 Domäne, ein 25 Aminosäuren langes, zwei d^{10} Metallionen koordinierendes Polypeptide. Die 3D Struktur der γ-E_c-1 Domäne wurde als Zn_2- und Cd_2-Form mittels multidimensionaler NMR gelöst. Die Untersuchung des tetraedrischen tetrathiolat $M^{II}{}_2Cys_6$ Metallclusters erfolgte via ^{113}Cd-NMR. Zusätzlich zu strukturellen Eigenschaften erfolgte eine detaillierte Untersuchung der Metallbindung mittels diversen spektroskopischen Techniken, wie F-AA(S), UVvis, CD, MCD und EXAF(S) Spektroskopie, welche auf eine stärkere Cd^{II} (pK_s = 3.95 ± 0.06) als Zn^{II} (pK_s = 4.79 ± 0.06) Bindung hinweisen, sowie auf eine nicht-kooperative Metallbindung. Zusätzlich wurden fundamentale Aspekte der d^{10} M^{II} Metallionenbindung mit tetraedrischen Tetrathiolatliganden beleuchtet, um genauere Einblicke in die chiralen, magnetisch induzierten chiralen, sowie elektronischen Eigenschaften von M^{II}-S-Cys (M^{II}: Zn^{II} and Cd^{II}) Bindungen zu gewinnen. Besonderen Fokus wurde auf den molekularen Ursprung der Absorptionsbanden gelegt. In der Literatur wird ein Ladungsübergang vom Ligand zum Metall (LMCT) vorgeschlagen, den wir bezüglich seiner Eigenschaften auf terminale Cysteine (ein gebundenes Metallion) und verbrückenden Cysteine (zwei gebundene Metallionen) untersuchten. Hierbei zeigten sich Zn/Cd Substitutionsexperimente als nützlich. Diese können mit Hilfe von NMR Spektroskopie verfolgt werden, wobei sich eine neue Probenpräparationsmethode namens GHOST als besonders nützlich erwiesen hat. Diese ermöglicht im Falle von γ-E_c-1 eine schnelle, einfache und verlässliche Probenpräparation in Kombination mit einer besseren Signal Auflösung, sowie einer Stabilisierung von anderweitig nicht beobachtbaren Metallierungszuständen – in unserem Fall der ZnCd-Form von γ-E_c-1.

Die Validierung des GHOST System erfolgte mittels Cd^{II} Substitution von $Zn_2\gamma$-E_c-1, wobei die isolierte γ-Domäne mit dem gelierten GST Fusionsprotein, welches den Schlüsselaspekt des GHOST Systems darstellt, verglichen wurde. Hierzu wurde Massenspektrometrie, UVvis- und NMR Spektroskopie benutzt, sowie die resultierenden 3D Strukturen verglichen.
Ausgehend vom einfachsten binuklearen Zn_2- und Cd_2-Cluster ($M^{II}_2Cys_6$) haben wir das etwas komplexere Neclu_MT1 Protein studiert. Neclu_MT1, ist das erste nur durch Cd^{II} induzierbare Metallothionein, welches aus einem aquatischen Pilz isoliert wurde und acht Cysteine sowie ein Histidin zur Metallionenkoordination besitzt. Neclu_MT1 wird auf Cd^{II} Exposition hin in dem aquatischem Hyphomyceten *Heliscus lugdunensis* exprimiert, welcher aus einem verlassenen Bergbauareal im Mansfelder Land, Deutschland, isoliert wurde. In einem ersten Untersuchungsschritt erfolgte die Validierung der Cd^{II} Selektivität am rekombinant exprimierten Protein. Es konnte die Cd^{II} Preferenz auch auf molekulare Ebene gezeigt werden, da unter physiologisch relevanten Bedingungen eine stöchiometrisch unterschiedlicher Metallbindung für Cd^{II} und Zn^{II} (Cd_3 und Zn_2) beobachtet wurde. Zusätzlich konnte für Zn^{II} Neclu_MT1 eine konzentrationsabhängige Metallierung nachgewiesen werden, wobei ein Zn_2- oder bei höheren Proteinkonzentrationen ein Zn_3-Cluster gebildet wird, die sich aufgrund ihrer Bindungsstärke unterscheiden (Zn_3 : pK_s = 4.56 ± 0.03; Zn_2 : pK_s = 4.87 ± 0.03). In einem weiteren Schritt erfolgte eine tiefgreifendere Untersuchung des Metallierungsprozesses, sowie der resultierenden Metallcluster. Unter der Verwendung der Methodik, die für die Untersuchung der MT-Domäne γ-E_c-1 vorgestellt wurde, schlagen wir die Existenz eines bisher nicht beschriebenen Metallcluster vor - $M^{II}_3Cys_8His$ (M^{II}: Zn^{II} und Cd^{II}) – welcher topologisch dem gut untersuchten β-cluster ($M^{II}_3Cys_9$) aus Säugetiermetallothioneinen ähnelt. Zusätzlich weisen unsere Ergebnisse auf einen zweiten Clustertypen in Neclu_MT1 hin, ein $M^{II}_3Cys_8$ (M^{II}: Zn^{II} and Cd^{II}) Cluster, welcher als solcher weder in biologischen noch in biomimetischen Systemen bekannt ist. Eines der Schlüsselexperimente, das zur Identifizierung dieser Clusterarchitekturen geführt hat, ist die photo-spektroskopische Untersuchung zum Übergang von Thiolen zu Thiolaten, einhergehend mit der Ausbildung von Disulfidbrücken am unterschiedlich metallierten, sowie konzentrierten Neclu_MT1 Protein. Wir schlagen vor, dass diese Thiolattitration als Standardexperiment im Portfolio für struktur- und funktionsaufklärende Untersuchungen von Metallproteinen aufgenommen wird.

Chapter I : General Introduction

I 1 Metallothioneins

From a chemical point of view cellular components can be divided into two classes: the macromolecules, consisting of sugars, fatty and nucleic acids as well as proteins and the metabolites, including chemically diverse organic molecules, inorganic salts and metal ions. In general macromolecules regulate metabolite levels in a complex system relying on a multitude of specifically designed proteins carrying out various tasks, which all can be associated to import/synthesis, export/degradation and storage/regulation. In case of essential d^{10} metal ions such as Cu^{I} or Zn^{II}, a protein super-family termed metallothioneins (MTs) is involved in these processes. Those proteins, in contrast to most others, rely on thermodynamics in order to coordinate their co-factors by providing an unusual high degree of cysteine thiols for metal ion coordination, which coined the name metallothioneins. According to the *hard and soft acids and bases* (HSAB) concept that provides a guideline for coordination chemistry, the well polarizing cysteine thiolates are rated as *soft bases* that may coordinate to *soft acids*, especially closed shell metal ions, including all d^{10} metal ions like essential Cu^{I} and Zn^{II} but also non-essential Cd^{II} and Hg^{II}. The chemical reactivity owing to the relatively high oxidation potential of the cysteine thiolates (-145 mV in proliferating HT29 cells[1]) and their preference for toxic higher period group 2b metal ions constitutes a major challenge when investigating metallothioneins *in vitro* and *in vivo*.

Historically MTs have been indentified in equine kidney cortex in the late 1950s[2] as natural Cd^{II}-binding protein. In the last 50 years a myriad of proteins have been identified that were taxonomically classified as metallothioneins according to their primary amino acid sequence[3] resulting in a heterogeneous non-function related classification (**Fig. I 1**). According to the widely accepted definition MTs are low molecular mass (<10 kDa), cysteine (up to 33 %)- and metal ion-rich proteins containing multiple Cys-Xxx-Cys, Cys-Cys or Cys-$(Xxx)_2$-Cys amino acid stretches.

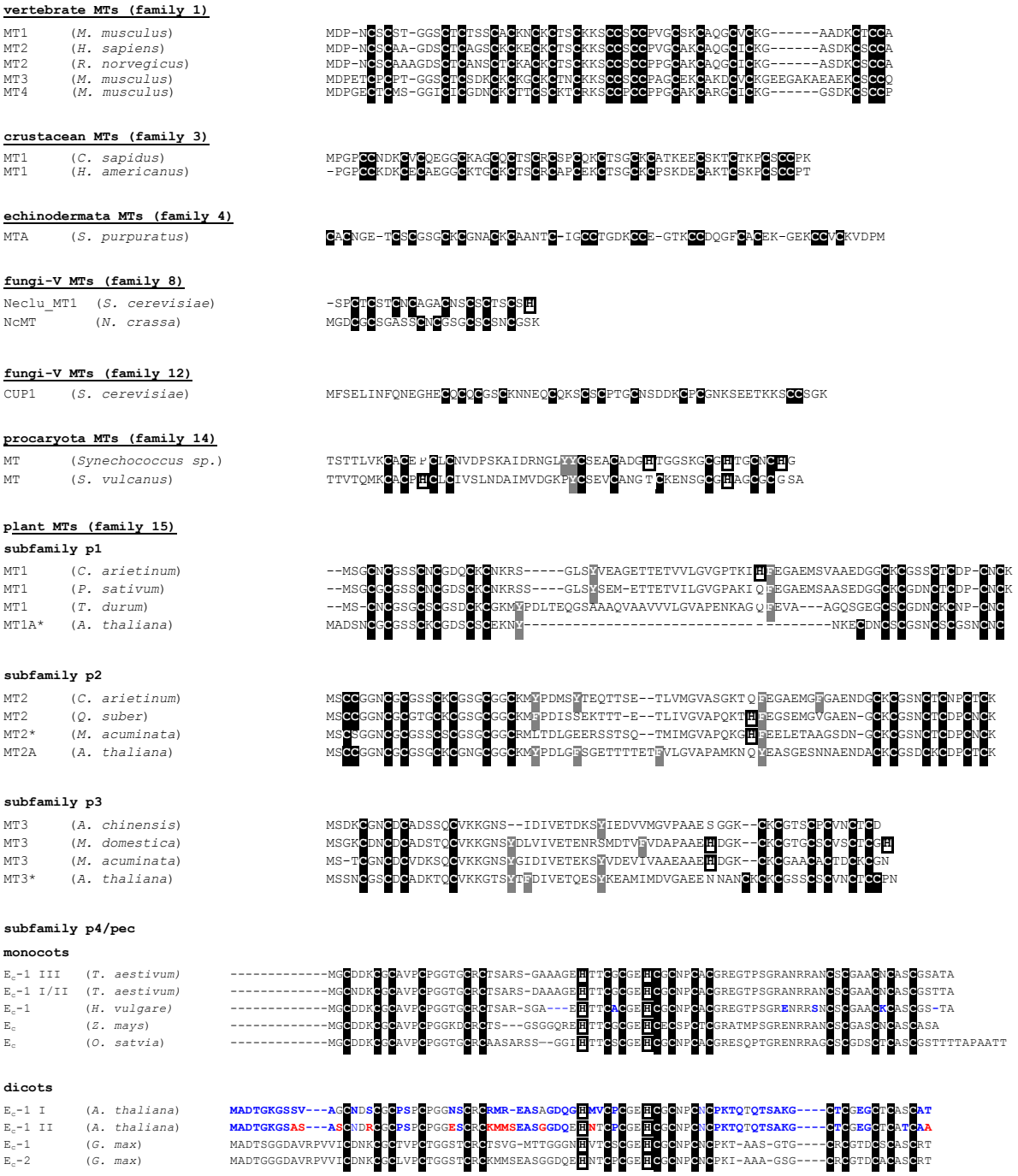

Fig. I 1 Classification of metallothioneins into different taxonomical families according to *Binz et al.*[3] of those families were structures are known or significant functional characterization on the protein level were carried out. Cysteine patterns are highlighted in black while histidines are enclosed in black boxes. In the sequence alignment of E_c-1 proteins (I, II vs. III) from bread wheat the differing amino acids are marked in bold grey (figure was adapted from[4-5]). Furthermore, differences form *A. thaliana* E_c-1 proteins to wheat E_c-1 III are marked in blue. Additionally, amino acids varying among E_c-1 I and E_c-1 II from *A. thaliana* are highlighted in red.

mt genes were isolated from basically all living phyla except *archaea*. Those MTs, which were investigated on the protein level, all comprise a sulfur-based metal ion cluster. A more recent metallothionein classification is oriented on the metal binding selectivity differentiating among Zn^{II} and Cu^{I} associated MTs[6] and claiming that according to the difference in binding geometry MTs are either involved in Zn^{II} or in Cu^{I} homeostasis. The increasing complexity in MT research is also reflected in the finding that a further amino acid, histidine, was reported to be involved in metal ion coordination in SmtA, a bacterial metallothionein[7]. Furthermore the structure of the first plant metallothionein, E_c-1 from bread wheat, displayed a mononuclear $M^{II}Cys_2His_2$ metal center[8-9]. While the NMR solution structure of the β_E-domain (**Fig. I 2**), containing the $M^{II}Cys_2His_2$ metal center, was obtained for the Zn^{II}-form doubts were raised, whether an isostructural replacement of Zn^{II} by Cd^{II} occurs[10].

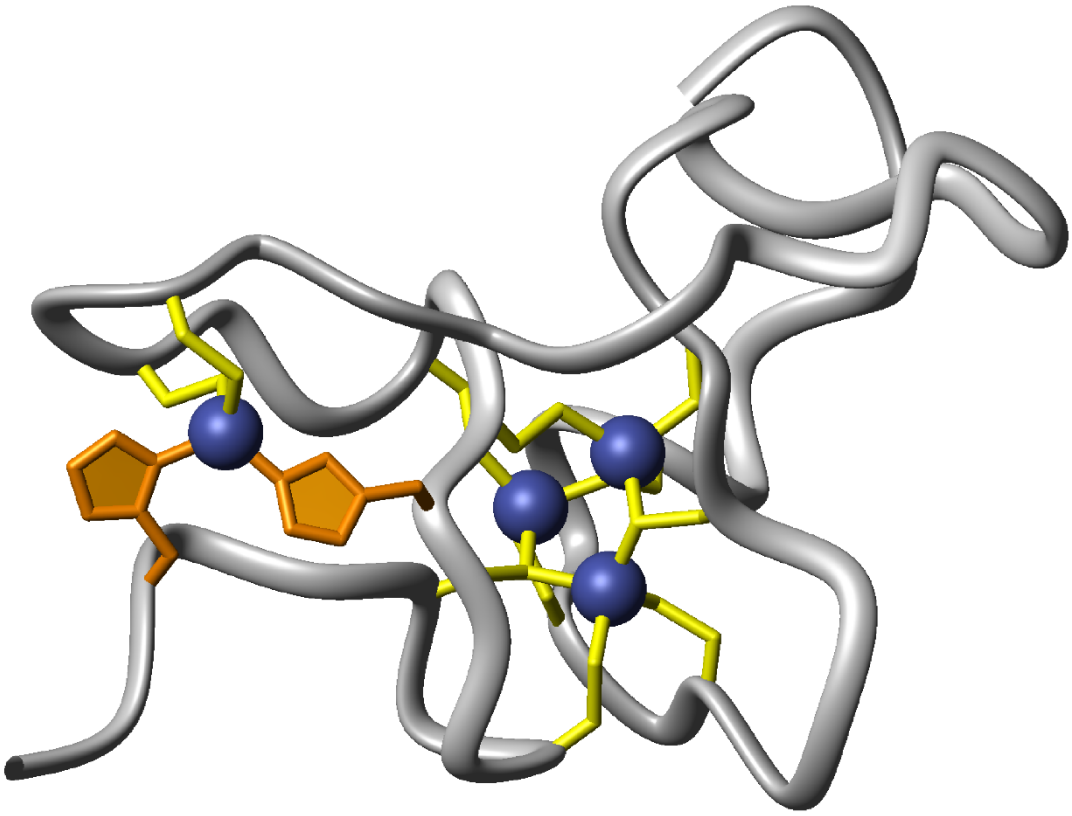

Fig. I 2 The protein backbone of $Zn_4\beta_E$-E_c-1 is depicted in ribbon shape (grey). The larger domain of E_c-1 contains eleven cysteines (yellow bonds) and two histidines (orange bonds) coordinating four Zn^{II} ions depicted as blue spheres. The metal ions are organized in two metal centers: a $Zn^{II}{}_3Cys_9$ metal

thiolate cluster and an isolated mononuclear binding site $Zn^{II}Cys_2His_2$ representing a common zinc finger motive as evidenced in numerous transcription factors.

Moreover a general discrimination between essential Zn^{II} and toxic Cd^{II} is hypothesized on the basis of imidazole nitrogen involvement of histidine in MTs. Here again the HSAB concept is exploited. The "harder" nitrogen ligand histidine (base) prefers the "harder" metal ion Zn^{II} (acid)[11]. So far, however, no direct experimental proof was provided, in particular chemical shift patterns of the $Zn_4\beta_E$-E_c-1 and $Cd_4\beta_E$-E_c-1 [^{15}N,^{1}H] HSQC NMR spectra and intensities of the ^{15}N-(^{1}H)-NOE steady state nuclear overhauser enhancement experiment are identical, indicating a comparable fold of the β_E-domain for the Zn_4- and Cd_4-form[9]. The second smaller domain of E_c-1, the γ-domain, embedding a binuclear tetrahedral tetrathiolate $M^{II}_2Cys_6$ (M: Zn, Cd, Hg) metal cluster remained to be structurally elaborated, which constitutes one of the two main aspects of this thesis. Besides its structural particularity, E_c-1, which belongs to the pec subfamily of plant MTs[12], received considerable interest from plant biologists. When in 1983 Lane et al. investigated the major sulfur associated compounds in imbibiting wheat grains from *Triticum aestivum* they discovered along with the early methionine rich protein (E_m) the early cysteine labeled protein (E_c-1)[13], which was later identified as the first plant MT[14]. The E_c proteins occur in three isoforms I, II and III. While I and II are identical, III differs in three amino acids. The E_c proteins are encoded in the hexaploidic chromosome set as single copy genes on chromosomes 1A, 1B, 1D[12]. The E_c-1 MT represents the major cysteine containing translate (25%), when heterologously expressing the stored mRNA of the wheat grain[13]. Moreover E_c-1 is reported to be only induced during the mid and late wheat grain filling stage[15-16]. Based on the cysteine pattering, homologues of E_c-1 are reported in all crops including rice, maize, barley, soybean and sesame as well as in *Arabidopsis thaliana* the model organism of plant biologists[17].

In *A. thaliana* two 70 % homologous isoforms have been described, with E_c-1 I possessing a tendency to provide Zn^{II} resistance, and E_c-1 II to foster Cd^{II} resistance in genetically engineered *Saccharomyces cerevisiae*[18]. Another recent study in *A. thaliana* claims the E_c proteins to be determinants for grain size. Ren et al.[19] showed that *knock out* mutants of neither E_c-1 I nor E_c-1 II were viable and siRNA suppressed E_c-1 I/II mutants displayed a reduction in *A. thaliana* grain weight and size, whereas overexpression of the E_c proteins let to a 20% increase in the size of the grain. Owing to the high E_c-1 transcripts levels in the dried wheat grain along with a 57 % homology in primary amino acid structure to E_c-1 I from *A.*

thaliana, this protein might generate a substantial agronomical interest. To further understand the mechanism of E_c-1 involvement in determining the grain size of wheat or other cereals more detailed investigations on this subject are required. In a first line of investigation the structure and metallation properties of the protein need to be elaborated, more specifically, the so far uncharacterized γ-domain of E_c-1 required an in-depth analysis as has been done in chapter 2 to 5 of this thesis.

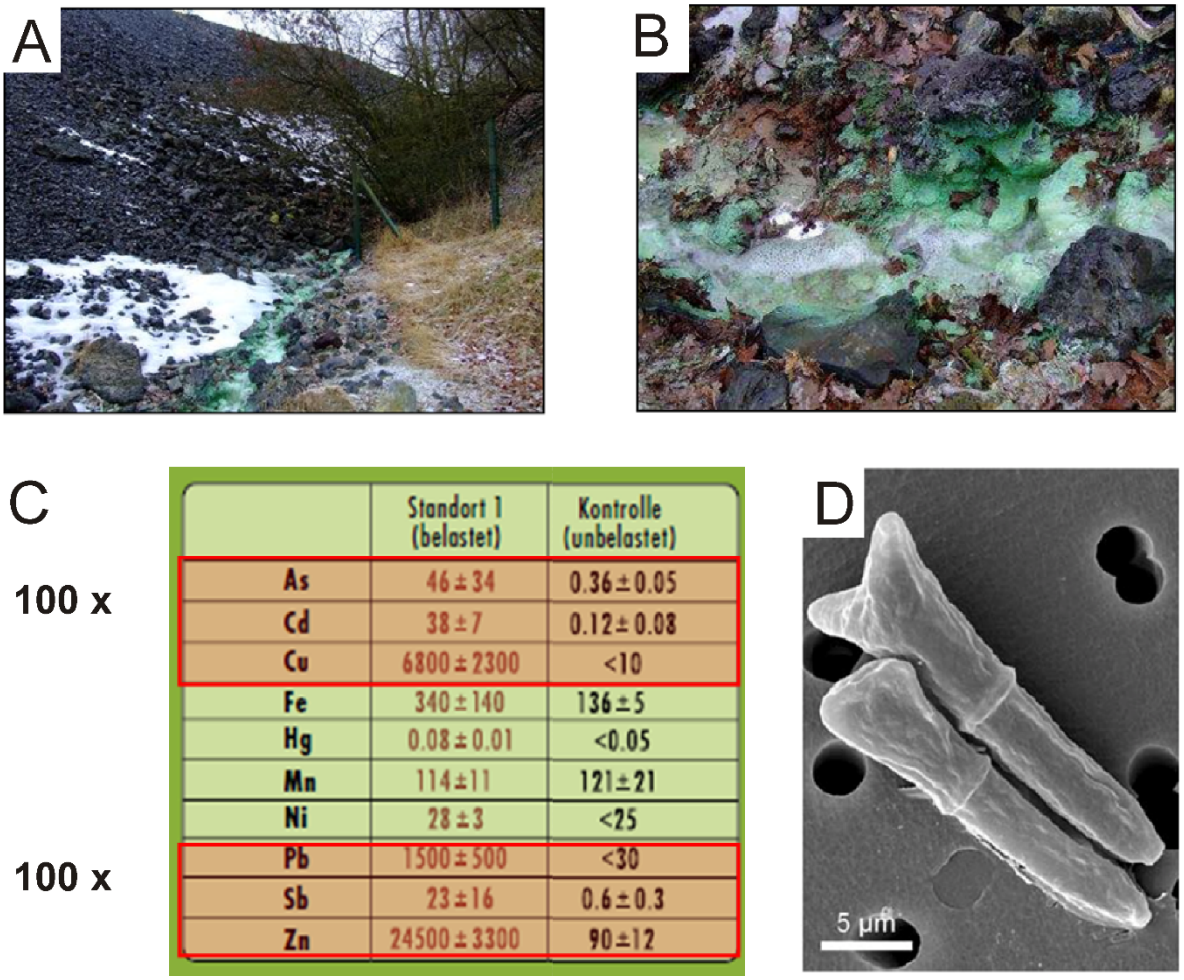

	Standort 1 (belastet)	Kontrolle (unbelastet)
As	46 ± 34	0.36 ± 0.05
Cd	38 ± 7	0.12 ± 0.08
Cu	6800 ± 2300	<10
Fe	340 ± 140	136 ± 5
Hg	0.08 ± 0.01	<0.05
Mn	114 ± 11	121 ± 21
Ni	28 ± 3	<25
Pb	1500 ± 500	<30
Sb	23 ± 16	0.6 ± 0.3
Zn	24500 ± 3300	90 ± 12

Figure I 3 Pictures of the site of isolation and the conidia of *H. lugdunensis* along with a statistics of the metal ion content of the spring is depicted. ***A)*** and ***B)*** Site of isolation H.4.2.4 in Stadtborn/Hergisdorf near Eisleben (Mansfelder Land; 01/2009). The spring of a former copper shale mine contains green Zn^{II} deposition[23]. ***C)*** Metal ion content of site H.4.2.4, the reddish framed metal ions are 100 times over-represented in comparison to the control condition. ***D)*** SEM image of conidia of *H. lugdunensis* strain H.4.2.4.[24].

In order to expand the findings derived from γ-E_c-1, a chemically related second small metallothionein (smMT), Neclu_MT1 from the aquatic fungus *Heliscus lugdunensis*, was investigated. Comparable in size (Neclu_MT1: 2378 Da/ 24 amino acids; γ-E_c-1: 2448 Da/25 amino acids) it provides eight cysteines and one histidine for metal ion coordination instead of six cysteines as in case of γ-E_c-1. So far no structural features of the protein backbone nor the embedded metal cluster are known, yet detailed studies elaborating the physiological situation, in which Neclu_MT1 is evidenced, exist[20-22]. The *H. lugdunensis* strain H.4.2.4, from which the MT was identified, prospers in a spring of a former copper shale mine in the Mansfelder Land area, Germany (**Fig. I 3**), being exposed to extraordinary high transition metal ion concentrations, i.e. 40 mM Zn^{II}, 208 μM Cu^{II}, 25 μM Cd^{II}, and 61 μM As^{V}.

In order to cope with the fierce conditions of its habitat, *H. lugdunensis* enzymatically synthesizes a wide range of thiol containing redox-active lower molecular mass species including, cysteines, γ-glutamylcysteines (γ-ECs), glutathione (GSH), and phytochelatins (PCs)[24]. Moreover a genetically encoded metallothionein Neclu_MT1 could be identified and classified as a Cd^{II} binding MT via mass spectrometry[22]. Neclu_MT1 is taxonomically rated as a member of the MT fungi family 8 along with the well-studied Cu_6MT from *Neurospora crassa*[25], raising the question, whether Neclu_MT1 can, in accordance with most other fungal MTs, be associated to Cu^{I} homeostasis. This question was addressed within this thesis (see **Chapter VI**). Moreover, sequence alignment based on the cysteine pattering of Neclu_MT1 using the UniProtKB/Swiss-prot data bank yielded two further MTs from glume blotch (*S. nodorum*) and blackleg fungus (*P. lingam*) not only sharing the same cysteine pattering but also the same number of amino acids as well as the *C*-terminal histidine (**Fig. I 4**).

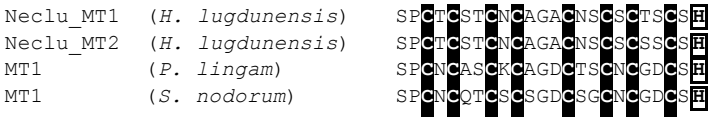

Figure I 4 Sequence alignment of Neclu_MT1 proteins sharing identical cysteine patterns with further fungi MT family 8 proteins. Cysteines are highlighted in black while histidines are enclosed in black boxes[26].

The MT from glume blotch is of special interest, since it genetically shares the same 5'-UTR upstream activation sequence (UAS) of the coding region as Neclu_MT1, namely the

TCnnGCAG sequence being identified as a metal responsive element (MRE)[27]. Additionally mRNA specific expressed sequence tag (EST) data are available, reporting that the wheat pathogen glume blotch expresses high copy numbers of the MT RNA[28].

I 2 Methods for Structural Investigation of Metallothioneins

Metalloproteins as such can be regarded as polypeptides embedding a metal center. In case of metallothioneins this perspective is even more valid owing to the size of the metal center constituting 20 to 33 % of the mass of the entire protein when accounting the cysteinyl thiolates ($-S^{1-}$) as part of the metal cluster. In consequence the structure of the protein backbone and the one of the metal cluster are separately investigated applying different experimental methods. Among the three standard methods for structure elucidation of biological macromolecules namely cryo-electron microscopy (cryo-EM), X-ray crystallography, and nuclear magnetic resonance (NMR) spectroscopy, NMR has gained prominence as most reliable method for predicting the correct structure of metallothioneins. While the spatial resolution of cryo-EM provides a rough estimate of the fold of the protein backbone it doesn't suffice to resolve the embedded metal ion cluster[29]. X-ray crystallography may yield the necessary atomic resolution, yet the topology on the metal cluster in case of the Zn^{II} and Cd^{II} binding mammalian MTs as well as the Cu^{I} associated Cup1 MT from yeast suggests optical and chiro-optical features differing from those evidenced in the crystal structure[30-32]. Moreover various extensive unsuccessful crystallization trials report from the intrinsic dynamic of the metal cluster, more precisely from kinetic processes within these thermodynamically stable metal clusters that inhibit high quality crystal growth. NMR on the other hand contributed largely to resolving the known structural diversity of MTs from e.g. humans[33], sea urchin, bacteria[7], and plants[9].

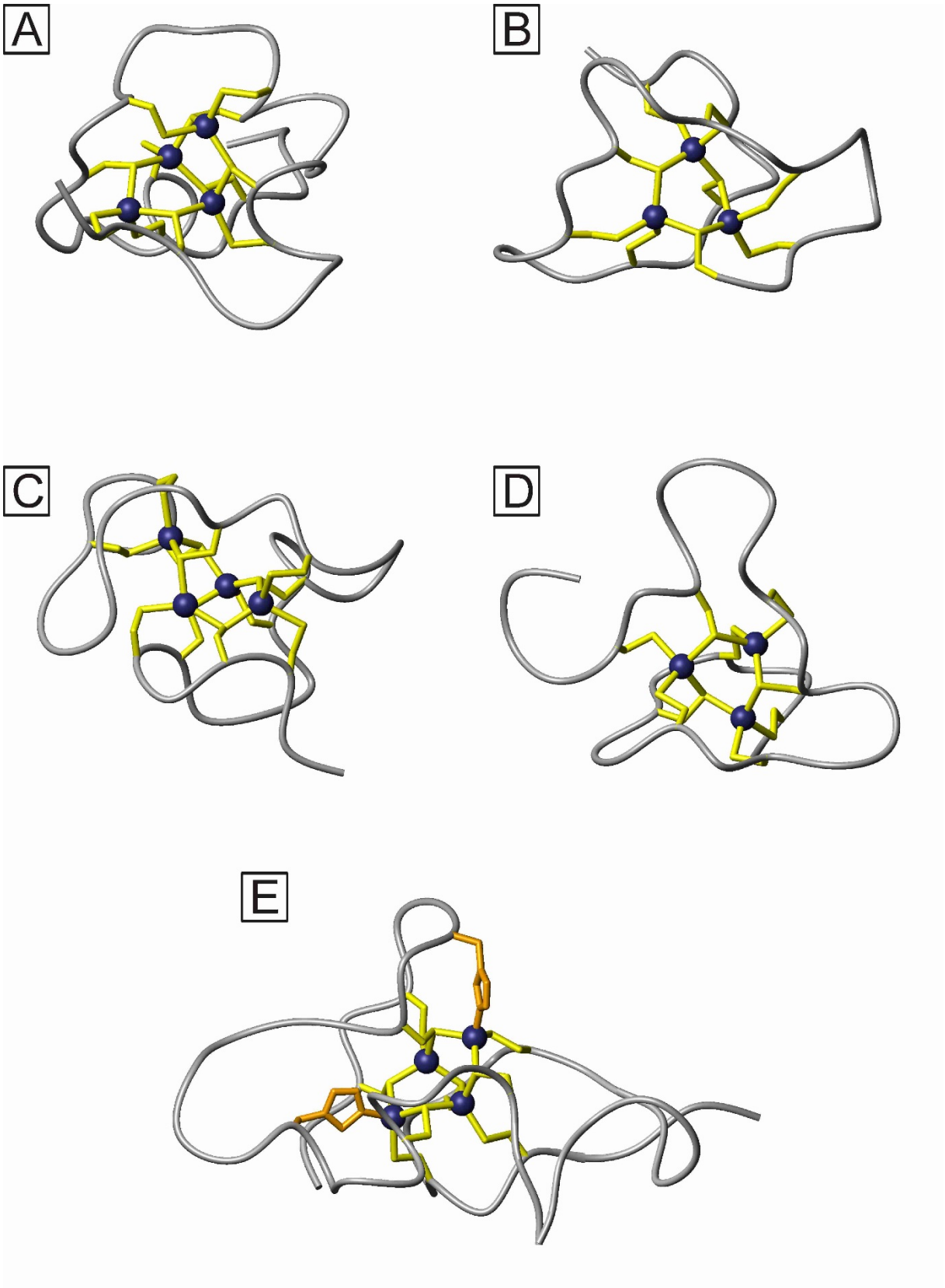

Figure I 5 Solution structures of selected MTs obtained by multidimensional NMR. The protein backbone is displayed in ribbon shape (grey), the divalent metal ions as spheres (blue) and the coordinating cysteines (yellow) and histidines (orange) as bonds. The solution structure of human

MT1 ***A)*** α-domain (pdb: 1MHU), ***B)*** β-domain (pdb: 2MHU), of sea urchin MT1 ***C)*** α-domain (pdb: 1QJL), ***D)*** β-domain (pdb: 1QJK) and the bacterial MT SmtA (pdb: 1JJD) are prepared employing the program MOLMOL®.

MT structure elucidation and biological NMR development proceeded concomitantly. In 1980 the first reported MT NMR analysis[34] probed the metal cluster employing ^{113}Cd NMR. Along with 2D [^{113}Cd,^{1}H] HSQC NMR experiments, allowing to establish the cysteine or in special cases histidine connectivities, 2D [^{113}Cd,^{113}Cd]-COSY NMR experiments were developed attributing the ^{113}Cd signals to the respective metal cluster[35-37], thus providing an entire set of ^{113}Cd NMR experiments to comprehensively dissect all the necessary information of the Cd-cluster for solution structure calculation of the entire MT, including the metal cluster. In order to investigate the protein backbone the group of Prof. Wüthrich developed the standard procedure for protein structure determination[38-39], where in a first step individual protons are grouped and allocated to spin-systems (generally representing one amino acid) using the 2D [^{1}H,^{1}H] TOCSY NMR spectra. In a next step the spin-systems are assigned to the respective amino acid via 2D [^{1}H,^{1}H] NOESY NMR spectra, which also yield NOEs providing the distance information of spatially close protons (<5 Å), that are used for solution structure calculation. This basic set of experiments has been further developed over the last two decades. Special labelling techniques, employing 2D, ^{13}C and ^{15}N isotopes have enabled NMR spectroscopists to venture to bigger size molecules. Also automated structure solution software packages have been engineered (UNIO) and greatly facilitated the otherwise difficult, time consuming process[40-42]. MTs, however, lacking regular secondary structure elements still require extensive manual engagement and controlling.

I 3 Methods for Functional Characterization of Metallothioneins

Understanding the (re)-metallation pathway and resulting metal ion cluster of MTs may yield information concerning possible physiological roles of the proteins. Characterizing metalloproteins in general and MTs in particular the chemical identity of the incorporated metal ion has to be indentified first. In case of MTs either d^{10} metal ions of group 2a (Zn^{II}, Cd^{II} or Hg^{II}) preferring tetrahedral coordination environments, or metal ions of group 1a (Cu^{I} or Ag^{I}), generally experiencing triangular and diagonal coordination geometry are

incorporated. If no biological data are available, e.g. gene induction, *in vivo* metallation state, etc., photospectroscopically followed metal ion titrations in comparison with mass spectrometrical data may provide a preliminary measure of judgment. Definite answers concerning the chemical indentify of the most likely bound metal ion *in vivo* can however only be provided by structure determination methods such as X-ray crystallography or NMR spectroscopy. In order to assess the purity of MTs size exclusion chromatography (SEC) and polyacrylamide gel electrophoresis (PAGE) are the methods of choice. Once the desired purity is obtained the concentration of the MT is determined via the 2-PDS assay[43], quantifying the amount of non-oxidized thiols, while the metal ion load is obtained by means of atomic absorption spectroscopy (AAS). Also the usage of inductively coupled plasma mass spectrometry (ICP-MS) quantifying both the ligand and the metal ion is possible. Having characterized the protein purity and identified the metal load, metal ion titrations to either the apo- or the holo-MT followed by UVvis spectroscopy constitute the most basic experiments for metal ion binding studies. According to the metal ion probed, the energy of the absorption bands along with their molar extinction coefficient (ε) are detailed in the literature[44-47]. In general the (re)-metallation process is considered to be finished when no increase in molar absorptivity despite addition of further metal ions is witnessed. The amount of incorporated $M^{I/II}$ ions can be determined based on the final extinction coefficient and on the number of metal ion equivalents added until this value is reached. In order to obtain further insight into the (re)-metallation process circular dichroism (CD) and magnetic circular dichroism (MCD) spectra can be recorded in addition to the UVvis spectra. While MCD data solely yield information regarding the point of formation of $M^{I/II}$ to S-Cys bonds, CD spectra foster the understanding of the cluster formation and rearrangement process. Together with SEC and MS the monomeric character and abundance of differently metallated species can be assessed, rendering this approach a powerful tool in order to investigate metal ion binding in MTs. Further attempts of applying optical spectroscopy including infra-red (IR)[48]- or Raman[49-50]. as well as fluorescence spectroscopy[51] are reported in the literature. For the interpretation of the experimental data, however, a comprehensive theoretical framework to map these data onto structural properties or functional processes still needs to be further developed. For metal ions with unpaired electrons such as Cu^{II} or Co^{II} electron paramagnetic resonance (EPR) spectroscopy may provide information concerning the geometry of the metal ions[52] owing to their electronic open shell configuration in comparison to the closed shell configuration of Zn^{II}, Cd^{II} or Hg^{II}. X-ray based methods, especially extended X-ray absorption fine structure

(EXAFS), probe the coordination environment of the otherwise spectroscopically silent d^{10} metal ions. By observing the K-edge of the metal ion the first coordination sphere of both Zn^{II} and Cd^{II} metal ions can be comprehensively predicted along with the prevailing ligand geometry[53] (see **Chapter VI**). Heteronuclear NMR can to a certain extend provide a wealth of information. $^{107/109}Ag$ and ^{199}Hg but most importantly $^{111/113}Cd$ NMR is employed to elucidate the metal cluster connectivities[54]. Due to the fact that $^{107/109}Ag^{I}$ only to a certain degree iso-structurally replaces Cu^{I} it is not as often applied as $^{111/113}Cd^{II}$ substitution for Zn^{II}. The same is true for $^{199}Hg^{II}$, which prefers a linear Cys-S-Hg^{II}-S-Cys coordination environment when added in excess. Mass spectrometry being the proteomics tool of the 21st century renders a multitude of data accessible to the scientist, which however necessitates careful interpretation relying on further spectroscopic or spectrometric experiments. Hyphenated techniques such as HPLC-ESI-MS or SE-HPLC-ICP-MS are powerful methods for investigating MTs from natural sources[55]. Moreover there have been a myriad of other experimental methods developed such as TD-PAC[56], CE-chromatography[57], SAXS[58] and a lot of other to study metal ion incorporation and the resulting structures[59]. In general, the parallel use and interpretation of various experimental techniques yield more concise and realistic information, than focusing merely on one method, when functionally characterizing MTs.

Chapter II : Protein and metal cluster structure of the wheat metallothionein domain γ-E_c-1. The second part of the puzzle.

Jens Loebus[a§] · Estevão A. Peroza[a§] · Nancy Blüthgen[a] · Thomas Fox[a] · Wolfram Meyer-Klaucke[b] · Oliver Zerbe[c] · Eva Freisinger[a]

[a]Jens Loebus · Estevão A. Peroza · Nancy Blüthgen · Thomas Fox · Eva Freisinger (✉)

Institute of Inorganic Chemistry, University of Zurich,

Winterthurerstr. 179

8057 Zurich, Switzerland

e-mail: freisinger@aci.uzh.ch

[b]Wolfram Meyer-Klaucke

European Molecular Biology Laboratory (EMBL), Outstation Hamburg at Deutsches Elektronen-Synchrotron (DESY),

22603 Hamburg, Germany

[c]Oliver Zerbe (✉)

Institute of Organic Chemistry, University of Zurich,

8057 Zurich, Switzerland

e-mail: zerbe@oci.uzh.ch

[§] both authors contributed equally

II 1 Abstract

Metallothioneins (MTs) are small cysteine-rich proteins, coordinating various transition metal ions including Zn^{II}, Cd^{II}, and Cu^{I}. MTs are ubiquitously present in all phyla indicating a successful molecular concept for metal ion binding in all organisms. The plant MT E_c-1 from *Triticum aestivum*, common bread wheat, is a Zn^{II} binding protein that comprises two domains and binds up to six metal ions. The structure of the C-terminal four metal ion binding β_E-domain was recently described. Here we present now also the structure of the N-terminal second domain, γ-E_c-1, determined with NMR spectroscopy. The γ-E_c-1 domain enfolds a $M^{II}_2Cys_6$ cluster and was characterized as part of the full-length Zn_6E_c-1 protein as well as in form of the separately expressed domain, both in the Zn^{II}- and the Cd^{II}-containing isoform. EXAFS analysis of $Zn_2\gamma$-E_c-1 clearly shows the presence of a ZnS_4 coordination sphere with average Zn-S distances of 2.33 Å. ^{113}Cd NMR experiments were used to identify the M^{II}-Cys connectivity pattern, revealing two putative metal cluster conformations. In addition, the general metal ion coordination abilities of γ-E_c-1 were probed with Cd^{II} binding experiments as well as by pH titrations of the Zn^{II}- and Cd^{II}-forms, the latter suggesting an interaction of the γ- and the β_E-domain within the full-length protein.

Keywords Plant metallothionein · Metal-thiolate cluster · Electronic absorption spectroscopy · EXAFS · NMR spectroscopy

II 2 Introduction

Metallothioneins (MTs) are low molecular mass (2–10 kDa) and cysteine-rich proteins with a preference for the coordination of metal ions with d^{10} electron configuration, e.g. Zn^{II}, Cu^{I}, and Cd^{II} [60], Their occurrence is reported throughout the animal kingdom, in plants, several eukaryotic microorganisms, as well as in some prokaryotes[3]. The plant MT E_c-1 from wheat consists of 81 amino acids. All of the 17 cysteine and two histidine residues are involved in the coordination of six divalent metal ions that are arranged in two separate metal-binding domains (**Fig. II 1**)[61].

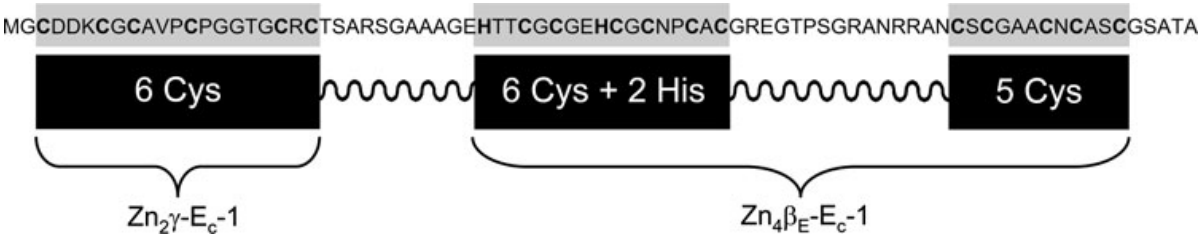

Figure II 1 Amino acid sequence of full-length wheat E_c-1 with the cysteine-rich metal ion coordinating regions highlighted in grey (top) as well as a schematic representation giving the sort and number of coordinating amino acids. The N-terminal Cys-rich region harbors the herein described Zn_2Cys_6 cluster, while the central and C-terminal regions together form the $Zn_4\beta_E$-domain.

E_c-1 is the first and so far only plant MT, which could be successfully isolated from plant material[13]. E_c-1 is most abundant in wheat embryos and present in the Zn^{II} form[14]. Unlike the majority of MTs, E_c-1 recruits also two His residues for Zn^{II} binding, a feature so far only observed in a cyanobacterial MT form[7]. This ligand specificity usually distinguishes MTs from Zn^{II} binding enzymes, where the Zn^{II} coordination sphere often consists of a mixture of S, N, and O donor ligands. In consequence, the resulting metal clusters show a limited variety of possible structures. This is demonstrated by the fact that only two basic cluster arrangements have been structurally described for divalent metal ions so far: The $M^{II}_3Cys_9$ cluster of the β-domain of vertebrate, crustacean, and echinodermata MTs and the $M^{II}_4Cys_{11}$ cluster of the α-domain from vertebrates and echinodermata MTs (e.g. PDB codes 4MT2, 1DMC, 1DME, 1QJK, and 1QJL[62-64]). The $Zn_4Cys_9His_2$ cluster of the cyanobacterium

Synechococcus PCC 7942 is structurally related to the Zn_4Cys_{11} cluster with exchange of two terminal thiolate ligands by imidazole moieties[7]. A Zn_3Cys_9 cluster with similarity to the $M^{II}{}_3Cys_9$ cluster mentioned above can be also found in the β_E-domain of wheat E_c-1, but the Zn^{II} coordinating residues are interleaved with the two Cys and His ligands of the additional mononuclear Zn^{II} site[9]. This $ZnCys_2His_2$ site, while known from certain Zn-finger proteins, was unprecedented in the MT superfamily and is so far uniquely found in the plant E_c proteins. The limited structural variability of the metal ion binding sites in MTs goes along with the constricted biological functionality known so far, mainly the participation in metal ion homeostasis and detoxification as well as protection against oxidative stress[12, 65-66]. Wheat E_c-1 seems to have a potential role in plant development as inferred from its high abundance during embryogenesis[63]. Interestingly, the only regulatory element found so far in the upstream 5' flanking region of the wheat E_c-1 mRNA is an abscisic acid (ABA) responsive element (ARBE) simile[15]. Even more striking than the putative regulation by one of the major plant hormones, involved in abscission, grain filling, desiccation, and embryogenesis[67], is the absence of a metal responsive regulatory element (MRE)[15]. In addition, it is known that 25% of an entire ^{35}S-labelled cysteine pool is found in E_c-1, when wheat grain embryo mRNA is expressed in a cell free expression system[13]. This indicates either a high rate of mRNA translation or a massive accumulation of E_c-1 mRNA and/or a failure of its degradation in the dried embryo, possibly regulated at the transcriptional level. From further studies, using 8K cDNA microarray technology, the E_c-1 transcript abundance was shown to correlate with grain dry weight only[16]. This behaviour is found for only three other proteins, the defense proteins γ-purothionin and remorin-like protein as well as asparagine synthetase 2, a "housekeeping" enzyme. In this study it was further shown that gene expression during wheat grain development can be divided into 10 clusters. The E_c-1 transcript belongs to the 10^{th} cluster, which comprises only 10 of the 2295 differentially expressed genes. The E_c-1 transcript level peaks at 35 days post anthesis, hence in the maturation and desiccation state, and disappears abruptly during the first hour of imbibition[15-16]. Generally, such rapid decline of transcripts is indicative for redundant mRNA remaining from post anthesis. This view is supported by the concomitant decrease of the E_c-1 protein level. Yet, despite the wealth of information the role of E_c-1 still remains illusive.

In the following, we will present the first three-dimensional structure of the N-terminal, 24 amino acid residues comprising, γ-domain of wheat E_c-1 as determined by NMR

spectroscopy. In total, three structures of different γ-E_c-1 forms are presented: the Cd^{II} and Zn^{II} forms of the separately expressed domain as well as the Zn_2γ-E_c-1 form as part of the full-length protein. All forms contain a $M^{II}_2Cys_6$ cluster, which is unprecedented for any MT. EXAFS studies confirm such an arrangement. Moreover, the metal ion binding properties of γ-E_c-1 are probed via pH titration and metal ion reconstitution experiments.

II 3 Material and methods

II 3 1 Chemicals and solutions

$^{113}CdCl_2$ and $^{15}NH_4Cl$ were purchased from Cambridge Isotope Laboratories Inc. (Innerberg, Switzerland), d_{11}-Tris from Euriso-top (Saint-Aubin, France), enzymes used for plasmid construction and protein cleavage from Promega (Catalys AG, Wallisellen, Switzerland), Roche (Rotkreuz, Switzerland), GE Healthcare Europe GmbH (Glattbrugg, Switzerland) or New England Biolabs Inc. (Ipswich, MA, USA), LB Broth (Miller) from Chemie Brunschwig AG (Basel, Switzerland) and Chelex® 100 resin from Bio-Rad (Reinach, Switzerland). All other chemicals were ACS grade or comparable and purchased from Sigma-Aldrich Chemie GmbH (Buchs, Switzerland), Calbiochem (VWR International AG, Lucerne, Switzerland) or Acros organics (Chemie Brunschwig AG, Basel, Switzerland). All solutions were prepared using degassed millipore water. If appropriate, solutions were saturated with nitrogen or argon. Whenever complete absence of oxygen was required, millipore water was degassed by three consecutive freezing thawing cycles under vacuum.

II 3 2 Synthetic peptide

A synthetic γ-E_c-1 peptide (purity > 90%) consisting of the first 25 amino acids of the full-length E_c-1 protein

MGCDD KCGCA VPCPG GTGCR CTSAR

was purchased from Sigma-Genosys (Haverhill, UK) and used for EXAFS, ESI-MS, pH and metal ion titration experiments as well as for the 2D [^{1}H-^{1}H] TOCSY and NOESY NMR spectra of the Cd_2γ-E_c-1 form. All other experiments were conducted with the peptide overexpressed using the pGEX-4T-gEc1 construct.

II 3 3 Plasmid construction

The cDNA sequence encoding for the first 24 amino acids of wheat E_c-1 without the N-terminal translation initiator Met was optimised for *E. coli* codon usage. Two additional Gly

and Ser residues were added to the N-terminus of the protein to ensure optimal thrombin cleavage yielding the sequence

GS GCDD KCGCA VPCPG GTGCR CTSAR.

The resulting construct was cloned into to the pGEX-4T expression vector (GE Healthcare) using the BamH1 and EcoR1 restriction sites and the construct identity (pGEX-T4-gEc1) was subsequently verified by DNA sequencing. The constructed plasmid was transferred into the protease deficient *E. coli* expression strain BL21(DE3).

II 3 4 Protein expression and purification

γ-E_c-1 was overexpressed in form of the glutathione-*S*-transferase-MT fusion protein according to the GST purification manual (GE Healthcare). After induction with 1 mM isopropyl-β-D-thiogalactopyranosid (IPTG) at OD_{600} = 1 cells were harvested after 4 to 7 h at 37 °C and lysed by sonification. The supernatant was loaded on a pre-equilibrated GST-affinity column (GE Healthcare). After washing, the fusion protein was stripped from the column using 10 mM glutathione (GSH) and cleaved with 1 unit thrombin per mg GST-MT fusion protein for 60 h at 25 °C. Final purification of γ-E_c-1 was performed by size exclusion chromatography using a Superdex 30pg column (GE Healthcare) and the molecular identity verified with ESI-MS (**Fig. II 2**). Crucial for GST-MT protein cleavage with thrombin was the demetalation of the fusion protein with 10 mM EDTA during the GST-affinity column wash step. All chromatographic steps were conducted in phosphate buffer saline (PBS - 10 mM Na_2HPO_4, 1.8 mM KH_2PO_4, 140 mM NaCl, 2.7 mM KCl) at pH 7.3. Purified and completely oxidized γ-E_c-1 was dialysed twice against 20 mM Tris/HCl pH 8.0, lyophilized and stored at -80 °C. Average yields are 4 mg of purified protein per L cell culture medium. The full-length E_c-1 protein was prepared as described elsewhere[61].

II 3 5 Apoγ-E_c-1 preparation

Apoγ-E_c-1 was prepared freshly prior to each experiment. Typically 1 to 3 mg of oxidized γ-E_c-1 was incubated with 200 mM DTT in a 100 mM Tris/HCl solution (pH 8.0) for 1 h prior to acidification to pH 2 with 1 M HCl. The sample was applied to a G10 size exclusion column (GE Healthcare) pre-equilibrated with 10 mM HCl and eluted under constant argon flow. The residual Zn^{II}, Cd^{II}, and $Cu^{I/II}$ content of apoγ-E_c-1 was below the detection limit of

flame atomic absorption spectroscopy (F-AAS) (0.001 ppm). Prior to the subsequent metal ion reconstitution step, the solution of apoγ-E_c-1 was argon saturated for 1 h in a N_2-flushed glove box and the protein concentration determined via thiol quantification using the 2,2'-dithio-dipyridine (2-PDS) assay[43].

II 3 6 Preparation of Zn_2γ-E_c-1, Zn_6E_c-1, and Cd_2γ-E_c-1

For all experiments the exact amount of 2 or 6 equivalents of metal ions was titrated to the respective apo-form in a N_2-flushed glove box. Subsequently, the pH was raised to 8.6 using Tris/HCl or d_{11}-Tris/HCl for the NMR samples. Reconstituted samples were dialysed against 20 mM of the respective Tris/HCl solution or 5 mM NH_4Ac for ESI-MS measurements and concentrated by lyophilization.

II 3 7 pH titrations followed by UV spectroscopy

800 µL of the respective reconstituted E_c-1 form (ca. 10 µM each) in 1 mM Tris/HCl 8.6 and 10 mM NaCl were titrated with diluted HCl as described[61]. For the concurrent titration of both domains, γ- and β_E-E_c-1 were mixed in equimolar amounts. Plots of molar absorptivity at 230 nm for the Zn^{II}-forms and at 250 nm for the Cd^{II}-loaded species against pH were fitted in the program Origin 7.0® (OriginLab corporation, MA, USA) using three different functions, considering either one or two common apparent pK_a values for the cysteine residues in presence of the respective metal ions as described[61, 68].

II 3 8 Titration of apoγ-E_c-1 with Cd^{II}

For each titration point 90 µL of 32 µM apoγ-E_c-1 were mixed with the appropriate amount of a 1.25 mM $CdCl_2$ solution in a nitrogen-purged glove box. The pH was raised to approximately 8.6 with 100 mM Tris that was pretreated with Chelex 100 resulting in samples with 20 µM E_c-1, 20 mM Tris/HCl, and 10 mM NaCl. Samples were transferred into cuvettes, sealed, and UV spectra were recorded.

II 3 9 Mass spectrometry

Samples of $Zn_2\gamma$-E_c-1 in 100 mM NH_4Ac (pH 8) were treated with 2 equiv. Zn^{II} or 4 equiv. Cd^{II} and injected directly or with a prior acidification step into a quadropole time-of-flight (TOF) Ultima API spectrometer (Waters, UK). 10 mM NH_4Ac in 50% MeOH (pH 7.5) or 50% acetonitrile with 0.2% formic acid (pH 2-3) were used as a solvent. Scans were accumulated and further processed by the software MassLynx 3.5 (Micromass). Deconvolution of mass spectra was done by applying the maximum entropy algorithm of the MassLynx tool MaxEnt1. Electrospray parameters were capillary 2.8 V, cone 60 V and source temperature 80 °C.

II 3 10 X-ray absorption spectroscopy

In order to determine the average Zn^{II} binding motif K-edge X-ray absorption spectra of $Zn_2\gamma$-E_c-1 were recorded at beamline D2 of the EMBL Outstation Hamburg at DESY, Germany, as described[8]. Data reduction, such as background removal, normalization and extraction of the fine structure, was performed with KEMP[69] assuming a threshold energy of $E_{0,Zn}$=9662 eV. The extracted K-edge EXAFS data were converted to photoelectron wave vector k-space and weighted by k^3. Initial evaluation of the spectra by ABRA[70], which is based on EXCURV[71], included a systematic screening of ~400 potential binding motifs. The subsequent meta-analysis identified structural Zn sites, and thus in the final refinement the total number of ligands was fixed to four. The absence of multiple scattering contributions indicative for the binding of imidazole rings to the Zn^{II} ion limited the refinement to the following parameters for each structural model: namely the atomic distances (R), the Debye-Waller factors ($2\sigma^2$), and a residual shift of the energy origin (EF) were refined, minimizing the Fit Index (Φ). An amplitude reduction factor (AFAC) of 1.0 was used throughout the data analysis.

II 3 11 NMR spectroscopy

$Zn_2{}^{15}N$-γ-E_c-1, $Cd_2{}^{15}N$-γ-E_c-1, $^{113}Cd_2\gamma$-E_c-1 and $Zn_6{}^{15}N$-E_c-1 samples were prepared as described above. The lyophilised proteins were dissolved in 10% D_2O/90% H_2O, 15 mM d_{11}-Tris/HCl pH 6.9 and 50 mM NaCl to a final concentration of 1 mM protein for ^{1}H-NMR and 3 mM for ^{113}Cd-NMR studies. Proton NMR experiments to elucidate the protein backbone structure were recorded at 25 °C on Bruker Avance 700- and 600-MHz spectrometers. ^{113}Cd-

NMR experiments to investigate the binding sites of the Cd^{II} ions were performed on a Bruker DRX 500-MHz spectrometer. Assignment of resonances in $Cd_2\gamma$-E_c-1 and Zn_6E_c-1 was performed using 3D ^{15}N resolved TOCSY[72-73] and NOESY[74-75] spectra recorded with 80 ms and 120 ms mixing times, respectively. Distance restraints were derived from the 120 ms mixing time 3D ^{15}N resolved NOESY and 2D NOESY experiments. Resonance assignments for the $Zn_2\gamma$-E_c-1 domain were conducted using 2D TOCSY and 2D NOESY spectra with 80 and 120 ms mixing times, respectively. Additionally, a 120 ms mixing time 3D ^{15}N resolved NOESY spectra as well as the information from the $Cd_2\gamma$-E_c-1 and Zn_6E_c-1 form were used to validate the assignment. Distance restraints were again derived from the 3D ^{15}N resolved NOESY and 2D NOESY experiments. In all cases zero-quantum interference in the spectra was suppressed using an appropriate filter[76-77]. $^{15}N,^{1}H$ correlation maps were derived from a gradient-enhanced [$^{15}N,^{1}H$]-HSQC experiment using the Rance-Palmer trick for sensitivity enhancement[78-79]. 1D-^{113}Cd-NMR**,** 2D-[$^{113}Cd,^{1}H$]-HSQC spectra and 2D-[$^{113}Cd,^{113}Cd$]-COSY experiments were recorded to investigate the metal cluster[35]. $^{3}J[H_\beta,Cd]$ couplings derived from a 2D [$^{113}Cd,^{1}H$]-HSQC spectrum allowed to establish the individual Cd-Cys connectivities.

Sequence-specific resonance assignment was performed using the methodology developed by Wüthrich[38]. Assignments were achieved based on information from 2D TOCSY, NOESY, 2D [$^{15}N,^{1}H$]-HSQC, 3D ^{15}N-resolved NOESY, and 3D ^{15}N-resolved TOCSY experiments. The 2D and 3D spectra were evaluated with the programs XEASY[80] and CARA[81], respectively. As a first step, the spin systems were identified in the 2D TOCSY or 3D ^{15}N-resolved TOCSY experiments. Subsequently, spin systems were linked based on NOE information derived from 2D NOESY and 3D ^{15}N- resolved NOESY. Once longer stretches had been identified, they were mapped onto the sequence of γ-E_c-1.

For the structure calculations NOE peaks were picked and integrated using the program XEASY for 2D and CARA for 3D experiments employing identical lower integration thresholds. Torsion angle dynamics[82] were performed with the *noeassign*[42] algorithm of the program CYANA 2.1[83]. Structure calculations were started from 100 conformers with randomized torsion angle values. The 20 conformers with the lowest final target function value were further subjected to restrained energy minimization in explicit solvent against the AMBER force field[84] using the program OPALp[85-86]. The resulting structures were deposited in the Protein Data Bank under the accession codes 2I61 and 2I62. Structure figures were generated with the program MOLMOL[87].

II 4 Results and discussion

II 4 1 Initial quantification of metal ion binding

Reconstituted forms of γ-E_c-1 with Zn^{II} and Cd^{II} were analysed for their metal ion content using flame-AAS and the 2-PDS assay and yielded M^{II} to thiol group ratios of 1:3 indicating the binding of two divalent metal ions per protein. The proposed metal stoichiometry was confirmed with mass spectrometry. For this two equivalents of Zn^{II} or four equivalents of Cd^{II} ions were added to a solution of Zn_2γ-E_c-1, and the resulting mixture was analyzed with ESI-MS either at acidic or neutral pH. The spectrum at acidic pH shows the apoγ-E_c-1 species as expected, while at neutral pH exclusively Zn_2γ-E_c-1 or Cd_2γ-E_c-1 are observed despite the addition of an excess of the respective metal ion (**Fig. II 2**).

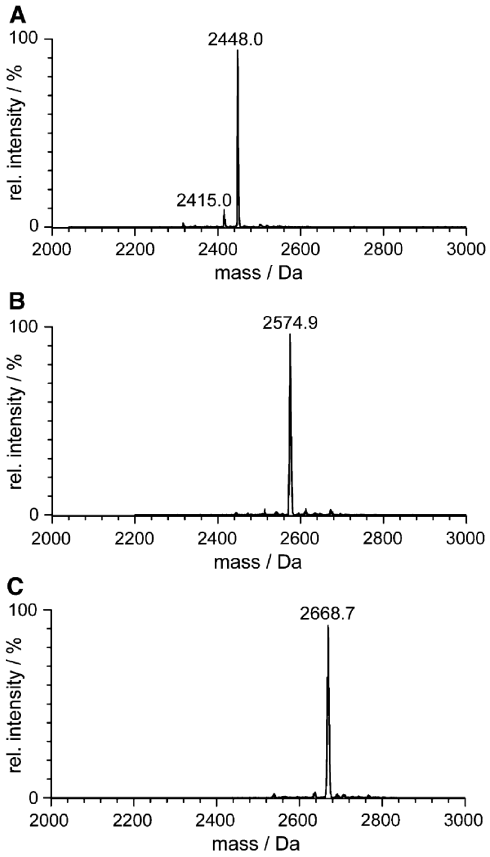

Figure II 2 Deconvoluted ESI-MS spectra of ***A)*** γ-E_c-1 in form of the metal-depleted apo-form at pH 2 (calc. mass 2448.0 Da), ***B)*** Zn_2γ-E_c-1 (calc. 2574.7 Da) or ***C)*** Cd_2γ-E_c-1 (calc. 2668.8 Da), both at pH 7.5.

To corroborate this result, apoγ-E_c-1 was titrated with increments of Cd^{II} and UV-spectra were recorded (**Fig. II 3**). They show the formation of the typical ligand-to-metal charge transfer (LMCT) bands at 245-250 nm indicative for Cd^{II} coordination to thiolate groups.

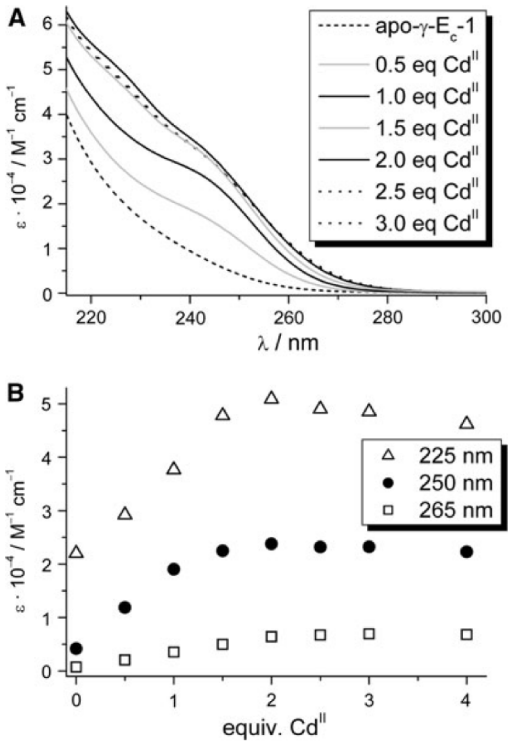

Figure II 3 ***A)*** UV spectra of the stepwise reconstitution of apoγ-E_c-1 with Cd^{II} ions showing the evolution of the S→Cd^{II} LMCT bands around 250 nm. ***B)*** Plots of molar absorptivity at 225 nm, 250 nm, and 265 nm against the number of equiv. of Cd^{II} ions added all reaching the maximum value after addition of two equiv.

These bands increase in absorptivity up to the addition of two equivalents Cd^{II} and remain constant thereafter. It was already shown that the full-length E_c-1 protein is able to coordinate six divalent metal ions and that four of them can be accommodated in the C-terminal β_E-domain[9, 61]. That the remaining two metal ions are bound within the N-terminal γ-domain was evidenced with ESI-MS measurements on a proteolytically digested Zn_6E_c-1 sample revealing the presence of a Zn_2γ-E_c-1 species[8]. In the same publication, a [^{113}Cd,^{113}Cd]-COSY spectrum of $^{113}Cd_6$Ec-1 shows cross peaks between two ^{113}Cd signals that originate from metal ions coordinated within the γ-domain and let to the proposal of a Cd_2Cys_6 cluster.

The results with the separate γ-E_c-1 peptide presented here clearly demonstrate that the binding ability for two divalent metal ions is not restricted to the domain within the full-length protein. This validates our experimental approach to use the separate γ-E_c-1 sequence for the in-depth spectroscopic characterisation of the γ-domain of wheat E_c-1.

II 4 2 pH titrations of Zn_2γ-E_c-1 and Cd_2γ-E_c-1

pH titrations followed by UV spectroscopy were performed to investigate the pH dependent

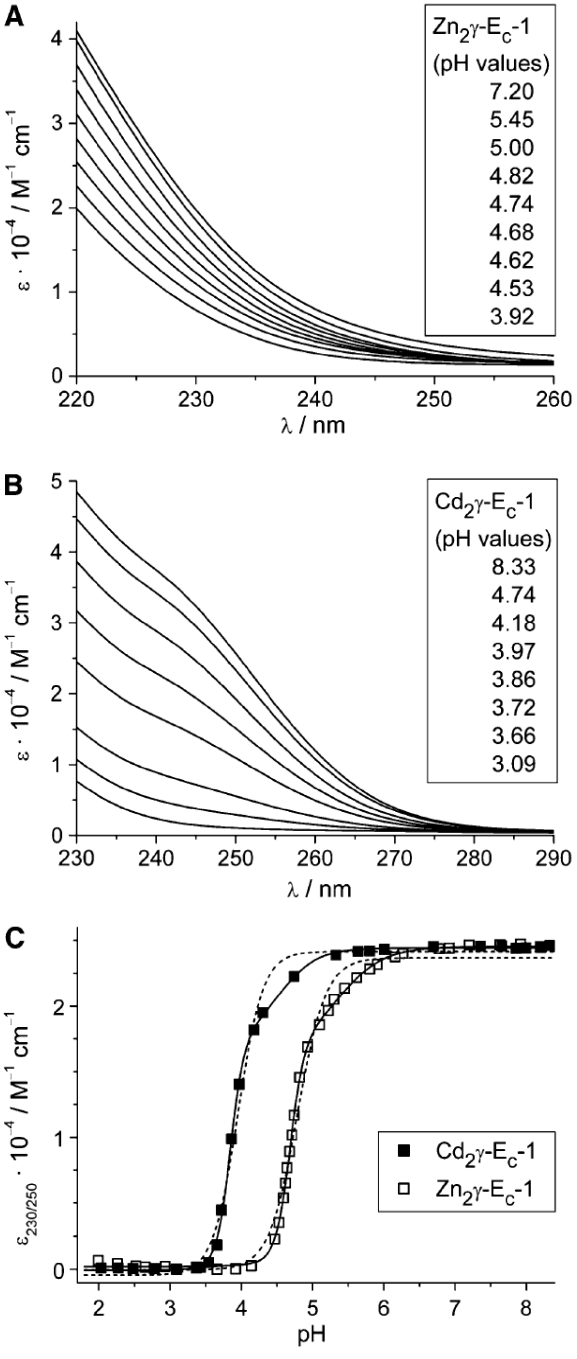

Figure II 4 Representative UV spectra of the titration of ***A)*** Zn_2- and ***B)*** $Cd_2\gamma$-E_c-1 with increasing amounts of HCl. ***C)*** Plots of molar absorptivity at 230 nm for the Zn^{II}- and at 250 nm for the Cd^{II}-form versus pH. To allow better comparability, the values obtained for the apo-forms in both titrations were shifted to zero and in addition the plot of the Zn^{II}-form was normalized to the values obtained for the Cd^{II}-form. Curve fits were performed with equations considering one (dashed lines) or two apparent pK_a values (solid lines) as described in the Suppl. Mat.

metal ion release. Though not tantamount, the obtained apparent pK_a values of the Cys residues in presence of the respective metal ion are a good indication for the relative binding affinity of the metal ion to the MT. A number of apparent pK_a values for different Zn^{II} and Cd^{II} MTs were recently reviewed[12]. In the context of the study presented here, the pH stability of γ-E_c-1 in comparison to the full-length protein and the β_E-domain is of special interest. The UV spectra of the pH titration of Zn_2- and $Cd_2\gamma$-E_c-1 are depicted in **Figure II 4** as well as the plots of molar absorptivity at 230 nm (Zn^{II}-form) and 250 nm (Cd^{II}-form) against the respective pH values. Fitting of the data was performed as described[69, 70] and the results are presented in more detail in the **Supplementary Material**. As the pK_a values obtained for both $Zn_2\gamma$-E_c-1 and $Cd_2\gamma$-E_c-1 were significantly higher than determined for the respective β_E- and full-length forms (**Fig. II 5**), also a titration of an equimolar mixture of both domains was performed. The resulting pK_a values for the mixed domains are settled in-between the values obtained for the respective γ- and β_E-domains, but are still significantly higher than the values for the full-length E_c-1 forms (**Fig. II 5**).

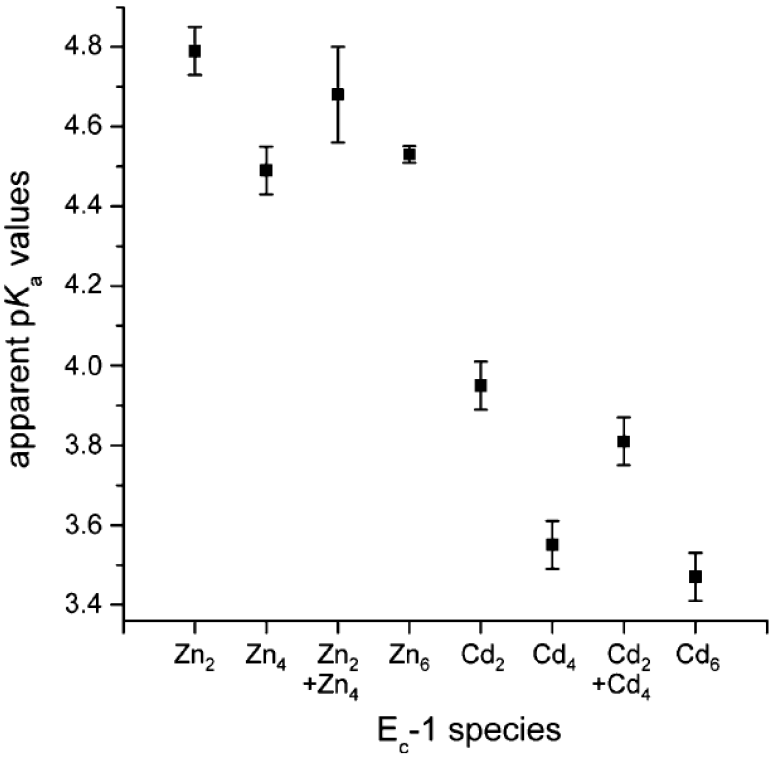

Figure II 5 Apparent pK_a values of the Cys residues in γ-, β_E- and full-length wheat E_c-1 in presence of Zn^{II} or Cd^{II} ions. The error bars show the 3σ error range. From left to right: 4.79(6), 4.49(6), 4.68(12), 4.530(21), 3.95(6), 3.55(6), 3.81(6), and 3.47(6).

Hence it appears that not the mere presence but rather the close proximity of the respective other domain leads to the observed increased pH stability of the full-length protein. While basically possible it seems unlikely that the nature of the five amino acids SGAAA between the γ- and the β_E-domain, which were removed in the separately expressed domains, has a major influence as the residues are neither charged nor especially bulky or hydrophobic. So far, also no indications for any sort of interactions between the two domains were observed judging from the lack of corresponding NOE signals in the NMR experiments. Furthermore, ^{15}N dynamics data, in particular values of the ^{15}N-(^1H)-NOE, indicate that the linker comprising residues 26 to 30 is fully flexible[9]. One possible explanation for the low pK_a values of the full-length protein could be that the spatial proximity of the respective other domain leads to a reduced solvent accessibility and hence to a deferred metal ion displacement by protons. Alternatively, formation of intermediate species in the full-length protein at decreasing pH values could occur slowing down the metal ion release process, i.e.

migration of metal ions between the two domains or even transient generation of a new cluster arrangement. However, such species would not be detected in the structural investigation presented here, as the NMR experiments were performed at pH 6.9, while metal ion release only starts below 6.5 for the Zn^{II}- and 5.5 for the Cd^{II}-forms. Interesting to note is that the stabilizing effect of the respective other domain is obviously much more pronounced for the γ-domain, while the β_E-domain shows within the error limits the same apparent pK_a values as the full-length protein. Shifts in pK_a values present subtle probes into thermodynamic protein stability, and our data indicate that the γ-domain is intrinsically less stable than the β_E-domain when in isolation, although both are structured and capable of metal binding.

An additional surprising result was obtained, when evaluating the pH titration data for Zn_2γ-E_c-1 and Cd_2γ-E_c-1 more closely. The absorptivity values obtained from the curve fit with the equation considering two apparent pK_a values reveal a decrease by approximately one third for the first protonation step, characterized by pK_{a2}, i.e. Δε 2900 ± 400 M^{-1} cm^{-1} for Zn_2γ-E_c-1 and Δε 7200 ± 1700 M^{-1} cm^{-1} for Cd_2γ-E_c-1, and a decrease by two thirds for the second step, characterized by pK_{a1}, i.e. Δε 5700 ± 400 M^{-1} cm^{-1} for Zn_2γ-E_c-1 and Δε 17300 ± 1700 M^{-1} cm^{-1} for Cd_2γ-E_c-1 (see **Supplementary Material**). Disregarding the contribution of bridging thiolate ligands to the LMCT bands, which is considerably lower than the contribution of terminal thiolate ligands, the absorptivity decreases suggest the loss of two terminal metal-thiolate bonds in the first step and of four metal-thiolate bonds in the second. This suggests that in the first step one metal ion is released and hence the contribution of two terminal and two bridging metal-thiolate bonds is lost, while in the second step the second metal ion is released and hence the contribution of the residual four metal-thiolate bonds disappears. As a result, the two metal ions in γ-E_c-1 seem to be released at pH values approximately 0.6-0.7 units apart and this might also be an indication that γ-E_c-1 contains two metal ion binding sites with different affinities.

II 4 3 Extended X-ray absorption fine structure (EXAFS) spectroscopy of Zn_2γ-E_c-1

EXAFS spectra were recorded to analyse the coordination environment of the Zn^{II} ions in Zn_2γ-E_c-1. The results reveal the presence of four sulfur ligands and no contribution of lighter ligands with N- or O-donor atoms within the error limits. Zn-S distances are with 2.332(3) Å in the normal range for Zn^{II} coordination by thiol ligands (**Fig. II 6, Table II 1**).

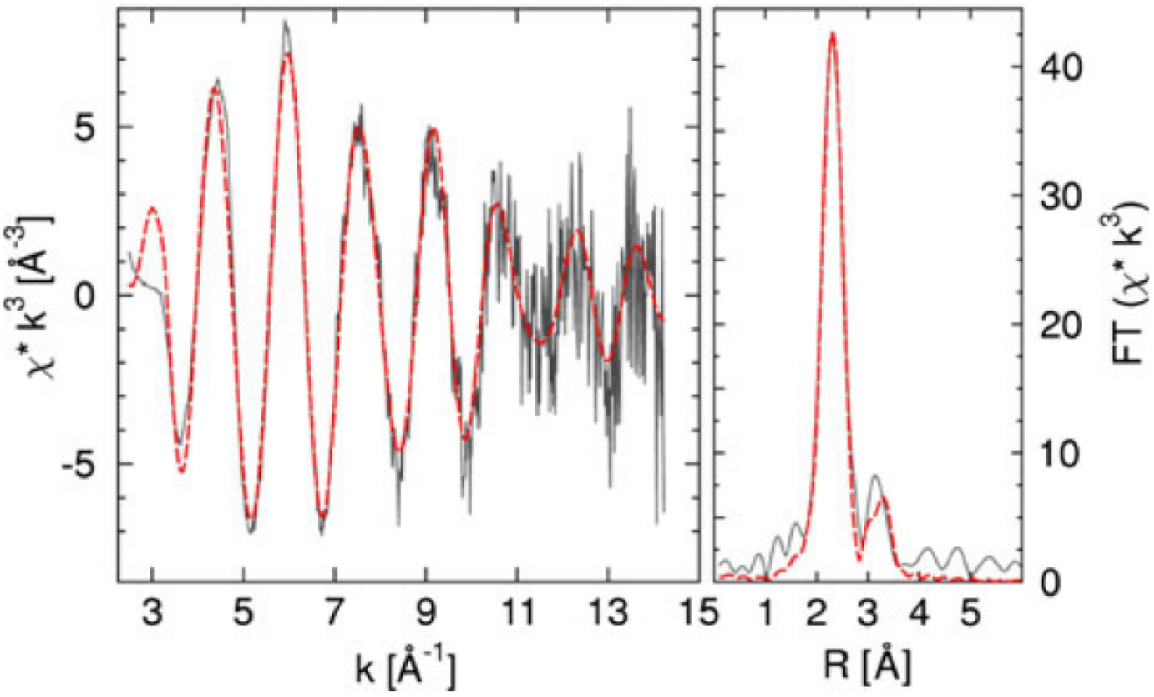

Figure II 6 EXAFS (left) and corresponding Fourier transform (right) of $Zn_2\gamma$-E_c-1. The EXAFS is dominated by a single frequency, originating from sulfur backscattering. In the refinement no other first shell contribution could be identified. In line with this result the Fourier transform is dominated by a single peak at 2.3 Å. The additional peak above 3 Å is refined as metal-metal contribution, indicative of bridging sulfur ligands. The corresponding parameters are given in **Table II 1**.

Table 1 EXAFS refinement parameters for $Zn_2\gamma$-E_c-1

N	*M ··· L*	*R (Å)*	*2σ² (Å²)*	*EF (eV)*	*Φ*
$Zn_2\gamma$-E_c-1		ΔE= 13 eV – 770 eV		$E_{0,Zn}$= 9662 eV	
4	Zn ··· S	2.332(3)	0.0134(5)	-7.6(5)	0.2141
0.5(3)	Zn ··· Zn	3.163(6)	0.006(3)		

Best models with average numbers (N) of ligand atoms (L), their distance to the metal ion (R), the respective Debye-Waller factor ($2\sigma^2$), the Fermi energy for all shells (EF), and the Fit Index (Φ), indicating the quality of the fit are shown. The total error is estimated to 0.01 Å or smaller for first shell distance and 0.05 to 0.1 Å for the metal-metal contribution. In parentheses the numerical error margins are given on the 2σ level.

Assuming the presence of a Zn-Zn interaction with a distance of 3.163(6) Å improves the Fit Index significantly from 0.2988 to 0.2141. However, the error range for the corresponding average number of ligands is relatively high. These findings together with the results from concentration and ESI-MS measurements presented above strongly suggests the formation of a Zn_2Cys_6 metal-thiolate cluster with four terminal and two bridging thiolate groups. Such a cluster is in accordance with the Cd_2Cys_6 cluster proposed to be formed in $^{113}Cd_6E_c$-1 based on the [^{113}Cd,^{113}Cd]-COSY spectrum mentioned above[8].

II 4 4 NMR solution structures of the separate $Zn_2\gamma$-E_c-1 and $Cd_2\gamma$-E_c-1 peptides

Except for the first two amino acids Gly and Ser, which were engineered to improve proteolytic cleavage of the GST fusion protein by thrombin all residues could be identified

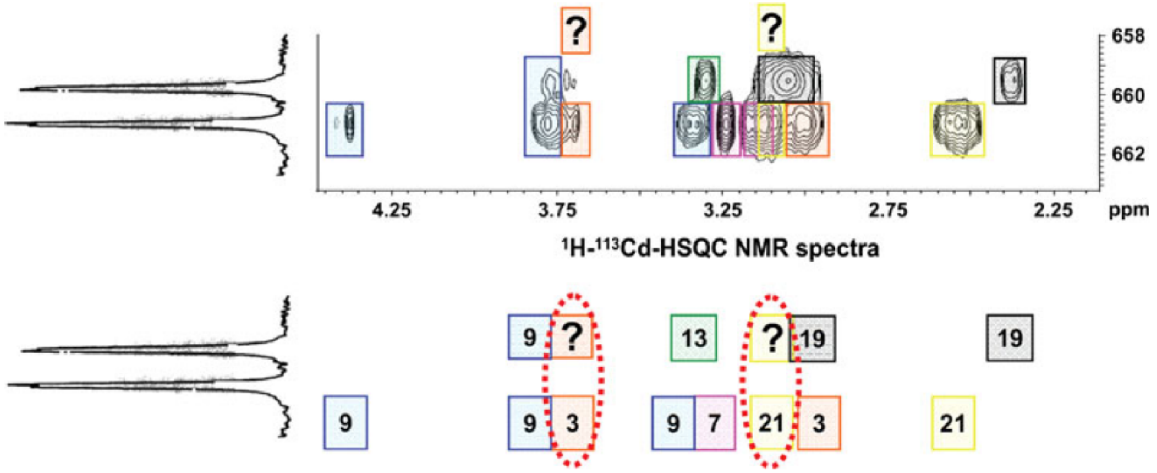

Figure II 7 The 1D ^{113}Cd NMR spectrum of $Cd_2\gamma$-E_c-1 shows two doublets representing the two Cd^{II} ions. The 2D ^{113}Cd-^{1}H-HSQC NMR spectrum allows two possible solutions for the bridging Cys residues: Cys-9/3 and Cys-9/21. The assignment of cross peaks to Cys residues is schematically depicted in the lower part.

with 3D ^{15}N-resolved NOESY and TOCSY NMR experiments in case of the Cd^{II} form or with 3D ^{15}N-resolved NOESY, 2D TOCSY and [^{15}N,^{1}H]-HSQC experiments for the Zn^{II} form. Experiments with the NMR active ^{113}Cd nucleus were performed to probe the metal ion

coordination sphere. [^{113}Cd,^{1}H]-HSQC spectra allow observing cross peaks based on ^{3}J couplings between the H_{β} protons of the Cys residues and the respective coordinated Cd^{II} ions. In theory, each of the 12 H_{β} protons of the six Cys residues present in the peptide should display a ^{3}J coupling to one $^{113}Cd^{II}$ ion, or in the case of bridging thiolate ligands, to two Cd^{II} ions. As shown in **Figure II 7** indeed the majority of Cys residues correlate to metal ions, however, not two as expected but rather three possible bridging Cys residues were identified.
Despite differences in size and electronegativity Cd^{II}- and Zn^{II}-forms of MTs have been interchangeably used for structural studies[30, 35, 88]. In case of the γ-E_c-1 domain such an assumption is justified by the reasonable agreement of proton chemical shifts in the two forms (**Fig. II 8**).

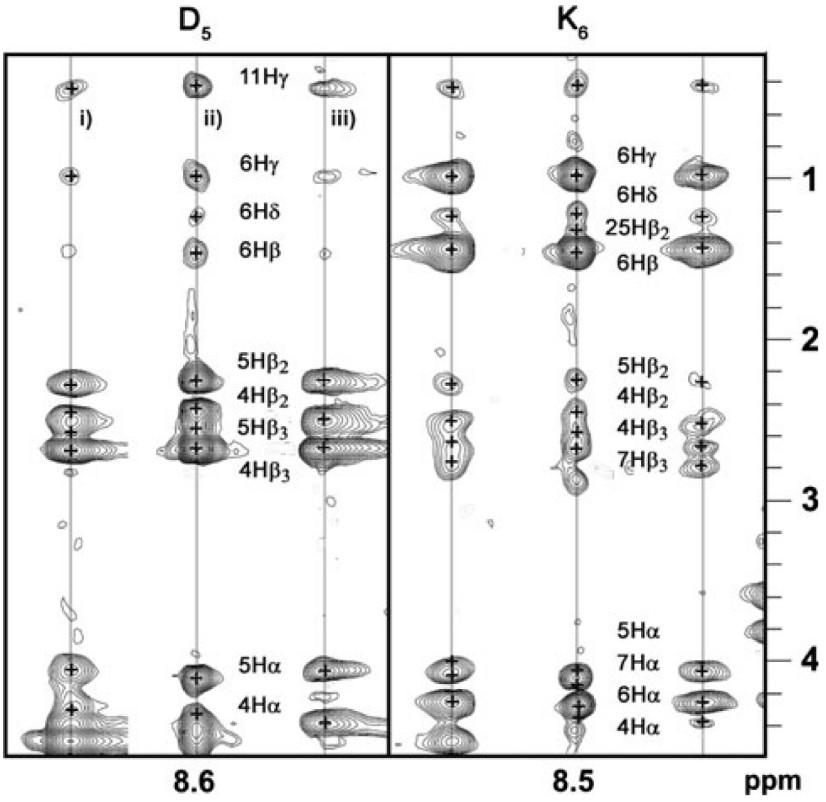

Figure II 8 Comparison of the 3D ^{15}N-^{1}H-^{1}H NOESY NMR slices of Asp-5 and Lys-6 depicted for the separate Zn_2γ-E_c-1 (i) and Cd_2γ-E_c-1 (ii) peptides as well as for the Zn_2γ-E_c-1 domain (iii) within the full-length protein. Assigned NOE cross peaks are labelled. The high degree of NOE pattern homology is apparent.

Chemical shift assignment was based on the sequence-specific sequential resonance assignment procedure developed by Wüthrich and coworkers[38]. Overall, completeness of proton assignment was 99%. No long-range NOEs reflecting contacts of residues from the C- and N-terminal region were observed in the NOESY spectra. Pro-12 (in contrast to Pro-14) was shown to be connected via a cis peptide bond to the previous residue in both metal isoforms (**Supplementary Fig. II 1**), as deduced from comparably strong NOEs of the sequential alpha protons. The comparison of backbone amide ^{1}H and ^{15}N chemical shifts for residues of the γ-domain indicates that differences as large as 0.4 or 1.1 ppm are observed between the Zn- and Cd-species, respectively (**Supplementary Fig. II 2**). The largest differences are not limited to residues that are involved in metal coordination, but also include some of the residues in the small loop regions. A comparison of the amide proton and nitrogen chemical shifts of $Zn_2\gamma$-E_c-1 with the values previously determined on the full-length Zn_6E_c-1 protein reveals that chemical shift differences are negligible and limited to the terminal residues (**Supplementary Fig. II 2**). The latter are expected to be different due to the slightly N-terminally modified sequence (GlySer instead of Met) or due to the additional presence of the C-terminal β_E-domain in the full-length species. As mentioned above, a somewhat surprising result of the analysis is that while the analysis of the pK_a values indicated differences between corresponding segments in the isolated γ-domain compared to the full-length protein no such differences could be detected in the backbone amide chemical shifts. We speculate that there may be contacts between the two domains that, however, are very transient (and possibly also unspecific) in nature.

Initial structures calculated without addition of explicit metal-Cys(Sγ) restraints (**Supplementary Fig. II 3**) converge for the amino acid residues Gly-2 to Gly-18. However the positions of the C-terminal residues and of the thiol groups of the Cys residues deviate substantially. When upper distance restraints were added that enforced tetrahedral geometry and metal sulphur distances derived from EXAFS experiments also the calculations for the C-terminal part of the structure converged. While Cys-9 (numbering according to amino acid sequence given in **Fig. II 1**) could be unambiguously identified as a bridging Cys residue based on the [^{113}Cd,^{1}H]-HSQC experiment, the nature of the second bridging Cys residue could not be experimentally established. Accordingly, independent structure calculations were started assuming the bridging residues to be i) Cys-9 and 21, ii) Cys-9 and 3 and iii) Cys-9 and 13 with all other Cys residues coordinating in terminal fashion. The calculation using

Cys-9/13 as bridging residues resulted in no low-energy conformer and was therefore excluded from further analysis. The resulting structures containing the metal cluster arrangements Cys-9/21 and Cys-9/3 are representatively shown for $Zn_2\gamma$-E_c-1 in **Figure II 9**, and the statistics from the corresponding structure calculations are summarized in **Table II 2**.

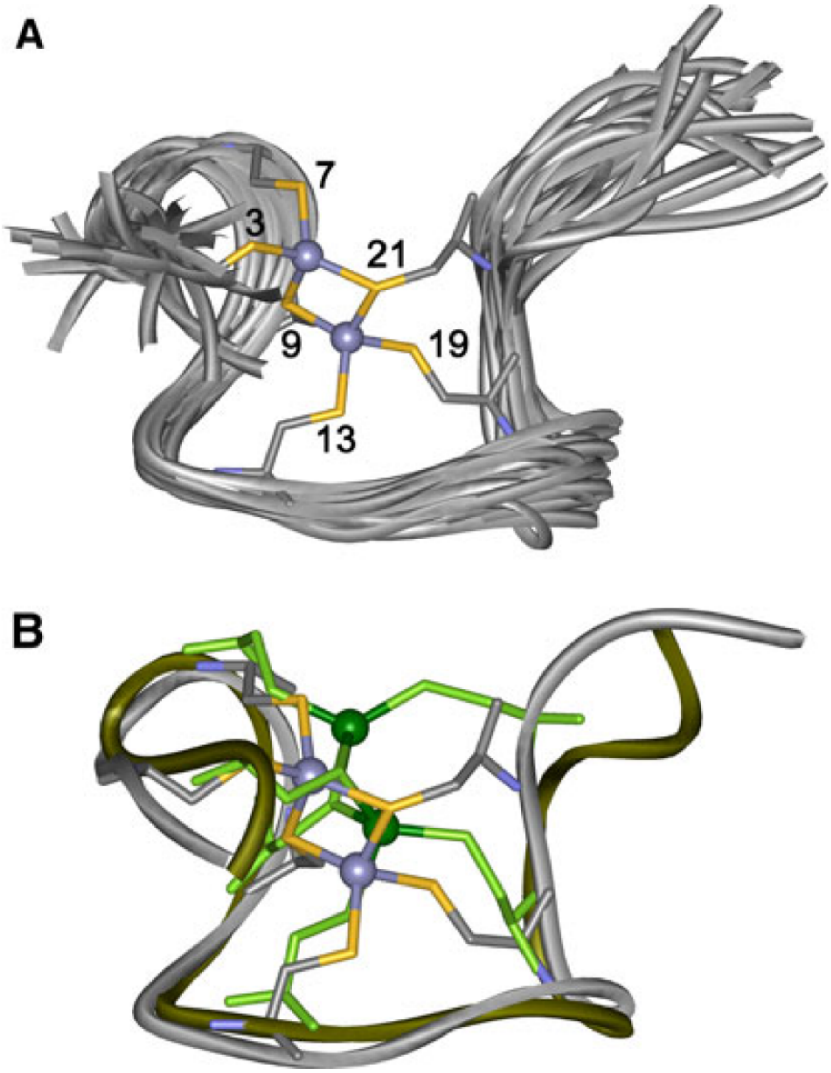

Figure II 9 ***A)*** Structure bundle for $Zn_2\gamma$-E_c-1 showing the metal cluster arrangement Cys-9/21. The backbones are shown in gray, the Cys residues of one representative structure in stick mode and the two corresponding Zn^{II} ions as light blue spheres. Cys residues are numbered according to their position in the amino acid sequence given in Fig. 1. ***B)*** Backbone overlay of two representative structures of $Zn_2\gamma$-E_c-1 with Cys-9/21 connectivity as in (A) and with Cys-9/3 arrangement (olive backbone, Cys residues as green sticks, Zn^{II} ions as dark green spheres).

Similar to previously determined structures of metallothioneins the γ-domain of E_c-1 is devoid of regular secondary structure. Superposition of backbone atoms result in RMSD values of 0.62 to 0.8 Å for backbone atoms of residues 2 to 22, and 1.3 to 1.5 for all heavy atoms, and the values are very similar for the Cd^{II}- or Zn^{II}-loaded isoforms (see **Table II 2**). The overall fold resembles a hook, in which the stem part is formed by the segments comprising Cys7-9 and Cys19-21, and the loop by the coordination of Cys-13 to the metal. Two loops bridge the latter residue to the next metal-anchoring residues Cys-9 and Cys-19. Coordination of Cys-3 brings the *N*-terminal segment into proximity. No significant differences in conformation that were unambiguously supported by the NOEs were observed between the Cd^{II}- and Zn^{II}-loaded peptides despite the fact that in part substantial chemical shift differences are observed (*vide supra*). A superposition of the backbone atoms of conformers, in which either Cys-3 or Cys-21 were constrained to be the bridging ligands, revealed that only small structural adaptations were necessary to transform one form into the other. Considering that only upper-distance limits were derived from the NOEs and taking the inherent dynamics of the system as well as the low proton density in metallothioneins, that are largely devoid of regular secondary structure or tertiary contacts, into account we feel that no sound statements on structural differences of the Zn^{II}- or Cd^{II}-loaded species can be made on the basis of the present data. Moreover, the lack of explicit ^{113}Cd-Cys(Hβ) cross peaks in the [^{113}Cd,^{1}H]-HSQC experiment for these residues, and the fact that the target functions of the calculated conformers are very similar precludes unambiguous determination of the nature of the second bridging Cys residue. Whether this is due to the fact that the coordination mode in the peptide changes dynamically or whether the NMR data simply are insufficient to describe a unique coordination mode remains unclear presently.

A $M^{II}_2Cys_6$ cluster as identified in the γ-domain is unprecedented for MTs so far, but a very similar Zn_2Cys_6 cluster was previously observed in the transcription factor GAL4 from *Saccheromyces cerevisiae*[88]. Also here the metal-Cys connectivities were probed by replacement of Zn^{II} ions by $^{113}Cd^{II}$. Since the two ^{113}Cd resonances at 669 and 707 ppm are well separated it was possible to identify the bridging Cys residues using selectively decoupled [^{113}Cd,^{1}H]-HSQC spectra. However, such an experiment is not feasible in the case of Cd_2γ-E_c-1 owing to the very small chemical shift difference of only 2 ppm. Nevertheless, two further peculiarities in the NMR spectra corroborate the concomitant presence of two different, probably interchanging cluster arrangements. Firstly, in $^{113}Cd_2$γE_c-1 TOCSY spectra

cross peaks due to the geminal $H\beta_2$- $H\beta_3$ correlation for the putative bridging Cys residues 3 and 21 are significantly broadened, and the corresponding correlation for Cys 9 is broadened beyond detection, indicating the presence of exchange processes. Secondly, in contrast to spectra recorded on the full-length protein[8], no mutual coupling was observed in the [^{113}Cd,^{113}Cd]-COSY spectrum of $^{113}Cd_2\gamma$-E_c-1, which might again be explained by intermediate exchange processes occurring in the isolated domain.

II 4 5 NMR solution structure of $Zn_2\gamma$-E_c-1 as part of the full-length Zn_6E_c-1 protein and comparison to the separate $Zn_2\gamma$-E_c-1 peptide

Spectroscopic and spectrometric studies[5, 8-9, 30] have revealed that wheat Zn_6E_c-1 is a two-domain protein. The larger *C*-terminal domain, termed extended-β or β_E, consists of 51 amino acids and embeds a mononuclear $ZnCys_2His_2$ site as well as a trinuclear Zn_3Cys_9 metal-thiolate cluster with similarity to the β-domain of the vertebrate MTs. As described above the smaller 24 amino acids long N-terminal domain, γ-E_c-1, folds around a Zn_2Cys_6 cluster. Chemical shift mapping accompanied by ^{15}N relaxation experiments was used to confirm identical folds of both the β_E-domain in form of the separately expressed peptide as well as being part of the full-length Zn_6E_c-1 protein. To confirm that this is also true for the γ-domain, chemical shift assignment and identification of close contacts from NOESY spectra was performed for both the isolated peptides (Cd^{II}- and Zn^{II}-isoforms) of the γ-domain and for the corresponding part in the full-length protein. Similar chemical shifts and NOESY crosspeaks (**Fig. II 8**) indicate analogous peptide folding. A comparison of the solution structure bundle calculated for the embedded and for the independent γ-domain (Zn^{II}-isoform, Cys-9/21 bridging) is displayed in **Table II 2**. Indeed, only minor differences between the two conformations are observed.

Table 2 Statistics of structure calculations:

	Cd3*	**Cd21***	**Zn3***	**Zn21***	**Zn3(full)***	**Zn21(full)***
NMR distance restraints						

Total NOE	374	372	462	463	307	310
Short range: |i−j|≤1	322	321	396	395	268	268
Medium range: 1>|i−j|>5	61	58	69	70	47	44
Long range: |i−j|≥5	15	13	20	20	13	15
Maximal distance restraint violation (Å)	0.11	0.11	0.11	0.19	0.16	0.44
AMBER energies (kcal/mol)						
Total (mean±SD)	−679 ± 76	−711 ± 43	−697 ± 70	−693 ± 75	−679 ± 52	−641 ± 67
van der Waals	−14 ± 4	−7 ± 5	−12 ± 5	−12 ± 6	−9 ± 5	−8 ± 7
RMSDs from idealized geometry						
Bond lengths (Å)	0.0142 ± 0.0002	0.0138 ± 0.0002	0.0136 ± 0.0002	0.0142 ± 0.000**2**	0.0138 ± 0.0002	0.0138 ± 0.0002
Bond angles (°)	2.15 ± 0.06	2.03 ± 0.06	1.94 ± 0.06	2.42 ± 0.06	2.11 ± 0.06	2.11 ± 0.06
Ramachandran plot statistics (%)						
Residues in most favored regions	80.9	70.9	74.4	69.4	65.6	63.5
Residues in additionally allowed regions	18.2	28.5	24.7	28.5	32.4	32.4
Residues in generously allowed regions	0.9	0.6	0.9	1.8	2.1	3.2
Residues in disallowed regions	0	0	0	0.3	0	0.9
RMSDs from the mean coordinates (Å)						

N, Cα, and C′ of residues 2-22	0.70±0.14	0.69 ± 0.33	1.06 ± 0.34	0.97 ± 0.25	1.29 ± 0.44	1.50 ± 0.45
Heavy atoms of residues 2-22	1.37±0.26	1.45 ± 0.37	1.76 ± 0.35	1.54 ± 0.27	1.97 ± 0.43	2.26 ± 0.46

* The number describes the residue that presents the second bridging Cys moiety (in addition to Cys-9; see text). Numbering is performed with respect to the sequence of the full-length protein as given in **Fig. II 1**.

II 4 6 Comparison of $Zn_2\gamma$-E_c-1 with the Zn_2Cys_6 cluster in GAL4

As mentioned above, Zn_2Cys_6 clusters were so far only structurally described in yeast transcription factors[89-91]**.** Amino acid sequence alignments of the latter reveal a completely conserved Cys distribution pattern and a high conservation of Lys residues, which play a major role for the interaction of these proteins with DNA (**Fig. II 10**). In contrast, the Cys distribution pattern of the γ-E_c-1 domain differs significantly from that of the transcription factors, and only three positively charged residues, one Lys and two Arg, are present. In addition, while the fold of the protein backbone in the yeast transcription factors can be described as a loop, the backbone of γ-E_c-1 is S-shaped or resembles a hook (**Fig. II 9** and **10**). Taken together, despite the similarity of the metal-thiolate clusters, recognition of DNA by γ-E_c-1 in the same fashion as observed for the yeast transcription factors seems unlikely.

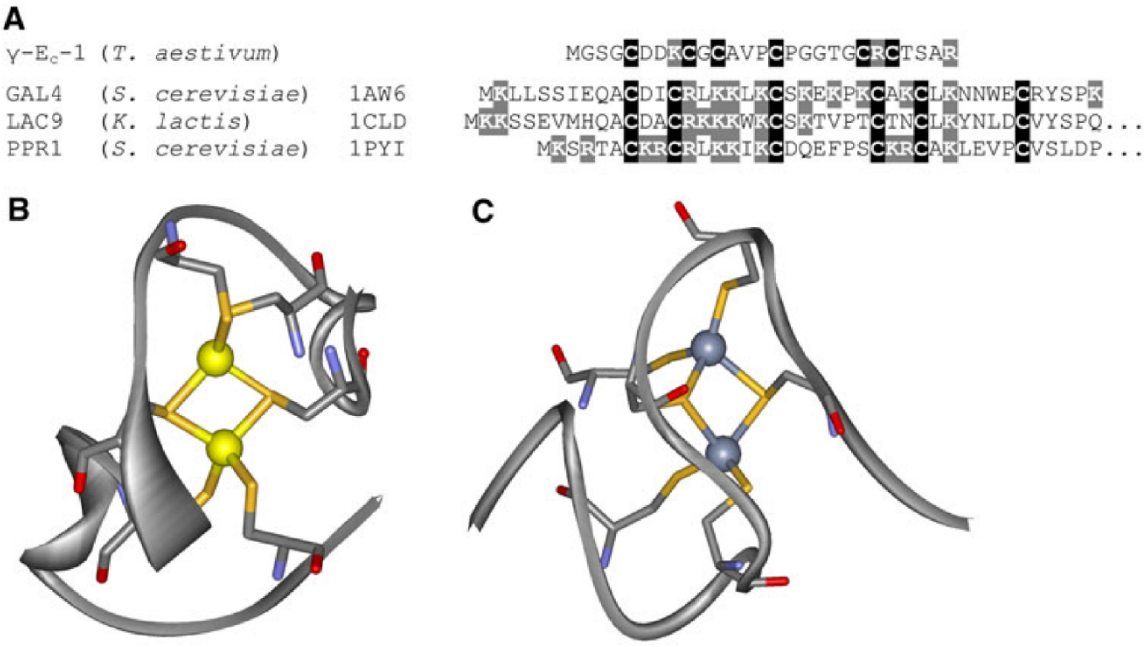

Figure II 10 ***A)*** Amino acid sequence of γ-E_c-1 and alignment of the sequences from the three yeast transcription factors GAL4, LAC9, and PPR1 with the species name and PDB accession code given. Cys residues are highlighted with a black, Lys and Arg residues with a grey background. NMR solution structure of ***B)*** Cd_2GAL4[89] and ***C)*** Zn_2γ-E_c-1 with the metal ions drawn as yellow or blue-grey spheres and the Cys residues presented in stick mode. The *N*-terminus is positioned to the (upper) right, respectively.

II 5 Conclusions

Complementing our investigation of the $Zn_4\beta_E$-E_c-1 domain including the determination of its solution structure by NMR[8-9] we complete now the second part of the puzzle by presenting a study of the properties and the solution structure of the γ-domain of wheat E_c-1. ESI-MS experiments in conjunction with F-AAS measurements and metal ion titrations followed with UV spectroscopy clearly confirm the ability of the *N*-terminal E_c-1 fragment to coordinate two Zn^{II} or Cd^{II} ions even in the absence of the β_E-domain. Tetrahedral tetrathiolate coordination of the bound Zn^{II} ions is established by EXAFS measurements in addition to the presence of a short Zn-Zn distance of 3.16 Å. pH titrations of $Zn_2\gamma$-E_c-1 and $Cd_2\gamma$-E_c-1 reveal higher apparent pK_a values of the Cys residues than previously determined for the β_E-domain and full-length E_c-1. This earlier protonation of thiolate ligands is paralleled by an increased peptide backbone flexibility compared to the β_E-domain[9]. A pH titration of an equimolar mixture of the γ- and the β_E-domain yields intermediate pK_a values, which however differ from the values obtained with the full-length protein. This might indicate a yet unidentified interaction between the two domains in the full-length protein that increases the pH stability especially of the $M^{II}_2Cys_6$ cluster of the γ-domain. Owing to the low percentage or even lack of regular secondary structure in MTs the metal clusters critically contribute to the overall protein fold. Hence only when the metal-coordinating residues have been identified the structure can be determined correctly. In case of the γ-domain [^{113}Cd,^{1}H]-HSQC spectra indicated three possible metal ion-to-Cys connectivities, one of which could be eliminated during the structure calculation. Based on the ^{113}Cd NMR and ^{1}H NMR studies of the separate $Zn_2\gamma$-E_c-1 and $Cd_2\gamma$-E_c-1 peptides as well as of the embedded domain in the full-length protein we propose the presence of a highly dynamic metal cluster, possibly switching between two slightly different cluster arrangements recruiting either Cys-3 or Cys-21 as the second bridging thiolate ligand. This flexibility is in line with the observed decreased rigidity of the γ-domain compared to the β_E-domain as observed in ^{15}N relaxation experiments[9]. Overall, the structures of the separate $Zn_2\gamma$-E_c-1 and $Cd_2\gamma$-E_c-1 peptides show only minor differences within the error limits. In addition, when monitoring the chemical shifts of the backbone amide protons and nitrogen atoms in the 24-residue *N*-terminal segment of Zn_6E_c-1 and in the

separate $Zn_2\gamma$-E_c-1 peptide only small differences are observed. Hence the solution structure of the separately expressed γ-E_c-1 peptide can be reliably taken as a model for the γ-domain in the full-length E_c-1 protein.

II 6 Acknowledgements

We thank Prof. Peter Güntert for refining the CYANA structures with a full force field. This work was supported by the Swiss National Science Foundation (SNF Förderungsprofessur PP002-119106/1 to E.F.)

II 7 Supplementary Material

Table S1 Apparent pK_a values of Cys residues in different E_c-1 species

Curve fitting of pH titration data for $Zn_2\gamma$-E_c-1, $Zn_2\gamma$ + $Zn_4\beta_E$- E_c-1, $Cd_2\gamma$-E_c-1, and $Cd_2\gamma$ + $Cd_4\beta_E$-E_c-1 using three different equations.[a]

Eq. 1	$Zn_2\gamma$-E_c-1	$Zn_2\gamma$ + $Zn_4\beta_E$-E_c-1	$Cd_2\gamma$-E_c-1	$Cd_2\gamma$ + $Cd_4\beta_E$-E_c-1
A_{MT}	13413 ± 105	48885 ± 694	25237 ± 236	56145 ± 498
A_{MTH_n}	5003 ± 140	10113 ± 858	648 ± 354	3114 ± 766
pK	4.79 ± 0.02	4.68 ± 0.04	3.95 ± 0.02	3.81 ± 0.02
n	2.2 ± 0.2	1.7 ± 0.2	2.5 ± 0.2	1.8 ± 0.1
Eq. 2				
A_{MT}	13747 ± 24	50257 ± 261	25609 ± 54	58163 ± 147
A_{MTH_m}	9671 ± 813	37291 ± 488	-354405±1183529	41186 ± 2051
$A_{MTH_{n+m}}$	5143 ± 18	10823 ± 164	1147 ± 84	4098 ± 92
pK_1	4.693 ± 0.007	4.56 ± 0.01	4.1 ± 0.3	3.716 ± 0.004
pK_2	5.1 ± 0.2	5.3 ± 0	2 ± 2	4.41 ± 0.09
n	4.05 ± 0.09	3.1 ± 0.1	3.9 ± 0.3	3.03 ± 0.06
m	1.0 ± 0.1	1.0 ± 0.1	0.81 ± 0.06	1.2 ± 0.1
Eq. 3				
A_{MT}[b]	13746 ± 24	50225 ± 273	25653 ± 74	58161 ± 142
A_{MTH_m}[b]	10814 ± 351	37607 ± 3401	18442 ± 1720	43177 ± 1844
$A_{MTH_{n+m}}$[b]	5143 ± 26	10832 ± 263	1147 ± 106	4011 ± 107
pK_1	4.685 ± 0.003	4.55 ± 0.01	3.857 ± 0.007	3.713 ± 0.005
pK_2	5.32 ± 0.08	5.3 ± 0.2	4.5 ± 0.2	4.50 ± 0.08
n	4.4 ± 0.2	3.4 ± 0.3	4.5 ± 0.4	3.2 ± 0.1
m	1.30 ± 0.1	1.1 ± 0.2	1.6 ± 0.4	1.3 ± 0.1

[a] $$A_{total} = \frac{A_{MT} + A_{MTH_n} 10^{n(pK-pH)}}{1+10^{n(pK-pH)}} \quad \text{(Eq. 1)}$$

$$A_{total} = \frac{A_{MT} + A_{MTH_m} 10^{m(pK_2-pH)} + A_{MTH_{n+m}} 10^{n\cdot pK_1+m\cdot pK_2-(n+m)pH}}{1+10^{m(pK_2-pH)} + 10^{n\cdot pK_1+m\cdot pK_2-(n+m)pH}} \quad \text{(Eq. 2)}$$

$$A_{total} = \frac{A_{MTH_m} + A_{MTH_{n+m}} 10^{n(pK_1-pH)}}{1+10^{n(pK_1-pH)}} + \frac{A_{MT} + A_{MTH_m} 10^{m(pK_2-pH)}}{1+10^{m(pK_2-pH)}} \quad \text{(Eq. 3)}$$

A_{MT} is the absorptivity of the fully metal ion-loaded protein (=A_{max}), A_{MTH_n} (Eq. 1) and MTH_{n+m} (Eqs. 2 and 3) denote the value obtained for apo-MT after acidification (=A_{min}), MTH_m (Eqs. 2 and 3) is the absorptivity of the protein species obtained after the first protonation step characterized by pK_2, and m (Eqs. 2 and 3) as well as n (Eqs. 1, 2, and 3) are a measure for the slope of the curves.

[b] the absorption values obtained from the original curve fitting with Eq. 3 were shifted by [$A_{MTH_{n+m}}$ (Eq. 2) - $A_{MTH_{n+m}}$ (Eq. 3)] to allow direct comparison with values from Eq. 2.

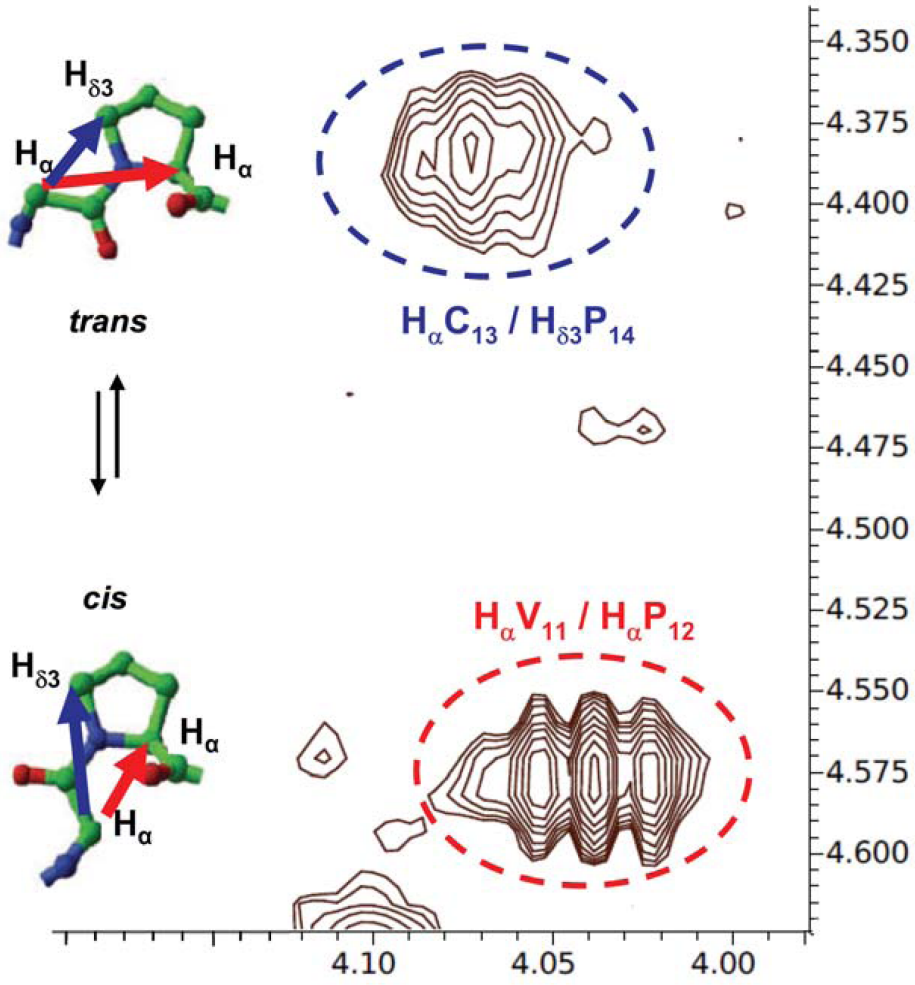

Figure II S 1 Section of the ^{1}H-^{1}H NOESY NMR spectrum of $Zn_2\gamma$-E_c-1 showing the two proline residues. Pro-14 shows a strong $H_\alpha X_i/H_{\delta 3}P_{i+1}$ cross peak indicative for the *trans*-conformation, whereas Pro-12 displays a strong for $H_\alpha X_i$ /$H_\alpha P_{i+1}$ cross peak, which is characteristic for the *cis*-conformation.

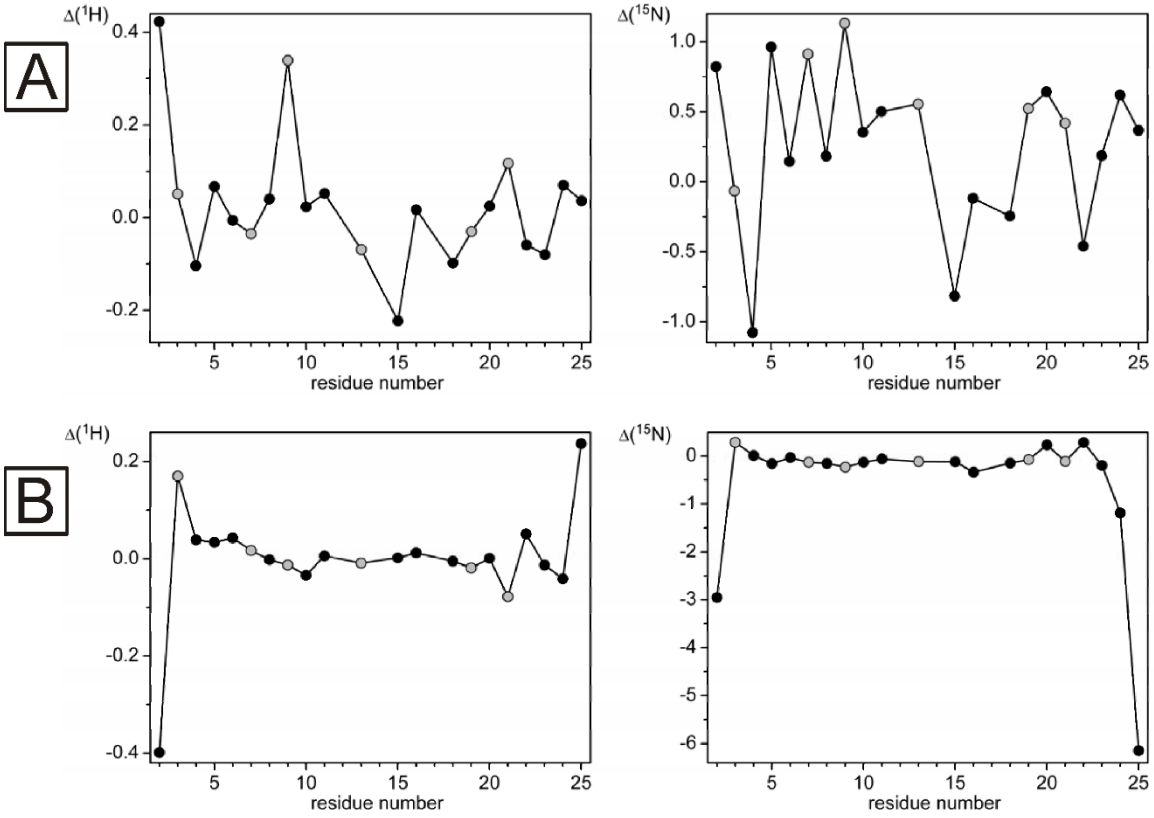

Figure II S 2 ***A)*** Differences in amide proton (left) and nitrogen (right) chemical shifts between $Zn_2\gamma$-E_c-1 and $^{113}Cd_2\gamma$-E_c-1. The positions of the Cys residues are highlighted with gray circles. ***B)*** Differences in amide proton (left) and nitrogen (right) chemical shifts between $Zn_2\gamma$-E_c-1 and full-length Zn_6E_c-1. The positions of the Cys residues are highlighted with gray circles.

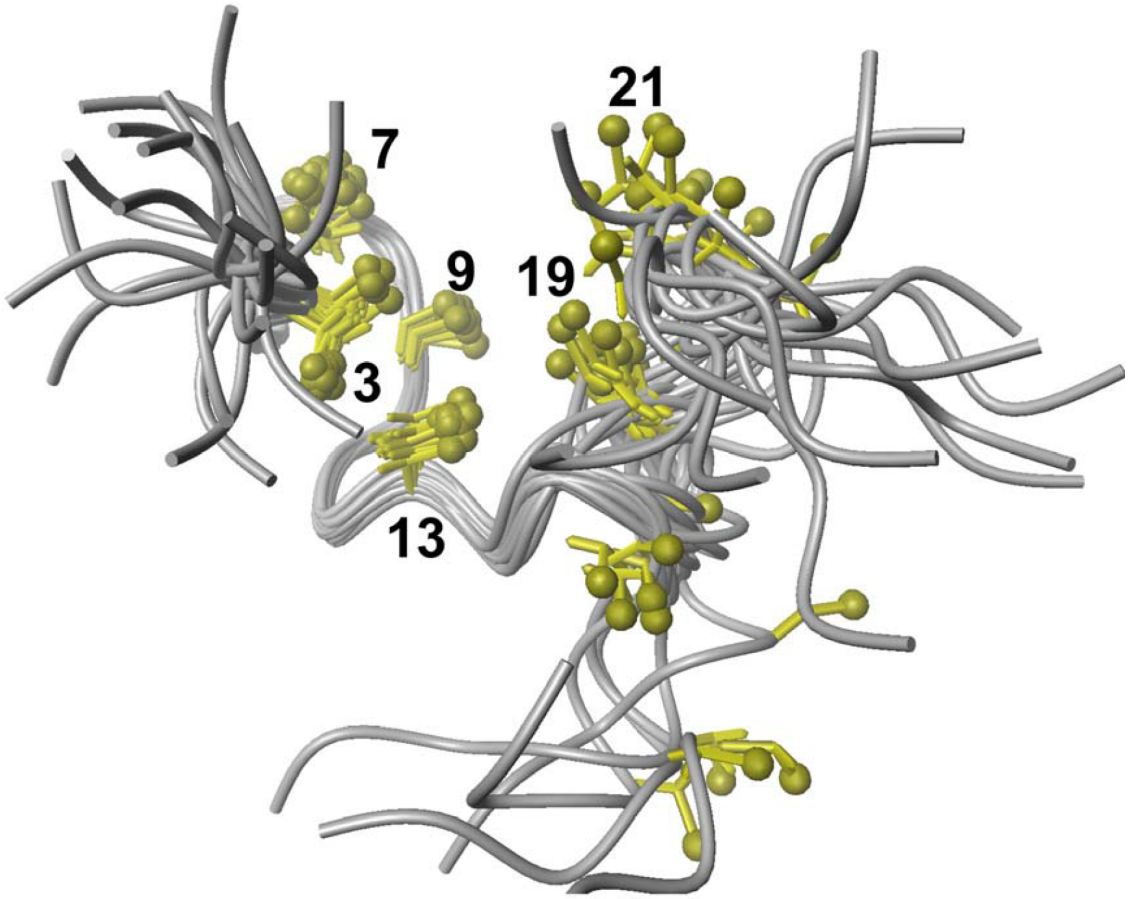

Figure II S 3 Initial structure bundle for $Zn_2\gamma$-E_c-1 calculated without addition of explicit metal-Cys(S) constraints. The structures converge for the amino acid residues Gly-2 to Gly-18. However, the positions of the C-terminal residues and of the thiol-groups of the Cys residues deviate substantially

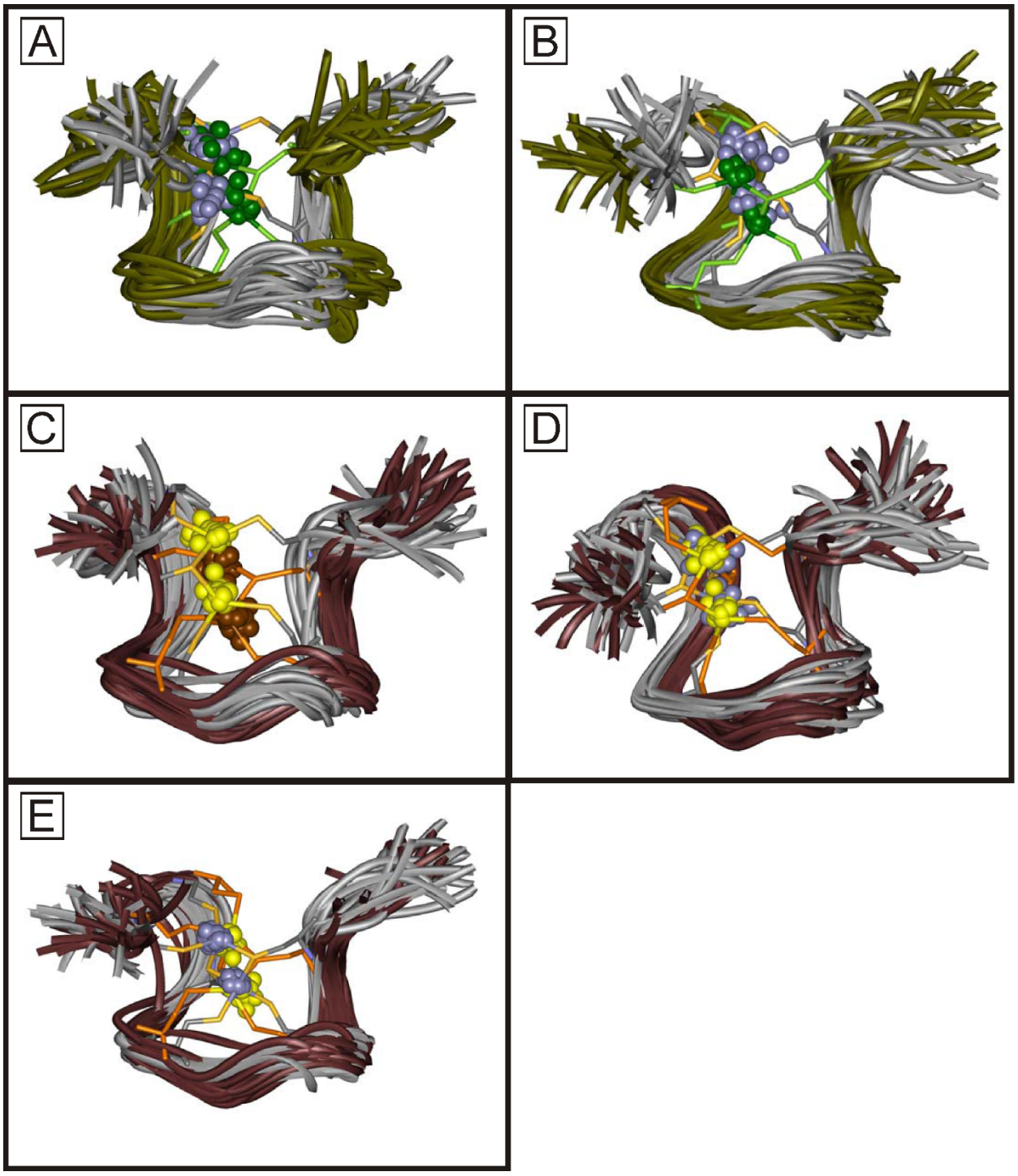

Figure II S 4 Backbone overlays of structure bundles (20 lowest energy structures) for the ***A)*** Zn^{II}-isoforms Cys-9/3 (grey backbone, Cys residues in stick mode, Zn^{II} ions as light blue spheres) and Cys-9/21 (olive backbone, Cys residues as green sticks, Zn^{II} ions as dark green spheres) of the γ-domain embedded in the full-length protein and ***B)*** of the independent γ-domains. ***C)*** Cd^{II}-isoforms Cys-9/3 (grey backbone, Cys residues in stick mode, Cd^{II} ions as yellow spheres) and Cys-9/21 (brown, Cys residues as orange sticks, Cd^{II} ions as brown spheres) of the independent γ-domains ***D)*** Zn^{II}-isoform

Cys-9/3 (grey backbone, Cys residues in stick mode, Zn^{II} ions as light blue spheres) and the Cd^{II}-isoform Cys-9/3 (brown, Cys residues as orange sticks, Cd^{II} ions as yellow spheres) of the independent γ-domains ***E)*** Zn^{II}-isoform Cys-9/21 (grey backbone, Cys residues in stick mode, Zn^{II} ions as light blue spheres) and the Cd^{II}-isoform Cys-9/21 (brown, Cys residues as orange sticks, Cd^{II} ions as yellow spheres) of the independent γ-domains.

Chapter III : GHOST – A GST Hydrogel System for rapid NMR structure determination and spectroscopic characterization of small proteins

Jens Loebus[§] · Silke Johannsen[§] · Eva Freisinger

Jens Loebus · Silke Johannsen · Eva Freisinger (*)

Institute of Inorganic Chemistry, University of Zurich,

Winterthurerstr. 179

8057 Zurich, Switzerland

e-mail: freisinger@aci.uzh.ch

[§] both authors contributed equally

III 1 Abstract

Providing low-cost and fast structural and functional information of proteins is essential in the ever-growing fields of structural and systems biology. Moreover it is vital for pharmaceutical drug discovery processes, as lead compounds for medical applications are derived from various sources, including small proteins found in venoms of various insects, crustaceans or snakes but also in fungi as elicitor peptides and in plants as defense peptides. Therefore we have developed a i) faster, ii) less-expensive and iii) more reliable process for analyzing the structure and function of small proteins with different co-factors by employing the well-known glutathione *S*-transferase (GST) fusion protein system in standard experimental procedures including UVvis, circular dichroism, and NMR spectroscopy as well as mass spectrometry.

Selecting a plant metallothionein (MT) domain termed γ-E_c-1 containing a well characterized Zn_2Cys_6 zinc finger motive, we compared metal binding properties as well as NMR solution structures of the free domain with a GST-tagged form. Next to the decrease of preparation time required to obtain sufficient amounts of purified protein from 3 weeks to 3 days, we observed improved quality of NMR spectra and consequently of the resulting solution structure of the GST-γ-E_c-1 fusion protein. Additionally, we investigated the fungal metal binding protein Neclu_MT1 and observed comparable metallation patterns relative to the isolated target protein, emphasizing the potential value of the GST Hydrogel system GHOST as a screening platform.

Keywords: Expression platform · Metallothionein · GST fusion system · Electronic absorption spectroscopy · NMR spectroscopy · Lead compound screening · GHOST

III 2 Introduction

Recombinant protein expression is a powerful tool in unravelling cellular processes as proteins can be studied and manipulated under various well-devised conditions, assisting in the thorough understanding of the protein. For high-throughput structural biology processes, efficient fast and straight forward protein purification is vital. For this purpose fusion gene system assisted affinity chromatography is the most widely applied technique. Here, a genetically encoded fusion peptide or protein, designated as fusion tag, is *C*- or *N*-terminally linked to the protein of interest in order to facilitate gene and protein expression and detection as well as protein purification via affinity chromatography based on fusion tag binding partner recognition[92]. Many fusion tag systems have been developed such as maltose binding protein[93], His-tag[94], Strep-tag[95], Intein-tag[96-97], FLAG-tag[98], and probably the most widely used GST-tag[99]. These systems vary in size, affinity towards their binding partners and biocompatibility[92]. GST is a ubiquitously expressed, multifunctional protein[100-103]. With a size of 27 kDa the GST-tag is a relatively large tag, yet possesses a high affinity towards its natural ligand glutathione (GSH) as well as to synthetic GSH derivatives and shows an exceptional biocompatibility due to its inherent role in cellular detoxification processes[100, 104], hereby rendering it an excellent fusion protein partner in immunoprecipitation and pull down experiments[105].

Despite its tremendous advantage for protein expression, purification, and detection, expressed fusion tags are themselves proteins or polypeptides with certain properties and hence suspected to inherently infer with the functional or structural elucidation of the target proteins. Especially for small target proteins (<10 kDa) or even polypeptides also the size of the fusion tag potentially can have a large influence. Very problematic for the study of metalloproteins such as e.g. zinc-finger proteins or metallothioneins (MTs) is also the use of the rather short polyhistidine tags due to the intrinsic metal ion coordination capacities of histidine. Consequently, fusion tag systems often offer the possibility to remove the fusion tag by digestion with a protease such as thrombin or factor Xa after purification with affinity chromatography. A very neat system in this respect is the self-cleavable Intein-tag, where cleavage requires simply incubation of the fusion protein with a thiol containing reducing agent. Nevertheless, removal of the fusion tag requires at least one additional step in the purification protocol, generally lowering the final yield and rendering the whole procedure more expensive and time consuming.

MTs are typical examples for small metal ion binding proteins and derive their name from their elevated cysteine content (15% - 33%) and hence their ability to coordinate metal ions such as Zn^{II} and Cu^{I} in form of metal-thiolate clusters. MTs can be found in almost all living phyla (besides archaea)[3]. Despite of more than 50 years of intensive research especially on the mammalian forms still only limited insight into the physiological role of MTs were obtained so far. Several MTs from different families, e.g. the mammalian and crustacean forms, contain two metal-thiolate clusters. As these clusters for the most part do not interact with each other they have been studied separately including the determination of their solution structures with NMR spectroscopy. Another example for a two domain MT is the E_c-1 protein from *Triticum aestivum* (common bread wheat), the first metallothionein evidenced in plants[14]. Naturally, wheat E_c-1 is a Zn^{II} binding protein, but it may also coordinate to toxic d^{10} metal ions such as e.g. Cd^{II} with even higher affinity[8, 61, 106]. Next to the metal ion arrangement in the larger β_E-E_c-1 domain it features a Zn_2Cys_6 cluster in the smaller 25 amino acids long γ-E_c-1 domain. This Zn_2Cys_6 cluster is the smallest metal-thiolate cluster arrangement possible and is structurally similar to the one observed in the GAL4 zinc finger protein[89, 107]. As MTs occur in a multitude of different phyla they display a high sequence diversity and accordingly it can be expected that many of the yet unstudied forms will contain novel metal cluster architectures and overall protein folds. Neclu_MT1 is an example for such MTs with unique amino acid sequences. While Neclu_MT1 has been initially characterized by a variety of spectroscopic methods three-dimensional structural information is not available so far. Neclu_MT1 is a Cd^{II} coordinating metallothionein from the aquatic fungus *Heliscus lugdunensis* featuring eight Cys and one His residue as potential metal binding ligands[22] (see **Chapter VI**). There are strong indications that the metallation pattern of Neclu_MT1 differs depending on whether Cd^{II} or Zn^{II} is coordinated by the protein as investigated via electronic and chiro-optic spectroscopy. Both types of spectroscopy are also ideally suited for drug-protein screening since they open up low budget, easy to use screening procedures. NMR experiments provide valuable information about the structure and site specificity of drug-protein interaction. Here a fast, low-cost, easy to use, and rich in content screening procedure would be highly beneficial. In order to tackle the need for such as straight forward high throughput screening method for structure and folding assessment, structure determination, and spectroscopic characterization we propose the GST Hydrogel System (GHOST) as a tool especially applicable for the screening of small proteins in biomedical and life science research.

III 3 Material and methods

III 3 1 Chemicals and solutions

$^{113}CdCl_2$ and $^{15}NH_4Cl$ were purchased from ReseaChem GmbH (Burgdorf, Switzerland), d_{11}-Tris from Euriso-top (Saint-Aubin, France). All other chemicals were ACS grade or comparable from Sigma-Aldrich Chemie GmbH (Buchs, Switzerland), Calbiochem (VWR International AG, Lucerne, Switzerland) or Acros organics (Chemie Brunschwig AG, Basel, Switzerland). All solutions were prepared using filterd, degassed, bidestilled water (ddH_2O). If appropriate, solutions were saturated with nitrogen or argon. Whenever complete absence of oxygen was required, ddH_2O was degassed by three consecutive freezing thawing cycles under vacuum.

III 3 2 Plasmid construction, protein expression and purification as well as removal of GST tag

The coding sequences for γ-E_c-1

GS GCDDKCGCA VPCPGGTGC RCTSAR

and Neclu_MT1

G SPCTCSTCNC AGACNSCSCT SCSH

were cloned into pGEX-4T (GE Healthcare) using the BamH1 and EcoR1 restriction sites and expressed in *Escherichia coli* as described[106] (see **Chapter VI**). Purification of γ-E_c-1 and Neclu_MT1 was performed as published[106] (see **Chapter VI**).

III 3 3 Preparation of apoγ-E_c-1 and apoNeclu_MT1

Apoγ-E_c-1 and apoNeclu_MT1 were prepared freshly prior to each experiment. Typically 1 to 3 mg of oxidized protein as obtained after thrombin cleavage and size exclusion chromatography was incubated with 200 mM 1,4 dithreitol (DTT) in 100 mM Tris/HCl (pH 8.0) for 1 h prior to acidification to pH 2 with 1 M HCl. In a glovebox the sample was applied to a Superdex Peptide 10/300 GL size exclusion column (GE Healthcare) pre-equilibrated with 10 mM HCl and eluted under constant argon flow. The residual Zn^{II}, Cd^{II},

and $Cu^{I/II}$ content of apo-γ-E_c-1 and apoNeclu_MT1 was below the detection limit of flame atomic absorption spectroscopy (F-AAS, AA240FS spectrometer (Varian AG, Zug, Switzerland)) i.e. below 0.001 ppm. Prior to metal ion reconstitution experiments as described below, apo-protein solutions were argon saturated for 1 h in a N_2-flushed glove box and the protein concentration determined via thiol quantification using the 2,2'-dithio-dipyridine (2-PDS) assay[43].

III 3 4 Preparation of Zn^{II} forms of GST-γ-E_c-1 and GST-Neclu_MT1

To obtain the Zn^{II} loaded GST fusion proteins LB growth media was supplemented with 100 μM $ZnCl_2$ after induction of protein expression. Following cell harvest, lysis and recuperation of cytoplasmatic proteins trough centrifugation, GST fusion proteins were purified employing a glutathione sepharose affinity column according to the manufacturer's manual (GE Healthcare)(110). The fusion proteins are eluted from the affinity column with 50 mM GSH in 50 mM Tris/HCl, pH 8.0 yielding approximately 20 mL of fusion protein with a concentration of 10 mg mL^{-1} per L of cell culture. From here on, all buffer exchange and concentration steps of the protein were performed in a Series 8050 stirred ultracentrifugation cell (Millipore AG, Zug, Switzerland) pressurized with argon. Following concentration of the fusion protein solution to approximately 5 ml, (DTT) was added to a final concentration of 100 to 200 mM to ensure reduction of all Cys residues and the pH was adjusted to 8.5 with 1 M Tris/HCl, pH 8.9.

After 30 min incubation, the protein solution was twice diluted with 50 ml of 50 mM Tris/HCl, pH 8.0 and re-concentrated. Then the concentrated GST fusion protein solution was diluted a third time with 50 mM Tris/HCl pH 8.0, and subsequently a 100 mM $ZnCl_2$ solution was slowly titrated into the sample to result in a final concentration of approximately 200 μM Zn^{II}, which equals a slight excess relative to the Zn^{II} binding capacities of the respective fusion protein. Following one further buffer exchange cycle with 50 mM Tris/HCl pH 8.0 three wash cycles with 1 mM d_{11}-Tris/HCl pH 8.0 were performed to remove remaining DTT, non-deuterated Tris/HCl, and unbound Zn^{II} ions. Subsequently, the protein concentration was determined via the absorption at 280 nm assuming extinction coefficients of 41'760 M^{-1} cm^{-1} (www.expasy.ch/protparam) for GST-γ-E_c-1 and GST-Neclu_MT1. In addition, protein concentrations were also quantified with the 2-PDS assay accounting for two more Cys residues of the GST tag in addition to the MT thiols agreeing excellently with the values

obtained by the A_{280nm} method. Although the GST-tag features four Cys residues, we found that only two are accessible for modification with the PDS assay after purification of the GST-tag alone. The metal concentration of the GST fusion protein solution was determined via F-AAS prior to aliquoting the protein and storage at -80°C. Final protein concentrations varied from 0.1 to 0.5 mM. For all preparations the final Zn^{II} load was adjusted to 2 (GST-γ-E_c-1) or 3 (GST-Neclu_MT1) equivalents per fusion protein.

III 3 5 Preparation of $^{113}Cd_3$ GST-Neclu_MT1, $^{113}Cd_2$ GST-γ-E_c-1, and $Zn^{113}Cd$ GST-γ-E_c-1

For all proteins the exact amount of 1, 2 (GST-γ-E_c-1) or 3 (Neclu_MT1) equivalents of $^{113}Cd^{II}$-ions were titrated to the diluted Zn-form (ca. 15 μM GST fusion protein) in 50 ml 1 mM d_{11}-Tris/HCl pH 8.0. Subsequently, two buffer exchange cycles with 1 mM d_{11}-Tris/HCl pH 8.0 were conducted to remove released Zn^{II} ions and the protein concentration and metal concentration were analyzed (see **III 3 4**), and the samples further processed for NMR experiments (see **III 3 9**).

III 3 6 Preparation of Zn^{II}-forms for UVvis spectroscopy

Freshly prepared apo-γ-E_c-1 or apo-Neclu_MT1 in 10 mM HCl was mixed with two or three, respectively, equivalents of Zn^{II} ions prior to raising the pH to 7.2 with 1 M Tris/HCl pH 8.6 and 1 M NaOH in order to yield protein solutions containing approximately 10 mM Tris/HCl and 10 mM NaCl. The desired final protein concentration of ca 25 μM was adjusted by adding a solution containing 10 mM Tris/HCl, pH 7.2, and 10 mM NaCl giving a final sample volume of 1.8 mL. The volume and pH of the Zn GST-γ-E_c-1 or Zn GST-Neclu_MT1 forms prepared in 1 mM d_{11}-Tris/HCl (see **III 3 4**) was adjusted via the identical 10 mM Tris/HCl, pH 7.2, 10 mM NaCl solution. Owing to the higher stock protein concentration (> 300 μM), the slight dilution of the buffer was neglected.

III 3 7 Metal ion titrations followed with UVvis spectroscopy

The respective Zn^{II}-forms of γ-E_c-1, GST-γ-E_c-1, Neclu_MT1, and GST-Neclu_MT1 were titrated with Cd^{II} ions, Neclu_MT1 and GST-Neclu_MT1 were also titrated with Hg^{II} ions. 1.8 mL of the respective protein solution were transferred into a 1-cm septum sealed cuvette

and the respective metal ion solution into a 25 µl Hamilton syringe. After each incremental metal ion addition followed by short mixing through slide manual slewing of the cuvette UVvis spectra were recorded. Once the titration was completed, the protein and metal ion concentrations were again determined with the 2-PDS assay or by F-AAS, respectively, to exclude protein oxidation and titration errors. Finally size exclusion chromatography (SEC) was performed to affirm the monomeric character of the Cd^{II} and Hg^{II} loaded protein species.

III 3 8 Mass spectrometry

Samples of 50 µM Zn_2 and Cd_2 GST-γ-E_c-1 were dialyzed against 50 mM NH_4Ac (pH 7.6) and injected directly or with a prior acidification step into a quadrupole time-of-flight (TOF) Ultima API spectrometer (Waters, UK). 10 mM NH_4Ac in 50% MeOH (pH 7.5) or 50% acetonitrile with 0.2% formic acid (pH 2-3) were used as a solvent. Scans were accumulated and further processed by the software MassLynx 3.5 (Micromass). Deconvolution of mass spectra was done by applying the maximum entropy algorithm of the MassLynx tool MaxEnt1. Electrospray parameters were capillary 2.8 V, cone 60 V and source temperature 80 °C.

III 3 9 Preparation of GST fusion protein forms for NMR

The GST-tagged forms of Zn_2-, ZnCd-, and Cd_2γ-E_c-1, as well as of Zn_3- and Cd_3Neclu_MT1 were prepared as described above and concentrated to final concentrations of approximately 1 mM in a Series 8003 stirred ultracentrifugation cell (Millipore). D_2O was added to give a 10 % solution. Samples were transferred into NMR shigemi tubes (Shigemi Inc.) and heated for 24 h at 37°C in order to generate the hydrogel.

III 3 10 Preparation of Zn_2- and Cd_2γ-E_c-1 as well as Zn_3- and Cd_3Neclu_MT1 for NMR

For all experiments the exact amount of 2 or 3 equivalents of metal ions was titrated to the respective apo-form in a N_2-flushed glove box. Subsequently, the pH was raised to 8.6 using Tris/HCl or d_{11}-Tris/HCl. Reconstituted samples were dialyzed against 100 µM d_{11}-Tris/HCl, pH 7, and concentrated by lyophilization. The proteins were dissolved in 10% D_2O/90% H_2O containing 15 mM d_{11}-Tris/HCl, pH 6.9, and 50 mM NaCl for the γ-E_c-1 samples or 10 mM

d_{11}-Tris/HCl, pH 7.3, and 10 mM NaCl for the Neclu_MT1 samples to a final concentration of 1 mM protein.

III 3 11 NMR spectroscopy

The NMR spectra and the solution structures of ^{15}N-labelled Zn_2- and $^{113}Cd_2\gamma$-E_c-1 were reported previously[106]. ^{1}H NMR experiments to elucidate the protein backbone structure of ^{15}N labelled and non ^{15}N labelled Zn_2 GST-γ-E_c-1, $^{113}Cd_2$ GST-γ-E_c-1, GST-tagged and cleaved Zn_3Neclu_MT1 as well as Cd_3Neclu_MT1 were recorded at 310 K on Bruker Avance 700- and 600-MHz spectrometers. ^{113}Cd-NMR experiments to investigate the binding sites of the Cd^{II} ions were performed on a Bruker DRX 500-MHz spectrometer. Assignment of resonances in GST-γ-E_c-1 were performed using 3D ^{15}N resolved TOCSY[72-73], NOESY[74-75] and 2D TOCSY spectra recorded with 100 ms (TOCSY) and 250 ms (NOESY) mixing times, respectively. Distance restraints were derived from both the 3D ^{15}N resolved NOESY and 2D NOESY experiments. In all ^{15}N resolved samples zero-quantum interference in the spectra was suppressed using an appropriate filter[77, 108]. 1D ^{113}Cd**,** 2D [^{113}Cd,^{1}H]-HSQC and 2D [^{113}Cd,^{113}Cd]-COSY NMR spectra were recorded to investigate the metal cluster[35]. $^3J[H_\beta,Cd]$ couplings derived from a 2D [^{113}Cd,^{1}H]-HSQC spectrum allowed to establish the individual Cd-Cys connectivities. In case of Zn_3- and Cd_3Neclu_MT1 2D NOESY and 2D TOCSY spectra were recorded with 150 ms and 100 ms mixing time, respectively. Zn_3 and Cd_3 GST-Neclu_MT1 2D NOESY and 2D TOCSY spectra were recorded with 250 ms and 100 ms mixing time, respectively.

Sequence-specific resonance assignment was performed using the methodology developed by Wüthrich[38]. Assignments were achieved based on information from 2D TOCSY, NOESY, 2D [^{15}N,^{1}H]-HSQC, 3D ^{15}N-resolved NOESY, and 3D ^{15}N-resolved TOCSY experiments. The 2D and 3D spectra were evaluated with the programs XEASY[80] and CARA[81], respectively. As a first step, the spin systems were identified in the 2D TOCSY or 3D ^{15}N-resolved TOCSY experiments. Subsequently, spin systems were linked based on NOE information derived from 2D NOESY and 3D ^{15}N- resolved NOESY. Once longer stretches had been identified, they were mapped onto the sequence of γ-E_c-1.

For the structure calculations NOE peaks were picked and integrated using the program XEASY for 2D and CARA for 3D experiments employing identical lower integration thresholds. Torsion angle dynamics[82] were performed with the *noeassign*[42] algorithm of the program CYANA 2.1[83]. Structure calculations were started from 100 conformers with

randomized torsion angle values. Structure figures of the 20 conformers with the lowest final target function value were generated with the program MOLMOL[87]. To determine the hydrodynamic radii r_H of Zn_2 and $Cd_2\gamma$-E_c-1 and Cd_2 and Zn_2 GST-γ-E_c-1 DOSY spectra were recorded using the standard BRUKER pulsprogram ledbpgp2s_es applying stimulated echoes using bipolar gradient pulses for diffusion. The hydrodynamic radii r_H is calculated from the Stokes-Einstein equation employing the measured diffusion coefficient (D_H), at the temperature 298 K and the dynamic viscosity of H_2O ($0.89\ 10^{-3}$ N s m^{-2}).

III 4 Results

III 4 1 Sample preparation strategy

The pGEX-T4 expression vector used produces a GST fusion protein, which contains a five amino acid long thrombin cleavage site between the GST-tag and the *N*-terminus of the desired protein The flexibility of this linker should confine a certain degree of motional freedom allowing unhindered folding and relatively free movement of the GST-tagged target protein. Employing this standard protein expression vector we developed a methodology for post GST fusion protein sample preparation (**Fig. III 1**) starting from the standard purification protocol for GST fusion tag protein (GE Healthcare). The key element of the sample preparation protocol is a "soft" protein denaturing step at low protein concentration (< 50 μM) and slightly basic pH (ca. 8.5) employing 1,4-dithiothreitol (DTT) as reducing agent. Tertiary and quaternary disulfide bridges are expected to be cleaved resulting in four reactive thiol containing moieties that may react amongst each other to again form disulfides if oxidation agents such as O_2 are present. The sample preparation strategy is devised as follows: **i)** GST fusion protein is eluted from the affinity column using 50 mM reduced glutathione providing the basis for a reducing environment; **ii)** GST fusion protein is denatured with 0.2 – 0.5 M DDT pH 8 for 30 min; **iii)** fast buffer exchange (factor ~ 1000) to enable **iv)** addition of co-factors (in this report M^{II} ions) to finally; **v)** concentrate the sample to the desired value. In case of the NMR sample preparation starting from step iii (buffer exchange) the NMR buffer solutions were used. During the protein sample concentration the solution already turns opaque providing optical prove for the onset of fusion protein polymerization (**Fig. III 1c)**. This is the most important step for the successful recording of the multidimensional NMR experiments using GST fusion protein and was initiated by a "soft" denaturing step resulting in reactive thiol moieties that form concentration dependent networks leading to partially disulfide linked hydrogels[109]. In order to facilitate and finalize the polymerization and gelation process as final step **vi)** an over night heat treatment of the NMR-tube at 37°C or

more[109] is conducted resulting in improved NMR spectra quality (**Fig. III 2d**).

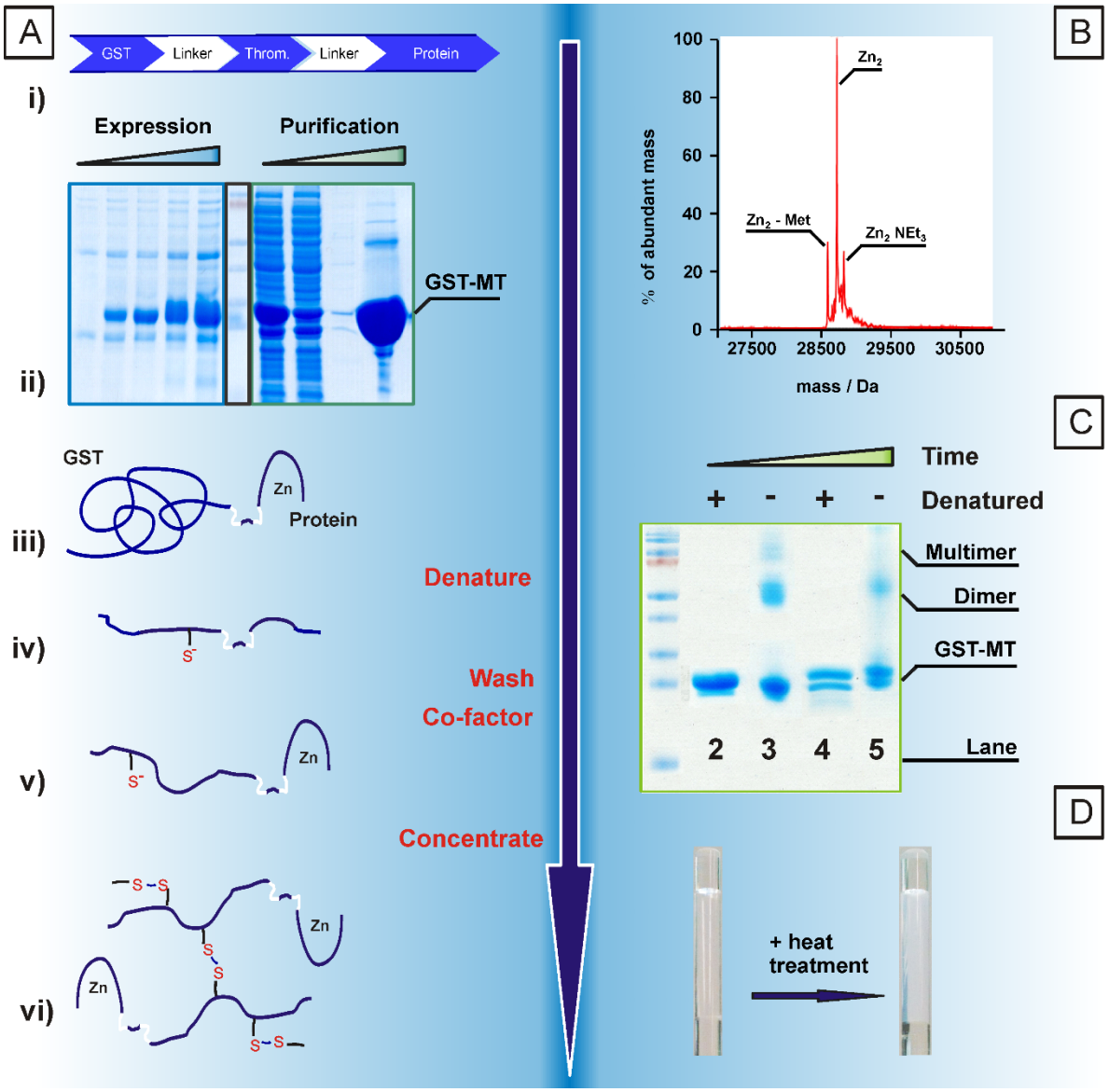

Figure III 1 GST fusion protein sample preparation and characterization is schematically displayed. ***A)*** To recombinantly over express and purify the GST fusion protein the pGEX expression vector contains a *N*-terminal GST-tag connected with a short flexible linker to the thrombin cleavage site, which is coupled to the non-structured amino acid stretch of the *C*-terminal target protein **(i)**. The gene product is over expressed and purified according to the GE Healthcare manual[110] **(ii)** concluding with the GST mediated elution of the GST fusion protein **(iii)** and is consequently reduced with DTT yielding reactive thiolates **(iv)**. In a next step the residual reducing agents are removed and the co-factors/ligands, in this case Zn^{II}-ions, are added **(v)**. In a last step the buffer is adjusted and the GST fusion protein sample is concentrated to the desired concentration, according to which, a hydrogel cross-linked via disulfides is formed **(vi)**. ***B)*** The molecular identity of the reduced and remetallated Zn_2 GST-γ-E_c-1 is probed via ESI-MS. Next to the correctly metallated fusion protein a form where

the *N*-terminal Methionine was not removed is observed as well as a triethylammonium adduct. ***C)*** The gelation process of the GST fusion protein after sufficient concentration is followed via SDS-PAGE. When the sample was completely denatured through incubation of standard Laemmli buffer at 99 °C for 5 min prior to SDS-PAGE only one band with the appropriate size was observed (2). In contrast a native, non-treated GST fusion protein sample displays monomers, dimers and some higher state aggregates (3) clearly evidencing a disulfide cross-linked polymerization. Following overnight incubation at 37°C the gelation to higher aggregates proceeds further (5), resulting in ***D)*** a formation into a hydrogel as evidenced comparing an NMR sample of the isolated protein (left) and the GST-γ-E_c-1 (right) in a shigemi NMR tube.

III 4 2 Analysis of GST fusion protein with NMR spectroscopy

1D ^{1}H NMR spectra of GST-γ-E_c-1 displayed broad peaks originating from the 26 kDa GST-tag, which lack baseline separation being characteristic for big molecules and dynamic processes. In addition sharp signals as witnessed for the isolated γ-E_c-1 domain modulating the GST signals were evidenced. Proton spectra of GST-γ-E_c-1 fusion protein, prepared as described above, were recorded at different relaxation delays D1 in order to evaluate the influence of the GST tag. No difference in signal was discernable. Surprisingly, when 2D [^{1}H,^{1}H] TOCSY NMR spectra were recorded both line widths and intensity of the cross-peaks were comparable with those of the isolated γ-E_c-1 domain. Indeed, the GST fusion protein line widths were even smaller (<10 Hz) than those for the isolated γ-E_c-1 domain. Moreover spin systems of the isolated γ-E_c-1 domain prior invisible (G_2, S_{23}) appear in the 2D [^{1}H,^{1}H] TOCSY NMR spectra of the GST fusion protein. Additionally four more spin systems are witnessed all of which belong to the engineered linker between GST and the target protein coding for a thrombin protease cleavage site (V, R, P, S) (**Fig. III 2a)**. In order to investigate on the influence of the GST fusion partner on the target protein the TOCSY mixing times were varied from 50 ms to 150 ms. As for the isolated γ-E_c-1 domain 100 ms was judged as the most appropriate mixing time and subsequently used for all other GST fusion proteins investigated. Almost identical chemical shift information derived from the 2D [^{1}H,^{1}H] TOCSY NMR spectra gave hope to assume a homolog protein structure, which can be calculated starting from proton distance information (NOEs) derived from NOESY NMR spectra. Hence a 2D [^{1}H,^{1}H] NOESY NMR spectra of the Zn-form of GST-γ-E_c-1 was recorded with 250 ms mixing time (**Fig. III 2b**) and overlayed with the isolated Zn_2γ-E_c-1 NOESY NMR spectra. In both cases the peaks are well dispersed with half-linewidth of about

10 Hz, resulting in a straightforward assignment of NOE cross peaks. Strikingly, there are ca. 60 more NOEs discernable for GST-γ-E_c-1, not considering those NOEs arising from the additional spin systems assigned to the thrombin cleavage site. When mixing times were varied from 120 ms to 250 ms a significant decrease of residual GST signals (not appearing in the TOCSY spectra) was witnessed in contrast to spin diffusion crossover. In consequence mixing time 250 ms was set as default for all further 2D NOESY NMR measurements. To circumvent a certain degree of ambiguity in NOE assignment caused by residual GST signals, ^{15}N resolved 2D and 3D NMR spectra were recorded. An overlay of the [^{15}N,^{1}H] HSQC spectra of the Zn-form of the GST-γ-E_c-1 fusion protein and the isolated γ-E_c-1 domain (**Fig. III 2c**) clearly displays an identical chemical shift pattern with additional cross-peaks for so far unresolved amide nitrogen shifts (G_2, S_{23}) of the isolated γ-E_c-1domain and three further peaks, which were assigned to the thrombin protease cleavage site residues (V, R, S). 3D ^{15}N resolved TOCSY and NOESY experiments were recorded with the same

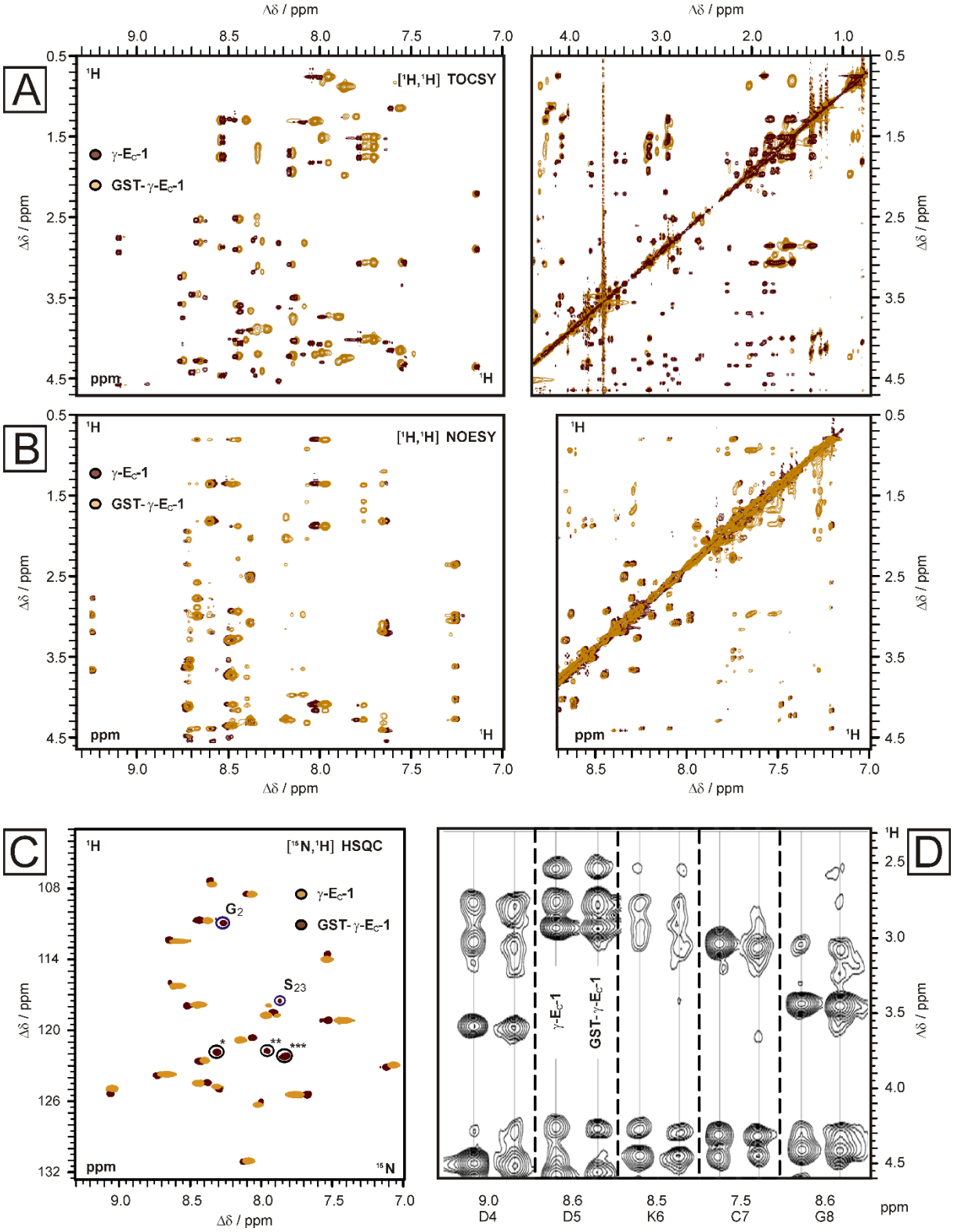

Figure III 2 2D and 3D NMR spectra overlays of GST-γ-E_c-1 with the isolated γ-E_c-1 domain as Zn_2- and Cd_2-form. ***A)*** 2D [^{1}H,^{1}H] TOCSY NMR spectra overlay of Zn_2 GST-γ-E_c-1 (light brown) and Zn_2γ-E_c-1 (dark brown). On the right side the aliphatic spectral region is depicted, while on the left side the amide region is displayed exhibiting four more spin systems for GST-γ-E_c-1 presumably all

belonging to the thrombin cleavage site and the flexible linker. ***B)*** 2D [^{1}H,^{1}H] NOESY NMR spectra overlay of Cd_2 GST-γ-E_c-1 (light brown) and Cd_2γ-E_c-1 (dark brown). Besides the identical NOE pattern in both spectra regions, a higher number of NOEs is discernible for Cd_2 GST-γ-E_c-1 form. ***C)*** 2D [^{15}N,^{1}H] HSQC NMR spectra overlay of Zn_2 GST-γ-E_c-1 (dark brown) and Zn_2γ-E_c-1 (light brown). The five additional peaks for the GST fusion protein are grouped into two signals arising from so far unresolved γ-E_c-1 residues (G_2 and S_{23}) and three signals belonging to the thrombin cleavage site or linker (V, R, S). ***D)*** 3D [^{15}N,^{1}H,^{1}H] NOESY NMR spectra overlay of the aliphatic region of Zn_2γ-E_c-1 (left) and Zn_2 GST-γ-E_c-1 (right), respectively for the 3D strips of D_4 to G_8.

conditions as for γ-E_c-1 yielding almost identical proton chemical shifts (Δδ > 0.01 ppm). The NOE cross peaks derived from the 3D NOESY NMR spectra are identical in pattern and intensity (**Fig. III 2d**).

III 4 3 Solution structure calculation of GST fusion protein

NOEs derived from 2D [^{1}H,^{1}H] NOESY NMR spectra were integrated based on the chemical shifts assigned in the 2D [^{1}H,^{1}H] TOCSY NMR spectra while only considering those NOE cross peaks which lay in a chemical shift range of Δδ > 0.01 ppm to an assigned proton chemical shift. In case of the Cd and Zn form of γ-E_c-1 and the GST fusion protein all NOEs of the 2D [^{1}H,^{1}H] NOESY NMR spectra were integrated and employed for solution structure calculation. Notably, in case of the GST fusion protein structure calculation the correct fold of the Cd_2-form of the entire γ-E_c-1 domain was achieved without restraining the metal cluster (**Fig. III 3a**), which was required for the isolated γ-E_c-1 domain[106]. This was mainly due to a 15 % increase in the number of distance information NOEs, which do not restrain the *N*-terminus of γ-E_c-1 to which the GST is fused, but surprisingly helped to predict the correct fold of the so far unstructured *C*-terminus (**Supplementary Material, Table S III 1 and Fig. S III 1, 2**).

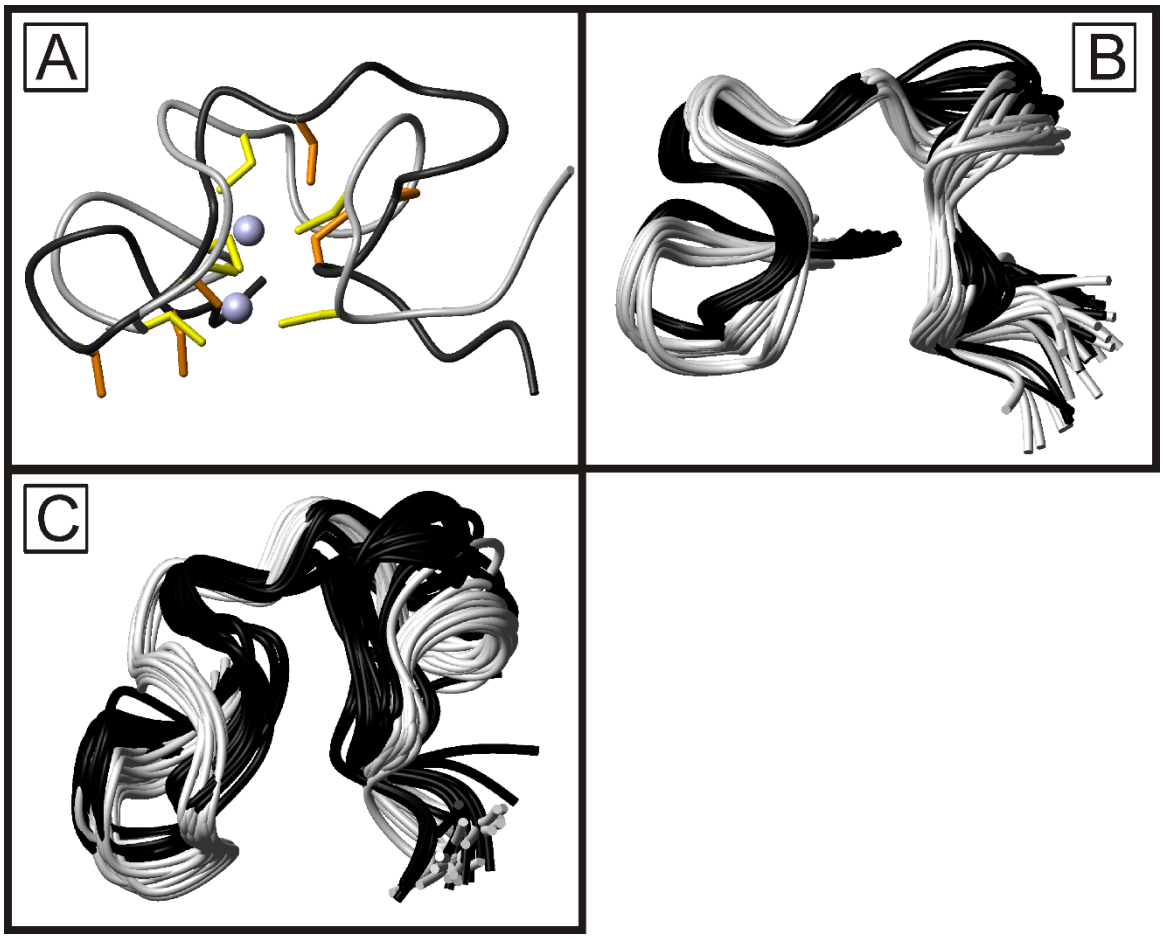

Figure III 3 NMR solution structure overlays of GST-γ-E_c-1 and the isolated γ-E_c-1 domain as Zn_2- and Cd_2-form. For all proteins (B, C) a backbone overlay of the calculated 20 lowest energy structures is depicted. ***A)*** Overlay of the Cd_2 GST-γ-E_c-1 calculated with (grey ribbon, Cys residues yellow sticks, Cd^{II} ions blue spheres) and without (black ribbon, Cys residues orange sticks) metal cluster restraints. ***B)*** Overlay of the Zn_2 GST-γ-E_c-1 (black ribbon) with the isolated Zn_2γ-E_c-1 domain (grey ribbon) in bridging cysteine 3 and 9 conformation. ***C)*** Overlay of Cd_2 GST-γ-E_c-1 (black ribbon) with the isolated Cd_2γ-E_c-1 domain (grey ribbon) in bridging cysteine 21 and 9 conformation.

Hence, assumption regarding stabilization effects due to the existence of a *N*-terminal protein domain can readily be discarded. To further refine the structure calculation of both Zn and Cd metallated species ^{15}N resolved distant restraints derived from the 3D NOESY NMR spectra were used. As mentioned above the number and intensity of the 3D GST fusion protein NOEs is virtually identical to those of the separate domain, resulting in an almost identical protein fold (**Fig. III 3b,c**). Furthermore diffusion NMR experiments for both Zn and Cd GST-γ-E_c-1 as well as isolated Zn and Cd-γ-E_c-1 were performed resulting in monomeric species. While isolated γ-E_c-1 yields a hydrodynamic radius of 1 nm, γ-E_c-1 attached to the GST fusion tag

appears to be slightly larger, i.e. 1.4 nm most likely owing to the linker and thrombin cleavage site, increasing the amino acid chain by nearly 30 %.

III 4 4 GST fusion protein for the characterization and screening of the target protein

In order to additionally validate the possibility of using the GST fusion protein preparation system (GHOST) to substitute the isolated target protein we performed further spectroscopic and spectrometric experiments. First re-metallation studies of the Zn-form of GST-γ-E_c-1 with Cd^{II} ions were performed followed by UVvis spectroscopy (**Fig. III 4a**). Traditionally the incorporation of Cd^{II} ions into tetrathiolate binding sites is monitored by plotting the extinction coefficient at 250 nm versus the amount of Cd^{II} ions added to the solution. The evolution of the extinction coefficient in the range of 270 nm to 230 nm gives information about the nature of the coordinating ligands, i.e. cysteine thiolates groups, as well as the bound metal ion, the number of coordinating ligands, i.e. four, and the coordination geometry, i.e. tetrahedral. In order to follow the exact metallation pathway however, it was suggested to distinguish between electronic contributions from terminal and bridging cysteines[45], which can in this case be observed at 243 and 253 nm (**Fig. III 4b**). The shape of the UV spectra for each metal ion equivalent added is identical for the fusion protein and the isolated target protein. Insignificant, yet chemically meaningful differences are discernable when an excess of Cd^{II} equivalents is added, i.e. more than 2 eq. of Cd^{II}. The extinction coefficient at 243 nm is slightly rising owing to the four putatively non-oxidized cysteine residues indigenous to the GST protein. Nevertheless a clear step in the slope of metallation is visible. This is also corroborated by mass spectrometric (MS) experiments stated above proving the existence of the monomeric form along with the correct metal ion load and the correct molar mass for Zn_2GST-γ-E_c-1 (**Fig. III 1b**) (see **Chapter V**) Hence, MS spectrometry can be used as a further experimental technique for investigating small proteins engineered as part of the here presented GST fusion protein preparation system using μM sample concentration.

Applicability of the samples prepared with GHOST for spectroscopiccal characterization was also shown for titrations of Zn_2 GST-Neclu_MT1 fusion protein with Hg^{II} ions. The highly thiophilic Hg^{II} ion may substitute tetrahedral tetrathiolate Zn^{II}-binding sites, yet it generally prefers a linear dithiolate coordination environment. In consequence after addition of two to three metal ions a shift in tetrahedral to linear Hg^{II} complexes is expected. In the case of the GST fusion protein the transition of Hg^{II} coordination occurs more gradually, than observed

for the isolated protein and the absorption maxima in the 250 nm and 310 nm plots are less pronounced.

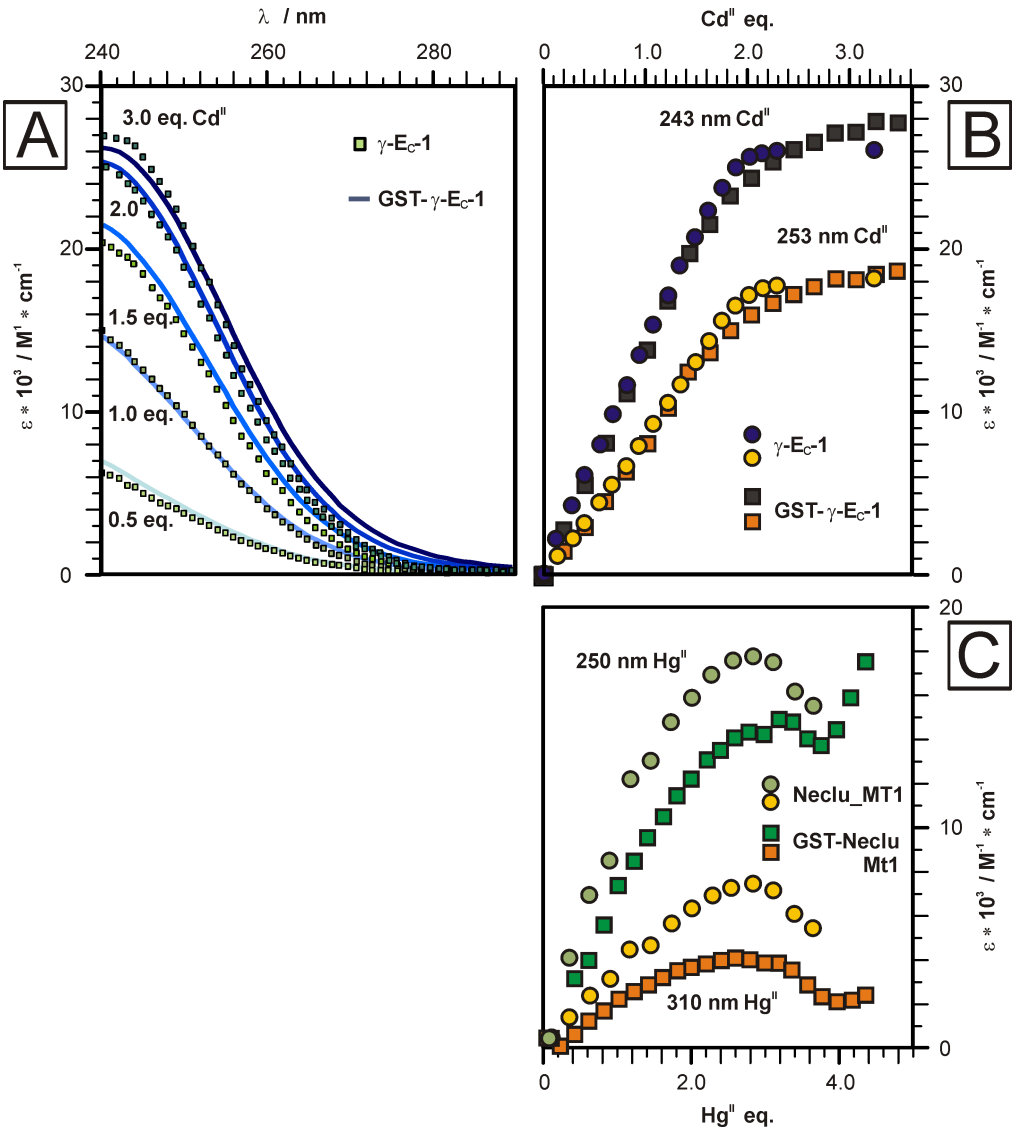

Figure III 4 Spectroscopic assessment of GST fusion protein in comparison to the isolated target protein. ***A)*** Zn^{II} to Cd^{II} exchange titration of Zn_2 GST-γ-E_c-1 (15 μM, squares) and the isolated Zn_2γ-E_c-1 domain (30 μM, solid line) followed by UVvis spectroscopy. ***B)*** The increase of the characteristic ligand-to-metal-charge-transfer (LMCT) band of terminal ligands in a tetrathiolate Cd^{II} binding site (243 nm; blue-black) and bridging ligands tetrathiolate Cd^{II} binding site (253nm; yellow-orange) is plotted against the added Cd^{II} equivalents; GST-γ-E_c-1 (squares); isolated γ-E_c-1 domain (circles). ***C)*** The increase of the characteristic ligand-to-metal-charge-transfer (LMCT) band of an isolated tetrathiolate Hg^{II} binding site (250 nm; blue-black) and a cluster embedded tetrathiolate Hg^{II} binding site (310 nm; yellow-orange) is plotted against the added Hg^{II} equivalents; GST-Neclu_MT1 (15 μM, squares); isolated Neclu_MT1 (15 μM circles).

III 5 Discussion

The concept of using a GST fusion protein for target protein analysis is well established. Several analysis methods in protein science rely on GST fusion protein usage including protein-protein interaction utilizing GST pull-down experiments[105]. Also for the biochemical characterization of proteins and their ligands GST fusion proteins have been applied[111-112] owing to a number of advantages: The GST fusion protein is inexpensive, applicable in all host organisms, it enhances generally protein expression and solubility and it offers high substrate selectivity and affinity in purification[113]. Also structural biologists have applied GST fusion proteins successfully in crystallization and NMR spectroscopy deciphering the structure and correct fold of the protein under investigation[114-115]. In crystallography GST fusion protein usage for template assisted crystallization is well established[116], yet potential interaction between the target protein and the fusion protein in the crystal lattice, possibly enforced by packing effects are more likely to perturb the native folded state. In 2008 *Kong Liew et al.* first reported GST fusion protein assisted screening of folding states of proteins via [^{15}N,^{1}H] HSQC NMR with only a negligible number of signals arising from the GST protein[117]. The authors explain the disappearance of GST related NMR signals in the spectra by dimerization of the homodimeric GST fusion partner.

In contrast, our sample preparation strategy for GST fusion proteins leads not only to dimerization processes but results in polymerization of the GST fusion proteins, arranging into a hydrogel (**Fig. III 1**) with novel advantageous properties. Hydrogel formation of proteins is widely used in pharmaceutical and medical application, with elastin, calmodulin and leucine zipper being the most prominent protagonist[118]. The gelation process of GST fusion protein, however, is poorly understood, especially after mild denaturation with a reducing agent DTT, which has been reported as being essential for hydrogel formation of lysozyme at 20 mM DTT concentration and neutral pH. It was shown that at low mM protein concentration lysozyme uses its reduced thiol groups in order to aggregate into fibrils forming solid hydrogels after 5 min of 85°C heating[109]. Judging from the SDS-PAGE (**Fig. III 1c**) applying denaturing and non-denaturing sample preparation conditions reduction with DTT during protein preparation does not interfere with the dimerization ability of the GST-tag or to form even higher aggregates via intermolecular disulfide bridges or other physical interactions. (**Fig. III 1a**). Additional over night heating at 37°C or more fosters the formation of higher aggregates (**Fig. III 1c**) rendering the proteinous hydrogel more compact resulting

in drastically decrease of water signal in 1D ^{1}H NMR spectra in all investigated GST fusion protein samples.

When examining small proteins (<5 kDa) solid phase synthesis (SPS) can be used for protein production. Large peptide libraries are easily synthesized in sufficient amounts. Nevertheless correct folding of the polypeptides is challenging especially when co-factors or chaperones are required. Moreover putatively interesting small target proteins for screening processes in pharmaceutical or biomedical application may contain a high degree of cysteines, which are difficult to process and to judge whether they are involved in disulfides or reduced or even coordinating metal ions. GST fusion proteins may be isolated from any organism carrying a variety of modifications and folds, which are not expected to interfered with the reducing conditions described here, rendering the GST fusion protein system more versatile and appropriate as substitute for the native protein. A convenient technique to probe proper folding is heteronuclear NMR. With the routine usage of automated assignment strategies such as UNIO ^{15}N and/or ^{13}C resolved NMR spectra have gained importance in analyzing folding conditions and ultimately in obtaining NMR solution structures of the target protein[40-42] Heteronuclear [^{15}N,^{1}H] HSQC NMR spectra of GST fusion proteins have already been reported in the literature[117], including protein expression amelioration method utilizing pCOLD-GST vectors systems[119]. New, however, is the finding that the target protein linked to the GST can be observed and analyzed by 2D [^{1}H,^{1}H] TOCSY NMR and 2D [^{1}H,^{1}H] NOESY NMR spectra, the key NMR experiment for NMR based protein structure solution[38]. Especially striking is the fact that the aliphatic region (**Fig. III 2a/b**) is so well resolved, providing information upon the spatial contact of amino acids side chains. These are of special interest for analyzing cis-trans isomerization of prolines[106] but more importantly on substrate/co-factorial binding pockets, which generally display a low proton density particularly of amino protons (H_N) examined in ^{15}N resolved 3D NMR experiments. Nonetheless residual signals of the GST fusion partner are witnessed in [^{1}H,^{1}H] NOESY NMR spectra resulting in a somewhat ambiguous assignment situation. Therefore ^{15}N resolved 3D TOCSY and NOESY NMR spectra have been recorded (**Fig. III 2c**) yielding identical NOE assignment and intensity patterns (**Fig. III 2d**) and hence equivalent NMR solutions structures of Zn_2- & Cd_2-form of γ-E_c-1 (**Fig. III 3b,c**). Surprising in this regard was the occurrence of 15% more NOEs in the 2D [^{1}H,^{1}H] NOESY NMR spectra allowing to calculate the correct fold of the γ-E_c-1 domain without restraining the proton devoid metal center (**Fig. III 3a**), which was not possible for the isolated γ-E_c-1 domain. This raised the

question whether the GST fusion partner may have a stabilizing effect on the target protein. The additionally found NOEs point to a stabilization of the *C*-terminus, albeit the GST-tag is fused *N*-terminally. The higher amount of well resolved NOEs might arise from the anticipated lack of interaction amongst the protein molecules in the hydrogel network, avoiding transient dimers or further destabilizing processes.

We believe that the hydrogel formation occurs during concentration of the GST fusion protein sample from low μM to mM concentration (**Fig. III 1**). Hence hydrogel formation has no relevance on optical or chiro-optical spectroscopy, where experiments are generally conducted at low μM protein concentration. Here non-colloidal monomeric structures (**Fig. III 1b**) are vital for accurate measurement in order to avoid Mie-scattering. Another aspect to consider are the aromatic amino acids of the GST fusion partner, which possess optical as well as chiro-optical absorption bands in the UV light and hence can overlap with those bands originating from the target protein. In addition optical and chiro-optical spectroscopy is generally employed to investigate interaction with chemical species under different physical conditions, relative to the properties of the native GST fusion protein. The resulting difference spectrum yield identical experimental results when compared with the isolated target protein (**Fig. III 4a**). Further advantages of the GST fusion system preparation method GHOST may arise from inhibiting target protein precipitation induced by altered experimental conditions.

III 6 Conclusion

The key to decipher cellular processes relies on the understanding of structure – function relationships. Proteins are of tremendous interest, both in natural science as well as pharmaceutical application. The need to develop fast and efficient processes, especially for target protein screening remains one of the great challenges in structural biology. The GST fusion protein system may foster this discovery process by providing a fast, cost-efficient alternative for structural and functional analysis of small proteins and their ligands or co-factors.

III 7 Acknowledgements

This work was supported by the Swiss National Science Foundation (SNSF Professorship to E.F.).

III 8 Supplementary Material

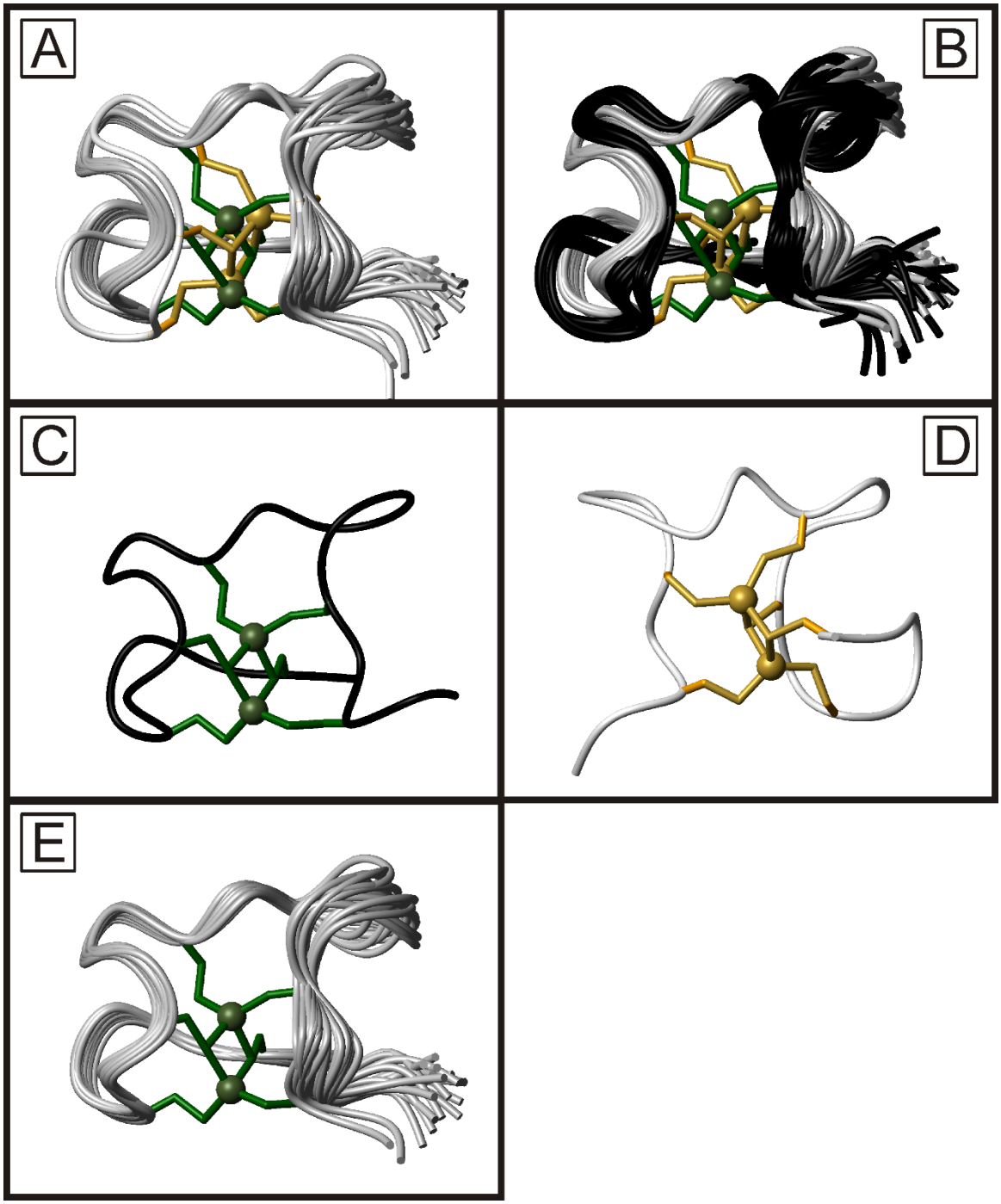

Figure III S 1 Comparison of Zn_2 GST-γ-E_c-1 with the isolated Zn_2γ-E_c-1 domain. ***A)*** Overlay of the 20 least energy structures of Zn_2 GST-γ-E_c-1 (grey ribbon, thiolates bonds green, Zn^{II} ions green spheres) with the average structure of the isolated Zn_2γ-E_c-1 domain (grey ribbon, thiolates bonds yellow, Zn^{II} ions yellow spheres). ***B)*** Overlay of the 20 least energy structures of Zn_2 GST-γ-E_c-1

(black ribbon, thiolates bonds green, Zn^{II} ions green spheres) with the 20 lowest energy structures of the isolated $Zn_2\gamma$-E_c-1 domain (grey ribbon, thiolates bonds yellow, Zn^{II} ions yellow spheres). ***C)*** Lowest energy structure of Zn_2 GST-γ-E_c-1 (black ribbon, thiolates bonds green, Zn^{II} ions green spheres). ***D)*** Lowest energy structure of $Zn_2\gamma$-E_c-1 (grey ribbon, thiolates bonds yellow, Zn^{II} ions yellow spheres). ***E)*** The 20 least energy structures of Zn_2 GST-γ-E_c-1 (grey ribbon, thiolates bonds green, Zn^{II} ions green spheres)

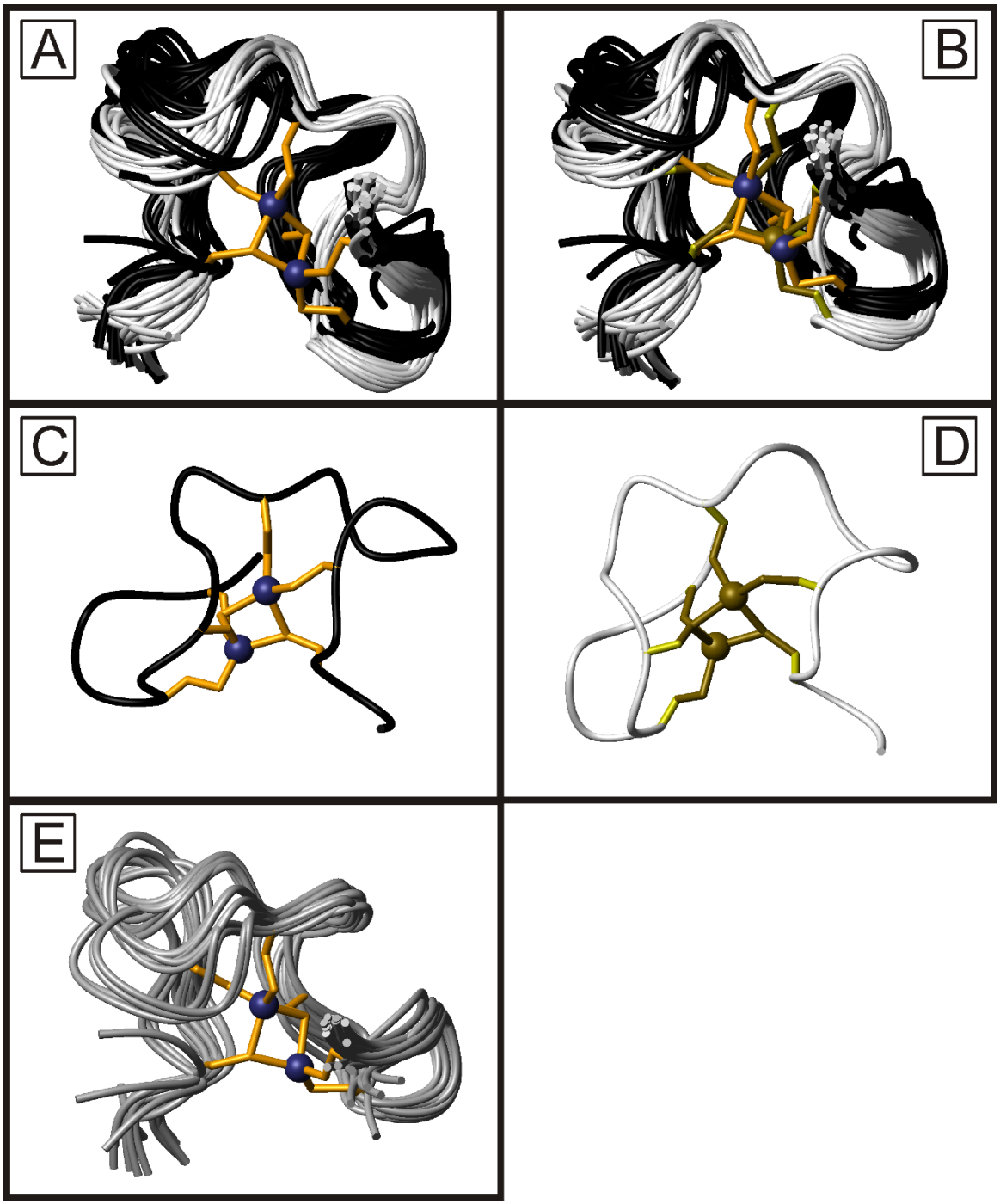

Figure III S 2 Comparison of Cd_2 GST-γ-E_c-1 with the isolated Cd_2γ-E_c-1 domain. ***A)*** Overlay of the 20 least energy structures of Cd_2 GST-γ-E_c-1 (black ribbon, thiolates bonds yellow, Cd^{II} ions blue spheres) with the 20 lowest energy structures of the isolated Cd_2γ-E_c-1 domain (grey ribbon). ***B)*** Overlay of the 20 least energy structures of Cd_2 GST-γ-E_c-1 (black ribbon, thiolates bonds yellow, Cd^{II} ions green spheres) with the 20 lowest energy structures of the isolated Zn_2γ-E_c-1 domain (grey ribbon, thiolates bonds green, Cd^{II} ions green spheres). ***C)*** Lowest energy structure of Cd_2 GST-γ-E_c-1 (black ribbon, thiolates bonds yellow, Cd^{II} ions blue spheres). ***D)*** Lowest energy structure of Cd_2γ-E_c-1 (grey ribbon, thiolates bonds green, Cd^{II} ions green spheres). ***E)*** The 20 least energy structures of Cd_2 GST-γ-E_c-1 (grey ribbon, thiolates bonds yellow, Cd^{II} ions blue spheres).

Table 1 Statistics of structure calculations:

	Cd3*	Cd21*	Cd3* GST	Cd21* GST	Cd** GST	Zn3*	Zn21*	Zn3* GST	Zn21* GST
NMR distance restraints									
Total NOE	374	372	427	423	430	462	463	480	479
Short range: |i−j|≤1	322	321	375	378	378	396	395	433	432
Medium range: 1>|i−j|>5	61	58	61	56	56	69	70	54	57
Long range: |i−j|≥5	15	13	32	26	26	20	20	23	28
Maximal distance restraint violation (Å)	0.11	0.11	0.15	0.22	0.20	0.11	0.19	0.13	0.11
AMBER energies (kcal/mol)									
Total (mean±SD)	−679 ± 76	−711 ± 43				−697 ± 70	−693 ± 75		
van der Waals	−14 ± 4	−7 ± 5				−12 ± 5	−12 ± 6		
RMSDs from idealized geometry									
Bond lengths (Å)	0.0142 ± 0.0002	0.0138 ± 0.0002				0.0136 ± 0.0002	0.0142 ± 0.0002		
Bond angles (°)	2.15 ± 0.06	2.03 ± 0.06				1.94 ± 0.06	2.42 ± 0.06		
Ramachandran plot statistics (%)									
Residues in most favored regions	80.9	70.9	56.2	65.9	66.5	74.4	69.4	62.6	57.1
Residues in additionally allowed regions	18.2	28.5	40.6	33.5	32.6	24.7	28.5	27.4	42.9
Residues in generously allowed regions	0.9	0.6	3.2	0.6	0.9	0.9	1.8	0	0

Residues in disallowed regions	0	0	0	0	0	0	0.3	0	0
RMSDs from the mean coordinates (Å)									
N, Cα, and C′ of residues 2-22	0.70±0.14	0.69 ± 0.33	0.80 ± 0.40	0.80 ± 0.40	2.10 ± 1.05	1.47 ± 0.66	0.97 ± 0.25	1.22 ± 0.26	1.00 ± 0.41
Heavy atoms of residues 2-22	1.37±0.26	1.45 ± 0.37	1.30 ± 0.40	1.30 ± 0.40	2.67 ± 1.19	2.02 ± 0.60	1.54 ± 0.27	1.87 ± 0.34	1.58 ± 0.48

* The number describes the residue that presents the second bridging Cys moiety (in addition to Cys-9; see text). The numbering and metal cluster features are detailed in[106].

Chapter IV : Spectroscopic studies on the γ-E_c-1 domain, a Zn_2Cys_6 zinc finger motive containing metallothionein

Jens Loebus · Katzyarina Tarasava · Silke Johannsen · Eva Freisinger*

Jens Loebus, Katzyarina Tarasava, Silke Johannsen, Eva Freisinger (✉)

Institute of Inorganic Chemistry, University of Zurich,

8057 Zurich, Switzerland

*e-mail: freisinger@aci.uzh.ch

IV 1 Abstract

Conveniently assessing metallation pathways of metalloproteins has been a long thought dream for spectroscopists and bio-inorganic chemists. For studying especially iron, copper, molybdenum, and manganese proteins a multitude of experimental methods were invented and applied. Zn^{II} containing enzymes representing the most diverse class of metalloproteins, however remained challenging system owing to both, the inherent spectroscopic silence of the closed shell metal ion and the predominant sulfur ligands. Structural and functional characterization of metallothioneins (MTs) constitute a perfect example. We have chosen the γ-domain of E_c-1 from bread wheat, a 25 amino acids long MT, in which six cysteine residues coordinate two M^{II} ions in a tetrahedral tetrathiolate fashion, in order to show that the evaluation of simple UVvis-spectra is sufficient to understand the metallation pathway and the resulting Zn_2- and Cd_2-cluster. Such a $M^{II}_2Cys_6$ metal cluster is also present in GAL4 like zinc finger transcription factors extending the scope of the work. We recorded UVvis-, CD-, and MCD spectra to distinguish the contributions from terminal and bridging cysteines. Presumably this approach should be extendable to more complex systems with different ligands greatly facilitating structural and functional characterization of Zn^{II} binding proteins.

Keywords: Zn^{II} binding proteins · Metallothionein · Electronic absorption spectroscopy · CD spectroscopy · MCD spectroscopy · Metal cluster

IV 2 Introduction

Most cellular processes require metalloproteins owing to their diverse structural motives derived from the organic envelope, and their catalytic potency conveyed through the inorganic metal ion core. While iron is the most abundant metal ion especially important for electron transfer and generally redox reactions, zinc is the most diversely employed metal ion facilitating a myriad of cellular processes including hydrolysis reactions or intracellular pH regulation, and provides functionality in case of e.g. protein-DNA recognition[120]. Zn^{II} coordinating donor atoms provided by the protein backbone can be either oxygen, nitrogen, or sulfur. The nature of the ligand has been correlated to the function of the zinc-binding site[121]. While oxygen ligands afforded as carboxylates from aspartates or glutamates or as alcohols from serines or threonines are found in catalytic zinc sites fostering the Lewis acid character of the Zn^{II} ions enabling e.g. substrate activation, peptide and imidazole nitrogens and more importantly cysteinyl thiolates as ligands constitutes structural Zn^{II} sites[122]. Especially tetrahedral tetrathiolate coordination of Zn^{II} is associated with stabilization of specific protein folds and witnessed in proteins involved in Zn^{II} homeostasis or regulation of transcription. A super-family of metalloproteins embedding tetrahedral tetrathiolate Zn^{II} metal ion clusters are metallothioneins (MTs) – ubiquitously expressed small (<10 kDa) cysteine-rich (<33 %) polypeptides[12]. Generally they are considered to be involved in Zn^{II} sensing and storage[65] and in some organisms also involvement in Cu^{I} homeostasis is described[6, 123]. Recent studies report specific bacterial and plant MTs to contain Zn^{II} centers evidenced in zinc-finger type transcription factors[7, 9, 106], highlighting the diversity of metallothionein fold. In these MTs the metal ion center is identical to those of transcription factors, including GAL4, that confer stability to structural motives responsible for nucleic acid recognition. The most prominent MT in this regard is E_c-1, a Zn^{II}-containing protein from the bread wheat *Triticum aestivum*. Taxonomically classified based on its primary amino acid sequence as a pec MT of the plant MT family 15[3], E_c-1 comprises 82 amino acids including 17 cysteines and 2 histidines, which coordinate up to 6 d^{10} metal ions i.e. Zn^{II} or Cd^{II} in two protein domains. The structure of the larger β_E-domain yielded a $M^{II}_3Cys_9$ metal cluster as well as a mononuclear $M^{II}Cys_2His_2$ metal center similar in constitution and fold to zinc knuckle transcription factors[9]. The smaller γ-E_c-1 domain contains a GAL4 like, Zn_2Cys_6 zinc finger motive, which has been structurally assessed as Zn_2- and Cd_2-form evidencing an almost isostructural

fold for both metal ions[106] (see **Chapter III** and **V**)) and provides the basis for further metallation studies.

Investigating kinetic and thermodynamic properties of tetrahedral tetrathiolate d^{10} metal ion binding sites in proteins still challenges spectroscopists, owing to the spectroscopical inaccessibly of the Zn^{II} ion complexed by the oxidation prone thiolate ligands and the dynamic of the enclosing protein backbone[59, 122]. From a structural perspective both X-ray crystallography and NMR provide high-resolution information concerning the metal centers, but require well-defined sample conditions resulting from time consuming but not necessary successful trial and error processes. Moreover these methods only yield snapshots of both a thermodynamically and kinetically optimized state at non-physiological conditions, rendering observation of energetically less preferred but biochemically more relevant processes impossible. A multitude of methods have been employed to overcome these limitations mostly relying on either optical or chiro-optical properties of the metalloproteins. Concerning accessibility and convenience UVvis absorption spectroscopy represents the method of choice in order to quickly assess biological properties. Major problems when interpreting UVvis spectra of Zn^{II}-binding proteins arise from the spectral overlap of the relevant absorption bands in the far UV and the lack of theoretical knowledge of their origin[45]. In case of thiolate-rich binding sites isostructural Cd^{II} substitution of Zn^{II} yields UVvis bands that are red-shifted and hence can be better separated from spectral contributions of the protein backbone. Additionally use of the ^{113}Cd isotope offers the opportunity to follow the metallation process via heteronuclear NMR spectroscopy[106] (see **Chapter V**). To understand the metallation pathway and the resulting tetrahedral tetrathiolate M^{II} cluster, it is vital to distinguish terminal (M^{II}-S-Cys) from bridging (Cys-S-M^{II}-S-Cys) cysteines. A semi-empirical theoretical framework developed for transition metal ions coordinated tetrahedrally by halides was extended to tetrathiolate sites in order to predict the energy level of the 1st absorption band assigned to the ligand to metal charge transfer (LMCT) band of the terminal thiolate ligand (Zn: 232 nm Cd: 249 nm)[45, 106, 124]. Despite the fact that these energy levels indeed *grosso modo* match the first transition band observed in MTs, no detailed account of the exact contributions of the thiolate or the group 2b metal ion could be provided. In addition to efforts elucidating the molecular origin of the absorption bands studies determining the molar extinction coefficient (ε) of the (M^{II}-S-Cys) band were conducted in several metallothioneins and rubredoxins, the later affording a mononuclear tetrahedral tetrathiolate binding site. For terminal cysteines coordinating to Cd^{II} ions a $\varepsilon = 5000\ M^{-1}\ cm^{-1}$ was

determined[125], which agrees well with most of the Cd^{II} tetrahedral tetrathiolate binding sites reported[44], yet neglects the contributions of bridging cysteines. Recent computational studies of protein embedded zinc-thiolate metal cluster structures[126] and lead-thiolate clusters[127] provide a promising approach towards unrevealing their spectral properties. Moreover they constitute the starting point of our investigation aiming to **i**) provide photospectroscopical data of the Zn^{II} and Cd^{II} (de)metallation as well as Zn^{II} /Cd^{II} substitution of the simplest well studied bi-nuclear tetrahedral tetrathiolate cluster ($M^{II}_2Cys_6$); **ii**) render chiro-optical and magnetically induced polarimetric features available for elucidating the Zn^{II} and Cd^{II} de- and re-metallation pathways.

IV 3 Material and methods

IV 3 1 Chemicals, solutions, plasmids and proteins

All chemicals were ACS grade or comparable. Solutions were prepared using double distilled and filtered water, which was further filtered, degassed and depending on the experiment either nitrogen or argon saturated and, if strictly anaerobic conditions were required, three times freeze-thawn under vacuum. The pGEX_γ-E_c-1 plasmid was engineered based on the pGEX-4T1 expression vector and the γ-E_c-1 with as *N*-terminal GST-tag as fusion protein expressed and purified as previously described[106] resulting in the amino acid sequence of the γ-E_c-1 domain:

GS GCDDKCGCA VPCPGGTGC RCTSAR

All protein preparation steps following purification of the protein were conducted in a nitrogen purged glove box (Coy Labs, Grass Lake, USA).

IV 3 2 Preparation of apo-, Zn_2-, Cd_2γ-E_c-1 for spectroscopic titrations

For all spectroscopic experiments the apo-protein was completely reduced with 0.1 M DTT, demetallated in 10 mM HCl, and purified directly prior to re-metallation with size exclusion chromatography (SEC: Superdex Peptide 10/300 GL) using 10 mM HCl as running buffer. Following 30 min of argon bubbling apo-γ-E_c-1 was either used for metal ion titrations of the apo-protein or metallated with exactly 2 equivalents of Zn^{II} or Cd^{II}, respectively. The pH and desired protein concentration (25 μM) was adjusted using 10 mM NaCl and 10 mM Tris/HCl pH 7.2, 8 or 8.9. Finally the γ-E_c-1 concentration was determined via quantification of –SH groups, employing the 2-PDS assay[43] and correlated with M^{II} concentration, quantified by flame atomic absorption spectroscopy (F-AAS) before and after γ-E_c-1 metallation, if applicable[106].

IV 3 3 Metal ion titration of apo-γ-E_c-1 followed by UVvis-, CD-, and MCD spectroscopy

Freshly prepared argon-saturated apo-γ-E_c-1 dissolved in 10 mM HCl was adjusted to a protein concentration of around 25 μM in 10 mM Tris/HCl, pH 8, and 10 mM NaCl giving a final volume of 1.8 mL. The protein solution was transferred into a 1-cm path-length septum

sealed cuvette, and the Zn^{II}- or Cd^{II} solution was stepwise titrated to the γ-E_c-1 solution in 1 µl steps (~0.17 eq. M^{II}) using a 25 µl Hamilton syringe. After each metal ion addition UVvis- (Cary 500 UV-VIS-NIR spectrometer), CD- and MCD spectra (J-810 spectropolarimeter - JASCO, Japan) were collected. Subsequently, the protein concentration was determined via the 2-PDS assay and the metal ion concentration with F-AAS in order to recalculate the MT concentration and the amount of metal ions added. Changes in MT concentration measured before and after the titrations were minor as were the values of the amount of metal ions added. For all samples the monomeric character of the metallated γ-E_c-1 species was verified via size exclusion chromatography (SEC).

IV 3 4 Metal exchange titration of Zn_2γ-E_c-1 with Cd^{II} followed via UVvis-, CD-, and MCD spectroscopy

Freshly prepared Zn_2γ-E_c-1 was adjusted to protein concentration of around 25 µM in 10 mM Tris/HCl, pH 7.2 or 8.9, respectively and 10 mM NaCl to a final volume of 1.8 mL. After transfer of the protein solution into a 1-cm path-length septum sealed cuvette a 4 mM Cd^{II} solution was stepwise titrated to the Zn_2-γ-E_c-1 solution in 1 µl steps (0.33 eq. M^{II}) using a 25 µl Hamilton syringe followed by UVvis-, CD- and MCD spectroscopy. Post-titration analysis of concentrations was conducted as stated above.

IV 3 5 pH titrations followed by UVvis and CD spectroscopy

Zn_2 and Cd_2 metallated γ-E_c-1 species diluted to ca 30 µM protein concentration in 10 mM NaCl, 10 mM Tris/HCl pH 8.9 were titrated with 1, 0.1 and 0.01 M HCl as described[61]. Plots of molar absorptivity at 230 nm for the Zn^{II} forms and at 250 nm for the Cd^{II}-loaded species against pH were fitted with the program Origin 8.0 (OriginLab, Northampton, MA, USA) using two different functions, considering either one or two common apparent pK_a values for the Cys residues in the presence of the respective metal ions as described[61, 68].

IV 4 Results

IV 4 1 Spectroscopic features of Cd^{II} and Zn^{II} metallation of apo-γ-E_c-1

To exclude experimental bias originating from sample preparation all metal ion titrations were performed with just a single sample, respectively, i.e., the apo-protein was transferred into a septum-closed cuvette, an incremental amount of Zn^{II} or Cd^{II} was added with a syringe and subsequently UVvis-, CD-, and MCD spectra were recorded. Metal addition was repeated until no further changes in the spectra were observed. **Fig. IV 1a** shows the absorption envelopes of the apo-form as well as Zn^{II} and Cd^{II} forms of γ-E_c-1. The absorption bands originating from metal ion binding to the protein thiolate groups can be visualized and analyzed most efficiently by plotting the difference spectra, i.e. by subtracting the spectra of the apo-protein from each spectrum (**Fig. IV 1b,e**). In case of the titration with Cd^{II} ions the metal-derived absorption envelope starts to evolve at 280 nm and shows a maximum at 227 nm. The subtraction of the succeeding from the preceding UVvis spectra resolves at least three major bands located at 227 nm, 242 nm and, 257 nm (**Fig. IV 1c**). Up to the addition of 1.1 eq. Cd^{II} the dominant band is centered around 227 nm with a shoulder at 242 nm, with the later increasing in intensity until 1.45 eq. of Cd^{II}. The relative extinction coefficient per eq. Cd^{II} drops from ε_{227nm} = 22'500 M^{-1} cm^{-1} to 18'000 M^{-1} cm^{-1}. A pronounced alteration of the absorption envelope is evidenced after 1.45 eq. Cd^{II} with a new electronic transition arising at 259 nm, the diminishing of the band at 242 nm, and the decrease in ε_{227nm} to 9'000 M^{-1} cm^{-1} (at 1.8 eq. Cd^{II}). The extinction coefficient at 250 nm usually used for quantifying Cd^{II}-cysteine coordination does not correspond to a major band, however qualitatively reproduces the changes at 227 nm (**Fig. IV 1d**) with ε_{250nm} at one eq. Cd^{II} of 14'500 M^{-1} cm^{-1} and at two eq. Cd^{II} of 21'000 M^{-1} cm^{-1} as previously reported[106]. The tendency, that after addition of one eq. of Cd^{II} 2/3 of the max. extinction coefficient at 227 nm is reached, is also reflected in the MCD spectra (**Fig. IV 4**). Zn^{II} and Cd^{II} ions coordinating to thiolate ligands show characteristic magnetically induced chirality bands assigned to degenerated energy levels in the metal thiolate center. The evolution of this bands originating from magnetic induced molar ellipticity allows to unambiguously investigate the metal ion binding processes, excluding major contribution of the protein backbone. The dominant band in the MCD spectrum of Cdγ-E_c-1 at 252 nm decreases steeply in magnetically induced chirality until 0.75

eq. Cd^{II} (θ_M per eq. Cd^{II} 160'000 deg^1 $dmol^{-1}$ cm^2 T^{-1}) and less pronounced until 1.6 eq. Cd^{II} (θ_M per eq. Cd^{II} 105'000 deg^1 $dmol^{-1}$ cm^2 T^{-1}), where the signal is saturated (**Fig. IV 4a-d**). Due to the indigent non-degeneracy of Cd-MT ground states[128] this band is part of an *A*-term, characterized by a di-phasic band[129].

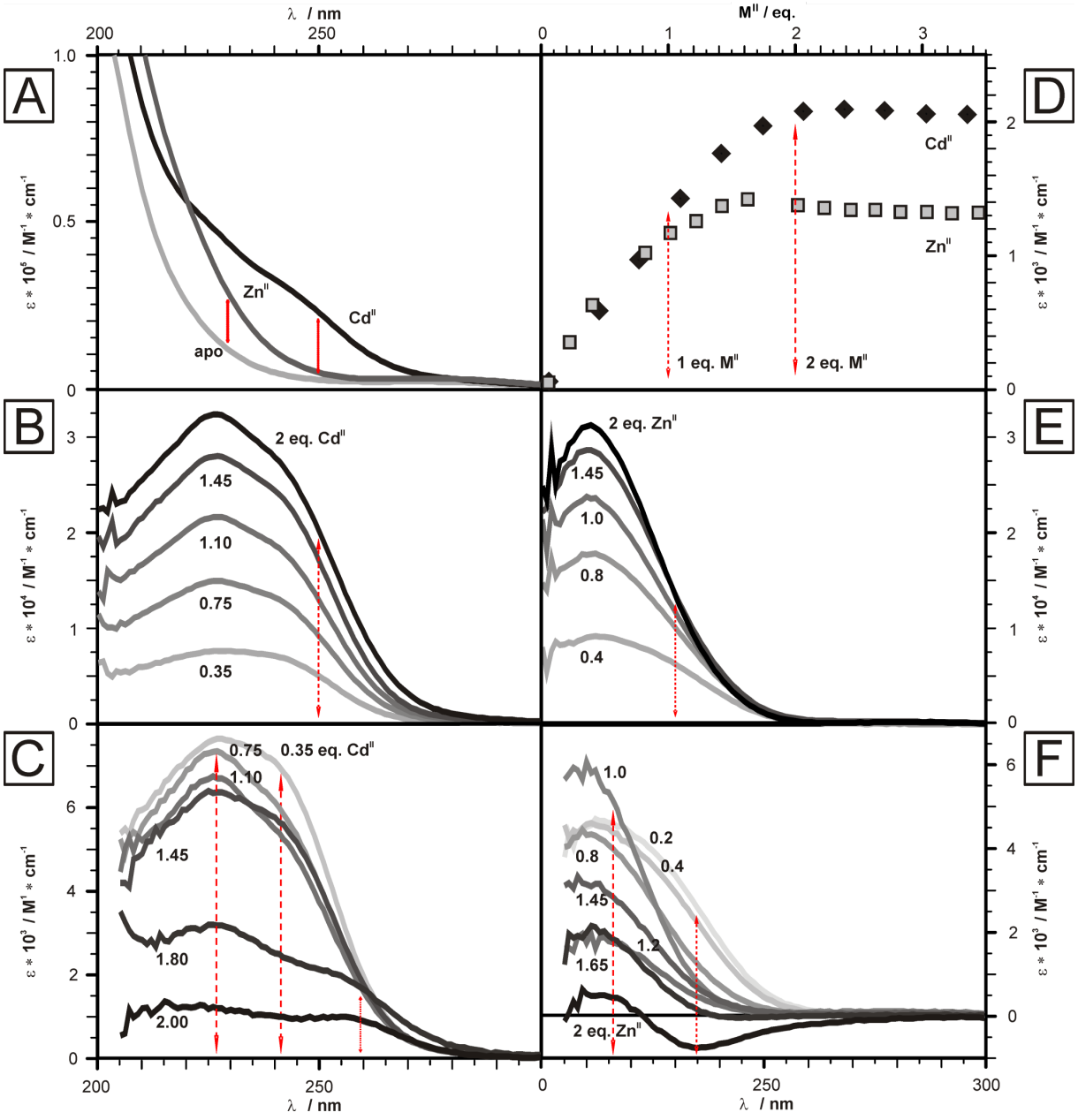

Figure IV 1 Metal ion titration studies of apo-γ-E_c-1 with Zn^{II} and Cd^{II} followed by UVvis spectroscopy. ***A)*** UVvis spectra of apo-γ-E_c-1 (light grey line), Zn_2- (dark grey line) and Cd_2γ-E_c-1 (black line). The red arrow indicates the maximum of the LMCT band at 230 nm and 250 nm, respectively. ***B)*** Difference spectra of the titration of apo-γ-E_c-1 with Cd^{II} ions obtained by subtracting

the apo-γ-E_c-1 absorption envelope from all other spectra (grey to black lines). The red arrow indicates 250 nm. ***C)*** Delta spectra of the titration shown in *(B)*. Each absorption spectra was subtracted from the previous. The respective Cd^{II} equivalents are labelled (increasing: grey to black lines) and the observed bands at 227 nm, 241 nm and 259 nm are marked with red arrows errors. ***D)*** Plot of molar absorptivity against equivalent of metal ions added for the titration of 25 μM apo-γ-E_c-1 with increasing amounts of Zn^{II} (grey squares) or Cd^{II} (black diamonds). While the molar absorptivity for the Cd^{II}-form levels out at ε = 21'000 M^{-1} cm^{-1} at exactly two Cd^{II} equivalents, for the Zn^{II}-form the maximum $\varepsilon_{230\ nm}$ = 14'000 M^{-1} cm^{-1} is reached at 1.6 equivalents. The red arrows indicate one and two equivalents of M^{II} added. ***E)*** In analogy to the Cd^{II} titration experiment, difference spectra of the Zn^{II} titration obtained by subtracting the apo-γ-E_c-1 absorption envelope from all other spectra (grey to black lines). The red error indicates 230 nm. ***F)*** Delta spectra of the Zn^{II} titration displayed in accordance to the Cd^{II} delta spectra (C). Absorption bands at 217 nm and 234 nm are indicated with red arrows.

More thorough evaluation of the metallation pathway by subtracting succeeding from preceding MCD spectra revealed Faraday effect induced bands at around 234 nm, 243 nm and 255 nm, all of which have an *A*-term shape (**Fig. IV 4c**). While both UVvis and MCD spectroscopy provide predominately information on the nature and number of bonds, CD spectroscopy render information on the geometry of the metal center available and thus also on rearrangement processes (Fig. IV 2). Zn^{II} and Cd^{II} ions show characteristic chirality bands assigned to the thiolate metal ion center. The evolution of the molar ellipticity envelope allows to investigate the metal ion binding processes, assuming that no further rearrangements occur once the MT is completely metallated. The final CD spectra is then indicative for the number of metal ions and the cluster arrangement in which the metal ion are bound. In particular Cd^{II}-thiolate cluster formation in MTs is proposed to be associated with dipolar excitonic splitting resulting in a di-phasic band[44, 130]. In case of Cd_2γ-E_c-1 ellipticity envelope originates from at least three bands centered at 225 nm, 242 nm and 257 nm. The two higher energy bands may be classified as absorption like shaped bands, while the band at 257 nm might show an excitonic character (**Fig. IV 2a-d**).

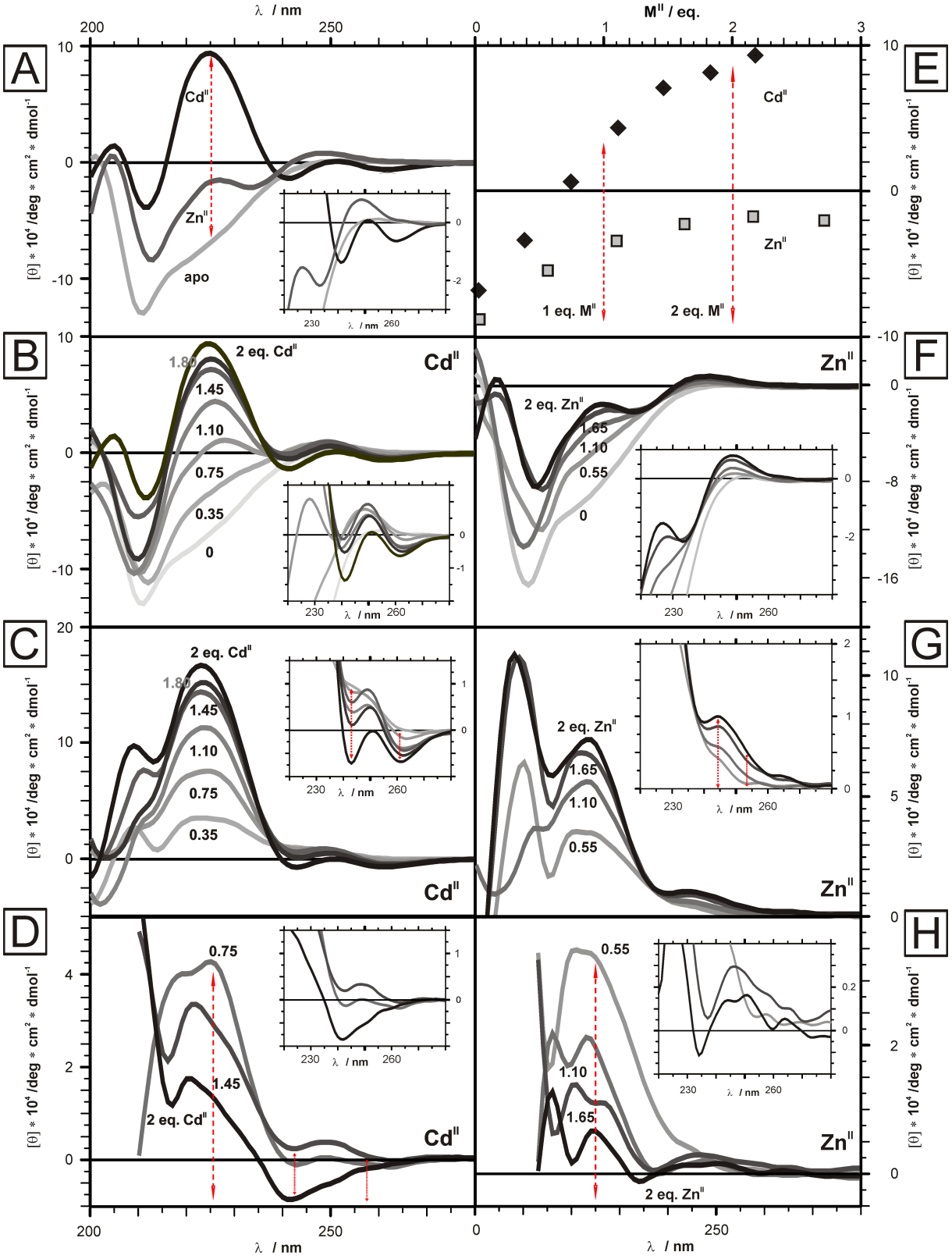

Figure IV 2 Metal ion titration studies of apo-γ-E_c-1 with Zn^{II} and Cd^{II} followed by CD spectroscopy. ***A)*** CD spectra of apo-γ-E_c-1 (light grey line) Zn_2- (dark grey line) and Cd_2γ-E_c-1 **(**black line). The red arrow at 225 nm indicates the wavelength used to evaluated metal ion incorporation, hence metal cluster formation. ***B)*** Spectra of apo-γ-E_c-1 titration with increasing amounts of Cd^{II} (grey to black). A

close up on the region between 220 nm and 280 nm is displayed in the inset. ***C)*** Difference spectra of the Cd^{II} titration obtained by subtracting the spectra of the apo-γ-E_c-1 from all other spectra (grey to black lines). A close up on the region between 220 nm and 280 nm is displayed in the inset. ***D)*** Delta spectra of the Cd^{II} titration. Each absorption spectrum was subtracted from the previous. Inset and style are as described in *(C)*. The red arrows indicate the different transition bands at 225 nm, 242 nm and 247 nm. ***E)*** The increase of molar ellipticity at 225 nm for Zn^{II} (grey squares) and Cd^{II} (black diamonds) is depicted as function of the M^{II} equivalents added. For both Zn^{II} and Cd^{II} no change in ellipticity is observed after addition of 2.2 equivalents of metal ions ($\theta_{max,225\ nm}$ (Cd) = 170'000 deg^1 $dmol^{-1}$ cm^2, $\theta_{max,225\ nm}$ (Zn)= 70'000 deg^1 $dmol^{-1}$ cm^2). ***F)*** CD spectra of the Zn^{II} titration of apo-γ-E_c-1 (grey to black lines). ***G)*** Difference spectra of the Zn^{II} titration obtained by subtracting the apo-γ-E_c-1 spectra from all other spectra (grey to black lines). ***H)*** Delta spectra of the Zn^{II} titration. Each absorption spectrum was subtracted from the previous.

In agreement with both UVvis- and MCD spectra after one eq. of Cd^{II} 2/3 of the band intensity at 225 nm is observed (θ = 110'000 deg^1 $dmol^{-1}$ cm^2; after two eq. Cd^{II} θ = 165'000 deg^1 $dmol^{-1}$ cm^2).

The Zn^{II} metallation pathway of γ-E_c-1 is spectroscopically more difficult to assess owing to its higher energy transitions. In UVvis absorption spectra two bands at 216 nm and 235 nm have been identified (**Fig. IV 1e-f**). During the addition of the first Zn^{II} equivalent the band at 235 nm is dominant and increases steadily with ε_{235nm} = 8'000 M^{-1} cm^{-1} per eq. Zn^{II} until one eq. Zn^{II} is added. During the addition of the second Zn^{II} eq. a steady decreases in intensity per Zn^{II} equivalent supplied is witnessed until at 1.8 eq. of Zn^{II} a negative band shape is observed (**Fig. IV 1f**), yielding an overall extinction coefficient for this band of ε_{235nm} = 4'500 M^{-1} cm^{-1} per eq. Zn^{II} (after the addition of two Zn^{II} eq.). The second electronic transition observed in the UVvis spectra during Zn^{II} addition occurs at 216 nm. The band increases to ε_{216nm} = 22'000 M^{-1} cm^{-1} after one eq. of Zn^{II} and levels off to ε_{216nm} = 28'000 M^{-1} cm^{-1} when two eq. of Zn^{II} are added. Generally the wavelength considered as indicative for Zn^{II}-tetrathiolate formation is 230 nm. When plotting the amount of incorporated Zn^{II} equivalents against ε_{230nm} after one eq. of Zn^{II} already 81% of Zn^{II}-S-Cys bonds are established (ε_{230nm} = 11'500 M^{-1} cm^{-}

[1]) with no further Zn^{II}-S-Cys bond formation evidenced after two or more equivalents (ε_{230nm} = 14'200 M^{-1} cm^{-1}) of Zn^{II} supplementation. The dominant increase in electronic absorptivity at 230 nm during the first Zn^{II} equivalent is in agreement with the observed increase of chirality at 225 nm (**Fig. IV 2e-h**) as judged by CD spectroscopy.

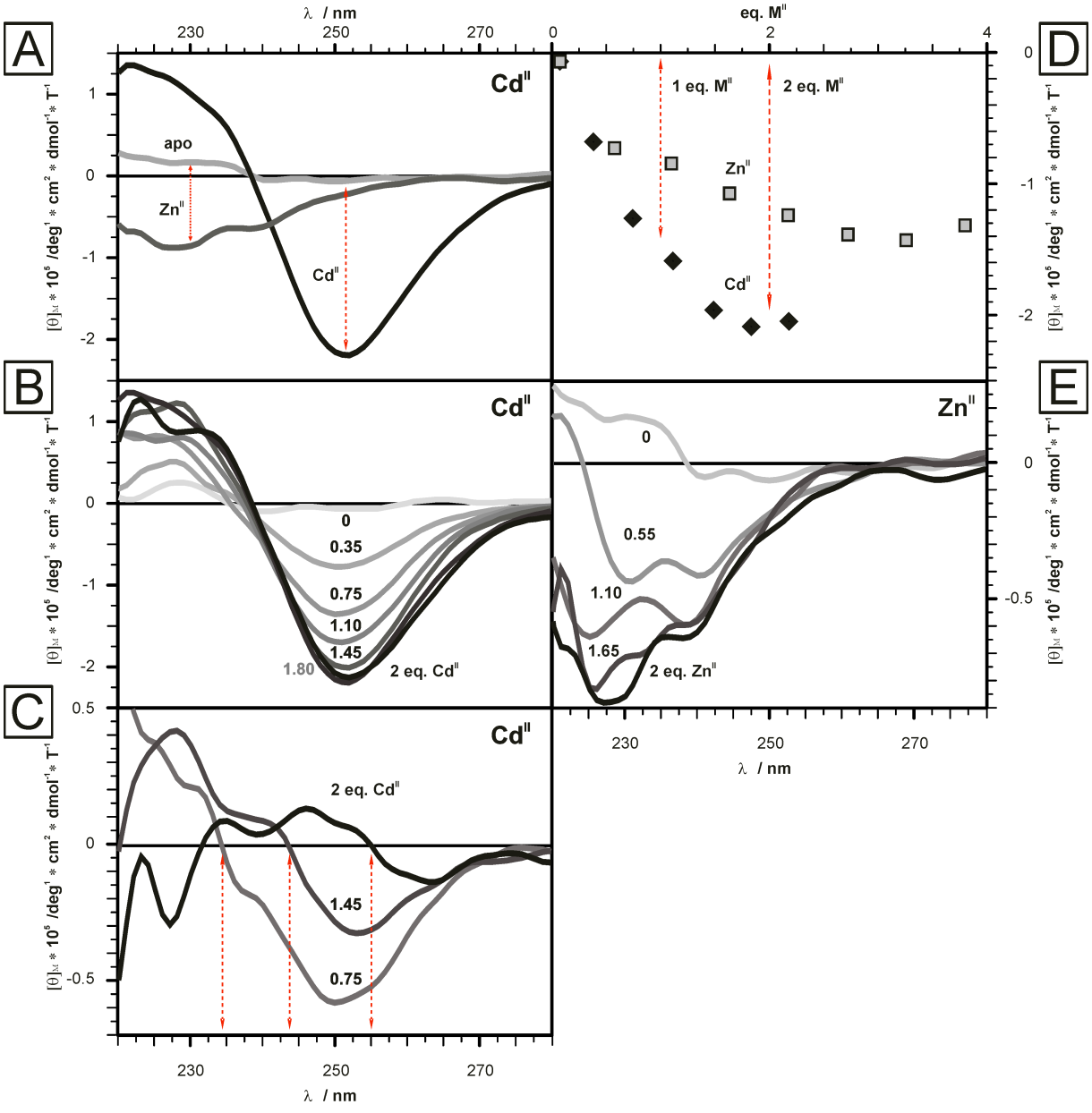

Figure IV 3 Metal ion titration studies of apo-γ-E_c-1 with Zn^{II} and Cd^{II} followed by MCD spectroscopy. ***A)*** apo-γ-E_c-1 (light grey line) Zn_2 (dark grey line) and Cd_2γ-E_c-1 (black line). The red arrow indicates the wavelength used to evaluate metal ion incorporation (Zn^{II}: 230 nm, Cd^{II}: 252 nm). ***B)*** Spectra of subsequently added Cd^{II} equivalents to apo-γ-E_c-1 (apo-γ-E_c-1: light grey line – Cd_2γ-E_c-1: black line). ***C)*** Delta spectra of the Cd^{II} titration. Every second MCD spectra was subtracted from

the previous. Style as described in (*C*). The red arrows indicate the different infection points of the A-term transition bands at 234 nm, 243 nm and 255 nm. ***D)*** The increase in magnetically induced molar ellipticity for Zn^{II} (at 230 nm: grey squares) and Cd^{II} (at 252 nm: black diamonds) is depicted as function of the M^{II} equivalents added. The band at 252 nm assigned to Cd^{II}-S bond formation increases until 1.8 equivalents with θ_M = 210'000 deg^1 $dmol^{-1}$ cm^2 T^{-1}. In case of the Zn^{II}-form the magnetic ellipticity levels around 3 Zn^{II} equivalents with θ_M = 140'000 deg^1 $dmol^{-1}$ cm^2 T^{-1}, yet the magnetic ellipticity increases only by 8 % from 2 to 3 Zn^{II} equivalents. ***E)*** In analogy to the Cd^{II} titration experiment, MCD spectra of the titration with increasing amount of Zn^{II}-ions (grey to black lines) are depicted.

The molar ellipticity θ_{225nm} = 55'000 deg^1 $dmol^{-1}$ cm^2 after addition of one eq. of Zn^{II} (77 %) levels out following the addition of the second Zn^{II} eq. (θ_{225nm} = 72'000 deg^1 $dmol^{-1}$ cm^2). The evolution of the MCD spectra during Zn^{II} supplementation *grosso modo* agrees with the findings of a dominant increase in signal after one equivalent of Zn^{II}, yet exact quantification is limited owing to intrinsically weak Faraday effect (**Fig. IV 3e**).

IV 4 2 Spectroscopic features of Zn/Cd exchange of γ-E_c-1

The substitution of Zn^{II} through Cd^{II} in the γ-E_c-1 yields a well-defined absorption envelope (280 nm – 210 nm) (Fig.). The absence of high-energy bands (>200 nm) originating from spin-forbidden n-π* of the amide bond indicate a comparable fold of both differently metallated forms[45]. The metal ion exchange is probed at pH 7.3 and 8.9 in order to access putative free thiolates, which may occur in transition states (**Fig. IV 4**). The apo-Zn^{II} and apo-Cd^{II} titrations, have shown that the absorption band between 280 nm and 235 nm, arising from Zn^{II} to Cd^{II} exchange titration, contain only information concerning the Cd^{II}-thiolate cluster formation, due to the lack of absorption bands in this spectra region for the apo-Zn^{II} titration. Until 225 nm the absorptivity of the Cd^{II}-thiolate cluster is much more pronounced than the one of the Zn^{II}-thiolate cluster (**Fig. IV 1**) allowing at least a semi-quantitative judgment of the Cd^{II}-thilolate contributions during Zn^{II} to Cd^{II} exchange titrations.

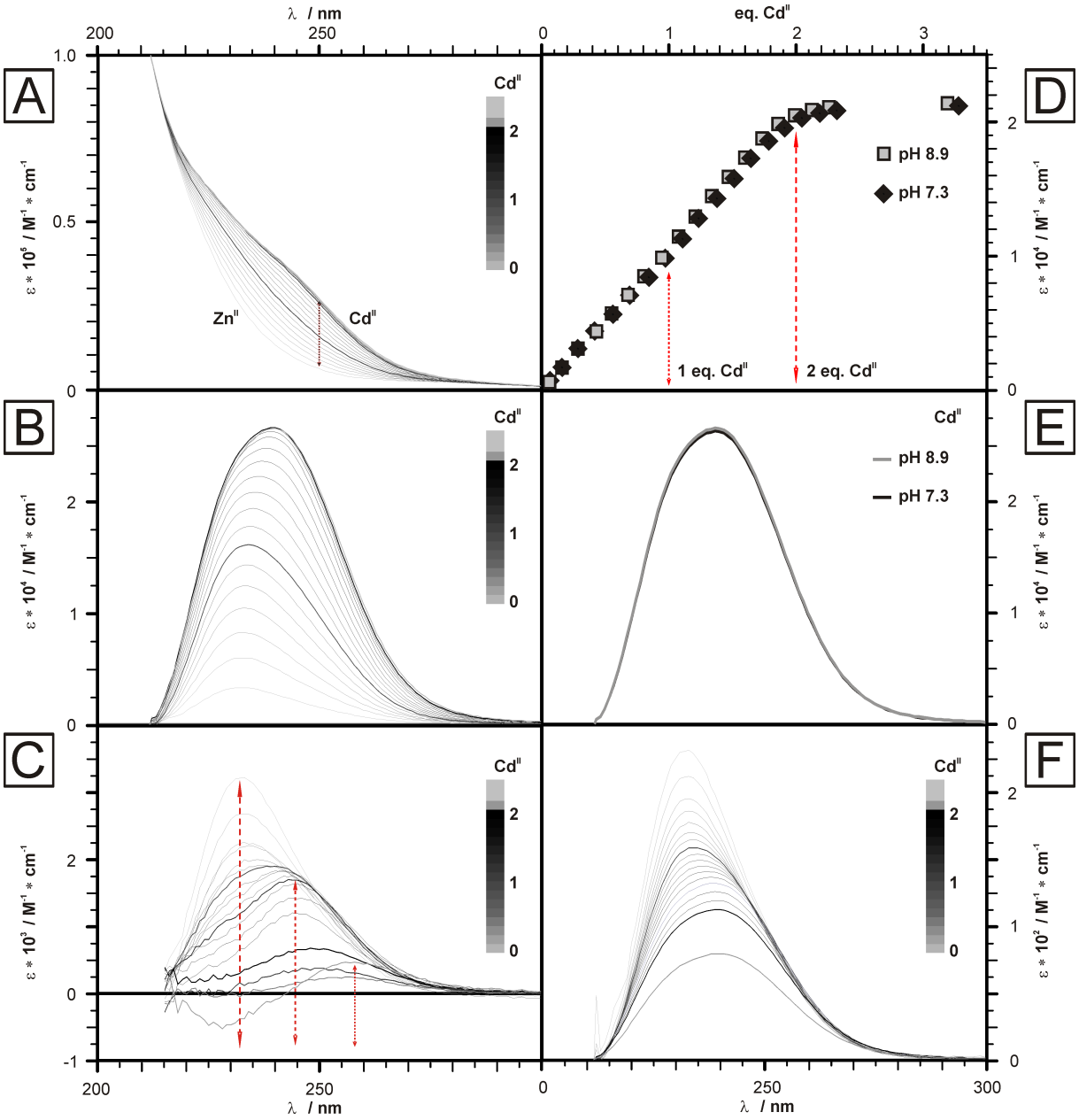

Figure IV 4 Metal exchange titration studies of $Zn_2\gamma$-E_c-1 with Cd^{II} at pH 7.3 and 8.9 followed by UVvis spectroscopy. ***A)*** Absorption spectra of stepwise addition of Cd^{II} ions to $Zn_2\gamma$-E_c-1 at pH 7.3 ($Zn_2\gamma$-E_c-1: light grey line – $Cd_2\gamma$-E_c-1: black line). ***B)*** Difference spectra and ***C)*** delta spectra of the Zn/Cd exchange titration at pH 7.3 (to compare: see fig. 1b). ***D)*** Plot of molar absorptivity against the equivalent of M^{II} ions added for the titration of 30 µM $Zn_2\gamma$-E_c-1 with Cd^{II} at pH 8.9 (grey squares) and pH 7.3 (black diamonds). The molar absorptivity for the Cd^{II}-form at both pH values increases until $\varepsilon_{250\ nm}$ = 21'000 M^{-1} cm^{-1} at exactly two Cd^{II} equivalents added. ***E)*** Difference absorption envelopes of $Cd_2\gamma$-E_c-1 (see B) at pH 7.3 and 8.9. ***F)*** Difference spectra were prepared by subtracting

the spectra at pH 7.3 from those at pH 8.9 for each titration step. In order to exactly quantify the pH induced changes of the absorption envelope the extinction coefficient is normalized to one eq. Cd^{II}.

The incremental subtraction (**Fig. IV 4c**) of the UVvis spectra reveals three major bands centered at 233 nm, 243 nm and 256 nm. Differences between the absorption envelopes at pH 7.3 and 8.9 differ negligible, i.e. less than 1 % (**Fig. IV 4e**) with minor bands at 233 nm until the first Cd^{II} equivalent added, which changes to 238 nm during incorporation of the second Cd^{II} equivalent (**Fig. IV 4f**). Moreover the extinction coefficient scored at 250 nm increases in the investigated pH range linearly and in agreement with the apo-Cd^{II} titration until ε_{250nm} = 21'200 M^{-1} cm^{-1}, when exactly two eq. Cd^{II} are provided. The linearity in of the Zn/Cd exchange is also witnessed in the MCD spectra recorded (**Fig. IV 5 a-d**). The maxima of the main MCD band at 252 nm and 225 nm originating from the chiral contributions of the degenerated excited states evolute identically in the observed pH range by peaking at exactly two Cd^{II} equivalents ($\theta_{M\ 252nm}$ = 200'000 deg^1 $dmol^{-1}$ cm^2 T^{-1} for pH 7.3 and 8.9 and $\theta_{M\ 234nm}$ = 150'000 deg^1 $dmol^{-1}$ cm^2 T^{-1} for pH 7.3 and $\theta_{M\ 234nm}$ = 160'000 deg^1 $dmol^{-1}$ cm^2 T^{-1} for pH 8.9). Both the *A*-term character of the magnetically induced transition and the energy level agree with those witnessed for the apo-Cd^{II} titration (234 nm, 243 nm and 251 nm). In addition the shape of the entire spectra of each metallation step of the apo-Cd^{II} addition corresponds to those evidenced for the Zn^{II}/Cd^{II} substitution (**Fig. IV 5c,d**). The chiral features evidenced in the CD spectra of the fully Cd^{II} loaded form of the $Zn_2\gamma$-E_c-1 domain in the investigated pH range (pH 7.3 - 8.9) are in accordance with those witnessed for $Cd_2\gamma$-E_c-1 obtained from the apo-form (**Fig. IV 5e-h**). Judging from the evolution of the CD spectra the formation of the Cd_2 cluster starting from the Zn_2-form precedes isostructural at pH 7.3 and 8.9 with a linear increase in chirality at 225 nm peaking at θ_{225nm} = 135'000 deg^1 $dmol^{-1}$ cm^2 after exactly two Cd^{II} equivalents (**Fig. IV 5h**). For the Zn^{II}/Cd^{II} exchange titration the ellipticity bands centered around 252 nm transforms at one eq. Cd^{II} from an absorption band shape, characteristic for the Zn_2-form, to a biphasic band shape evidenced in the Cd_2-form (**Fig. IV 5f, inset**), manifested in a linear decrease at 252 nm until supplementation of one eq. Cd^{II} (θ_{252nm} = 13'500 deg^1 $dmol^{-1}$ cm^2) without significant change in intensity during addition of the second Cd^{II} equivalent (**Fig. IV 5h**).

IV 4 3 Demetallation of Zn_2- and $Cd_2\gamma$-E_c-1

Proton driven demetallation of the Zn_2- and $Cd_2\gamma$-E_c-1 is followed by UVvis spectroscopy focusing on the M^{II}-S-Cys bonds and CD spectroscopy investigating the structural changes of the protein backbone and the metal center. The demetallation of the Cd_2-form proceeds inversely to the titration of apo-γ-E_c-1 with Cd^{II} ions (**Fig. IV 6a-c**) in terms of both changes in chirality and absorptivity (see figure IV 1 and 2). Moreover the evolution of the extinction coefficient at 250 nm is in absolute agreement with the one of the molar ellipticity at 225 nm (**Fig. IV 6c**) with an apparent pK_a value of the Cys residues in the Cd_2-form of 3.95 ± 0.02 as has already been reported[106]. For the demetallation of $Zn_2\gamma$-E_c-1 the situation looks complementary as the one described for $Cd_2\gamma$-E_c-1 (**Fig. IV 6c-e**). Both the LMCT and CD bands probed at 230 nm and 225 nm, respectively, yield apparent pK_a value of the Cys residues in the Zn_2-form of 4.79 ± 0.02 identical with the one previously reported[106]. A minor difference in-between proton driven Zn^{II} and Cd^{II} demetallation is pointed out in the inset of **Fig. IV 6d**, where a band centered around 280 nm with ε_{280nm} = 2'000 M^{-1} cm^{-1} occurs, indicating the formation of disulfide bridges whilst titrating.

IV 5 Discussion

IV 5 1 Spectroscopic features of Zn^{II} and Cd^{II} metallation of apo_γ-E_c-1

Starting from the metal-free protein, we investigated the changes in electronic properties during Zn^{II} and Cd^{II} metal ion incorporation (**Fig. IV 1, 2, 4)**. By subtracting the apo-spectra from those of the metallated forms the absorption envelope or change in chirality reflects the electronic contributions of the metal ion coordination, which originate from M^{II}-ligand binding and the refolding of the protein. When subtracting the UVvis- and CD spectra of each subsequently added equivalent from the previous the changes in the shape of the absorption and chiral bands provide information on the metallation pathway and resolve more precisely contributions of bridging and terminal cysteines[45], which eventually reveal a cooperative or non-cooperative character of the cluster formation process. In the detectable range of UVvis-, CD-, and MCD spectroscopy appreciable bands originating from coordination of Cd^{II} to cysteine are reported from 280 nm on to 210 nm from where amide backbone derived $\sigma^* - \pi$ interactions strongly bias accurate measurements[128]. In photo-spectrometrically followed Cd^{II} titrations the maximum of absorptivity of the first (227 nm) and the last (257 nm) fractional Cd^{II} equivalent added may indicate the contribution of only terminal ligands (1^{st}) and predominantly bridging ligands (last), resulting in a expected bathochromic shift due to the transition from a bent to a trigonal binding mode at the thiolates sulfur atom[44]. In case of the Zn^{II} metallation a hypsochromic shift from terminal (235 nm) to bridging (216 nm) cysteines is witnessed. The evolution of the magnetically induced chiral band for the Cd^{II} titration reproduces the bathochromic shift of terminal to bridging cysteines, suggesting that the origin of the non-degenerated ground state excitation resulting in orbital splitting in the excited state might correlate with the photo-spectrometrically observed transition. The predominant chiral band is centered around 225 nm independent of the probed metal ion.

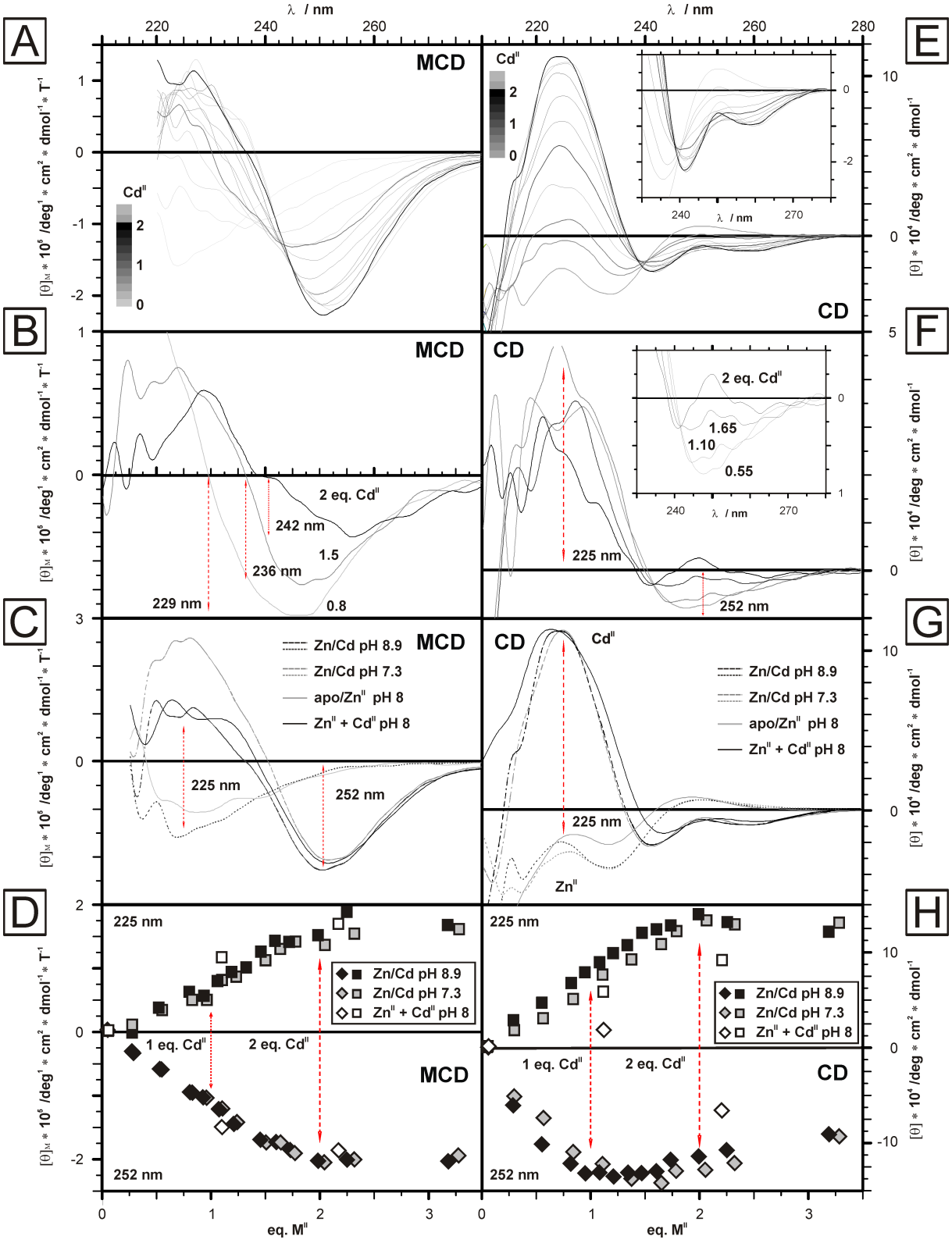

Figure IV 5 Metal exchange titration studies of $Zn_2\gamma$-E_c-1 with Cd^{II} at pH 7.3 and 8.9 followed by CD and MCD spectroscopy. ***A)*** MCD spectra of $Zn_2\gamma$-E_c-1 titration with Cd^{II}. Spectra of subsequently added Cd^{II} equivalents are depicted ($Zn_2\gamma$-E_c-1: red line – $Cd_2\gamma$-E_c-1: black line). ***B)*** Dark grey spectra of the Zn/Cd exchange titration. Each MCD spectra was subtracted from the previous. The *A*-term

transition bands are observable at 229 nm, 236 nm and 242 nm. ***C)*** Comparison of MCD spectra of $Zn_2\gamma$-E_c-1 and $Cd_2\gamma$-E_c-1 spectra of the Zn/Cd γ-E_c-1 exchange titration at pH 7.3 and 8.9 with the Cd_2 spectra of γ-E_c-1 when the resulting Cd_2 spectra of the apo /$Cd_2\gamma$-E_c-1 titration is subtracted from Zn_2 spectra resulting from the apo/$Zn_2\gamma$-E_c-1 titration. ***D)*** The increase of magnetically induced molar ellipticity at 225 nm (squares) and 252 nm (diamonds) as a result of Cd^{II} ion addition to the apo protein is depicted. Comparing Zn/Cd exchange (pH 7.3 grey; pH 8.9 black) titrations with the apo-Cd subtracted from the apo-Zn titration no significant differences in metallation are observed (white). ***E)*** CD spectra of $Zn_2\gamma$-E_c-1 titration with Cd^{II} (same representation as in A). ***F)*** Delta spectra of the Zn/Cd exchange titration. Each CD spectra was subtracted from the previous (style as in B). ***G)*** Comparison of CD spectra of $Zn_2\gamma$-E_c-1 and $Cd_2\gamma$-E_c-1 spectra of the Zn/Cd γ-E_c-1 exchange titration at pH 7.3 and 8.9 with the Cd_2 spectra of γ-E_c-1 when the resulting Cd_2 spectra of the apo /$Cd_2\gamma$-E_c-1 titration is subtracted from Zn_2 spectra resulting from the apo/$Zn_2\gamma$-E_c-1 titration. ***H)*** The increase of molar ellipticity at 225 nm (squares) and 252 nm (diamonds: 10 times enlarged signal) as a result of Cd^{II} -ion addition is depicted (as in C).

During the titration with Cd^{II} and Zn^{II} ions the chirality increases linerarly until 1.5 eq. M^{II} what is in excellent agreement with the absorptivity at 225 nm during the titration with Cd^{II} and Zn^{II} ions. The evidenced biphasic features of the Cd^{II} and Zn^{II} CD spectra between 235 and 270 nm are comparable in shape (for Cd^{II} slightly shifted to the red) whereas the contribution of the negative bands at 242 nm and 262 nm are more pronounced for Cd^{II}. In analogy, the bi-phasic shape was also evidenced for the β- and α-cluster of mammalian MTs[44, 131] and was explained as excitonic splitting of the two involved dipolar moments[128].

IV 5 2 Spectroscopic features of Zn/Cd exchange of γ-E_c-1

The lack of absorption changes in the far UV (below 220 nm) of the Zn/Cd exchange titration manifests the already reported[106] isostructural exchange of Zn^{II} ions by Cd^{II} in γ-E_c-1 in the pH range of 7.3 to 8.9. The ε_{250nm} plot (**Fig. IV 3d**) suggests a gradually exchange visible as a clear change in absorption envelope during re-metallation. The subtle differences between pH 7.3 and 8.9 in Zn/Cd substitution may be accounted to a short intermediate protonation state (H/Cd^{II} exchange) of the terminal cysteine at pH 7.3, that is in constant exchange with the solvent as has been suggested from computational studies on $ZnCys_4$ metal center[132]. This would lead to a decrease in extinction coefficient for a terminal bridging cysteines

accompanied with an increasing band originating from a thiol to thiolate transition described at around 235 nm (see **Chapter VII**).

The difference in chiral features of the Cd^{II} substitution of $Zn_2\gamma$-E_c-1 relative to the Cd^{II} to apo-γ-E_c-1 titration are of special interest owing to the fact that UVvis-, CD-, and MCD followed Cd^{II} titration of apo-γ-E_c-1 exclude the existence of an isolated Cd_1Cys_6 intermediate state after the addition of one equivalent Cd^{II}. Otherwise in all three type of spectra a pronounced change at exactly one eq. Cd^{II} from bridging to terminal cysteine contribution should be witnessed, which is not the case. Moreover the differing evolution of the chiral bands manifests the only pronounced difference between Cd^{II} addition to Zn_2- or apo-γ-E_c-1. Generally, in Zn/Cd exchange titration only the larger ionic-radius accompanied with the lower electron density at the Cd^{II} nuclei can explain the substitution of Zn^{II}. This physical difference may also result in changes of Cd^{II} metallation pattern of Zn_2- versus apo-γ-E_c-1. In $Zn_2\gamma$-E_c-1 a more non-cooperative metallation may occur owing to a preferred binding site for Cd^{II} or Zn^{II}. The linear increase of the CD band at 225 nm until ca. 1.5 eq. Cd^{II} suggests that the observed chiral center during Cd^{II} metallation occurs more often, or is more distorted than the respective Zn^{II} binding site. Moreover the existence of only a biphasic line shape in-between 235 and 270 nm until one eq. of Cd^{II} (**Fig. IV 5f, h**) supports the notion of a predominant non-cooperative Zn/Cd exchange yielding a stable $Zn_1Cd_1\gamma$-E_c-1 metallation intermediate. Otherwise a more complex CD spectra originating from cluster formation and accompanied excitonic splitting would be expected (**Fig. IV 5f**).

IV 5 3 Demetallation of Zn_2- and $Cd_2\gamma$-E_c-1

In parallel to metal ion association studies, the demetallation of the Zn_2- and Cd_2-form of the γ-E_c-1 domain was investigated. The degree of demetallation cooperativity and the driving force of the metal ion removal was probed by fitting the shape of the pH dependent extinction coefficient at 250 nm (Cd^{II}) or 230 nm (Zn^{II}), respectively to Hill type equation with one or two apparent pK_a values[68]. If the demetallation of wheat E_c-1 is a physiological relevant process during imbibition of the wheat grain[13], a proton gradient might well be the driving force. In consequence acid titration followed photospectro- and polarimetrically yield information concerning: **i**) the apparent stability constant of the (individually) bound metal ions, **ii**) the degree of demetallation cooperativity and in combination with metallation studies **iii**) the reproducibility of metallation. Furthermore **iv**) it can be distinguished whether the

demetallation is a kinetically (first protein backbone rearrangement) or thermodynamically (first cluster disassembly) driven process. The apparent stability constants (pK_D) are expressed in terms of cysteinyl thiolate acid constant at half protonation (pK_a).

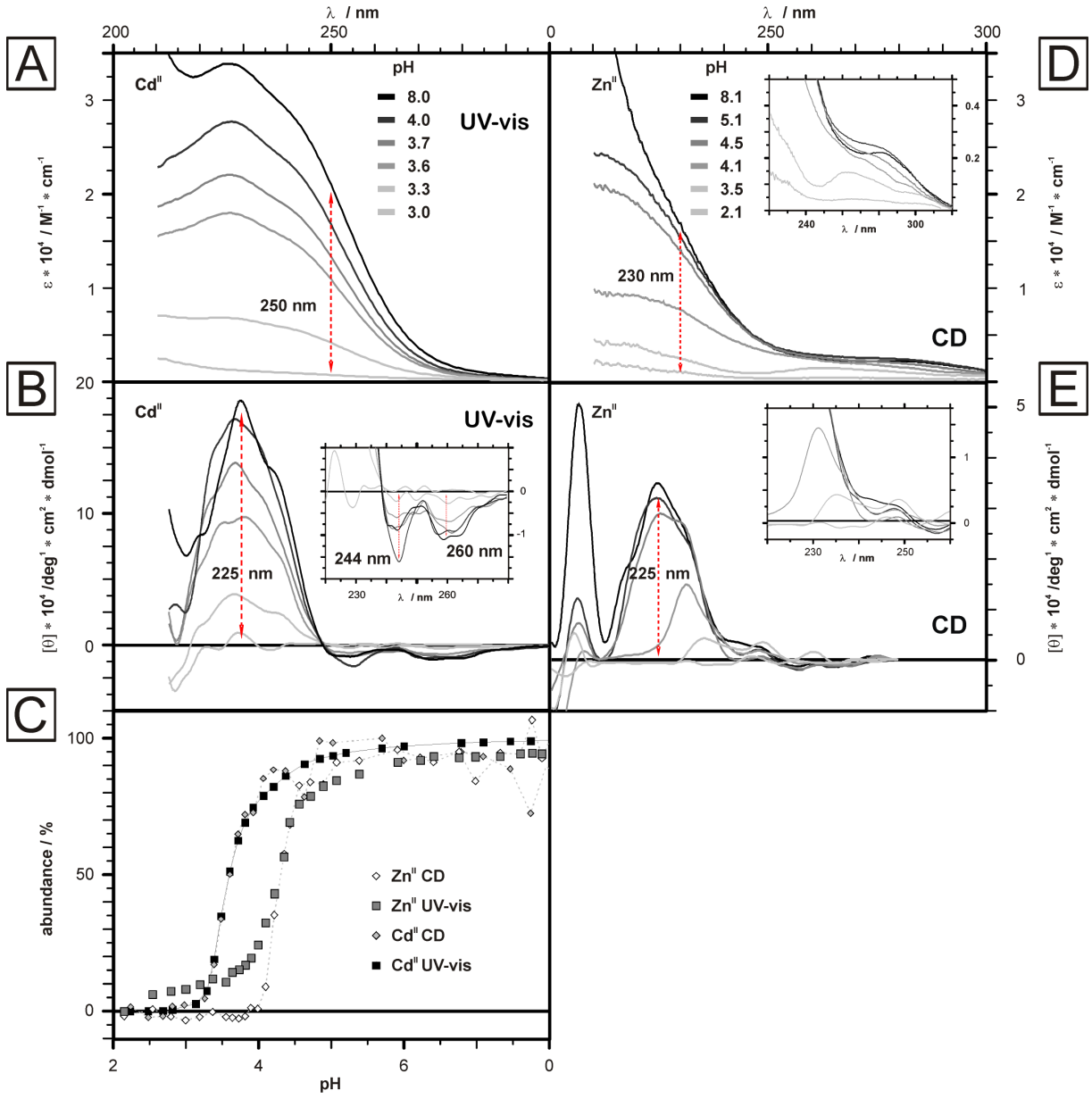

Figure IV 6 pH-titration of $Cd_2\gamma$-E_c-1 and $Zn_2\gamma$-E_c-1 followed by UVvis- and CD spectroscopy. In A and D the wavelength is plotted against the extinction coefficient, in B and E against the molar ellipticity. ***A)*** pH-titration of Cd^{II}-form is observed photo-spectrometrically. The displayed bands at different pHs (grey line: pH 3: black line: pH 8.9) are subtracted from the absorption envelope at pH 2. The red arrow indicates the wavelength (250 nm) of demetallation quantification. ***B)*** pH-titration of Cd^{II}-form observed photo-polarimetrically. Style and layout are detailed in A. The inset resolves the

spectral features around 250 nm more in detail. ***C)*** The percentual demetallation of $Cd_2\gamma$-E_c-1 and $Zn_2\gamma$-E_c-1 as function of pH is displayed for both UVvis- and CD spectroscopy. The characteristic preference of stronger Cd^{II} than Zn^{II} binding is observed. For both metallated forms the chiral and electronic absorption envelopes show a comparable demetallation pattern. ***D)*** pH-titration of Zn^{II}-form observed photo-spectrometrically and ***E)*** photo-polarimetrically. Inset, style and layout are depicted as in A, B.

γ-E_c-1 coordinates Zn^{II} and Cd^{II} rather weak in comparison to other MTs[12]. The pH dependent evolution of the dichroic properties, namely the steady decrease of all chiral bands without the appearance of new chiral features allow the conclusion that the solvent accessible Zn_2 or Cd_2 clusters are first partially dissociated and as a result the protein unfolds. Otherwise a change in chiral feature especially 230 nm and 270 nm for both the Zn_2- and the Cd_2-form would have been expected. So the demetallation process is cooperative as is also reflected in the lack of a pronounced second pK_a value[106] and thermodynamically driven due to the fact that first the metal ions are released and only then the protein unfolds as judged from CD spectroscopy.

IV 6 Conclusion

We have chosen the γ-domain of E_c-1 from bread wheat a small metalloprotein termed metallothionein embedding a binuclear tetrahedral tetrathiolate $M^{II}_2Cys_6$ metal cluster as study system to investigate **i)** the absorption envelope originating from tetrahedral tetrathiolate Cd^{II} and Zn^{II} sites in respect to the contribution derived from terminal and bridging cysteines, **ii)** the chiro-optical and magnetically induced chiro-optical bands of those Cd^{II} and Zn^{II} sites and **iii)** the synergetic character of the information derived from all three spectroscopic techniques.

We were able to assign absorptive contributions from terminal and bridging cysteines for the Cd^{II}-form at 259 nm (bridging) and 242 nm (terminal), which agreed with the center of the *A*-term shaped MCD signals. For the Zn^{II}-form contributions at 215 nm (bridging) and 235 nm (terminal) were evidenced. We are confident that the methodology employed herein will allow to draw further conclusion on the metallation of metallothioneins.

IV 7 Acknowledgements

This work was supported by the Swiss National Science Foundation (SNSF Professorship to E.F.).

Chapter V : Identification of a site preference during Cadmium poisoning of a Zn_2Cys_6 zinc finger motive: comparing the results of the GST hydrogel system GHOST to those obtained for the isolated protein

Jens Loebus[§] · Silke Johannsen[§] · Thomas Fox · Eva Freisinger*

Jens Loebus · Silke Johannsen · Thomas Fox · Eva Freisinger (✉)

Institute of Inorganic Chemistry, University of Zurich,

8057 Zurich, Switzerland

*e-mail: freisinger@aci.uzh.ch

[§] both authors contributed equally

V 1 Abstract

Zinc tetrathiolate coordination represents the major motive of Zn^{II} structural binding sites in proteins, evidenced in transcription factors and metallothioneins (MTs) owing to the inherent thermodynamic and redox-chemical stability. Their identification and investigation on a molecular level, however remains a challenging task for spectroscopists, due to the fact that both Zn^{II} ions and thiolates especially in tetrathiolate coordination, are generally considered as being spectroscopically silent. Besides X-ray based experimental approaches, isostructural substitution of Zn^{II} with the NMR active nuclei ^{113}Cd provide direct information on the metal centre. Zn^{II} substitution in proteins by the Cd^{II} is considered a major pathway for Cd^{II} toxicity, rendering investigation of Zn^{II} exchange by Cd^{II} beneficial from a structural perspective as well as from a toxicological.

In this study we employed the plant metallothionein domain γ-E_c-1, containing a GAL4 like transcription factor Zn_2Cys_6 metal cluster, to probe the Cd^{II} remetallation pathway. We compared the experimental results for mass spectrometry, UVvis- and NMR spectroscopy of the isolated γ-E_c-1 domain and validated them by utilizing a GST fusion protein prepared according to the recently reported GST Hydrogel System (GHOST). By this approach, we **i)** identified four differently metallated isoforms (Zn_2, Cd_2, ZnCd, CdZn); **ii)** quantified their relative abundance, **iii)** evidenced a site specificity of the metallation pathway (ZnCd-form) and **iv)** solved the structure of the ZnCd GST-γ-E_c-1 isoform via NMR.

In summary: the Zn/Cd exchange in a model protein system was elaborated, providing evidence for the complementary use of MS, UVvis- and NMR spectroscopy.

Keywords Cd toxicity · Metallothionein · GHOST system · Electronic absorption spectroscopy · NMR spectroscopy · Zinc finger motive

V 2 Introduction

Cadmium exposure to the environment is one of the unfortunate side effects of metal ore mining and processing. As side-product in phosphate-based fertilizer it is introduced into the food chain[133], where it is readily taken up by crops such as wheat, barley or rice[134]. In consequence, besides inferring with the cultured plants, i.e. reduced plant size, grain number and size, animals and human will be exposed to Cd^{II}, which accumulates in the kidney[101, 135] and liver[136] triggering carcinogenic, mutagenic and teratogenic processes[137-138]. In order to prevent toxification through Cd^{II} the molecular identity of the chemical species involved in **i)** uptake; **ii)** sequestration and **iii)** storage are under investigation and agronomical strategies to limit the entry into the food chain through crop uptake are developed.

It is well accepted that Cd^{II} toxicity propagates through interference with Zinc dependent processes largely owing to their comparable chemical properties. Especially the high affinity towards thiols, which represents the major ligand for structural zinc binding sites occurring in a variety of proteins including transcription factors, so-called zinc fingers, is a key to understand Cd^{II} toxification. As a surprisingly well-suited study system we investigated the metallothionein (MT) domain γ-E_c-1, which is part of the E_c-1 protein[8] a major zinc storage protein in wheat grains[14]. One reason to study γ-E_c-1 is the occurrence of homologues in a variety of crop grains including rice, maize and barley as well as in the plant model organism *Arabidopsis thaliana*[17] providing a putative target for Cd^{II} poisoning in all major crops. Moreover γ-E_c-1 is a GAL4 like zinc finger protein coordinating two Zn^{II} ions via six thiolate residues, hence the Zn^{II} ions can easily be substituted by Cd^{II} ions, which coordinate significantly stronger[106], rendering γ-E_c-1 susceptible to Cd^{II} poisoning. With the already solved NMR solution structures of Cd_2γ-E_c-1 and Zn_2γ-E_c-1 at hand[106], complemented by EXAFS data of the Zn_2-form, the protein embedded homo metallated clusters were already carefully examined yielding the following properties: **i)** tetrahedral tetrathiolate coordination; **ii)** the two tetrahedron are connected via two bridging cysteines **iii)** two alternating bridging cysteine coordination with one position either occupied by Cys_3 or Cys_{21} and the other position fixed to Cys_9; **iv)** the change of connectivity is restricted to one metal binding site (Site A); **v)** a non-enzymatically formed cis-proline adjacent to Cys_{13} (see **Chapter III**).

The metal cluster of γ-E_c-1 is embedded into a relatively small (2.5 kDa) protein envelope, rendering it a suitable target for metallation studies to understand the poisoning of a zinc finger like protein by Cd^{II}. To simplify experimental procedures we have employed the

recently developed GHOST (GST Hydrogel System) GST fusion protein system to study small proteins with different co-factors. This technique allows **i)** faster, **ii)** cheaper and **iii)** reliable experiments by employing the well-known Glutathione-*S*-transferase (GST) – fusion protein system, in standard experimental procedures including UVvis-, CD-, and NMR spectroscopy as well MS for analyzing structure and function (see **Chapter III**). The GHOST GST fusion protein system is based on the post-purification sample preparation of a Glutathione-*S*-transferase, a 27 kDa, ubiquitous expressed, multifunctional homodimeric protein[100-101, 103]. Besides its advantages in protein expression and purification GST possesses an exceptional biocompatibility due to its inherent role in cellular detoxification processes[104], hereby rendering it a versatile fusion protein partner for biochemical methods, including immunoprecipitation and pull down experiments[105]. The main step of the sample preparation method for GHOST GST fusion protein preparation is a "soft" protein-denaturing step at low concentration (< 50 μM) and slightly basic pH employing 0.1 to 0.3 M of the reducing agent 1,4-dithiothreitol DTT. Hereby reactive cysteine thiolates are formed, which may form intra- and intermolecular disulfides during fusion protein concentration leading to the formation of a hydrogel structure. Furthermore a heat treatment step facilitates the formation of the hydrogel[109]. The advantages of the GHOST GST fusion system comprise the inexpensive, simple and straight forward methodology, which allows the substitution of the isolated target protein in experiments aiming to elucidate the **i)** structure and folding as well as the **ii)** spectroscopic properties of the protein under investigation.

In this work we provide information upon the Cd^{II} toxification process of a GAL4 like zinc finger motive containing metal protein from bread wheat, the γ-E_c-1 domain. The re-metallation process is followed by UVvis-, multidimensional NMR spectroscopy and mass spectrometry for the GST γ-E_c-1 fusion protein as well as for the isolated γ-E_c-1 domain and the experimental outcome is compared amongst the two protein species. Moreover the use of GHOST for GST fusion protein preparation, applicable to a myriad of spectroscopic and spectrometric techniques, is further validated. Additionally, its promising qualification and quantification ability is underlined by solving the structure of the ZnCd-form of the γ-E_c-1 domain as part of the GST fusion protein, which was impossible for the isolated MT.

V 3 Material and methods

V 3 1 Chemicals, solutions, plasmids and proteins

$^{113}CdCl_2$ and $^{15}NH_4Cl$ were purchased from Cambridge Isotope Laboratories Inc. (Innerberg, Switzerland), d_{11}-Tris from Euriso-top (Saint-Aubin, France). All other chemicals were ACS grade or comparable and purchased from Sigma-Aldrich Chemie GmbH (Buchs, Switzerland), Calbiochem (VWR International AG, Lucerne, Switzerland) or Acros organics (Chemie Brunschwig AG, Basel, Switzerland). Solutions were prepared with degassed, nitrogen or argon saturated millipore water and if necessary three times freeze-thawn. The pGEX_γ-E_c-1 plasmid was engineered based on the pGEX-4T1 expression vector coding for a *N*-terminal GST fusion protein, expressed and purified as previously described[106] (see **Chapter III**). The GST γ-E_c-1 fusion protein consists of the *N*-terminal GST protein, a linker followed by the amino acid sequence of γ-E_c-1:

GS GCDDKCGCA VPCPGGTGC RCTSAR

which has already been reported[106].

V 3 2 Preparation of Zn-forms of GHOST GST-γ-E_c-1 and isolated γ-E_c-1

Procedures for GHOST GST fusion protein (see **Chapter III**) and Zn_2γ-E_c-1[106] preparation were already detailed previously. In short: All buffer exchange and concentration steps were performed in a Series 8050 stirred (Millipore) ultracentrifugation cell.

The GST fusion protein freshly eluted off the GST affinity column was concentrated to around 5 ml. All buffer exchange and concentration steps were performed in a Series 8050 stirred (Millipore) ultracentrifugation cell. In a next step, 0.1 to 0.3 M DTT at pH 8.5 (1 M Tris/HCl, pH 8.9) were incubated for 30 min, afterwards twice diluted with 50 ml of 50 mM Tris/HCl pH 8.0 and re-concentrated. Following dilution with 50 mM Tris/HCl pH 8.0, micromolar excess of $ZnCl_2$ was added, completed by one further buffer exchange cycle with 50 mM Tris/HCl pH 8.0 and three cycles with 1 mM d_{11}-Tris/HCl pH 8.0. Finally the protein concentration was determined photo-spectrometrically at 280 nm and compared to the 2,2'-dithio-dipyridine (2-PDS) assay (accounting 6 Cys of γ-E_c-1 and 2 Cys of GST)[43] (see **Chapter III**). The metal concentration was scored via flame atomic absorption spectroscopy (F-AAS) prior to aliquoting the protein and storage at -80°C.

For the isolated protein, apo-γ-E_c-1 was prepared freshly prior to each experiment and remetallated with two equivalents of Zn^{II}. Protein concentration was scored via the 2-PDS assay and Zn^{II} as well as Cd^{II} concentration were quantified via F-AAS.

V 3 3 Re-metallation of Zn_2 GST-γ-E_c-1 and isolated Zn_2γ-E_c-1 with ^{113}Cd for heteronuclear and homonuclear NMR spectroscopy

Procedures for GHOST GST fusion protein (see **Chapter III**) and Zn_2γ-E_c-1[106] preparation were already detailed previously. In short:

In case of the isolated γ-E_c-1 domain the Zn_2-form was dialyzed twice for 24 h against 100 μM d_{11}-Tris/HCl pH 8.0 prior to lyophilization and resolubilisation in 10% D_2O/90% H_2O, 15 mM d_{11}-Tris/HCl pH 6.9, 50 mM NaCl to yield a final concentration of ca 0.8 mM protein. In subsequent steps (0, 0.33, 0.5, 0.67, 1.0, 1.33, 1.5, 1.67 or 2 equivalents) ^{113}Cd ions were titrated from a 10 mM $^{113}CdCl_2$ solution directly into the NMR tube.

In case of the GST fusion protein ca. 5 ml of the Zn_2-form of GST-γ-E_c-1 were concentrated to a final concentration of ca 0.8 mM in 10 % D_2O, 1 mM d_{11}-Tris/HCl pH 7.5. For all experiments the exact amount of 0, 0.33, 0.5, 0.67, 1.0, 1.33, 1.5, 1.67 and 2 equivalents of Cd^{II} ions was calculated and subsequently titrated to the previous equivalent prior to transferring the respective solution into NMR shigemi tubes (Shigemi Inc) and heated for 24 h at 37°C in order to polymerize.

Aliquots from all NMR samples were taken and protein concentrations were scored via the 2-PDS assay and the metal ion concentration was measured by F-AAS. Both protein concentration and MT to M^{II} ratio were recalculated from these values. Finally size exclusion chromatography (SEC) was applied to prove the monomeric character of the isolated γ-E_c-1 domain.

V 3 4 Sample preparation and titration of Cd^{II} to apo-γ-E_c-1 and Zn_2 GST-γ-E_c-1 followed by UVvis spectroscopy

The production of apo-protein was detailed previously (see **Chapter II**). To the freshly prepared apo-γ-E_c-1 dissolved in 10 mM HCl two equivalents of Zn^{II}-ions were added prior to adjusting the buffer to 10 mM Tris/HCl, 10 mM NaCl, pH 7.2, and diluting the sample to ca 25 μM in a final volume of 1.8 ml.

Zn^{II} GST-γ-E_c-1 dissolved in 1 mM d_{11}-Tris/HCl, pH 8.0 was adjusted to 15 μM protein concentration in 10 mM Tris/HCl, 10 mM, NaCl pH 7.2 to a final volume of 1.8 ml. Owing to the higher stock protein concentration (> 300 μM), dilution effects on the buffer composition were neglected.

The protein solution was transferred into a septum sealed cuvette with a 1-cm pathlength and the Cd^{II} solution was titrated using a 25 μl Hamilton syringe in steps of 1 μl (0.17 eq. Cd^{II}) followed by UVvis spectroscopy. After subsequent addition of all Cd^{II}-equivalents the protein concentration were determined via the 2-PDS assay and the A_{280}-method (for GST fusion protein; extinction coefficient ε = 41760 M^{-1} cm^{-1} (see **Chapter III)**), while the metal-ion concentration was scored via F-AAS in order to recalculate the MT to M^{II} ratios. Size exclusion chromatography (SEC) was applied to prove the monomeric character of both the GST fusion protein and the isolated γ-E_c-1 domain.

V 3 5 Mass spectrometry

Samples of Zn_2-, Cd_2- and mixed ZnCd- forms of GST-γ-E_c-1 and the isolated γ-E_c-1 domain are dialyzed (GST-γ-E_c-1: SnakeSkin Dialysis Tubing, 3.5K MWCO, Thermo Scientific, γ-E_c-1: Tube-O-DIALYSER^{TM} Micro 1K MWCO, G-BIOSCIENCES) twice overnight against 50 mM NH_4Ac (pH 7.6) and were subsequently injected directly or with a prior acidification step into a quadrupole time-of-flight (TOF) Ultima API spectrometer (Waters, UK). 10 mM NH_4Ac in 50% MeOH (pH 7.5) or 50% acetonitrile with 0.2% formic acid (pH 2-3) were used as a solvent. Scans were accumulated and further processed by the software MassLynx 3.5 (Micromass). Deconvolution of mass spectra was done by applying the maximum entropy algorithm of the MassLynx tool MaxEnt1. Electrospray parameters were capillary 2.8 V, cone 60 V and source temperature 80 °C.

V 3 6 NMR spectroscopy

The NMR spectra and solution structure of Zn_2γ-E_c-1 and Cd_2γ-E_c-1[106] and their respective GST fusion protein forms were previously reported (see **Chapter III**). All proton and ^{15}N resolved NMR experiments were recorded at 310 K on Bruker Avance 700- and 600-MHz spectrometers. 2D [^1H,^1H] TOCSY experiments following the metallation process were recorded at 100 ms mixing time for all NMR samples. ^{113}Cd-NMR experiments to investigate the binding sites and stoichiometries of the Cd^{II} ions were also performed at 310 K on a

Bruker DRX 500-MHz spectrometer. $^{3}J[H_{\beta},Cd]$ couplings derived from a 2D [^{113}Cd,^{1}H] HSQC spectrum were used to establish the individual Cd-Cys connectivities of the ZnCd-, CdZn- and Cd_2-form as well as providing the basis to follow the metallation pathway from the Zn_2 to the Cd_2 species[35]. Assignment of resonances in Zn_1Cd_1 GST-γ-E_c-1 was conducted using 3D ^{15}N resolved TOCSY[72-73], NOESY[74-75] and 2D TOCSY spectra recorded with 100 ms (TOCSY) and 250 ms (NOESY) mixing times, respectively. Distance restraints were derived from the 3D ^{15}N resolved NOESY NMR and the 2D NOESY NMR experiments. Zero-quantum interference in the ^{15}N resolved spectra was suppressed using an appropriate filter[77, 108]. Sequence-specific resonances were assigned based on the methodology developed by Wüthrich[38]. For the assignment process 2D TOCSY, NOESY, 2D [^{15}N,^{1}H] HSQC, 3D ^{15}N-resolved NOESY, and 3D ^{15}N-resolved TOCSY experiments were used. Both 2D and 3D spectra were evaluated with the programs XEASY[80] and CARA[79, 81], respectively as previously described[106]. Simulation of torsion angle dynamics[82] were performed with the *noeassign*[42] algorithm of the program CYANA 2.1[83]. Structure calculations were started from 100 conformers with randomized torsion angle values. Structure figures of the 20 conformers with the lowest final target function value were generated with the program MOLMOL[87].

V 4 Results

V 4 1 Mass spectrometry of the isolated γ-E_c-1 domain

ESI-MS is a convenient method to study chemical identity and relative abundance of differently metallated MTs[8]. The differently metallated species starting from the Zn_2-form of γ-E_c-1 exposed to an increasing number of Cd^{II} equivalents were identified by MS (**Fig V 1a**). While the relative abundance of the Zn_2-form hyperbolically decreases, the Cd_2-form increases exponentially. Already at 0.33 equivalents of Cd^{II} titrated to the isolated γ-E_c-1 domain a third species is observable that peaks at one equivalents of Cd^{II} representing almost 60% of all metallated species and disappears at an overall stoichiometry of $Zn_{0.33}Cd_{1.67}$, suggesting the existence of a rather stable ZnCd (site A) and/or CdZn (site B) transition state during complete Zn^{II} exchange by Cd^{II} (**Fig. V 1b**). The predominance of ZnCd and/or CdZn can be visualized by comparing the relative distribution of the differently metallated isoforms. Assuming a Gaussian distribution, were all binding sites are equally occupied at, i.e. Zn_1Cd_1 the ratio of Zn_2 : ZnCd : Cd_2 should be 0.25 : 0.5 : 0.25. MS experiments, however yield a ratio of 0.2 : 0.6 : 0.2. At this point, it should be mentioned that an absolute quantification of ESI-MS data under these conditions is error prone and potentially misleading necessitating complementary approaches in order to follow the Cd^{II} metallation.

V 4 2 UVvis- and NMR spectroscopy of the isolated γ-E_c-1 domain

Zn^{II} to Cd^{II} exchange titration of the isolated γ-E_c-1 domain (**Fig. V 1c**) was followed in the UV region were ligand to metal charge transfer (LMCT) bands for tetrahedral tetrathiolate Cd^{II} binding sites have been predicted[139] and shown to occur at around 250 nm[45, 106]. The increase in absorptivity at 250 nm proceeds linearly until two equivalents of Cd^{II} are incorporated. In a second approach the Cd^{II} metallation pathway and the site specific incorporation of Cd^{II} into γ-E_c-1 was followed via 2D proton NMR and heteronuclear ^{113}Cd NMR spectroscopy. Both [^{113}Cd,^{1}H] HSQC NMR spectra and [^{1}H,^{1}H] TOCSY NMR spectra of Zn_2, $Zn_{1.67}Cd_{0.33}$, $Zn_{1.5}Cd_{0.5}$, $Zn_{1.33}Cd_{0.67}$ … Cd_2γ-E_c-1 were recorded and compared (**Fig. V 1 d, e, f, h**). Among all experimental methods employed, only [^{1}H,^{1}H] TOCSY NMR spectra yield information on the Cd^{II} dependent evolution of all differently metallated isoforms.

While during titration those spin systems originating from the pure Zn_2 form disappear in intensity until they are not detectable anymore ($Zn_{0.33}Cd_{1.67}$), spin systems belonging to the

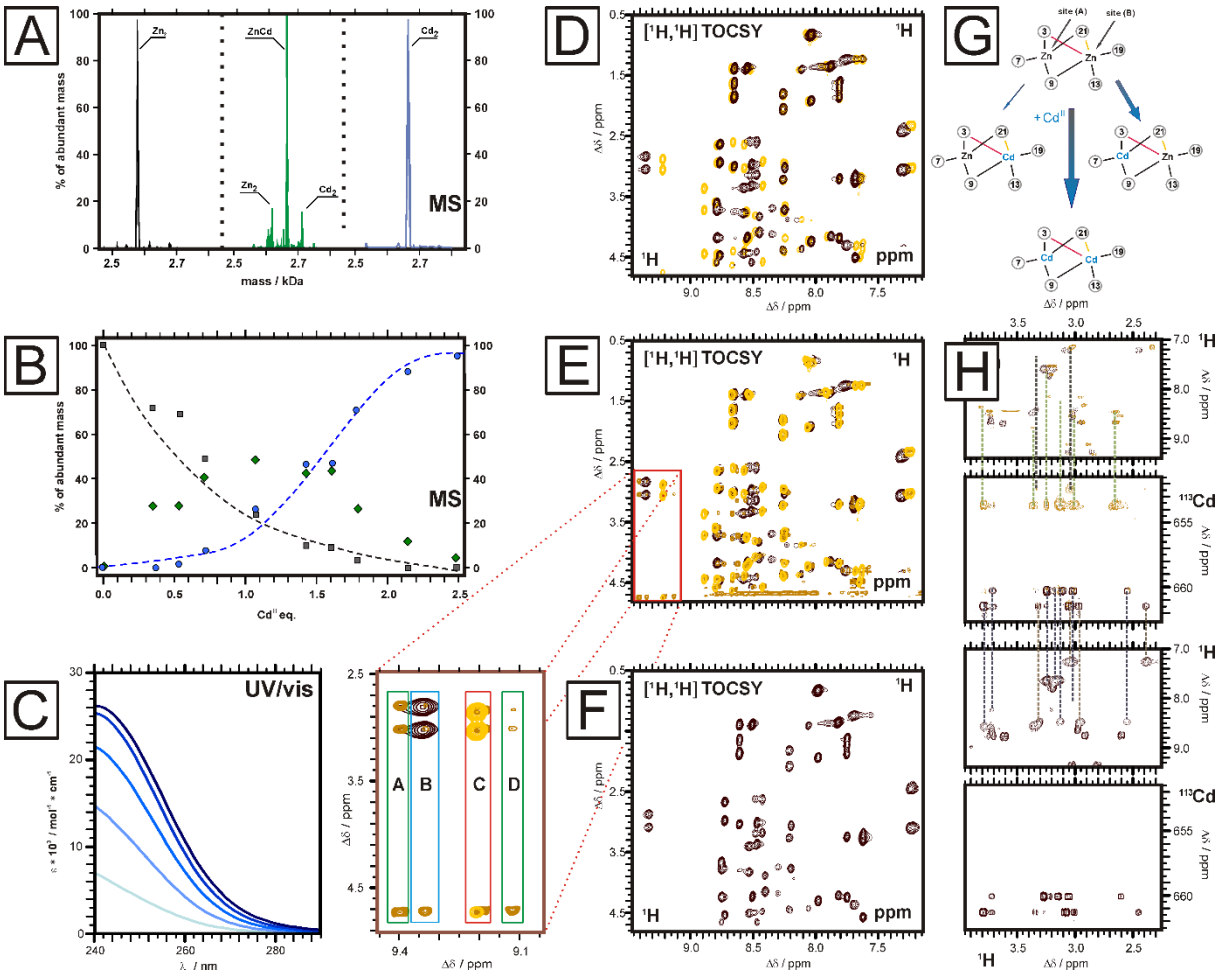

Figure V 1 displays the substitution of the Zn_2-form of the isolated γ-E_c-1 domain by Cd^{II}-ions evidenced through different experimental methods. In ***A)*** deconvoluted ESI-MS spectra of Zn_2 (black), ZnCd or CdZn (green) and Cd_2γ-E_c-1 (blue circles) and the relative abundance of the differently metallated isoform are depicted exemplarily. The evolution of distribution of the Zn_2 (black squares), ZnCd or CdZn (green diamonds) and Cd_2 (blue) isoforms for all titrated Zn^{II} to Cd^{II} ratios is displayed in ***B)***. ***C)*** The Cd^{II} titration steps followed by UVvis spectroscopy (left: steps of 0.5 Cd^{II} equivalents, Zn^{II}-form serves as baseline) are depicted. ***D-F)*** In the following three panels [^{1}H,^{1}H] TOCSY NMR spectra of the re-metallation process of Zn_2γ-E_c-1 by Cd^{II}-ions are displayed. In ***D)*** an overlay of the Zn_2- (yellow) with the Cd_2- (brown) form, in ***E)*** an overlay of the Zn_2- (yellow). Zn_1Cd_1- (light brown) and the Cd_2- (brown) form and in ***F)*** the spectra of the Cd_2-form is depicted. Exemplarily, the peak discrimination and integration of D_4 spin system (CdZn – (A) Cd_2 - (B), Zn_2 - (C), ZnCd – (D)) providing the basis of calculating the relative abundance of the respective metallated isoforms is

displayed in the red box. In ***G)*** the metal cluster and the deduced nomenclature for the differently metallated γ-E_c-1 isoforms is explained along with the metallation pathway. The thickness of the error indicates the preference of Cd^{II} substitution. In ***H)*** the [^{113}Cd,^{1}H] HSQC NMR spectra of the Cd_2γ-E_c-1 and the overlay of Cd_2- (brown) with the Zn_1Cd_1-form (light brown) is depicted. The $H_{B2/3}$ – Cd cross peaks are assigned to the respective Cd^{II} sites (Cd_2γ-E_c-1 brown cross peaks: site A dark green dashed line, site B violet dashed line; ZnCdγ-E_c-1 light brown cross peaks: site A dark green dashed line, site B violet dashed line) and the corresponding $H_{B2/3}$ protons (90° flipped amide region of [^{1}H,^{1}H] TOCSY NMR spectra).

mixed ZnCd- and CdZn-form (for metal cluster nomenclature see **Figure V 1g**) appear with rising Cd^{II} equivalents until an average $Zn_{1.33}Cd_{0.67}$-ratio is titrated to again diminish in relative intensity until they disappear at two Cd^{II} equivalents added. The fourth set of spin systems observed belongs to the Cd_2-form of γ-E_c-1. The Cd_2-form appears already with the 0.33 equivalents of Cd^{II} added ($Zn_{1.67}Cd_{0.33}$) dominating the NMR spectra from the $Zn_{1.5}Cd_{0.5}$-form on and remains the only set of spin systems visible when two Cd^{II} equivalents are supplemented. Owing to the pronounced chemical shift difference among the differently metallated forms in some N_H protons, the four isoforms (Zn_2, ZnCd, CdZn, Cd_2) are clearly distinguishable from each other as depicted in **Figure V 1e** displaying the Cd_2γ-E_c-1 form and the overlays of Cd_2- with Zn_1Cd_1- and Zn_2γ-E_c-1, respectively. Based on [^{1}H,^{1}H] NOESY NMR experiments of Zn_2-, ZnCd- and Cd_2-γ-E_c-1 species a sequential walk for all four differently metallated species of γ-E_c-1 was possible, resulting in the assignment of all spin systems to their respective metallated species.

In order to assess the relative abundance of the respective metallated species, we identified those spin systems, which are unique for the differently metallated γ-E_c-1 domains (all cysteines and aspartates as well as Gly_{10}) and integrated the corresponding H_{Ni}-H_{Xi} (X_i := A_i, B_i) cross peaks. In a next step invariable spin systems (Lys_6, Arg_{21} and Arg_{25}) are indentified and integrated. Finally, the ratios of the integrated cross peaks of Zn_2-, ZnCd-, CdZn and Cd_2-γ-E_c-1 relative to the integrated invariable spin systems is calculated and the sum for each cross peak e.g. Asp_4 (H_N-H_{B2}) is normalized to 100 %, assuming an equal weighted contribution of invariable cross peak intensity from all Zn_2, Cd_2 and mixed forms (**Fig. V 3)**.

Besides information derived from 2D [^{1}H,^{1}H] TOCSY NMR experiments 2D heteronuclear [^{113}Cd,^{1}H] HSQC NMR spectra of the differently metallated γ-E_c-1 (identical Zn to Cd ratios as described for MS, UVvis- and TOCSY NMR spectroscopy) were recorded (**Fig. V 1h**).

The chemical shifts of the Cd_2 species (Site A: 660 ppm; Site B: 661 ppm) and those of the CdZn- (Site B: 653 ppm) and the ZnCd species (Site A: 652 ppm), respectively, are easily discernable and baseline separated, enabling an accurate integration of all $H_{B2/3}$ – Cd cross peaks belonging to the respective Cd^{II} site. The ratio of the integrated cross peaks of the Cd_2 (Site A and B) is constant for all experiments (ratio A : B, 2:3) recorded at the coupling constant $^3J[H_\beta,Cd]$ of 50 Hz. To determine the relative abundance of the differently metallated γ-E_c-1 species the ratios between Cd_2 site A to CdZn site A and Cd_2 site B to ZnCd site B are determined and normalized to 100 % yielding the relative abundance of the respective Cd_2-, ZnCd- and CdZn-γ-E_c-1 species (**Fig. V 3**).

V 4 3 Mass spectrometry, UVvis- and NMR spectroscopy of the fusion GST-γ-E_c-1 protein

All experiments conducted with the isolated γ-E_c-1 domain were repeated with GST-γ-E_c-1 prepared with the GST Hydrogel System GHOST (see **Chapter III**), being hypothesized to facilitate functional and structural studies of small proteins. Indeed the protein preparation required much less financial and human resources yielding an acceptable deconvoluted ESI-MS spectra of Zn_2 GST-γ-E_c-1 representing the starting point for subsequent titration of Cd^{II} equivalents (**Fig. V 2a, b**). In accordance to the isolated γ-E_c-1 domain in MS experiments, the Zn_2- form decreases more or less hyperbolical until 1.66 eq. Cd^{II} are added. Despite small difference (15 %) in relative abundance, the distribution of ZnCd- and CdZn form progresses in agreement with the isolated γ-E_c-1 domain. Equally the Cd_2-form displays a comparable profile, starting to appear at 0.67 equivalents Cd^{II} added, being the most abundant species at 1.33 equivalents and the only metallated form discernable when 2 Cd^{II} equivalents are added. Concomitant to the mass spectrometric investigation, where the detectable charge state of the protein and hence the mass distribution pattern constituting the basis of the deconvoluted mass spectra is strongly dependent on the GST fusion partner, we performed Zn^{II} to Cd^{II} exchange titration followed by UVvis spectroscopy as previously reported (see **Chapter III**), clearly resembling the Zn/Cd exchange titration executed with the isolated γ-E_c-1 domain (**Fig. V 3c**). When deducting the Zn_2 GST-γ-E_c-1 (starting point of titration) from the consecutively recorded UVvis spectra during Cd^{II} addition, we can attribute the changes in absorption envelope witnessed between 270 nm and 240 nm to originate from the changes in electronic properties from the Zn_2- to the Cd_2-form of the protein. This procedure allows a

precise comparison of the GST-γ-E_c-1 derived absorption bands to those observed in the isolated γ-E_c-1 domain, which co-align reasonably (**Fig. V 1c and V 2c**).

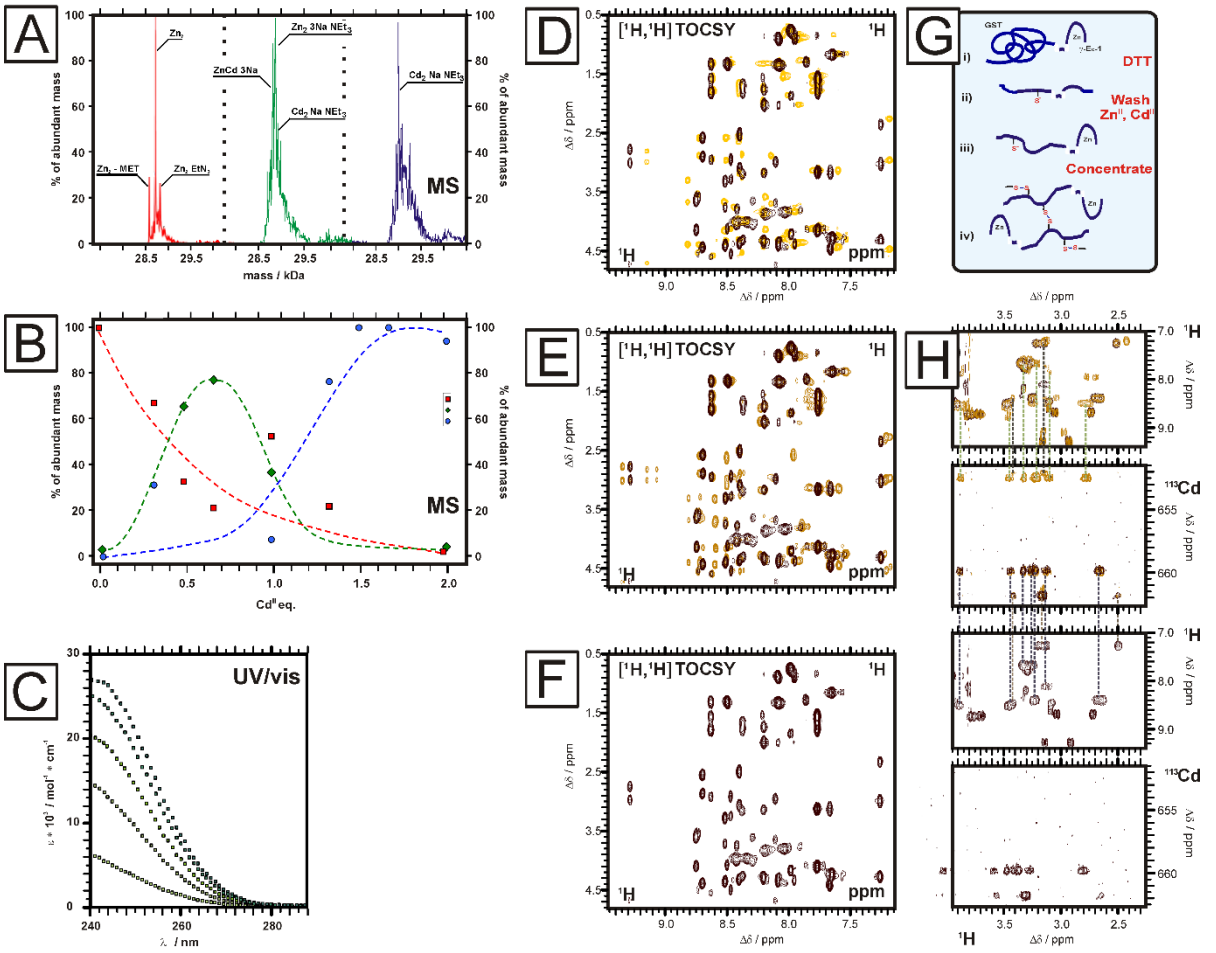

Figure V 2 shows the substitution of Zn_2 GST-γ-E_c-1 by Cd^{II}-ions using the same experimental methodology as for the isolated γ-E_c-1 domain. In ***A)*** the deconvoluted ESI-MS spectra of Zn_2 (red), ZnCd or CdZn (green) and Cd_2 GST-γ-E_c-1 (blue) and the relative abundance of the differently metallated isoform are depicted. The evolution of distribution of the Zn_2 (red), ZnCd or CdZn (green) and Cd_2 (blue) isoforms for all titrated Zn^{II} to Cd^{II} ratios is displayed in ***B)***. ***C)*** The Cd^{II} titration steps followed by UVvis spectroscopy (left: steps of 0.5 Cd^{II} equivalents) are depicted. In the following three panels NMR spectra of the re-metallation process of Zn_2 GST-γ-E_c-1 by Cd^{II}-ions are displayed. In ***D)*** an overlay of the Zn_2 (yellow) with the Cd_2 (brown) form, in ***E)*** an overlay of the Zn_2 (yellow). Zn_1Cd_1 (light brown) and the Cd_2 (brown) form and in ***F)*** the [^{1}H,^{1}H] TOCSY NMR spectra of the Cd_2-form of γ-E_c-1 alone is depicted. In ***G)*** a simplified scheme of GHOST GST fusion protein preparation is displayed. In short: affinity column eluted GST-γ-E_c-1 **i**) is softly denatured with 0.2-0.5 M 1,4-dithiothreitol (DTT) resulting in reduced thiol/thiolates **ii**). After buffer exchange and co-factor addition (Zn^{II}- or Cd^{II}-ions) **iii**), the GST fusion protein is concentrated **iv**) during which inter- and intra-molecular disulfide bridges are formed, constituting the basis for a hydrogel networking process,

which is finished after heat treatment[109] (see **Chapter III**). The [^{113}Cd,^{1}H] HSQC NMR spectra of the Cd_2 GST-γ-E_c-1 and the overlay of Cd_2 (brown) with the Zn_1Cd_1 (light brown) form are shown in ***H)***. The $H_{B2/3}$ – Cd cross peaks are assigned as described in **fig. V 1**.

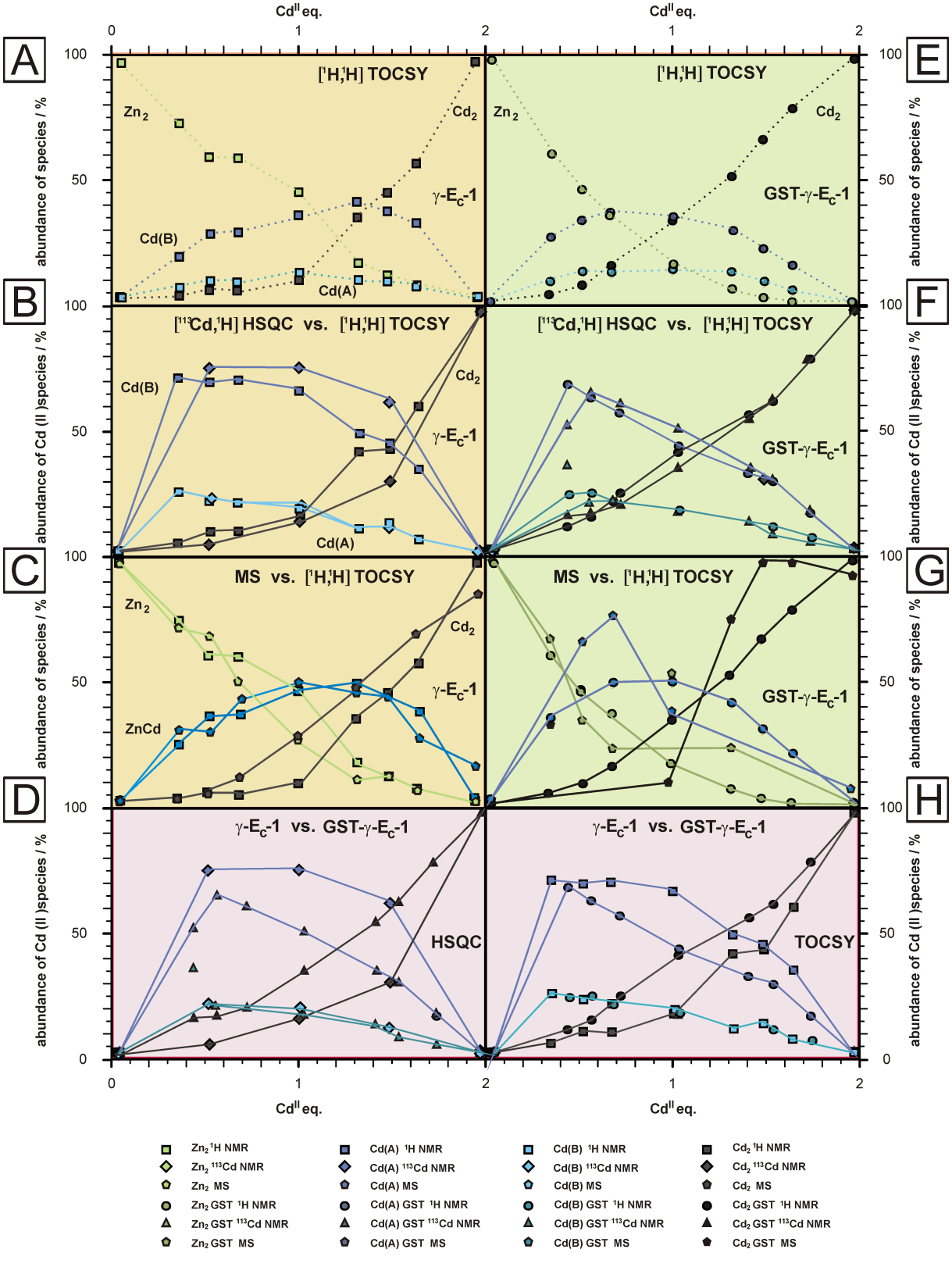

Figure V 3 depicts the distribution and formation of differently metallated species under Cd^{II} addition to $Zn_2\gamma$-E_c-1 and Zn_2 GST-γ-E_c-1. The comparison of the NMR and MS experiments with GST-γ-E_c-1 (yellow background) is put into perspective to those obtained for the isolated γ-E_c-1 domain (green background). Finally the proton ***D)*** and ^{113}Cd NMR spectra ***H)*** of both the GST and the isolated γ-E_c-1 are plotted (purple background). The evolution of all differently metallated isoforms integrated from [^1H,^1H] TOCSY NMR spectra of ***A)*** the GST fusion protein and ***E)*** the isolated γ-E_c-1 domain is shown. Cd^{II} equivalent dependent distribution of the ZnCd- (Cd (A) and Cd (B) site) and Cd_2-forms derived from [^{113}Cd,^1H] HSQC NMR spectra of GST-γ-E_c-1 ***B)*** and the isolated γ-domain ***F)*** are depicted along with the [^1H,^1H] TOCSY NMR spectra for comparison. In order to match the MS data to those obtained from NMR the Cd (A) and Cd (B) site are added to yield a ZnCd-form and plotted against the added Cd^{II} equivalents along with the Zn_2- and Cd_2-data of the [^1H,^1H] TOCSY NMR spectra for the GST fusion protein ***C)*** and the isolated γ-E_c-1 domain ***G)***.

In accordance to the NMR experiments conducted for the isolated γ-E_c-1 domain, 2D [^1H,^1H] TOCSY and [^{113}Cd,^1H] HSQC NMR spectra with the eight different Zn^{II} to Cd^{II} ratios have been recorded and evaluated regarding the abundance of the differently metallated GST-γ-E_c-1 isoforms. The spin system pattern observable in the 2D [^1H,^1H] TOCSY NMR spectra of the GST-γ-E_c-1 and isolated γ-E_c-1 domain are identical (**Fig. V 2d, e, f**), providing the starting point for the evaluation of abundance of the respective differently metallated isoforms as described for the isolated γ-E_c-1 domain. Despite small differences in cross peak intensity the chemical shifts of the Cd^{II} sites evidenced in the [^{113}Cd,^1H] HSQC NMR spectra as well as the $H_{B2/3}$ – Cd cross peak pattern are identical to the one observed for the isolated γ-E_c-1 domain (**Fig. V 1d, e, f**). The substitution of Zn^{II} by Cd^{II} ions of GST-γ-E_c-1 proceeds in accordance with the isolated γ-E_c-1 domain (**Fig. V 3**). Moreover the distribution of the Zn_2-, mixed ZnCd- and Cd_2-form investigated by mass spectrometry and NMR spectroscopy while titrating Cd^{II}-ions to the Zn_2-form of the isolated domain (**Fig. V 3f, g**) and the GST-γ-E_c-1 fusion protein is comparable (**Fig. V 3b, c**). Treating the Zn/Cd exchange of γ-E_c-1 as ordinary chemical reaction we witness for the isolated and the GST fused γ-domain: **i)** the Zn_2-form representing the educt of the Cd^{II} substitution decreases exponentially, while **ii)** the ZnCd-form first increase and then decreases exponentially, signifying the intermediate state and **iii)** the Cd_2-form being the product increases exponentially upon Cd^{II}-ion addition. The intermediate state can be subdivided into two reaction routes, where the metallation of site B

is favored in occupancy in respect to site A by a factor of three (**Fig. V 3a, b, e, f**). While differences in relative abundance of the respective isoforms observed among proton NMR, ^{113}Cd NMR and MS are in the range of the expected experimental error (**Fig. V 3b, c, f, g**) the occupancy of the Cd (B) site is somewhat increased for the isolated γ-domain during the addition of the 0.5th and 1.5th Cd^{II} equivalent in comparison to the GST fusion protein (**Fig. V 3d, h**).

V 4 4 NMR Solution structure of ZnCd GST-γ-E_c-1

Judging from the 2D [^{1}H,^{1}H] TOCSY NMR spectra of the Zn/Cd re-metallation experiments, we hypothesized the existence of a stable ZnCdγ-E_c-1 domain, whose structure could be calculated from distance information (NOEs) derived from 2D [^{1}H,^{1}H] NOESY NMR spectra. However, we were not able to record suitable 2D and ^{15}N resolved NOESY NMR spectra for the isolated γ-E_c-1 domain. As previously reported (see **Chapter III**), the GST fusion protein preparation system GHOST may facilitate NMR solution structure elaboration. In consequence we tested the method for ZnCd GST-γ-E_c-1. In contrast to the isolated domain we were able to record both 2D and ^{15}N resolved NOESY NMR spectra that allowed the

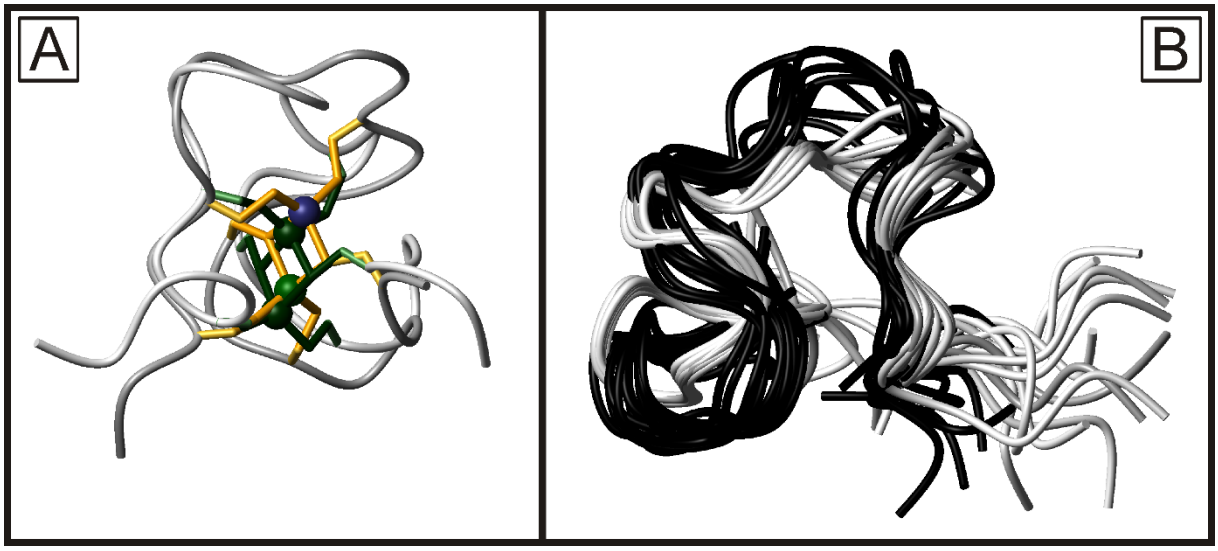

Figure V 4 depicts overlay of the NMR solution structures of ZnCd GST-γ-E_c-1 with Zn_2 GST-γ-E_c-1. ***A)*** Overlay of the lowest energy structure of ZnCd (white ribbon) - and Zn_2 GST-γ-E_c-1 (grey ribbon) displayed in bridging cysteines 3 and 9 conformation. Cysteine thiolates are depicted as sticks (ZnCd: orange; Zn_2: green), the metal ions as spheres (Zn^{II}: green, Cd^{II}: blue). The different metal clusters are

slightly shifted, while the overall topology remains. ***B)*** Overlay of the 20 lowest energy structures of ZnCd (white ribbons) - and Zn_2 GST-γ-E_c-1 (black ribbon) in a backbone bond representation, in the bridging cysteine 3 and 9 conformation.

calculation of a ZnCd GST-γ-E_c-1 structure. We attempted to exclude bias of other metallated forms by only considering those NOEs, which belong to the spin system clearly attributable to the ZnCd-form and those being previously identified as invariable (**Fig. V 4a**).In comparison to Zn_2 GST-γ-E_c-1 different NOEs were observed while previously assigned distance information was not witnessed, resulting in slightly altered solution structure (**Fig. V 4b**). However, conclusive difference in folding of the differently metallated forms of GST-γ-E_c-1 cannot be reported, owing to a lack of proton density and hence resolution around the $M^{II}_2Cys_6$ metal cluster.

V 5 Discussion

V 5 1 Spectrometric and spectroscopical methods for studying Zn^{II} to Cd^{II} re-metallation of tetrahedral tetrathiolate binding sites

Tertiary structural stabilization in proteins can be achieved amongst other by bridging disulfide or metal-ion interaction, especially Zn^{II} tetrathiolate binding sites, conferring a high degree of thermodynamic stability without being easily prone to alteration via redox reactions as witnessed in zinc finger proteins or some heat shock proteins[140]. However, the coordinating thiolates may very well trigger redox-sensing and signalling events[141] as well as determine the metal ion specificity of the metal binding site. Following these processes on a molecular level remains challenging. Besides X-ray based methods[142] mass spectrometry is commonly used to follow metallation pathways[124] in metallothioneins[59] as well as photometric spectroscopy and ^{113}Cd NMR spectroscopy[54]. The different experimental methods inquire different properties of the Zn_2Cys_6 metal cluster. Mass spectrometric analysis may provide information on the distribution of metal species with low concentration in the gas phase, which, however, tend to destabilize tetrathiolate metal binding sites[132], hereby rendering exact quantification speculative. UVvis experiment on the other hand, likewise performed at low, physiological more relevant concentration, in buffer solutions, mimicking cytoplasmatic conditions may render insights on the electronic environment around the metal centre. Especially electronic contribution of the terminal and bridging cysteines to the metal ion give rise to broad absorption bands, which have been examined from an experimental and theoretical point of view (see **Chapter IV**). Gaussian fitting is needed to extract the number of terminal cysteines and the onset of bridging cysteines formation, indicative for homometallic cluster formation. Again quantification is hampered owing to the limits of the Gaussian fit conditions additionally the Zn_2 species of γ-E_c-1 is not detectable under these conditions[142].

Alternatively 2D homonuclear [^1H,^1H] and heteronuclear [^{113}Cd,^1H] NMR spectroscopy may be employed to distinguish the differently metallated γ-E_c-1 species. This is possible owing to the slightly bigger ionic radius of Cd^{II}- versus Zn^{II}-ions, resulting in a larger metal cluster manifesting subtle changes in amide backbone proton (H_N) shifts, which constitute the basis of the differentiation between the differently metallated species in the homonuclear proton 2D NMR spectra. As expected all protons of the six cysteines experience an alteration in

electronic environment witnessed in 2D [^{1}H,^{1}H] TOCSY NMR spectra. Moreover the H_N protons of the two aspartates (D_4, D_5) are also strongly affected by a change in cluster metallation as well as the H_N proton of Gly_{10} (**Fig. V 1e, f**). This could either be due to spatial proximity to the metal cluster, which could be readily excluded from the solution structure, or to an involvement in the cluster stabilization for instance through hydrogen bridging so far not evidenced in 2D [^{113}Cd,^{1}H] HSQC TOCSY NMR experiments. Finally, a participation in the cysteine connectivity switching process is imaginable. As previously reported[106], we believe that the γ-E_c-1 domain can easily harbor both a Zn_2 or a Cd_2 metal cluster necessitating only minor structural rearrangements around the metal centre, without drastically changing its overall fold. This isostructural exchange is also witnessed for some other MTs[128], while others including the fungal MT Neclu_MT1 differentiate between Zn^{II} and Cd^{II} (see **Chapter VI** and **VII**).

Besides already reported Zn^{II} EXAFS experiments[106] both, the existence of invariable chemical shifts for some spin systems (Arg, Lys) in any metallation of the M_2Cys_6 metal cluster and [^{113}Cd,^{1}H] HSQC NMR experiments provide strong evidence of an isostructural Zn/Cd exchange pathway. Especially ^{113}Cd NMR spectroscopy is a highly valuable tool. One may conclude on **i)** the coordination sphere, **ii)** the number of ligands, **iii)** their chemical identity and in concomitance to 2D proton NMR **iv)** the metal to ligand connectivities. In [^{113}Cd,^{1}H] HSQC NMR spectra recorded, a moderate ^{113}Cd downfield chemical shift change (9 ppm) from the Cd_2 to the ZnCd or CdZn cluster was witnessed. This can only be explained by the deshielding of the observable tetrahedral tetrathiolate ^{113}Cd signal, owing to the reduced ionic radius from Cd^{II} ion to Zn^{II} ion, respectively. The cysteine connectivities of the heterometallic cluster could be unambiguously established assigning the ZnCd- and CdZn-form derived cysteine H_B protons to the respective Cd-proton cross peaks, allowing to allocate the cross peaks at 652 ppm to the metal ion site A and those at 653 ppm to the metal ion site B (**Fig. V 1h**). With this data at hand integration of the differently proton-proton cross peaks in the 2D TOCSY NMR spectra and the respective cadmium-proton cross peaks in the 2D HSQC NMR spectra allow exact quantification of the individual differently metallated species. The only drawback of using NMR for this type of quantification is the high, i.e. 1mM, concentration of the protein, putatively resulting in non-physiological relevant aggregation events. In order to evaluate the influence of such processes and due to its other advantages we used the GHOST GST Hydrogel System to validate the reported finding for the isolated γ-E_c-1 domain with those for GST γ-E_c-1.

V 5 2 Comparing the Cd^{II} substitution pathway of the Zn_2-form of the GST fusion protein with the isolated γ-E_c-1 domain.

Employing GST fusion proteins for target protein analysis is a standard method for analyzing protein-protein interaction in GST facilitated pull-down experiments[105] and biochemical characterization of proteins and their ligands[111-112]. Moreover structural biologists investigated GST fused target proteins in crystallization[115-116] and NMR spectroscopy[117] to decipher the structure and correct fold of the protein under investigation. Recently we developed the sample preparation strategy for GST fusion proteins – the GHOST GST fusion protein - based on the polymerization of the GST tag resulting in a hydrogel (**Fig. V 2g**) formation (see **Chapter III**). While proteinous hydrogels are widely use in biomedical applications in cases of homodimeric proteins such as leucine zippers[118], the key processes for GHOST GST fusion protein agglomeration constitutes a mild denaturation step with a reducing agent DDT, also leading to a hydrogel formation of lysozyme at 20 mM concentration and neutral pH after heat treatment[109]. Surprisingly the hydrogel formation fosters NMR based structure investigation. It was shown that the structure of the Zn_2 and Cd_2 GST-γ-E_c-1 is identical to the isolated γ-E_c-1 domain (see **Chapter III**). Based on theses consideration the metallation pathway of Zn_2 to Cd_2γ-E_c-1 was investigated with both the GST-γ-E_c-1 and the isolated γ-E_c-1 domain form (**Fig. V 3**). In case of the isolated γ-E_c-1 domain ^{1}H NMR, ^{113}Cd NMR and MS all experimental methods show a comparable evolution of the Zn_2-, ZnCd-, CdZn-, Cd_2-form.

Semi-quantitatively analyzing the relative abundance of differently metallated metallothionein species with mass spectrometry is routinely employed for deciphering MT metal ion coordination[8, 144]. For MTs the charge to mass ratio (m/z) is the decisive feature. In case of small proteins such as the isolated γ-domain the isotopic distribution of the different metal ions can be resolved, yet the number of protonated states observable in the sensitivity range of common ESI-MS detector may not suffice for automated spectral deconvolution. On the other hand average sized proteins e.g. GST yield excellent distributions of protonated states, only minorly affected by the fused small protein allowing to compare different fusion proteins, yet the isotopic sensitivity is diminished, rendering identification of the exact metallated state difficult, especially when salt adducts contaminate the sample. In case of the 2.5 kDa γ-domain the evolution of the differently metallated isoforms of the isolated domain more

closely resembles the one of the NMR spectra (**Fig. V 3c, g**), however the MS spectra could not be automatically deconvoluted. As already reported NMR spectroscopy employing the GST hydrogel system (GHOST) preparation method for GST fusion proteins yield excellent NMR spectra in case of GST-γ-E_c-1 (see **Chapter III**). This finding is reflected by the excellent agreement of Zn_2-, ZnCd- and Cd_2-form evolution evidenced in [^{113}Cd,^{1}H] HSQC NMR and [^{1}H,^{1}H] TOCSY NMR spectra during Cd^{II} addition (**Fig. V 3b, f**). As proton NMR spectroscopy is regularly applied to quantitatively assess different proteinous isoforms we can show that ^{113}Cd NMR is as well suitable for relative quantification of metal site occupancy, greatly facilitating investigations on the metallation state of metalloproteins lacking sufficient quality proton NMR spectra[143].

V 5 3 The structure of ZnCd GST-γ-E_c-1

Cd^{II} poisoning of a Zn_2Cys_6 zinc finger metal cluster proceeds either cooperatively or via a mixed metal transition state. Both the experimental and computational studies suggest the existence of a preferred ZnCd metallation site, which structure might be elucidative via NMR spectroscopy. Despite tremendous effort and favourable 2D TOCSY NMR spectra NOESY NMR spectra of the isolated γ-E_c-1 domain suitable for structure calculation could not be recorded. This might be due to aggregation processes among the differently metallated domains. In case of the GST-γ-E_c-1 form this problem was not evidenced. In order to avoid Zn_2 and Cd_2-form biased data for the calculation of the ZnCd GST-γ-E_c-1 form, only those NOE were considered for structural calculation that clearly originate from the ZnCd form and those, which are invariable, resulting in a lower structural resolution (**Supplementary material, Figure S V 1**).

In accordance to the subtle structural changes accompanying the re-metallation from the Zn_2- to the Cd_2-form[106], ZnCd GST-γ-E_c-1 displays the same overall fold, cysteine connectivity and metal cluster arrangement as the Zn_2- or Cd_2-form. Compared to the Zn_2 isoform the centre of the metal cluster as such is further pushed outward in the direction of the Cd_2-form (**Fig. V 4**). Neither detailed differences in the protein backbone originating from 20% different NOE cross peaks were witnessed nor further protein – metal cluster interactions. Together with the computational studies, the structure elucidation of ZnCd GSTγ-E_c-1 suggests a facile, low energy site-specific structural transition from the Zn_2 to the Cd_2 isoform.

V 6 Conclusion

Studying Cd^{II} toxification processes of the wheat MT domain γ-E_c-1, containing a GAL4 zinc finger like Zn_2Cys_6 cluster, on a structural level, requires a multitude of experimental techniques. We have designed an approach that utilizes **i)** mass spectrometry, providing information on the number of species (Zn_2, mixed ZnCd, Cd_2) and their distribution; with **ii)** UVvis spectroscopy, by fitting Zn^{II} – Cd^{II} exchange titrations, giving insight on the Cd^{II} first ligand shell environment (tetrahedral tetrathiolate) and the onset of Cd_2 cluster formation; complemented with **iii)** multidimensional – multinuclear NMR spectroscopy, yielding information concerning the site-specific Zn^{II} to Cd^{II} exchange, the distribution of the respective Cd^{II} – containing isoforms (CdZn, ZnCd, Cd_2) as well as the structure of the predominant ZnCdγ-E_c-1 domain. The combination of these three powerful methodologies allows drawing conclusion regarding **i)** the distribution of all the differently metallated species via MS and proton NMR, **ii)** the number and molecular identity of the Cd^{II}-ligands by UVvis and ^{113}Cd NMR, **iii)** the cooperativity of the re-metallation process through UVvis and ^{113}Cd NMR and the **iv)** site specificity of metal ion binding sites regarding Cd^{II} (**Fig. V 3**) as well as the solution structure of the ZnCd-form employing NMR spectroscopy (**Fig. V 4**) sonding electron and nuclear properties over a wide concentration (2 μM to 1 mM) and physiological pH range (6.9 to 8) in gas phase and aqueous solution. All experiments were conducted using the isolated γ-E_c-1 domain and the recently engineered GHOST GST fusion protein system employing a GST-γ-E_c-1 construct for the respective experimental procedures, which allowed the structure elaboration of the ZnCd form of GST-γ-E_c-1.

In this study we successfully report the strength of applying a set of experimental techniques to follow the poisoning of a binuclear Zn^{II} site by Cd^{II} ions, further isolated a transition state and finally validated the ease of using the GHOST GST fusion protein system for its structural calculation.

V 7 Acknowledgements

This work was supported by the Swiss National Science Foundation (SNSF Professorship to E.F.).

V 8 Supplementary Material

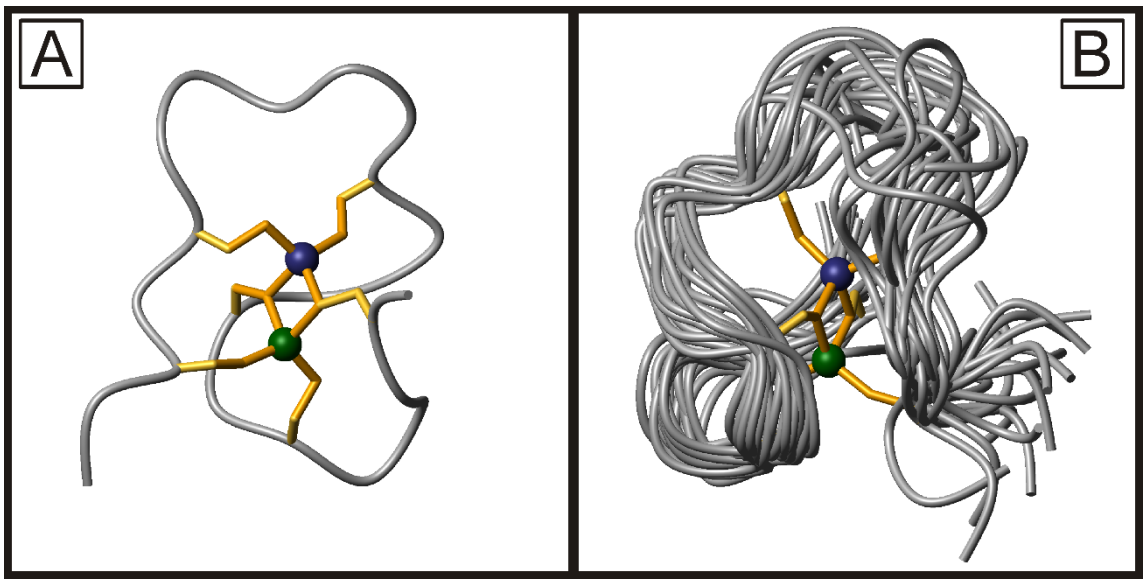

Table S V 1 Solution structure statistics and F**igure S V 1** overlays of 3D structure of ZnCd GST-γ-E_c-1. The protein backbone is displayed in grey ribbon shape while the metal cluster consisting of the metal ion (blue spheres Cd^{II}; orange sphere Zn^{II}) and the coordinating Cys (orange bonds) are depicted in color. ***A)*** Lowest energy solution structure of ZnCd GST-γ-E_c-1 displaying the metal cluster. ***B)*** The 20 lowest energy structures of ZnCd GST-γ-E_c-1 exemplarily displaying the metal cluster.

Table 1 Statistics of structure calculations:

	Cd3*	Zn3*	CdZn3* GST	ZnCd21* GST
NMR distance restraints				
Total NOE	374	462	196	205
Short range: |i−j|≤1	322	396	199	205
Medium range: 1>|i−j|>5	61	69	0	9
Long range: |i−j|≥5	15	20	11	7
Maximal distance restraint violation (Å)	0.11	0.11	0.11	0.11
AMBER energies (kcal/mol)				
Total (mean±SD)	−679 ± 76	−697 ± 70		
van der Waals	−14 ± 4	−12 ± 5		
RMSDs from idealized geometry				
Bond lengths (Å)	0.0142 ± 0.0002	0.0136 ± 0.0002		
Bond angles (°)	2.15 ± 0.06	1.94 ± 0.06		
Ramachandran plot statistics (%)				
Residues in most favored regions	80.9	74.4	56.8	58.2
Residues in additionally allowed regions	18.2	24.7	43.2	41.2
Residues in generously allowed regions	0.9	0.9	0	0.6
Residues in disallowed regions	0	0	0	0

RMSDs from the mean coordinates (Å)				
N, Cα, and C′ of residues 2-22	0.70±0.14	1.47 ± 0.66	2.14 ± 0.44	2.13 ± 0.49
Heavy atoms of residues 2-22	1.37±0.26	2.02 ± 0.60	2.78 ± 0.48	2.91 ± 0.51

* The number describes the residue that presents the second bridging Cys moiety (in addition to Cys-9). The numbering and metal cluster features are detailed in[106].

Chapter VI : A metallothionein from the aquatic fungus *Heliscus lugdunensis* shows cadmium specificity

Jens Loebus[a#] · Barbara Leitenmaier[a#] · Diana Meissner[b] · Bianca Braha[b] · Gerd-Joachim Krauss[b] · Dirk Dobritzsch[b*] · and Eva Freisinger[a*]

[a]Jens Loebus · Barbara Leitenmaier · Eva Freisinger

Institute of Inorganic Chemistry, University of Zurich,

8057 Zurich, Switzerland

[b]Diana Meissner · Bianca Braha · Gerd-Joachim Krauss · Dirk Dobritzsch

Institute of Biochemistry and Biotechnology, Ecological and Plant Biochemistry, Martin-Luther-University Halle-Wittenberg,

06120 Halle (Saale), Germany

[#]these authors contributed equally

[*]e-mail: freisinger@aci.uzh.ch; dirk.wesenberg@biochemtech.uni-halle.de

Keywords: Metallothionein · Cd detoxification · Electronic absorption spectroscopy · NMR spectroscopy

VI 1 Abstract

A spring from a former copper shale mine in the area *Mansfelder Land*, Germany, shows extremely high transition metal ion concentrations, i.e. 40 mM Zn^{II}, 208 μM Cu^{II}, 61.3 μM As^{V}, and 25 μM Cd^{II}. This makes it a challenging habitat for living organisms as they have to cope with metal ion concentrations by far exceeding the values usually observed in spring water. One of the surviving species found is the aquatic fungus *Heliscus lugdunensis*. Investigation of its redox related heavy metal tolerance revealed the presence of small thiol containing compounds as well as a small metallothionein, Neclu_MT1 (MT1_NECLU: P84865). Metallothioneins (MTs) form a superfamily of small (< 10 kDa), cysteine-rich metalloproteins physiologically linked to metal homeostasis and detoxification. Transcription of various *mt* genes in different organisms can be induced by Cd^{II} ions, but never exclusively. Hence with Neclu_MT1 it is shown here for the first time that induction of an MT is solely triggered by Cd^{II} but not by other metal ions such as Zn^{II} or copper ions. The present study suggests that discrimination between Zn^{II} and Cd^{II} ions can be also feasible on the protein level. Stoichiometric analyses of the recombinant protein in combination with photospectrometric metal ion titrations and ^{113}Cd-NMR experiments reveal that metal ion binding capacities and consequently the structures formed differ from each other. Concluding, we describe the first solely Cd^{II}-inducible metallothionein, Neclu_MT1 from *H. lugdunensis*, featuring a difference in the structure of the Cd^{II} *versus* the Zn^{II} metallated protein in a physiologically relevant concentration range.

VI 2 Introduction

The kingdom of fungi includes a huge variety of diverse and puzzling organisms, populating some of the harshest terrestrial and aquatic habitats, including metal contaminated sites like present and former mining areas[20-21, 144-145]. This raises the question, which mechanisms allow fungi to cope with such high metal ion concentrations. In yeast the tight regulation of essential Cu^{I} ions, which become toxic at higher concentrations, involves two metal sensing transcription factors, ACE1 and MAC1[146]. In many organisms non-essential or toxic metal ions including Cd^{II} are handled on a metabolic level via phytochelatin synthase (PCS)[147]. PCS uses heavy metal coordinated glutathione, an important thiol containing cellular redox state regulator, as a substrate to form poly(γ-glutamylcysteine)glycine (phytochelatin, PC: general structure $(\gamma\text{-EC})_nG$, n=2-6). Some fungi like *Saccharomyces cerevisiae* and *Heliscus lugdunensis* lack the enzyme PCS and hence are not capable of PC synthesis via PCS (*H. lugdunensis,* unpublished data). In *H. lugdunensis*, exposure to Cd^{II} leads to the intracellular up-regulation of glutathione as well as of the dipeptidic glutathione precursor γ-glutamylcysteine (γ-EC), the induction of a phytochelatin (PC2) possibly formed by a carboxypeptidase[20], and the induction of one metallothionein (MT) as defence mechanism[20, 22]. MTs are relatively small proteins (< 10 kDa) with a high Cys content that can reach up to 33% in the mammalian forms and are found in all living phyla[12, 20, 148-150], except *archaea*. Their exceptionally high affinity towards the soft d^{10} metal ions, e.g. both essential Zn^{II} and Cu^{I} ions and non-essential Cd^{II} and Hg^{II}, and their large metal ion binding capacity distinguish MTs from other metalloproteins. For the divalent metal ions, the binding strength increases in the order $Zn^{II} < Cd^{II} < Hg^{II}$ in line with increasing thiophilicity of the metal ions[151]. Generally, MTs are proposed to play a role in Zn^{II} and Cu^{I} homeostasis as well as in heavy metal ion detoxification[65], and it is often not easy to separate and decipher these two functions from each other due to the nearly unprecedented high thiol content of these proteins: Whenever an organisms is challenged with high concentrations of e.g. Hg^{II} or Cd^{II} any MT present will take up these thiophilic metal ions like a sponge due to the high thermodynamic stability of the corresponding Hg^{II}- and Cd^{II}-complexes. However, this "chemical" property can possibly mask a homeostatic function, i.e. binding of Zn^{II} or Cu^{I} in the unchallenged organism[151]. Recently, even a Ag^{I} containing MT form was isolated from the fruit bodies of

an ectomycorrhizal fungus, which was grown on naturally Ag^{I}-contaminated soil[152], further expanding the list of metal ions found associated with MTs *in vivo*. Additional yeast complementation assays showed that this MT can also function in Cu^{I} resistance. Again this leaves the unresolved question if this specific MT has physiologically a dual function including heavy metal detoxification, or was just "incidentally" loaded with Ag^{I} ions due to the higher thermodynamic stability of the resulting Ag^{I}-MT complex. One approach to separate MTs into Zn^{II} homeostasis or Cd^{II} detoxification linked proteins is based on the presence of histidine residues in the amino acid sequence as a contributing factor[10, 153]. Studies on a Zn-finger peptide model have shown that the stability constants for Zn^{II} and Cd^{II} binding to a Cys_3His site are roughly the same[154]. In contrast, the $ZnCys_2His_2$ complex is more and the $ZnCys_4$ complex less stable than the corresponding Cd^{II} complex. Hence, an increasing number of His residues should raise the affinity for Zn^{II} binding and favour a homeostatic function. An example corroborating this hypothesis is the seed-specific MT from *Triticum aestivum* (common bread wheat). This protein was isolated directly from the plant material and contains exclusively Zn^{II} ions in its native state[14] suggesting a role in zinc storage for germination. The solution structure of the protein solved by NMR spectroscopy revealed that the two highly conserved His residues participate in the formation of a $ZnCys_2His_2$ binding site[9] leading to the proposal of a discriminating function of these ligands against Cd^{II}.

The focus of the present study is set on the fungus *Heliscus lugdunensis* (Teleomorph: *Nectria lugdunensis*), which belongs to the group of aquatic hyphomycetes and was isolated in a highly heavy metal polluted spring in a former mining district in the area of *Mansfelder Land*, Germany[155]. The small MT Neclu_MT1 was first described in *H. lugdunensis* strain H 4-2-4 as part of the thiol-based defence mechanism of the fungus under Cd^{II} stress. While induction by Cd^{II} ions was shown for many *mt* genes from diverse organisms[156-159] results are most often not followed through to their logical conclusion: the evaluation of the gene translate levels. Quantification of protein expression levels in the host organism is much more complex and tedious experimentally compared to gene expression studies, however, results have by far the greater biological significance. For Neclu_MT1 this was accomplished, and indeed translation of the protein is induced by Cd^{II} ions. However, no induction of the Neclu_MT1 protein is observed in response to Zn^{II} or Cu^{I} ions. This is the major difference to most other MTs, which are also induced by other metal ions although this was again mostly shown on the genetic level. Additionally and very importantly, exclusively the Cd^{II} form of Neclu_MT1

was isolated from its native host[22]. In order to obtain a deeper insight into the regulation and detoxification mechanisms of organisms living in heavily Cd^{II} polluted environments, we also analyzed the metal ion binding and discrimination properties of the recombinantly expressed Neclu_MT1 in more detail.

VI 3 Experimental Procedures

VI 3 1 Materials

All reagents used in the experimental procedures were of high or highest grade or purity.

VI 3 2 Physiological experiments with *Heliscus lugdunensis* strain H 4-2-4

Isolation from its native site, *in vitro* growth and induction conditions as well as quantification of metal ions and cellular thiol compounds using post-column derivatization RP-HPLC has been described in detail before[20, 22, 24]. In summary, the fungus was pre-cultivated for five days on malt agar containing spring water from its native site (dissolved 1:1 in millipore water) to ensure identical starting conditions for metal ion stress experiments. Subsequently, *H. lugdunensis* was grown in liquid culture containing 25 μM Cd^{II} or 25 μM Zn^{II}, respectively. Quantification of thiol compound and metal ions was performed in at least five replicates at the log phase stage, i.e. after 3 days. In all experiments resazurin (7-hydroxy-3*H*-phenoxazin-3-one 10-oxide) as well as wet and dry weight was used to assay fungal viability.

VI 3 3 Plasmid construction, MT expression, purification, and preparation of apo-Neclu_MT1

For the synthetic gene encoding Neclu_MT1 two 75 nt long oligonucleotides were purchased from metabion GmbH, Martinsried, Germany (forward: 5'-tctccgtgca cctgctctac ctgcaactgc gcgggtgcgt gcaactcttg ctcttgcacc tcttgctctc acatg-3'; reverse: 5'-gtgagagcaa gaggtgcaag agcaagagtt gcacgcaccc gcgcagttgc aggtagagca ggtgcacgga gacat-3'). BamHI and EcoRI restriction sites were introduced by PCR and the digested product cloned into the pGEX-4T1 expression vector (GE Healthcare). The GST-Neclu_MT1 fusion protein was overexpressed in *Escherichia coli* BL21(DE3) cells and protein purification was performed as described in[106] yielding a final protein with a length of 25 amino acids and the following sequence

GSPCTCSTCNCAGACNSCSCTSCSH.

The *N*-terminal amino acid Gly is generated by the thrombin cleavage site. Preparation of a completely reduced and demetallated monomeric apo-Neclu_MT1 species was performed according to[61].

VI 3 4 Preparation of Cd^{II} and Zn^{II} Neclu_MT1 and Chelex® 100 treatment

All solutions used in the protein reconstitution and metal-ion titration experiments were rendered oxygen free by three freeze-pump-thaw cycles on a vacuum line, saturated with argon, and prepared or handled in an anaerobic chamber. To study the metal ion binding ability, five equivalents of Zn^{II} or Cd^{II} ions were added to apo-Neclu_MT1 at acidic pH followed by pH adjustment to 7.5 with 1 M Tris/HCl and dilution to the desired final protein concentration with ddH_2O. Samples were taken before the addition of 5% w/v Chelex® 100 and after each time interval. The residual Chelex® 100 resin in each sample was removed via centrifugation and the supernatant was analyzed with flame atomic absorption spectroscopy (F-AAS; Varian AA240FS Fast Sequential AAS) for the metal content and with the 2-PDS assay[43, 61] to determine the number of thiolate groups and hence the protein concentration.

VI 3 5 Titration of apo-Neclu_MT1 with Zn^{II}, Cd^{II}, and Co^{II}

Each metal-ion titration as well as the pH-titrations were carried out from one batch of apo-Neclu_MT1. Each set of titrations was performed in at least two replicates using different apo-Neclu_MT1 batches to ensure maximum reproducibility. The pH value of apo-Neclu_MT1 in 0.1 M HCl was adjusted with metal-free 1 M Tris to around pH 7.2. Inside the anaerobic chamber the apo-MT solution was transferred into a 1-cm septum sealed cuvette and the respective metal-ion solution was filled into a 25-µl Hamilton syringe. Protein concentrations used were 15 µM (for Cd^{II}), 25 µM (Zn^{II}), and 50 µM (Co^{II}). After each incremental metal ion addition UVvis spectra were recorded in the range of 200-400 nm for Zn^{II} and Cd^{II} and 200-800 nm for the Co^{II} titration. At the end of each metal titration experiment, the protein concentration was again determined with the 2-PDS assay to exclude protein oxidation and the metal ion concentration was measured with F-AAS to verify the total concentration of added metal ions and to exclude titration errors. Finally, size exclusion chromatography (SEC) was applied to show the monomeric character of the resulting Zn^{II}- and Cd^{II}-Neclu_MT1 species.

VI 3 6 pH titrations

The Zn^{II} and Cd^{II} Neclu_MT1 samples used for the pH titrations were prepared by addition of a small excess of approximately 3.3 equiv. of metal ions to apo-Neclu_MT1, which was adjusted to pH 8.9. Final protein concentration for the Cd_3Neclu_MT1 sample was 15 µM in 5 mM Tris/HCl, pH 8.9. For Zn^{II} Neclu_MT1 two protein concentrations were chosen, a lower one of 5 µM resembling the intracellular Neclu_MT1 concentration determined in the organism grown under conditions of the site of isolation and a higher concentration of 25 µM also used for the titration of apo-Neclu_MT1 with Zn^{II} ions, both in 5 mM Tris/HCl, pH 8.9. Plots of molar absorptivity at 230 nm for the Zn^{II}-form and at 250 nm for the Cd^{II}-form against the respective pH values were fitted with two different functions. The function considering the presence of just a single pK_a value was used to determine the average apparent pK_a value of all Cys residues in presence of the respective metal ion to enable the comparison with literature values. An additional data fit with two apparent pK_a values allows the closer evaluation of the curve shape, e.g. the identification of a two-step metal ion release. Detailed fitting parameters can be found in the **Supplementary Material VI**.

VI 3 7 ^{113}Cd NMR spectroscopy

NMR samples were prepared by reconstitution of the apo-forms with $^{113}Cd^{II}$. Final concentrations and buffer conditions of the samples were 1.5 mM $^{113}Cd_{2.5}$Neclu_MT1 in 20 mM Tris/HCl, pH 8.0, and 50 mM NaCl. The ^{1}H-decoupled ^{113}Cd NMR spectra were recorded with a Bruker DRX 500-MHz spectrometer relative to the signal of 1 M $Cd(ClO_4)_2$ at 310 K.

VI 4 Results

VI 4 1 Induction of the metallothionein Neclu_MT1

Neclu_MT1 protein induction was investigated in response to the addition of Zn^{II}, Cd^{II}, Cu^{II}, and As^{V} to the growth medium of the fungus. In addition to their direct toxicity at elevated concentrations, Cu^{II} and As^{V} can also induce MT expression by causing oxidative stress, e.g. via Fenton- and Haber-Weiss-like reactions in the case of Cu^{II}. While supplementation with 25 µM Cd^{II} or more induced Neclu_MT1 protein expression, neither 50-350 µM Zn^{II} nor 25-50 µM As^{V} or up to 208.5 µM Cu^{II} ions showed any effect, indicating that induction of Neclu_MT1 is neither triggered by metal ion stress in general nor by oxidative stress, but exclusively in response to Cd^{II} (**Fig. VI 1a**). Analyses of the fungus grown in the heavy metal

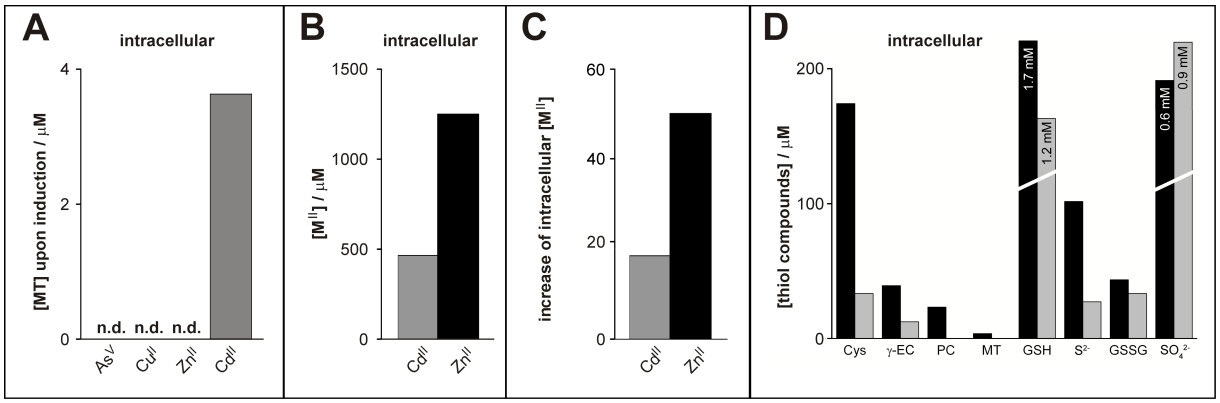

Figure VI 1. Induction of Neclu_MTs and other intracellular thiol containing compounds in dependence of Zn^{II}, Cu^{II}, and Cd^{II} ions. ***A)*** Neclu_MT1 induction under 350 µM Zn^{II}, 208 µM Cu^{II}, 61.3 µM As^{V}, or 25 µM Cd^{II}. ***B)*** Plot of intracellular Cd^{II} (grey) and Zn^{II} (black) concentrations at 25 µM extracellular Cd^{II} or Zn^{II} concentration, respectively. ***C)*** Display of intracellular Zn^{II} dilution (black) and Cd^{II} accumulation (grey) in *H. lugdunensis* grown in liquid media supplemented with 25 µM Zn^{II} or 25 µM Cd^{II}. ***D)*** Intracellular thiol concentrations of all relevant lower molecular mass cysteine compounds when grown in 25 µM Cd^{II} (black bars) in comparison to control experiments without additional metal ions (grey bars).

polluted water from the mining area of isolating show intracellular metal ion concentrations of up to 500 μM Cd^{II} and 1.25 mM Zn^{II} (**Fig. VI 1b**) and hence accumulation of Cd^{II} (**Fig. VI 1c**). *In vivo* Neclu_MT1 translate levels detected were in the range of 5 μM (intracellular) (**Fig. VI 1d**). Additionally, the concentrations of other low molecular mass Cys containing compounds were quantified in order to evaluate the potential cellular Cd^{II} binding capacity of the fungus. Moreover, elevated levels of glutathione (GSH), cysteines, sulfides, γ-ECs, or PCs may indicate a possible stress reaction in the fungus, which however is not witnessed when supplementing 25 μM Cd^{II} to the growth media.

VI 4 2 Metal ion binding capacity of Neclu_MT1

To obtain sufficient amounts of uniform material the protein was recombinantly expressed in *E. coli* in form of the glutathione *S*-transferase- (GST-) tagged fusion protein. After proteolytic cleavage of the GST-tag the metal-free apo-protein was prepared by acidification and purified under anaerobic conditions with size exclusion chromatography (SEC). To access the metal ion binding capacity, apo-forms of Neclu_MT1 at different concentrations, i.e. at 5 and 50 μM, were exposed to 5 equivalents of Zn^{II} ions at pH 7.5. Subsequently, the unbound or loosely bound metal ions were either removed with Chelex® 100 resin (Bio-Rad) or by SEC at pH 7.5. Metal ion quantification was performed with flame atomic absorption spectroscopy (F-AAS), the MT concentration was accessed via quantification of the Cys thiol groups using 2,2′-dithiodipyridine[43]. The measurements show the presence of two Zn^{II} ions per MT molecule in the 5 μM sample and a slightly increased amount, i.e. 2.4 equiv. of Zn^{II}, in the 10-fold concentrated sample. In contrast, analogously performed experiments with Cd^{II} yielded a Cd_3-Neclu_MT1 stoichiometry for both, the higher and the lower concentration (**Supplementary Material**). Analyses of the more concentrated samples with electrospray ionization mass spectrometry (ESI-MS) solely show signals for Zn_3 and Cd_3 forms, respectively. In addition, ESI-MS spectra were used to exclude the formation of oxidation products. No multimer formation was observed in the elution profile obtained during SEC (**Supplementary Material**). As pointed out above, the intracellular Neclu_MT1 concentration of the fungus grown under the conditions of the spring water are around 5 μM and hence the two forms obtained with the lowest concentration, i.e. Zn_2-Neclu_MT1 and Cd_3-Neclu_MT1, can be regarded as physiologically relevant.

VI 4 3 Spectroscopic features of Neclu_MT1

In absence of three-dimensional structural data, spectroscopic methods can give valuable details helping to decipher the nature of metal ion binding. The characteristic ligand-to-metal charge transfer (LMCT) bands observed in the UV spectra of the Zn^{II}- and Cd^{II}-bound forms at 230 and 250 nm, respectively, can be conveniently used to monitor the process of metal ion coordination (**Fig. VI 2a**). The stepwise titration of apo-Neclu_MT1 with Zn^{II} or Cd^{II} ions reveals the maximum metal ion binding capacity of the protein and allows to a certain extend the identification of the coordinating ligands.

Addition of the first two equivalents of metal ions causes an increase in absorptivity at 250 nm for Cd^{II} and 230 nm for Zn^{II}, and hence indicates a tetrahedral tetrathiolate coordination environment (**Fig. VI 2d**)[45]. A further increase of the LMCT bands is only observed up to 2.5 equiv., suggesting that binding of a third metal ion requires both thiolate groups as well as ligands from other amino acids, e.g. the C-terminal His residue (**Fig. VI 2b** and **d**). While the results from the titration experiments with Zn^{II} and Cd^{II} are closely similar indicating identical metalation pattern, a small but reproducible kink of the absorptivity increase is observed after addition of 2 equiv. of Zn^{II}, which might point to the formation of a defined and stabilized Zn_2-Neclu_MT1 intermediate (**Fig. VI 2d**). To analyze the cluster formation process, apo-Neclu_MT1 was titrated with Co^{II} ions (**Fig. VI 2c**). In contrast to Zn^{II} and Cd^{II}, the paramagnetic Co^{II} ion with its d^7 electron configuration, is not spectroscopically silent. Of special use is the sensitivity of its *d-d* transitions in the range of roughly 500-800 nm to changes in its coordination geometry[46].

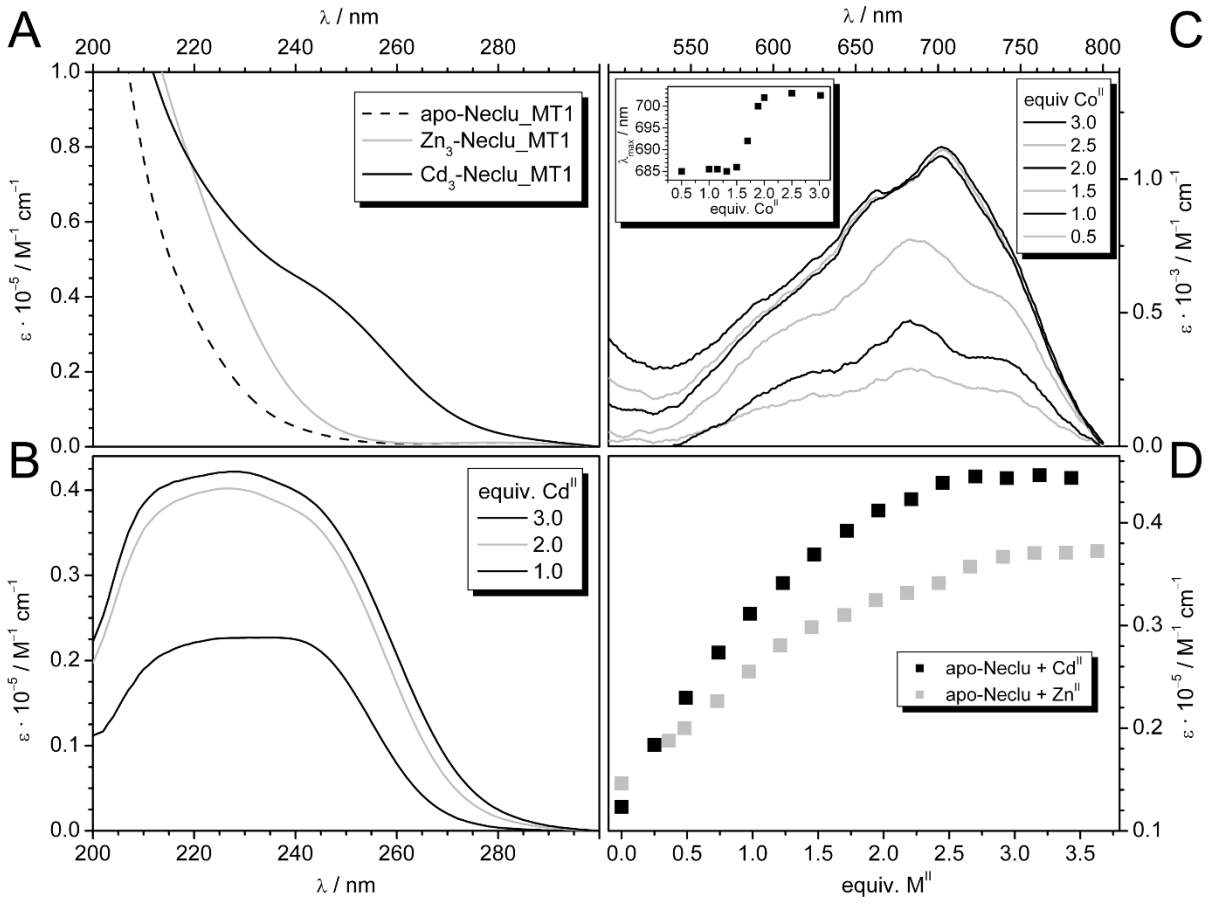

Figure VI 2. Metal ion titration studies of Neclu_MT1 with the divalent metal ions Zn^{II}, Cd^{II}, and Co^{II} were followed with UVvis spectroscopy. These metal ions prefer a tetrahedral tetrathiolate coordination sphere. Upon coordination characteristic ligand-to-metal charge transfer (LMCT) bands originating from the metal-thiolate bonds develop at 230 nm for Zn^{II} and at 250 nm for Cd^{II} coordination and allow to determine the metal ion binding capacity of a MT in a simple titration experiment[68]. ***A)*** UV spectra of apo-Neclu_MT1 (black dashed) and the completely metallated Zn_3- (grey) and Cd_3Neclu_MT1 forms (black). ***B)*** Difference spectra obtained by subtracting the apo-Neclu_MT1 absorption from Cd_1- (lower black spectrum), Cd_2- (grey), and Cd_3Neclu_MT1 (upper black spectrum). ***C)*** Difference spectra of the titration of 50 μM apo-Neclu_MT1 with Co^{II} ions. Absorption bands in the visible part of the spectra between 500 and 800 nm arise from metal *d-d* transitions. The absorption increase is proportional to the number of tetrahedrally coordinated Co^{II}-ions, while shifts of absorption maxima indicate a distortion of the tetrahedral coordination geometry originating from cluster formation, i.e. the transition of a structure with exclusively terminal thiolate ligands to an arrangement involving bridging thiolates. Such a transition to a clustered structure is observed after addition of 1.5 eq. Co^{II} in the visible region of the spectra (inset)[46]. ***D)*** 25 μM apo-Neclu_MT1 was titrated with increasing amounts of Zn^{II} (grey squares) or Cd^{II} (black squares), and

the molar absorptivity of the corresponding LMCT band at 230 nm and 250 nm, respectively, plotted against the number of Zn^{II} or Cd^{II} ions added. In analogy to the Cd^{II} titration experiment (see also B), the absorptivity increase suggests binding of a third Zn^{II} ion by a combination of Cys thiolates and ligands from other amino acids.

The onset of metal-thiolate cluster formation is accompanied by shifts of the absorption bands, both in the UV and visible regions of the spectra. Such a shift of absorption bands can be observed upon addition of more than 1.5 and up to 2.0 equiv. of Co^{II} ions and indicates that coordination of these metal ions requires the recruitment of bridging thiolates, i.e. indeed a cluster formation takes place.

VI 4 4 Metal ion binding affinities

pH titrations monitored by UV spectroscopy have been employed to investigate the metal ion binding affinities of different MT species as protons compete with the metal ions for the Cys thiolate groups with decreasing pH finally resulting in the complete loss of the metal ions. In this way, apparent pK_a values for the Cys thiolate groups in presence of the metal ion of interest can be obtained. The pH titration of the Zn^{II}-form was performed at two different protein concentrations as experiments with Chelex® 100 resin described above revealed a concentration dependence of the metal content found.

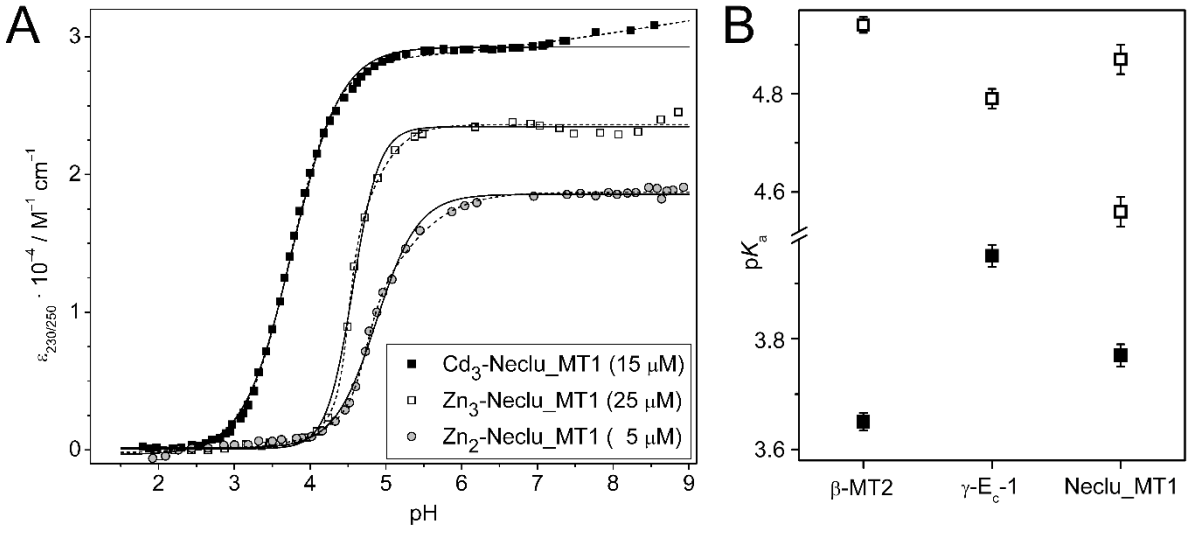

Figure VI 3. ***A)*** pH titration of Cd^{II}- and Zn^{II}- Neclu_MT1. Plots of the extinction coefficients at 230 nm for the Zn^{II}- and at 250 nm for the Cd^{II}-form against the pH value of the solution. The pH titration of the Zn^{II}-form has been performed at two different protein concentrations. At 25 μM the major

species is Zn_3Neclu_MT1, while at 5 μM the Zn_2-form prevails. The stoichiometry of the Cd^{II}-form, i.e. Cd_3Neclu_MT1, is not concentration dependent in the range used for the spectroscopic experiments described. Curve fitting of the plots allows determination of the apparent pK_a values of the Cys thiolate groups in presence of the respective metal ions and hence provides information about the metal ion binding affinities of Neclu_MT1. Curve fitting was performed assuming either one (solid lines) or two (dashed lines) pK_a values as described in the literature[68] and results in values of 3.77(2) for Cd_3Neclu_MT1, 4.56(3) for Zn_3Neclu_MT1, and 4.87(3) for Zn_2Neclu_MT1. The standard deviations are given as 3σ. ***B)*** The apparent pK_a values of Neclu_MT1 are compared with those of the β-domain of human MT2[160] featuring a $M^{II}_3Cys_9$ cluster and γ-domain of the wheat E_c-1 MT, which contains a $M^{II}_2Cys_6$ cluster[106] (Zn^{II}-forms open squares, Cd^{II}-forms black squares). Apparently, Zn_3Neclu_MT1 is slightly more stable, while the pK_a for Cd_3Neclu_MT1 ranges in between the values determined for the other two small metal-thiolate clusters. Compared to the full-length mammalian MTs, which show the highest affinities for metal ions, the apparent pK_a value of Cd_3Neclu_MT1 is by 0.2-0.8 log units and of Zn_3Neclu_MT1 by 0.3 log units larger and hence the metal ion affinity reduced. Interesting to note is the significantly reduced pH stability of the Zn_2Neclu_MT1 form.

The apparent pK_a values obtained for the different Zn^{II}- and Cd^{II}-Neclu_MT1 forms are 4.87(1) for Zn_2-, 4.56(1) for Zn_3-, and 3.76(1) for Cd_3-Neclu_MT1. These values are in all cases larger than the corresponding values obtained for mammalian M^{II}_7MTs, which are among the MTs with the highest metal ion affinities (**Fig. VI 3**)[12]. In comparison to other small metal-thiolate clusters, i.e. the $M^{II}_3Cys_9$ cluster in the β-domain of mammalian MTs[160-161] and the $M^{II}_2Cys_6$ cluster of the γ-domain of the wheat MT E_c-1[106], however, the differences are smaller (**Fig. VI 3**). In case of the Zn_3-species prevailing at the higher protein concentration a lower pK_a was found than for the Zn_2-form present at lower concentration indicating that the metal ion affinity of the Zn_3-form is higher. Additionally, the extinction coefficients at the Zn^{II}-S_{Cys} LMCT band (230 nm) for both forms vary, suggesting an incomplete incorporation of all cysteine ligands in the metal ion coordination of Zn_2-Neclu_MT1.

A comparison of the pH titrations of Zn_2- and Zn_3-Neclu-MT1 with each other suggests that the third metal ion in the Zn_3-form is not just coordinated in an additional binding site. If two different sets of binding sites were present a two step-behaviour of metal ion release would be expected corresponding to the subsequent release of one and two Zn^{II} ions, or *vice versa*. As this is not observed, it is probable that upon binding of the third metal

ion a rearrangement of the structure takes place resulting in a cluster structure with an overall higher stability as apparent from the lower pK_a value of Zn_3-Neclu_MT1.

VI 4 5 Probing the metal coordination environment with ^{113}Cd NMR spectroscopy

^{113}Cd NMR spectroscopy provides information about the number of metal ion binding sites with different chemical environments and the nature of the coordinating ligands. ^{113}Cd can be used as a spectroscopic probe for the spectroscopically silent Zn^{II} ion as replacement usually proceeds isostructurally. The one dimensional ^{113}Cd NMR spectrum of $^{113}Cd_3$-Neclu_MT1 reveals three rather broad signals, indicating a certain degree of dynamics within the cluster (**Fig VI 4a**). Importantly, treatment with Chelex® 100 resin, which is used to remove free and loosely bound metal ions, does not have an effect on the spectrum in accordance to the experiments presented above for the determination of the metal-to-protein stoichiometries at higher protein concentrations. Hence, also the third metal ion is tightly bound to the protein. A comparison of the ^{113}Cd chemical shifts observed for Neclu_MT1 with those obtained for other MTs reveals that two Cd^{II} ions are most likely coordinated in Cys_4 sites within a cluster structure, while the chemical shift of the third signal is in agreement with both, a metal ion in a Cys_4 or a Cys_3His environment within a cluster (**Fig. VI 4b**). Hence the ^{113}Cd spectra indicate that in Neclu_MT1 no isolated binding sites with high affinity are present.

VI 5 Discussion

Information about the metal-ion specificity of a protein can be derived at the physiological level from the analysis of gene induction or protein expression as well as by determining the metal ions bound by the protein *in vivo*. Experiments on the protein level are often hampered by low native expression levels or challenging purification procedures. In addition, *in vitro* experiments are frequently used to study the metal ion binding properties and affinities of the protein of interest in more detail. As an example, the metal-ion specificity of the Cu^{I}MTs from *Saccharomyces cerevisiae* and *Neurospora crassa* was shown by the inducibility of the encoding genes by copper ions[25, 146, 162] and by determining the metal content of the native protein isolated from the copper-challenged host[25, 163]. An alternative view on metal-specificity has been recently proposed, linking the nature of the preferentially bound metal ion with the cellular compartment, in which the protein folds[124]. For Neclu_MT1 no information concerning the subcellular localisation is available, yet characterization of the protein isolated from the Cd^{II}-treated host organism by mass spectrometry showed that Neclu_MT1 binds Cd^{II} ions *in vivo*[22]. Cd^{II}-inducibility of MTs is usually accompanied by a likewise inducibility by either Zn^{II} [65] or copper[164] and further heavy metals[165]. Expression of the Neclu_MT1 protein, however, is exclusively induced by Cd^{II} ions but not by Zn^{II} or copper nor the accompanied oxidative stress (**Fig. VI 1**). By setting the focus of the physiological studies on the actual translate levels the obtained results directly reflect the metal ion detoxification and sequestration abilities of *H. lugdunensis* in its natural habitat. Interestingly, as the intracellular Cd^{II} concentration is roughly 100 fold higher than the Neclu_MT1 concentration, only a maximum of around 3 % of the Cd^{II} pool can be coordinated by the protein. This suggests a transport function of Neclu_MT1 in the detoxification process rather them its role as a Cd^{II} sink. Indicated by the fact that Neclu_MT1 protein induction is not triggered by Zn^{II} or Cu^{II} ions, the protein is obviously not involved in the defence against reactive oxygen species, which is corroborated by the high concentration of glutathione, a potent cellular reducing agent (**Fig. VI 1d**). Metal ion coordination studies performed with physiological relevant Neclu_MT1 concentrations show that Neclu_MT1 binds three Cd^{II} but only two Zn^{II} ions. Generally, Cd^{II} coordinates isostructurally to Zn^{II}-binding sites of proteins[166]. The main difference, however, is the larger ionic radius and the higher thiophilicity of Cd^{II} compared to Zn^{II}, both key characteristics for the cellular discrimination of these metal ions. Given the

higher thiophilicity it is not surprising that the Cys-rich apo-MTs posses higher affinities towards Cd^{II} than Zn^{II} [45]. The difference in binding strength between Zn^{II} and Cd^{II} is protein specific and may indicate the preferentially bound metal ion *in vivo*. For MTs, the apparent pK_a values of the Cys residues in presence of the respective metal ions were shown to be a relatively easy accessible and reliable determinant of the metal ion binding affinity and specificity. For Neclu_MT1 the apparent pK_a values for the Cd^{II}- and Zn^{II}-forms are in the lower affinity range compared to full-length mammalian MTs, which have apparent pK_a values of approximately 3.3 and 4.4 for the Cd^{II} and Zn^{II} forms, respectively[12]. However, the metal-cluster(s) formed in Neclu_MT1 are as stable or even more stable than those of the plant MTs[12]. In **Figure VI 3b**, apparent pK_a values of Neclu_MT1 are compared with values for other small metal-thiolate clusters, i.e. the $M^{II}_3Cys_9$ cluster in the mammalian β-domain and the $M^{II}_2Cys_6$ cluster in the γ-domain of wheat E_c-1. The difference in the pK_a values for the Zn^{II} and Cd^{II} forms of the γ-domain is relatively small, as the Cd^{II} form is destabilized compared to the Zn^{II} form in this naturally Zn^{II}-binding MT. On the other hand, the difference in pK_a values for the β-domain of human MT2 is relatively large in line with a slight destabilization of the Zn^{II} form in this demonstrably cadmium detoxifying MT. Also for Neclu_MT1, the difference between the two forms relevant at physiological concentrations, i.e. Zn_2- and Cd_3Neclu_MT1, is relatively large and would corroborate a preference of the protein for the Cd^{II} bound form.

Very striking is the difference in metal ion binding capacity observed for the Zn^{II} form of Neclu_MT1 at physiological relevant and higher concentrations, i.e. 5 and 25 μM. Judging from the molar extinction coefficients at 230 and 250 nm all of the eight Cys residues are involved in metal ion coordination in Zn_3- and Cd_3-Neclu_MT1, respectively. In contrast, the extinction coefficient of Zn_2Neclu_MT1 is lower, i.e. approximately 18'600 M^{-1} cm^{-1} compared to 23'500 M^{-1} cm^{-1} for Zn_3Neclu_MT1 (**Fig. VI 3a**), indicating that only six of the eight Cys residues are bound to Zn^{II}. When the pH of a Zn_2Neclu_MT1 sample at neutral pH is increased to 8.9 a significant increase of the absorption band at 230 nm is observed, indicative for the deprotonation of Cys-thiol groups not coordinated to metal ions. No such change in absorbance is observed in the equivalent experiment with Zn_3Neclu_MT1, underlining the involvement of all Cys in Zn^{II}-thiolate bonds in this form. Apparently the metalation state of the Zn^{II} form is dependent on the protein concentration and even the presence of a slight excess of metal ions, i.e. 3.3 equivalents, produces solely the Zn_2 form at lower protein concentration.

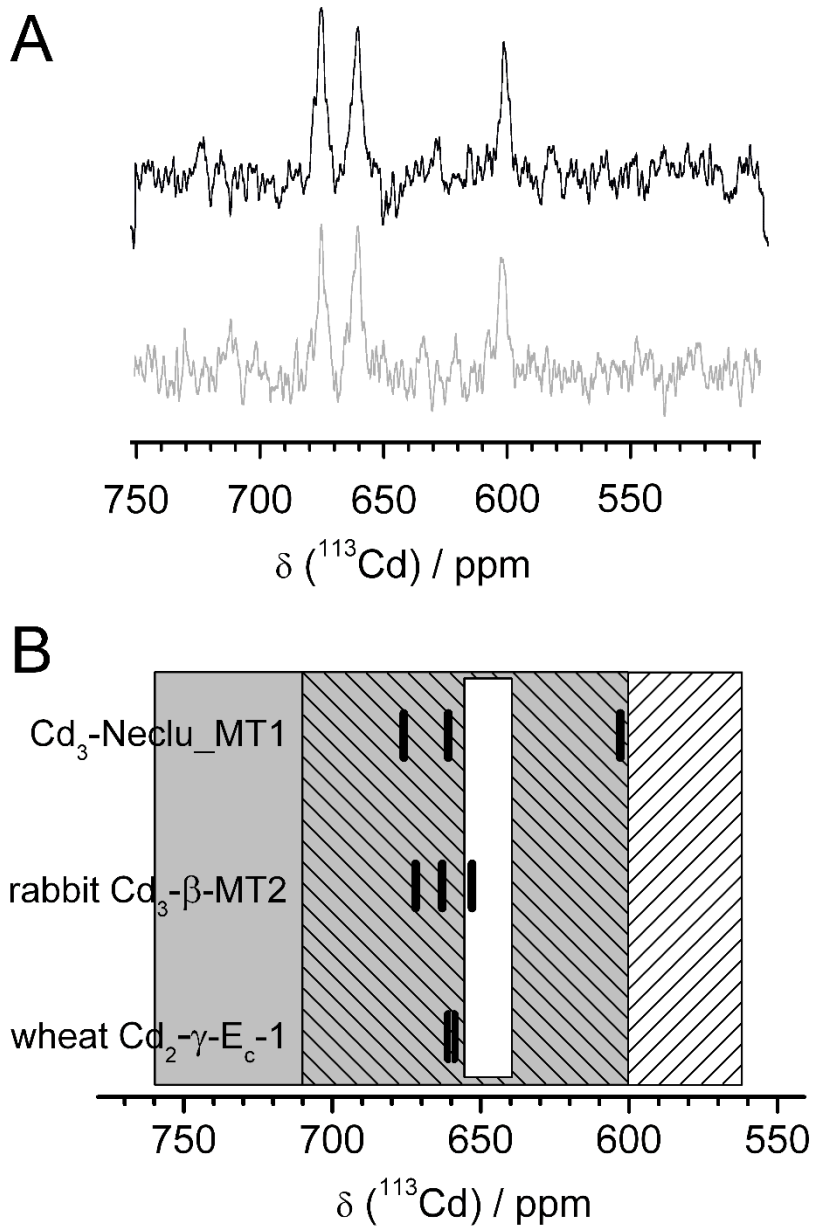

Figure VI 4. ^{113}Cd NMR experiments allow the determination of the number of different Cd^{II} binding sites based on the number of signals in the spectra. In addition, the chemical shift range of the NMR signals provides an estimate of the nature of the ligands and the coordination sphere of the respective metal ion. ***A)*** ^{113}Cd NMR spectra for $^{113}Cd_3$Neclu_MT1 before (black) and after (grey) Chelex® 100 treatment. Each spectrum contains three broad signals in the chemical shift range generally associated with tetrahedral tetrathiolate environments of ^{113}Cd ions in the clusters of mammalian MTs[54]. The chemical shift of the signal at higher field, i.e. at 603 ppm, agrees also with ^{113}Cd in a Cys_3N/O site.

The broadness of the signals indicates the presence of chemical exchange processes, i.e. a dynamic cluster structure. ***B)*** Comparison of ^{113}Cd chemical shift ranges for different coordination environments: Cys_3His sites within a cluster (white hatched box)[7, 167], isolated Cys_3His sites (white box)[168-172], Cys_4 sites within cluster (grey hatched box)[54], and isolated Cys_4 sites (grey box)[54]. In addition, chemical shifts of $^{113}Cd_3$Neclu_MT1, rabbit $Cd_3\beta$-MT2[33], and wheat $Cd_2\gamma$-E_c-1[106] are depicted as bars. $Cd_3\beta$-MT2 and wheat $Cd_2\gamma$-E_c-1 contain exclusively Cys_4 sites in their metal-thiolate clusters. Accordingly, the two ^{113}Cd resonances of Cd_3Neclu_MT1 observed at lower field (676 and 661 ppm) indicate two Cys_4 sites within a cluster structure, while the resonance at 603 ppm lies in a chemical shift range where both a tetrahedral Cys_4 or Cys_3His coordination within a cluster structure is possible.

Specific Cd^{II} isotopes are often used as probes for the spectroscopically silent Zn^{II} ions, e.g. the ^{113}Cd nucleus for NMR spectroscopy. In the present case, one-dimensional ^{113}Cd NMR spectra were used to determine the number of non-transient metal binding sites and clearly show the presence of three distinct broad peaks. The presence of these peaks was not abolished by treatment with the metal ion chelator Chelex® 100 indicative for the absence of low affinity metal ion binding sites in Cd_3Neclu_MT1. Comparing the chemical shift ranges of the observed ^{113}Cd signals with literature values[7, 54], two Cd^{II} ions, i.e. with signals at 676 and 661 ppm, are coordinated in tetrahedral tetrathiolate Cys_4 binding sites within a metal cluster while the third ion with a chemical shift of 603 ppm can be coordinated both in a Cys_4 or a Cys_3His site (**Fig. VI 4b**). While the Co^{II} titration experiments clearly show that a clustered structure is formed, no conclusion on the precise metalation process for the Cd^{II}- and the Zn^{II}-form can be presently deduced from the available data. Further investigations on this subject are required, which are currently in progress.

To summarize, this report focused on the metal coordination abilities of a metallothionein from an aquatic fungus. It was shown that Neclu_MT1 is the first solely cadmium-inducible metallothionein and that the Cd^{II} bound form differs from the Zn^{II} form in a physiologically relevant concentration range, which might indicate a mechanism on the protein level to discriminate between toxic Cd^{II} and essential Zn^{II} ions. The reported findings are anticipated to foster our understanding of Cd^{II} detoxification strategies in fungi, which might be extendable to more complex organisms.

VI 6 Acknowledgments

This work was supported by the Swiss National Science Foundation (SNSF Professorship to E.F.). D.M. acknowledges in addition the Halász-Foundation (Saarland University, Germany) and the *Graduiertenkolleg 416* of the German Research Foundation (DFG) for financial support. We especially thank Prof. Milan Vašák for numerous helpful discussions.

VI 7 Supplementary Material

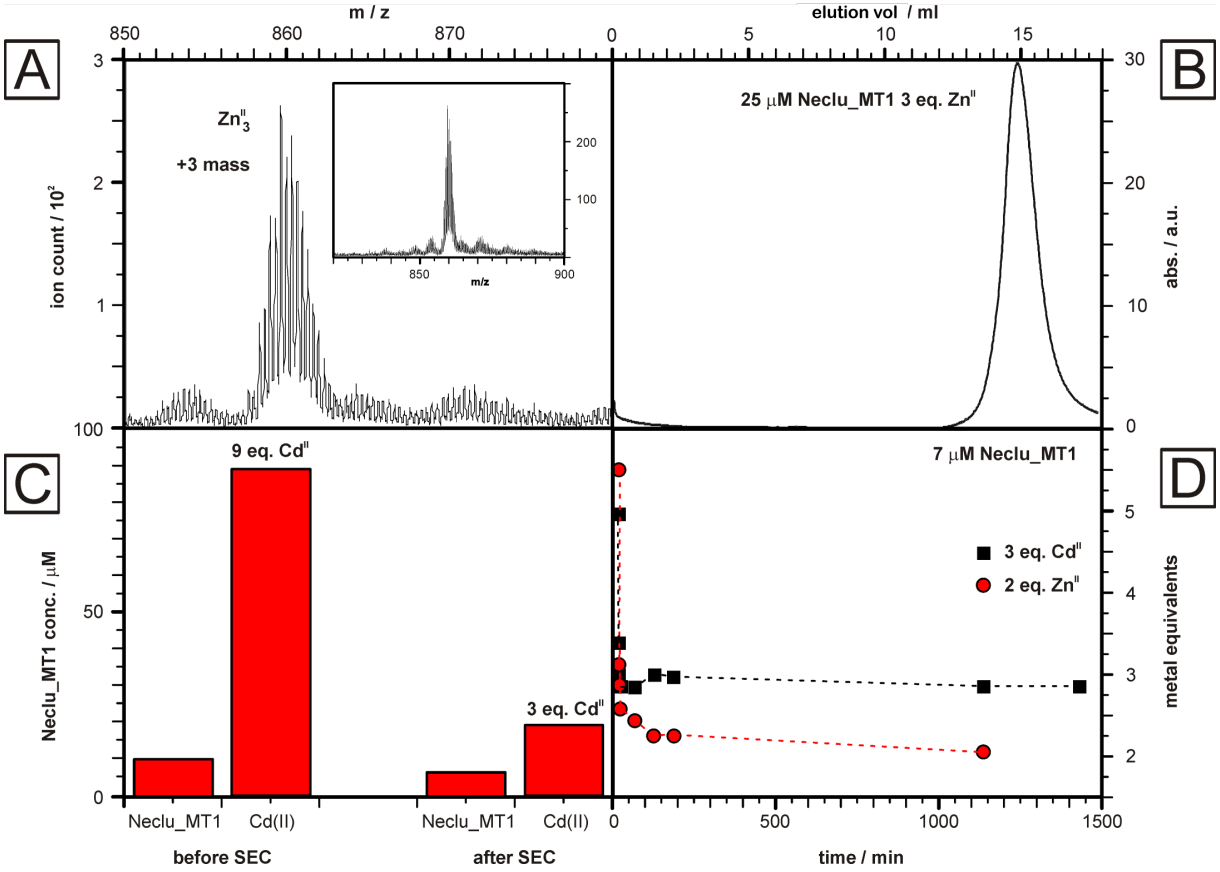

Figure S VI 1 Determination of the Zn^{II} and Cd^{II} metallation of Neclu_MT1. ***A)*** To prove the existence of the Zn_3Neclu_MT1 a higher protein concentration three Zn^{II} equivalents were added to a 25 µM Neclu_MT1 solution and analyzed via ESI-MS, yielding a Zn_3-species (3+ ion: 859.6 Da expected, 859.5 Da measured). ***B)*** To exclude a possible dimerization or aggregation of the metallated protein after titration or metallation experiments a representative size exclusion chromatography (SEC) chromatogram (Superdex Peptide 10/300 GL (GE, Healthcare), 10 mM Tris/HCl, 10 mM NaCl, pH 7.3) is displayed, showing a monomeric Neclu_MT1 peak. ***C)*** In order to validate the existence of a Cd_3Neclu_MT1 species, nine eq. of Cd^{II} were added to 10 µM Neclu_MT1, which were chromatographically separated employing the Superdex Peptide column, yielding a 7.4 µM Cd_3Neclu_MT1 species. ***D)*** In concomitance to SEC Chelex® 100 resin was added to 7 µM Neclu_MT1 being supplemented with either an excess of Zn^{II} and Cd^{II} in order to remove loosely bound metal ions, resulting in a Cd_3Neclu_MT1 and a Zn_2Neclu_MT1 species.

Chapter VII : Spectroscopic studies on the fungi metallothionein Neclu_MT1 reveal differences in Zn^{II} and Cd^{II} binding

Jens Loebus[§a] · Barbara Leitenmaier[§a] · Hendrik Küpper[b] · Eva Freisinger[a]*

[a]Jens Loebus · Barbara Leitenmaier · Eva Freisinger (✉)
Institute of Inorganic Chemistry, University of Zurich,
8057 Zurich, Switzerland

[b]Hendrik Küpper
Fachbereich Biologie, Universität Konstanz,
78457 Konstanz, Germany

*e-mail: freisinger@aci.uzh.ch
§ both authors contributed equally

VII 1 Abstract

Metal ion incorporation into proteins provides the key to their fascinating chemical functionality. Besides iron and copper, zinc is the most relevant metal ion fostering both chemical reactivity and structural stability in proteins. Owing to its preference towards soft ligands, mainly cysteinyl thiolates, Zn^{II} binding sites are prone to Cd^{II} poisoning, especially in heavy metal challenged habitats like mining areas. The aquatic fungus *Heliscus lugdunensis*, expressing the metalloprotein Neclu_MT1, was isolated from such a heavily polluted spring of an ancient metal ore dump, containing, besides other, 25 μM Cd^{II}- and 30 mM Zn^{II}-ions. Neclu_MT1 a 2.5 kDa, 33% cysteines containing metallothionein (MT) was reported to confer Cd^{II} resistance of *H. lugdunensis in vivo*. Moreover it was suggested to be the first Cd^{II} specific MT, which was further investigated herein. Employing optical, chiro-optical and magnetic induced chiro-optical spectroscopy together with heteronuclear multidimensional NMR and EXAFS, we investigated the Zn^{II} and Cd^{II} metallation pathways of Neclu_MT1 *in vitro* as well as the metal clusters formed. Surprisingly we evidenced a concentration dependency of Zn^{II} metallation resulting in a putative Zn_2Cys_6His cluster at 5 μM protein concentration or less in contrast to the Zn_3Cys_8His cluster formed at 25 μM protein concentration or higher. Additionally we witnessed a decisive difference in Zn^{II} and Cd^{II} metallation. The more thiophilic Cd^{II} coordinates either to all 8 cysteines resulting in a Cd_3Cys_8 metal cluster a so far unreported cluster motive or under more basic pH conditions in a novel Cd_3Cys_8His metal cluster, similar to those described in the β-cluster of mammalian MTs. By identifying these Zn^{II} and Cd^{II} Neclu_MT1 metallation pathways we might foster the understanding of molecular strategies organisms have developed in order to discriminate between essential and toxic metal ions.

Keywords Cd detoxification · Metallothionein · GHOST system · Electronic absorption spectroscopy · NMR spectroscopy · metal cluster · EXAFS

VII 2 Introduction

From a biological perspective transition metal ions are clustered in essential and non-essential elements. While the metal ions grouped in the 4th period of the table of elements are mostly involved in biochemical processes (e.g. Mn^{III}, Fe^{II}, Co^{II}, Ni^{II}, Cu^{I}, and Zn^{II}) those occurring in the 5th period are generally considered toxic (e.g. Tc^{II}, Ag^{I}, and Cd^{II}) except for molybdenum[173]. Both in plant science and health care Cd^{II} poisoning has caused significant interest resulting in a myriad of reports phenomenological describing causes and consequences of cadmium toxicity[135, 137-138]. Unfortunately, on a molecular level Cd^{II} homeostasis is not well understood. Little is known about the molecular identity of Cd^{II} specific proteins. While membrane embedded metal transporter, including ABC type, ZNT1[174] AtNramp3[175] and P-type ATPase-HMA transporters may more or less specifically transport metal ions to different cellular compartments or organs in eukaryotes[176], sequestering proteins are rarely described. In some plants and fungi short enzymatically synthesized peptides called phytochelatins (PCs) are involved in efficient Cd^{II} take up and detoxification. These PCs are formed from γ-glutamylcysteine (γEC) dipeptide building blocks by the enzyme phytochelatin synthase (PCS), which, organisms and isoform specific, polymerizes the dipeptide subunits to higher aggregates and finally attaches a *C*-terminal glycine, alanine, glutamate or glutamine residue[177-179]. Another class of Cd^{II} binding proteins are metallothioneins (MTs). These ubiquitous expressed small (<10 kDa), cysteine-rich (up to 33%) metalloproteins[12, 65] are generally considered to be involved in either Zn^{II} or Cu^{I} homeostasis[6]. Nevertheless, they can be induced and in most cases preferentially coordinate cellular available Cd^{II}-ions resulting in stable Cd^{II} thiolate clusters, which is why these proteins, especially in non-mammalians are hypothesized to contribute to Cd^{II} homeostasis and detoxification[180]. MTs are taxonomically classified according to their primary amino acid sequence[3] rendering this superfamily of proteins difficult to describe regarding their evolutionary function. Until the recent description of the MT Neclu_MT1 from *Heliscus lugdunensis* - an aquatic fungus[22] - no Cd^{II} specific metallothionein (see **Chapter VI**) and more strikingly only a few Cd^{II} specific proteins were reported so far, including the PCS and a Zn/Cd exchangeable carbonic anhydrase in a zinc deprived marine diatome *T. weissflogii*[166]. The Cd^{II} selectivity of Neclu_MT1 was established on the transcript as well as on the translate level. Under physiological condition using the growth solution of the heavily Cd^{II} and Zn^{II} exposed site of isolation[20], only Cd^{II} ions efficiently induce Neclu_MT1 expression (see

Chapter VI). Furthermore mass spectrometry (MS) based protein identification *in vivo* report a Cd_2Neclu_MT1 metallated species[22]. In order to formulate a hypothesis concerning the physiological relevance and thus the involvement of the MT Neclu_MT1 in Cd^{II} detoxification strategies of *H. lugdunensis* strain H.4.1.4, the gene sequence including the 5'UTR upstream region was decoded. A metal responsive element comparable to the one being recognized by the metal ion responsive transcription factor ACE1 from yeast, was identified along with the coding region of the protein, which templated the recombinant expressed Neclu_MT1 protein designed for further mechanistic and structural studies.

Following d^{10} metal ion, especially Zn^{II}, incorporation into proteins, including MTs, lacking crystal structure information has proven to be a challenging task, mostly owing to the spectroscopical inaccessibly of the Zn^{II} ion and the dominant oxidation prone thiolate ligands. Optical or chiro-optical spectroscopic methods could so far only establish the metal load of a protein and compare already otherwise identified metal binding site patterns. Recent computational studies of protein embedded metal cluster structures[126] represent promising efforts towards deriving spectral properties that enable to predict the metal ion cluster architecture and its formation pathways. In order to experimental identify the coordinating ligands of the Zn^{II} clusters X-ray absorption spectroscopy resolving the fine edge of the metal ion specific absorption band is analyzed (EXAFS). Generally, the ligand connectivity pattern is determined via Zn^{II} substitution by the NMR active, spin ½ nuclei ^{113}Cd or ^{111}Cd visualizing Cd^{II}-ligand-proton ^{3}J[Cd,H] interactions[37]. Applying both types of experiments the two archetypical MT metal clusters were identified: the α-cluster a M_4Cys_{11} metal cluster and the β-cluster a M_3Cys_9 architecture (**Fig. VII 1**).

From photo-spectrometric titration studies with Zn^{II}, Cd^{II} and Co^{II} as well as ^{113}Cd NMR experiments a three metal ion containing metal cluster was proposed, whose formation is probably concentration dependent in the case of Zn^{II}, resulting in a weakly coordinated Zn_2 species under physiological relevant protein concentration (see **Chapter VI**). In the following the difference in metallation and affinity among Zn^{II} and Cd^{II} forms of Neclu_MT1 is further investigated aiming on elucidating the metal cluster formation pathways for Zn^{II} and Cd^{II}.

VII 3 Material and methods

VII 3 1 Chemicals, solutions, plasmids and proteins

$^{113}CdCl_2$ and $^{15}NH_4Cl$ were ordered from Cambridge Isotope Laboratories Inc. (Innerberg, Switzerland), d_{11}-Tris from Euriso-top (Saint-Aubin, France). All other chemicals were ACS grade or comparable. Solutions prepared with millipore water were filtered, degassed and depending on the experiment either nitrogen or argon saturated. If necessary three times freeze-thawn cycles were conducted under vaccum. The pGEX_Neclu_MT1 plasmid was cloned based on the pGEX-4T1 expression vector as *N*-terminal fusion gene products and expressed and purified as previously described (see **Chapter VI**). A final protein with a length of 25 amino acids,

NECLU_MT1: G SPCTCSTCNC AGACNSCSCT SCSH

containing a *N*-terminal Gly, a relict from thrombin cleavage, resulted.

VII 3 2 Preparation of Zn- and Cd-forms of isolated Neclu_MT1 and GST-Neclu_MT1 for NMR

Procedures for GST hydrogel system (GHOST see **Chapter III**) and Zn_3Neclu_MT1, Zn_2Neclu_MT1 (see **Chapter VI**) preparation are reported elsewhere in detail. However, a short description is provided: For all buffer exchange or concentration steps a Series 8050 stirred (Millipore) ultrafiltration cell was used. The freshly eluted GST fusion protein from the GST affinity column (GE Healthcare, USA) was concentrated to around 5 ml. Then, DTT was added to a final concentration of 0.1 to 0.3 M and the pH of the solution adjusted to ca. pH 8.5 with 1 M Tris/HCl, pH 8.9. Following 30 min of incubation two dilution and re-concentration cycles were performed using 50 ml of 50 mM Tris/HCl, pH 8.0. After a third dilution with 50 mM Tris/HCl pH 8.0, micromolar excess of Zn^{II}-ions ($ZnCl_2$) was titrated to the protein solution and removed in one further buffer exchange cycle with 50 mM Tris/HCl, pH 8.0 and three cycles with 1 mM d_{11}-Tris/HCl, pH 8.0. After adjusting to the desired

volume, the protein concentration was determined applying the A_{280nm} method (extinction coefficient: 41'760 M^{-1} cm^{-1}) and compared to the 2,2'-dithio-dipyridine (2-PDS) assay accounting for 2 more cysteines of the GST-tag (total 10 Cys)[43] (see **Chapter III**). Finally the metal concentration was evaluated via F-AAS and the protein aliquoted and stored at -80°C or transferred into a shigemi tube, incubate overnight at 37°C and 20 min at 50°C for subsequent NMR experiments. In case of the Cd^{II}-form of GST-Neclu_MT1 exactly three equivalents of $^{113}Cd^{II}$ are added to the Zn^{II}-form of GST-Neclu_MT1. In the following the NMR sample preparation is identical to the Zn^{II}-form of GST-Neclu_MT1. For the experiments with isolated Neclu_MT1 the apo-protein was demetallated and purified freshly before re-metallation with exactly three equivalents of $^{113}Cd^{II}$ equivalents and pH 8 adjusted with 1M d_{11}Tris/HCl. Subsequently, the protein solution was twice dialyzed against 100 μM d_{11}Tris/HCl, pH 8.0 prior to lyophilization and resolubilisation in 10% D_2O, 10 mM d_{11}Tris/$HClO_4$, 10 mM Tris/$HClO_4$, pH 7.2 to yield a 1 mM protein sample. Finally the Neclu_MT1 concentration was determined (2-PDS assay) and correlated with Cd^{II} concentration, quantified by flame atomic absorption spectroscopy (F-AAS) and the Neclu_MT1 solution was transferred into a shigemi tube for successive NMR experiments.

VII 3 3 Sample preparation and titration of Zn^{II} and Cd^{II} to apo-Neclu_MT1 followed by UVvis-, CD-, and MCD spectroscopy

Freshly prepared argon-saturated apo-Neclu_MT1 dissolved in 10 mM HCl was adjusted to protein concentrations of 5 μM and 25 μM for Zn^{II} and of 25 μM for Cd^{II} titrations to yield Neclu_MT1 solutions of 1.8 ml 10 mM Tris/HCl, 10 mM NaCl, pH 7.2. Next the protein solution was transferred into a 1-cm septum sealed cuvette and the Zn^{II} or Cd^{II} solution were stepwise titrated to the Neclu_MT1 solution in 1 μl steps (0.17 eq. M^{II}) using a 25 μl Hamilton syringe followed by UVvis-, CD- and MCD spectroscopic measurements. Subsequently the protein concentration was determined via the 2-PDS assay, the metal ion concentration was scored via F-AAS in order to recalculate the MT to M^{II} ratio and for all samples the monomeric character of the metallated Neclu_MT1 species was verified via size exclusion chromatography (SEC).

VII 3 4 Thiolate titration followed by UVvis spectroscopy

Zn_2- and Zn_3Neclu_MT1 samples were prepared starting from apo-Neclu_MT1 (10 mM HCl, pH 2) in a N_2 saturated glove box as low (5 μM) and high (25 μM) protein concentration samples (final sample buffer: 10 mM Tris/HCl, 10 mM NaCl, pH 7), owing to the proposed concentration dependent difference in metallation (see **Chapter VI**). Cd_2- and Cd_3Neclu_MT1 samples were prepared identically, however as 25 μM protein concentration samples only. After transfer into a septum sealed 1-cm quartz cuvette 2.5 μl steps of 0.5 M NaOH solution were titrated to the protein solution until a pH of 11.5 was reached. After each titration step an UVvis spectra was recorded. The pH dependency was deduced performing the same procedure on a twin sample, determining the pH after each step. After each titration the protein sample in the cuvette was 20 min oxygen exposed, then photo-spectroscopically remeasured and the protein concentration (non oxidized thiols and thiolates) was determined with the 2-PDS assay along with the metal ion concentration using F-AAS. Finally the aggregation state of the protein sample was evaluated using size exclusion chromatography (SEC: pG peptide column – GE Healthcare, 10 mM NH_4Ac pH 7.4, 220 nm detector).

VII 3 5 Fine edge X-ray absorption spectroscopy (EXAFS)

In order to determine the average Zn^{II}-binding motif in Zn_2Neclu_MT1, Zn^{II} K-edge X-ray absorption spectra were recorded at SLAC facility at Stanford Synchrotron Radiation Lightsource Beam Line 9-3 in the spring of 2011. Data reduction, including background removal, normalization, and extraction of the fine structure, was detailed before[106]. In short: The software package was used KEMP[69] assuming a threshold energy of E_0, Zn = 9,662 eV. The extracted K-edge EXAFS data were converted to photoelectron wave vector k-space and weighted by k^3. Initial evaluation of the spectra by ABRA[70], which is based on EXCURV[71], included a systematic screening of approximately 400 potential binding motifs. The following meta-analysis identified structural zinc sites, defining a tetrahedral ligand environment in the final refinement step. Taking into account the multiple scattering contributions indicative for imidazole rings coordinating to the Zn^{II} ions lead to the refinement to the following parameters for each structural model: the atomic distances (R), the Debye–Waller factors (2r2), and a residual shift of the energy origin (EF) in order to minimize the fit index (U). An amplitude reduction factor (AFAC) of 1.0 was used throughout the data analysis.

VII 3 6 NMR spectroscopy

All ^{1}H, ^{113}Cd and ^{15}N resolved NMR experiments were recorded at 310 K on cryoprobe head equipped Bruker Avance 700- & 600-MHz spectrometers or on a broad band DRX 500-MHz Bruker spectrometer. Long range 2D [^{15}N,^{1}H] HSQC NMR experimental setup of Zn_3- and Cd_3GST-Neclu_MT1 sample was derived from a gradient-enhanced [^{15}N,^{1}H] HSQC NMR experiment using the Rance–Palmer trick for sensitivity enhancement[78-79] and optimized for ^{3}J[^{15}N,^{1}H] imidazole couling constants in order to investigate the tautomeric state of the *C*-terminal histidine[9]. 2D [^{113}Cd,^{1}H] HSQC NMR experiments of Cd_3Neclu_MT1 investigating the Cd^{II} binding sites and stoichiometries[35] were performed with $^{3}J[H_{\beta},Cd]$ couplings of 40 Hz at pH 7.2, 7.6 and 8.3.

VII 4 Results and Discussion

VII 4 1 The Cadmium Neclu_MT1 metallation pathway and the resulting metal cluster

From the UVvis spectra and the Chelex™ 100 experiments already reported, we know that three Cd^{II} ions may bind. The question remains on **i)** which and how many ligands are used, **ii)** what is their connectivity and **iii)** what is the metal cluster topology – does an isolated metal site exist. Furthermore the metallation pathway is under interrogation. **iv)** Is there cooperativity? If yes, at what metallation stage (0, 1, 2 eq.). **v)** Which ligands and binding sites are first occupied, is there a stable intermediate?

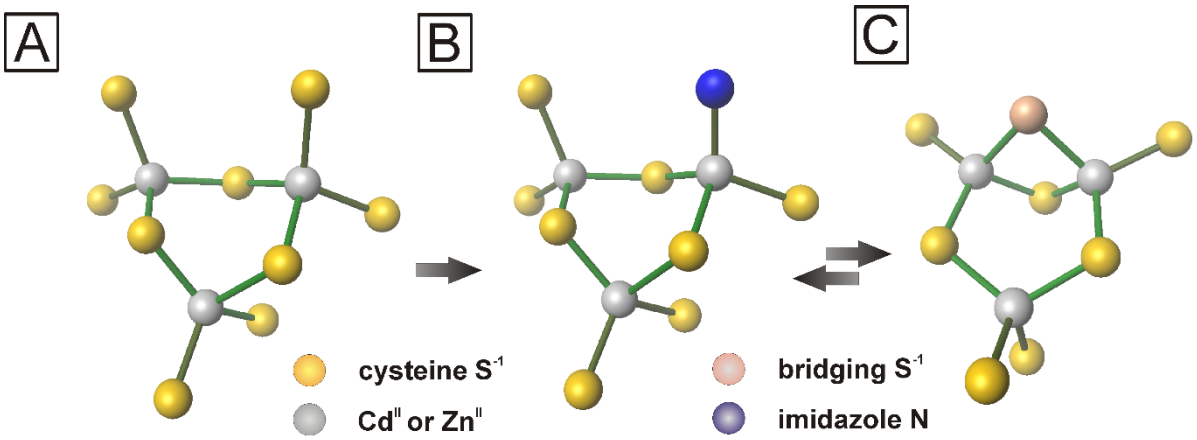

Figure VII 1 ***A)*** β-cluster of human MT2 (pdb: 2mhu) with a M_3Cys_9 metal cluster [102]. ***B)*** Proposed Zn_3Cys_8His and Cd_3Cys_8His metal cluster of Neclu_MT1 modeled starting from the β-cluster of human MT2. ***C)*** Envisioned Cd_3Cys_8 metal cluster. Starting from the Cd_3Cys_9 β-cluster of human MT2 two terminal thiolates were modeled to yield one bridging thiolate. The structure was energetically and structure optimized. Cysteines are depicted as yellow spheres, histidines as blue spheres, additional bridging cysteine as rose, while Cd^{II} or Zn^{II} are displayed as grey spheres. Bonds from terminal cysteines to M^{II} ions are colored in dark green and bridging in green.

Identifying the number and nature of all metal ligands is the first but also one of the most difficult steps in the path of elucidating the protein embedded Cd^{II} metal binding site. From 1D ^{113}Cd NMR (see **Chapter VI**) spectra as well as Cd^{II} EXAFS experiments (data not

shown) a non-thiolate most likely nitrogen derived ligand is suggested. Nevertheless the ^{113}Cd NMR chemical shift argument is rather weak and in case of evaluating the Cd^{II} EXAFS spectra a Cd_3Cys_8 instead of a Cd_3Cys_8His solution fits the data equally good. The involvement of all 8 cysteine in metal coordination was photo-spectrometrically verified in a thiolate titration (**Fig. VII 3**).

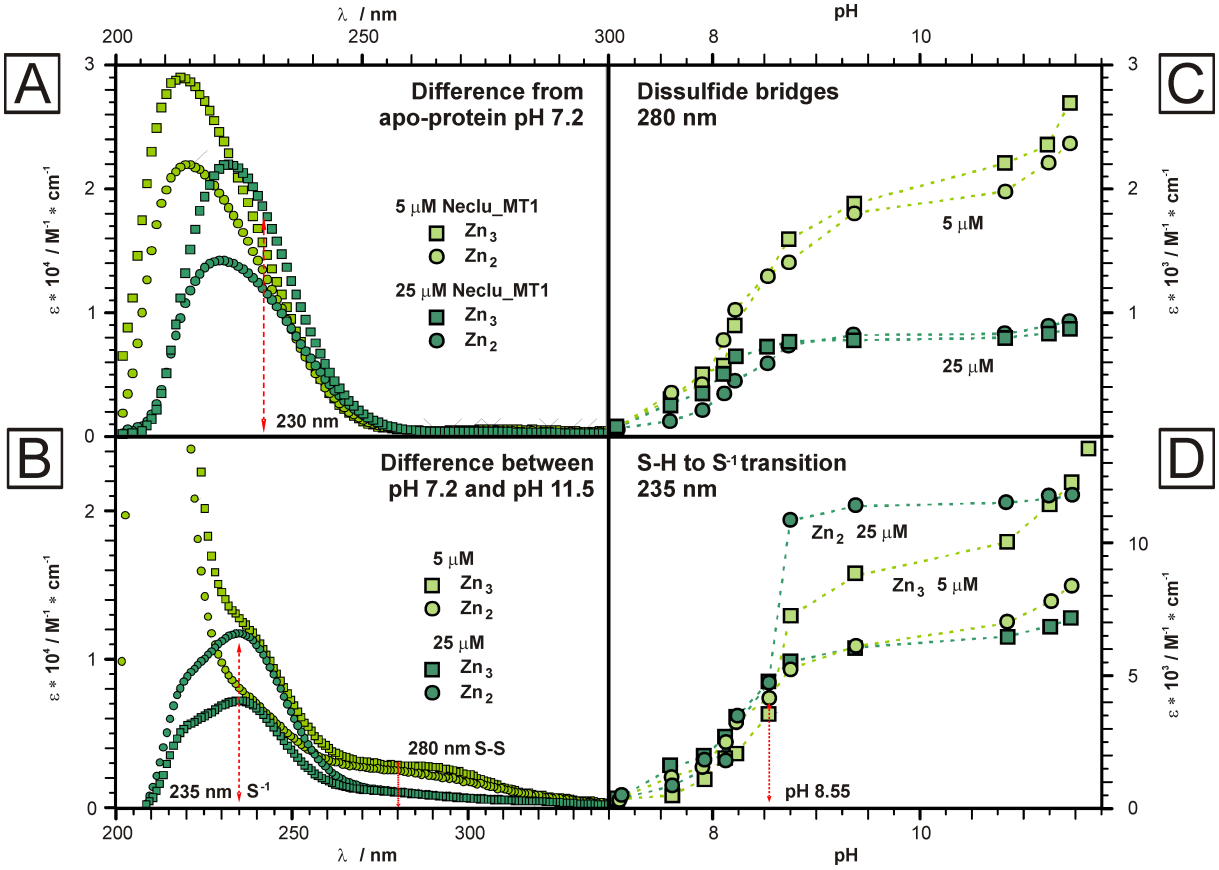

Figure VII 2 UVvis followed thiolate titrations of the Zn^{II} from of Neclu_MT1. 25 µM Zn_2Neclu_MT1 are indicated as dark green circles, 25 µM Zn_3Neclu_MT1 as dark green squares, 5 µM Zn_2Neclu_MT1 as light green circles, 5 µM Zn_3Neclu_MT1 as light green squares. ***A)*** Absorption envelope of $Zn_{2/3}$Neclu_MT1 at 25 µM protein concentration overlayed with the $Zn_{2/3}$Neclu_MT1 at 5 µM protein concentration. ***B)*** Difference of absorption between Zn^{II} Neclu_MT1 forms at pH 7.2 and pH 11.5. ***C)*** pH dependent evolution of absorption envelope of Zn Neclu_MT1 at pH 7.2 to pH 11.5 followed at 285 nm and at ***D)*** 233 nm, respectively.

By consecutively increasing the pH of a Cd_3Neclu_MT1 species from pH 7.2 to 11.5 non-coordinating – non-oxidized thiols should deprotonate giving rise to a strong absorption band at 233 nm, as can be witnessed for the Zn- but not the Cd-form of Neclu_MT1 (**Fig. VII 2,3**).

Metal cluster with 3 metal ions and 9 ligands are well described in metallothioneins, constituting the β-cluster, evidenced in mammalian and crustacean MTs[180].

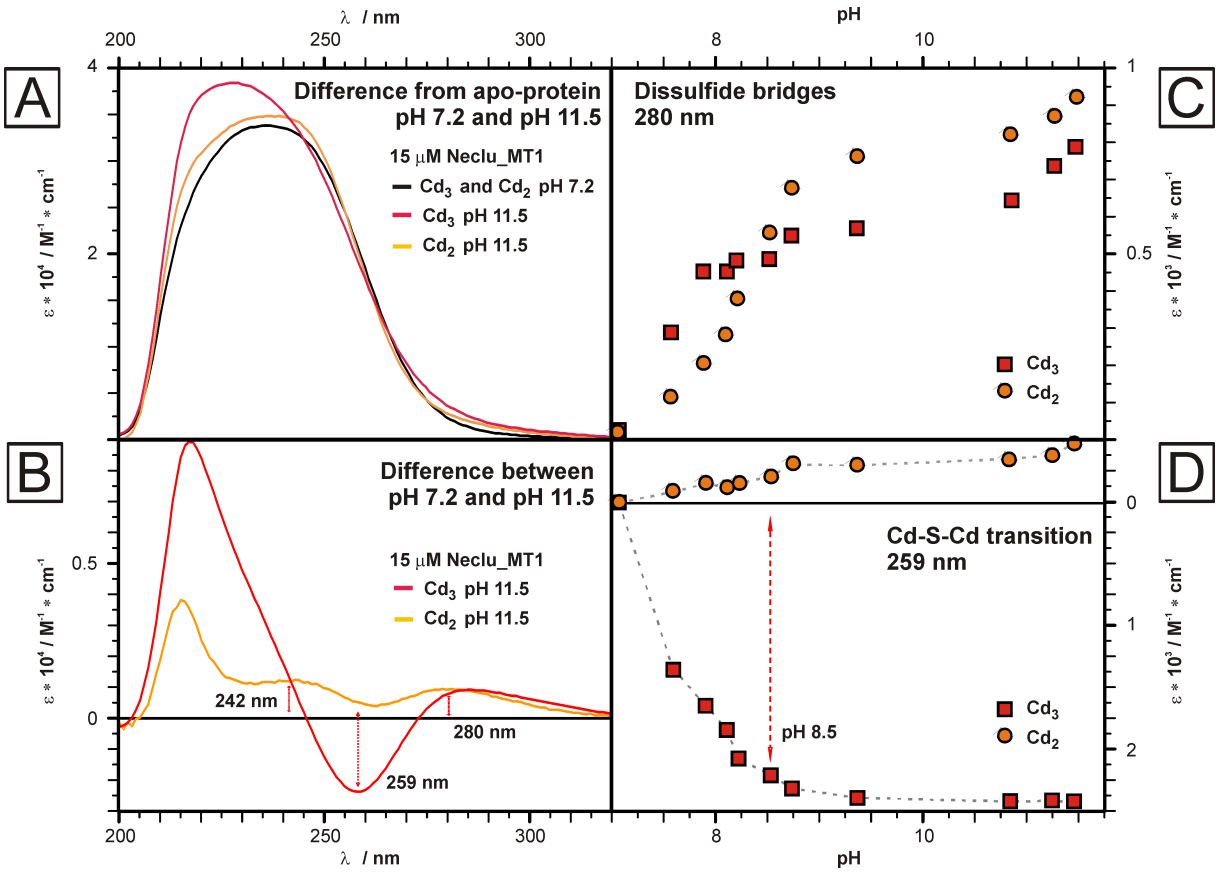

Figure VII 3 UVvis followed thiolate titration of Cd^{II} Neclu_MT1. ***A)*** Absorption envelope of $Cd_{2/3}$Neclu_MT1 at pH 7.2 (black) overlayed with the Cd_2Neclu_MT1 (orange) and Cd_3Neclu_MT1 (red) absorption spectra at pH 11.5. ***B)*** Difference of absorption between $Cd_{2/3}$Neclu_MT1 at pH 7.2 and Cd_2Neclu_MT1 (orange) as well as Cd_3Neclu_MT1 (red) at pH 11.5. ***C)*** pH dependent evolution of absorption envelope of Cd Neclu_MT1 at pH 7 to Cd_2Neclu_MT1 (orange) as well as to Cd_3Neclu_MT1 (red) at pH 11.2 followed at 285 nm and ***D)*** at 259 nm, respectively.

For the β-cluster no histidine involvement has been described in contrast to the bigger metallothionein metal cluster prototype the α-cluster (M_4Cys_{11}), where a two histidine ($M_4Cys_9His_2$) containing metal cluster was reported in a bacterial MT[7]. In case of exclusive thiolate coordination of the three Cd^{II} ions via 8 cysteines the metal cluster architecture would be of interest, since so far only a tetrahedral tetrathiolate Hg_3Cys_8 metal cluster has been reported[181] containing a three-fold coordinating thiolate ligand. Despite the fact that the

Cd_3Cys_8 cluster topology embedding a three-fold thiolate is not imaginable, a tetrahedral tetrathiolate Cd_3Cys_8 cluster is very well stoichiometrically conceivable (**Fig. VII 1c**) being easily converted to a Cd_3Cys_8His β-cluster-like arrangement (**Fig. VII 1b**). In consequence, from a structural perspective both a histidine involved Cd_3Cys_8His coordination or an exclusive thiolate Cd_3Cys_8 metal cluster coordination as well as a switching between both states could be imaginable.

Understanding the topology of the fully Cd^{II} loaded metal cluster may be fostered by elaborating the metallation pathway. Therefore we followed the metallation via different optical, chiro-optical and magneto chiro-optical spectroscopy at physiological pH (7.2) and slightly basic conditions (8.9) (**Fig. VII 4**). During the addition of the first equivalent of M^{II}-ions the tendency towards cooperativity or non-cooperativity can be probed.

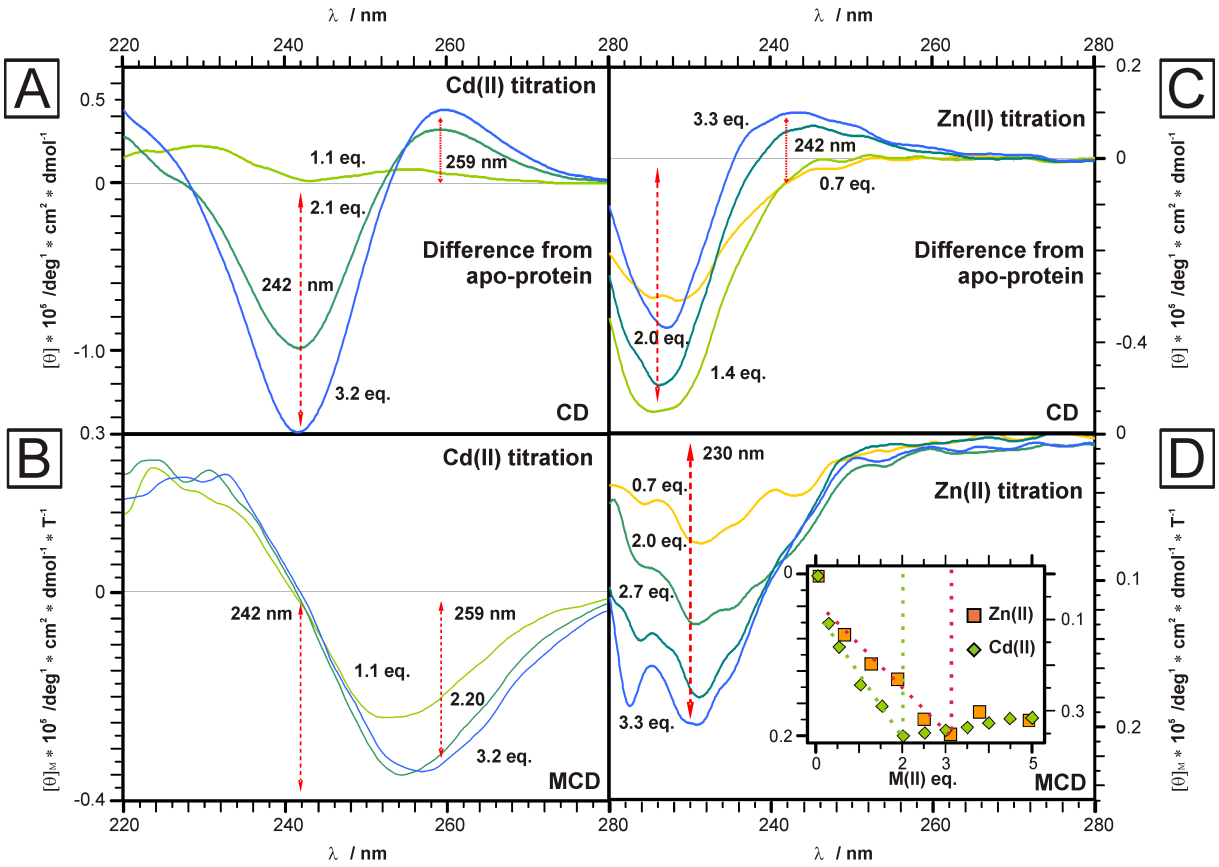
A
Cd(II) titration
1.1 eq.
259 nm
2.1 eq.
242 nm
Difference from apo-protein
3.2 eq.
CD
C
Zn(II) titration
3.3 eq.
242 nm
0.7 eq.
Difference from apo-protein
2.0 eq.
1.4 eq.
CD
B
Cd(II) titration
242 nm
259 nm
1.1 eq.
2.20
3.2 eq.
MCD
D
Zn(II) titration
230 nm
0.7 eq.
2.0 eq.
2.7 eq.
3.3 eq.
Zn(II)
Cd(II)
M(II) eq.
MCD
λ / nm
[θ] * 10⁵ /deg⁻¹ * cm² * dmol⁻¹
[θ]M * 10⁵ /deg⁻¹ * cm² * dmol⁻¹ * T⁻¹

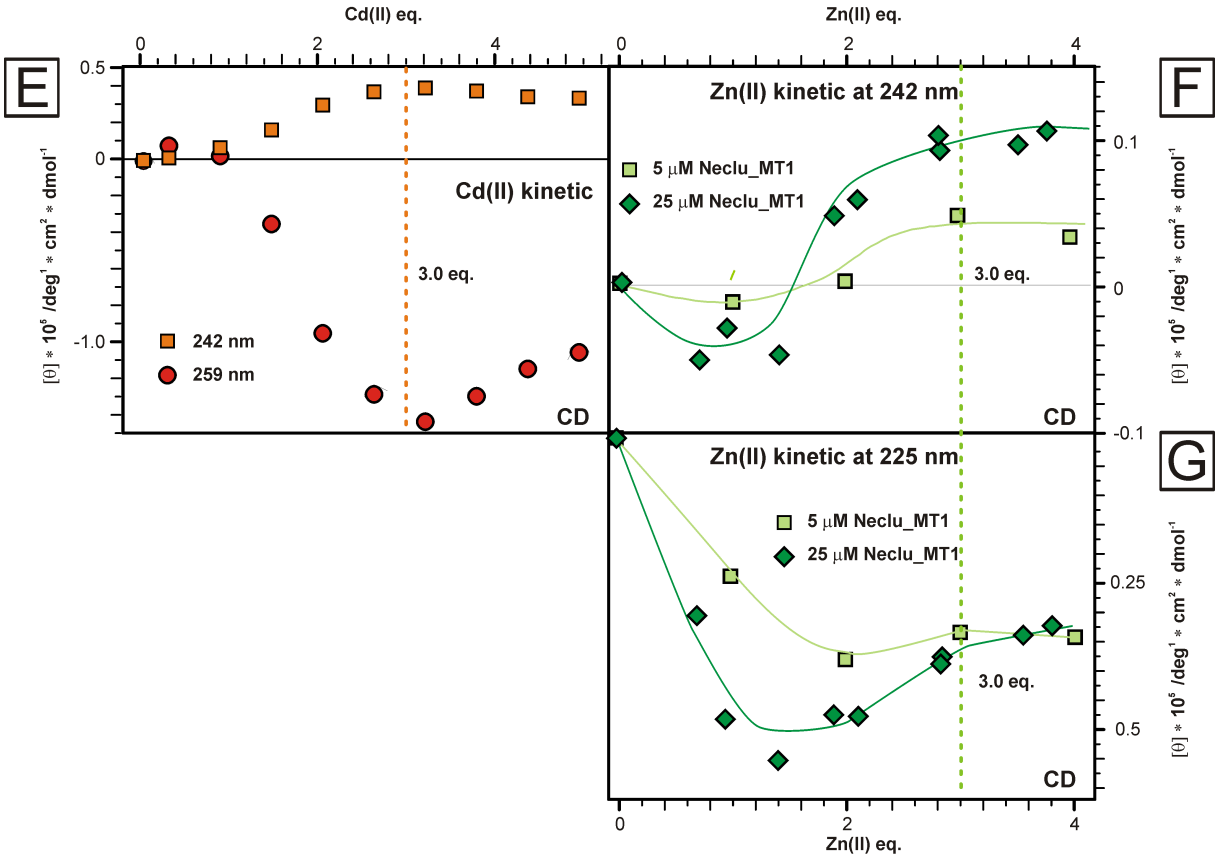
E
Cd(II) eq.
Cd(II) kinetic
3.0 eq.
242 nm
259 nm
CD
F
Zn(II) eq.
Zn(II) kinetic at 242 nm
5 μM Neclu_MT1
25 μM Neclu_MT1
3.0 eq.
CD
G
Zn(II) kinetic at 225 nm
5 μM Neclu_MT1
25 μM Neclu_MT1
3.0 eq.
CD
[θ] * 10⁵ /deg⁻¹ * cm² * dmol⁻¹

Figure VII 4 CD and MCD spectra of Zn^{II} and Cd^{II} titration to Neclu_MT1. ***A)*** apo-Cd^{II} and ***B)*** apo-Zn^{II} titration of Neclu_MT1 at pH 7 followed by CD spectroscopy ***C)*** apo-Cd^{II} and ***D)*** apo-Zn^{II} titration of Neclu_MT1 at pH 7 followed by MCD spectroscopy. The inset in D) displays the different magnetically induced chiro-optical band shape evolution of Zn^{II} (orange) and Cd^{II} (green) Neclu_MT1 at 259 nm (Cd^{II}) and 230 nm (Zn^{II}). ***E)*** Cd^{II} addition dependent evolution of the CD band at 242 nm (red) and 259 nm (orange) of Neclu_MT1 at pH 7. ***F)*** Zn^{II} addition dependent evolution of the CD band at 242 nm and ***G)*** 225 nm of Neclu_MT1 at pH 7 investigating different protein concentration (25 μM – dark green diamonds; 5 μM light green squares; accordingly colored solid lines are trendlines).

The different shape of the CD signal during the addition of the first Cd^{II} equivalent in comparison to the only in intensity increasing signal following the addition of the second Cd^{II} equivalent suggests a non-cooperative metallation pathway. After titrating the second Cd^{II} equivalent to the apo-Neclu_MT1 solution theoretically all possible cysteines could be incorporated in tetrahedral tetrathiolate coordination without cluster formation. According to the molar extinction coefficient at 250 nm, indicative for Cd^{II}- thiolate bond formation an average of around 7 cysteines are involved in Cd^{II} coordination (see **Chapter VI**). This notion is supported by the intensity of the Faraday effect induced negative ellipticity band at 255 nm, which, increased monotonic till 2 Cd^{II} equivalent, stagnates, and only shifts to lower wavelengths (265 nm) with further Cd^{II}-ions added (**Fig. VII 4c**). In consequence it is reasonable to assume that almost all thiolates are tetrahedrally bound to Cd^{II}-ions, which is further supported by thiolate titrations with a Cd_2Neclu_MT1 species evidenced to be devoid of free thiolates (**Fig. VII 3**). It appears that after subsequent addition of 2 equivalent of Cd^{II} ions the majority of Neclu_MT1 molecules occur as Cd_2Neclu_MT1 species in a saturated tetrahedral tetrathiolate non-cluster arrangement, which ought to be kinetically and thermodynamically stable. Nevertheless UVvis, NMR, MS and Chelex® 100 experiments proof the existence of a third Cd^{II} ion bound to Neclu_MT1 (see **Chapter VI**). CD spectroscopy supports these findings and may provide further inside. Until the addition of 1.0 to 1.5 equivalent no chiral ellipticity band shape develops, while from then on the bands increase steadily till 3.0 equivalents added (**Fig. VII 4d**). From 1.5 equivalents the typical negative sinus curve shape with two maxima at (-) 242 nm and (+) 255 nm appears, witnessed in the β-cluster of CE MTs and explained as excitonic coupling originating from the Cd_3Cys_9 metal cluster[183]. The evolution of the CD signal suggests that during the first equivalent of Cd^{II}-ions titrated only terminal ligands are coordinated without any preferences in shape or

ligand resulting in average a-chiral metal centers. Only when ca. 1.5 equivalent of Cd^{II} are supplemented a chiral metal center possessing chiral Cd^{II}–S^- LMCT (ligand to metal charge transfer) bands is evidenced, which increase linearly in intensity until three Cd^{II} ions are added. This behavior might either originate from an increase in number or in chirality of the respective chiral metal centers. It is difficult to imagine isolated chiral tetrahedral tetrathiolate Cd^{II} binding sites, especially if multiple metal ligand connectivities may occur in the ensemble of the dissolved protein. Hence there is reason to assume that the increased chirality originates from an amplification in number of chiral sites, thus the shape and intensity of the optical ellipticity band provides direct evidence on the formation of a Cd_3-metal cluster. Only the number and identity of the ligands remain uncertain. Therefore further experiments were conducted, including thiolate titration followed by UVvis and ^{113}Cd NMR spectroscopy, hinting the co-existence of a Cd_3Cys_8 and a Cd_3Cys_8His metal cluster. Especially ^{113}Cd NMR experiments may advance the understanding of the Cd_3 metal cluster. In consequence [^{113}Cd,^1H] HSQC NMR spectra were recorded at different pHs (**Fig. VII 5a,b**) all showing three Cd traces at 676 ppm, 660 ppm and 654 ppm containing proton cross peaks in the chemical shift range of 2.5 ppm to 3.8 ppm indicative for ^3J[Cd,H] coupled cysteine H_β-protons. Additionally the ^{113}Cd chemical shifts refer to tetrahedral tetrathiolate metal ion sites[36] (see **Chapter VI**). The ^{113}Cd signal at 654 ppm was not reported so far (see **Chapter VI**) however the 1D ^{113}Cd NMR spectra suggest the existence of a upfield shifted ^{113}Cd signal at 605 ppm hinting a histidine involved Cd^{II} binding site, which could be verified in [^{113}Cd,^1H] HSQC NMR spectra with increasing the pH (**Fig. VII 5c**).

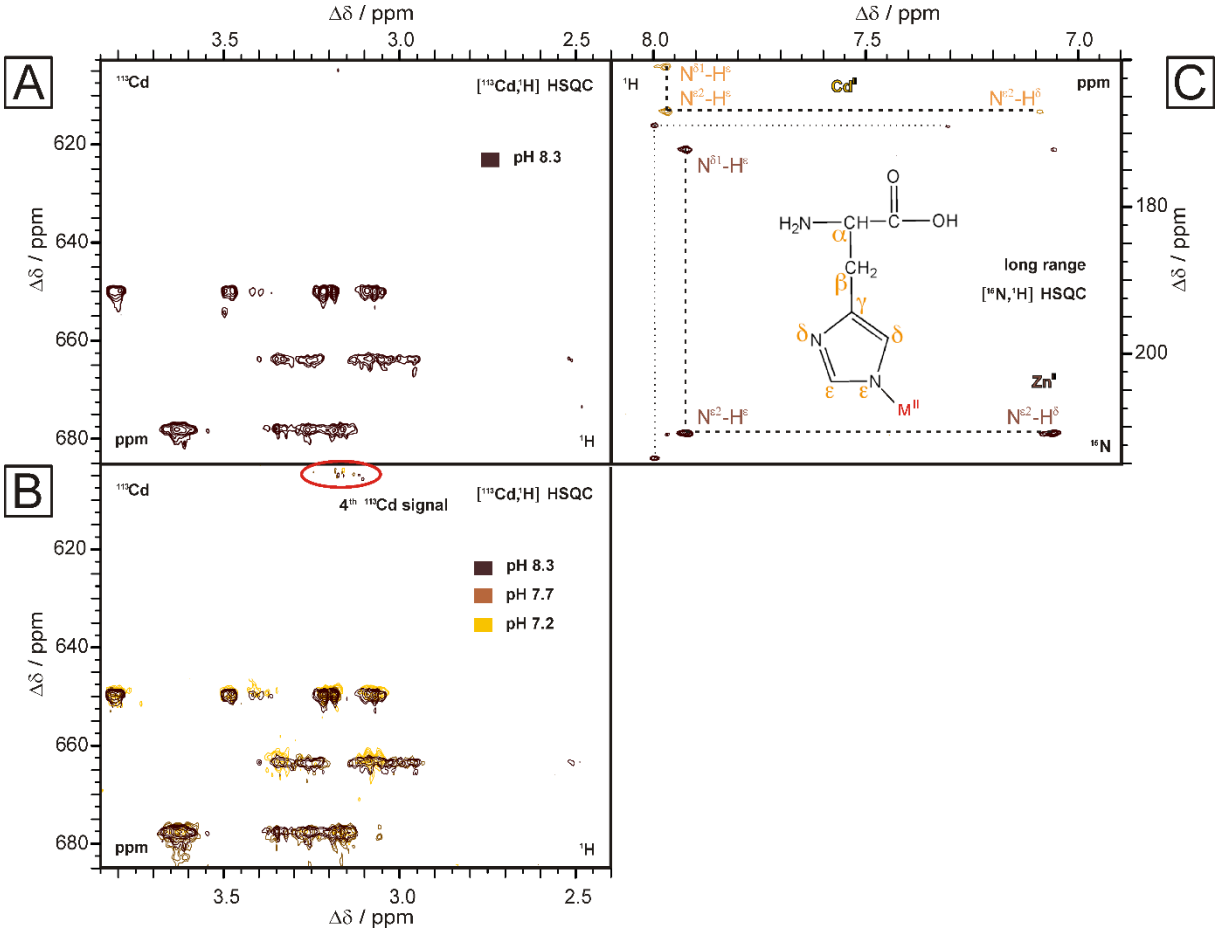

Figure VII 5. NMR spectra of Neclu_MT1. ***A)*** [^{113}Cd,^{1}H] HSQC NMR spectra of Cd_3Neclu_MT1 at pH 8.3. Four ^{113}Cd signals are discernable amongst three (676 ppm, 660 ppm and 654 ppm) show strong ^{3}J[Cd,H] couplings while the one at 605 ppm displays only weak ^{3}J[Cd,H] couplings. The proton chemical shifts between 2.5 ppm and 3.8 ppm indicate cysteinyl - $^{1}H_B$ coordination. ***B)*** Overlay of [^{113}Cd,^{1}H] HSQC NMR spectra of Cd_3Neclu_MT1 at pH 7.2 (yellow); 7.7 (light brown) and 8.3 (dark brown) is displayed. The pH dependent evolution of ^{3}J[Cd-H] coupling signals is visible. At more basic pH different protons couple to the $^{113}Cd^{II}$ at 676 ppm, 660 ppm and 654 ppm while the signal at 605 ppm only appears at pH 7.7 or higher. ***C)*** Overlay of long range [^{15}N,^{1}H] HSQC NMR spectra of Cd_3 (light brown) and Zn_3 GST-Neclu_MT1 (dark brown) used to determine the tautomeric form of the *N*-terminal histidine. The Zn_3-form shows a major (annotated) and a minor isomer. While the major form resides in the ε-tautomer the minor form prefers the δ-tautomer. For the Cd_3-form only the ε-tautomer is observed (see inset).

The Cd-$H_{B,CYS}$ cross peaks are rather weak at ^{3}J[Cd,H] coupling constant of 40 Hz. There was no Cd-$H_{D/E,HIS}$ cross peaks in the amide chemical shift region evidenced, being conclusive for

histidine coordination. When changing the pH from neural to slightly basic pHs the Cd-$H_{B,CYS}$ cross peak pattern shifts. This shift can also be photo-spectrometrically witnessed. The pH of a fully metallated Cd_3Neclu_MT1 is raised from pH 7.2 to 11.5. Besides the appearance of a band centered at around 280 nm possibly assignable to disulfide formation a negative band at 259 nm develops gradually till pH 8.5 (**Fig. VII 3**). Deducing the contribution of the band at 280 nm and those appearing at around 220 nm a difference in extinction coefficient at 259 nm of 4'000 M^{-1} cm^{-1} can be witnessed. The molar absorptivity of Cd-thiolate cluster at 259 nm was so far inferred as a contribution from the bridging cysteines to the absorption envelope[45] with a molar extinction coefficient of the bridging Cd-S-Cd thiolate of roughly 4'000 M^{-1} cm^{-1}. Thus it is well imaginable that with rising pH one of the four bridging thiolates of the Cd_3Cys_8 cluster transforms into a terminal thiolate while giving rise to imidazolic nitrogen coordination, which is favored in basic pH owing to the deprotonation of the imidazole nitrogen essential for metal ion – nitrogen bond formation (**Fig. VII 2**).

To sum up, we propose: **i)** the pH-dependent co-existence of a Cd_3Cys_8 and a Cd_3Cys_8His cluster, both describing novel Cd^{II} clusters in proteins; **ii)** the Cd_3Cys_8His cluster is identical in fold to the well known β-cluster of mammalian MTs with one terminal cysteine being substituted to a histidine; **iii)** the Cd_3Cys_8 represents a novel cluster motive with four bridging cysteines being derived from the MT β-cluster, with a transformation of two terminal cysteines into one bridging cysteine; **iv)** the metallation of the Cd_3 cluster proceeds largely non-cooperatively with a distinct Cd_2Cys_8 transition state. It needs, however, to be emphasized that further experiments are vital to support these hypotheses.

VII 4 2 The Zinc Neclu_MT1 metallation pathway and the resulting metal cluster

Metallothioneins are generally considered to either bind Zn^{II} or Cu^{I} *in vivo*[6]. Neclu_MT1 was proposed to be the first Cd^{II} specific MT without any evidence of Zn^{II} binding. In preliminary *in vitro* experiments using 25 μM protein concentration a Zn_3Neclu_MT1 was evidenced in photo-spectroscopic titration as well as Chelex®100 experiments. Physiological Cd^{II} concentration (metal concentration at site of organisms isolation) induced Neclu_MT1 *in vivo* to an average cytoplasmatic concentration below 5 μM rendering spectroscopic investigation at 5 μM and below physiological relevant. At those conditions *in vitro* spectroscopic investigation yield a Zn_2Neclu_MT1 species suggesting a concentration dependent metallation pathway (see **Chapter VI**). In order to elaborate the metal cluster structure **i)** the concentration dependent metal cluster stoichiometry; **ii)** the number and

chemical identity of the coordinating ligands and in a final step **iii)** the cluster connectivity was under investigation. Furthermore the metallation pathway was elaborated on **iv)** the degree of cooperativity and **v)** the concentration dependent occupation of the different binding sites.

Through apo to Zn^{II} (see **Chapter VI**) and thiolate (**Fig. VII 2**) titration as well as EXAFS (**Fig. VII 6**) and NMR spectroscopy (**fig. 5**) it is reasonable to predict a Zn_3Cys_8His metal cluster for Neclu_MT1 concentration of 25 µM or higher. From apo to Zn^{II} and thiolate titration experiments followed with UVvis, the involvement of all 8 cysteines is discernable. The extinction coefficient at 230 nm (ε_{230nm}), indicative for a Zn^{II}-S^{-1} ligand to metal charge transfer (LMCT) band[45], is 24'000 M^{-1} cm^{-1}, which assuming a Zn^{II}-S^{-1} extinction coefficient of 4'000 M^{-1} cm^{-1} would result in six tetrahedral tetrathiolate coordinated cysteines. In case two cysteines remain free thiols either the appearance of a thiolate band with increasing pH or the formation of disulfides, resulting in both an increase of absorptivity at 280 nm and a dimer/multimer formation witnessable in size exclusion chromatography (SEC) (data not shown) would be expected. Since neither effect was observed, moreover the thiol based protein concentration measurement before and after thiolate titration yield the same result, it

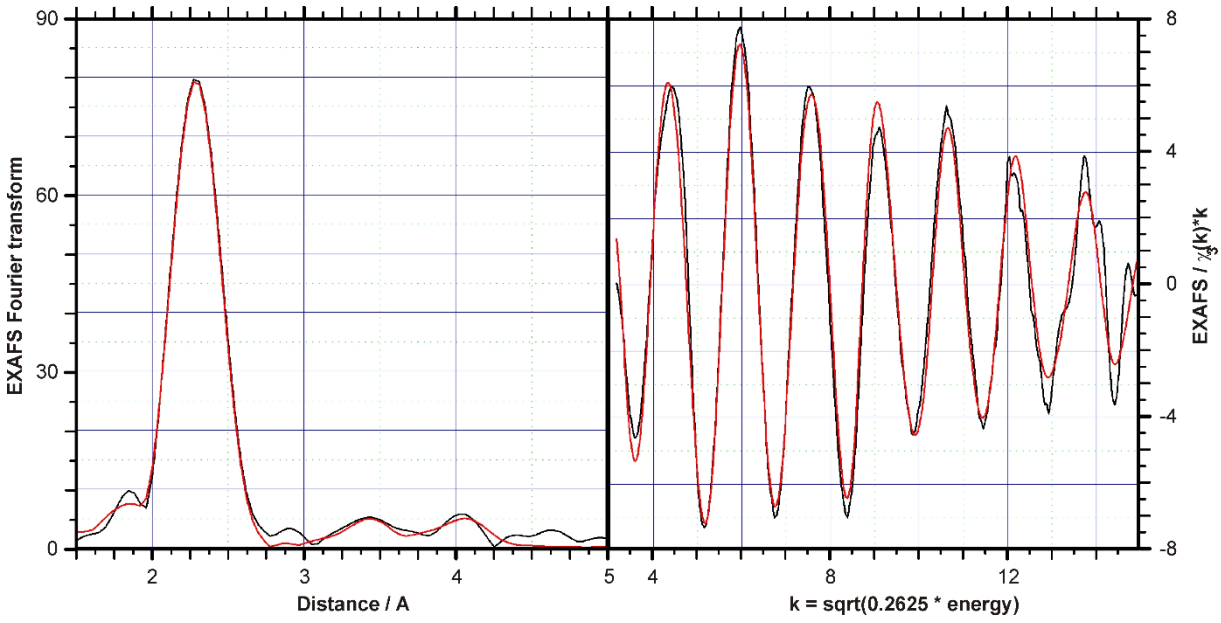

Figure VII 6. EXAFS data of Zn_2Neclu_MT1. ***A)*** Experimental EXAFS spectra (black) overlayed by calculated best fitting model (red) in k^3 space and ***B)*** real space. The model includes second shell contribution yielding an average Zn^{II} coordination of 0.4 nitrogen and 3.6 sulfur ligands.

can be readily inferred that all cysteines are involved in Zn^{II} coordination with a Zn^{II}-S^{-1} extinction coefficient of 3'000 M^{-1} cm^{-1}. In order to investigate the possible involvement of the *C*-terminal histidine Zn^{II} EXAFS experiments were performed, clearly proving the involvement of one nitrogen ligand (**Fig. VII 6**). Besides the imidazole ring the two asparagine as well as the protein backbone amides could coordinate to Zn^{II} via nitrogen necessitating further investigation. Heteronuclear 2D [^{15}N,^{1}H] HSQC NMR spectra have been proven as valuable tool to evaluate histidine involvement in metal coordination[9, 182]. Long range [^{15}N,^{1}H] HSQC NMR spectra allow elucidating the tautomeric state of histidine residues, indicative for the involvement of the respective nitrogen in any kind of binding event. In case the coordinating nitrogen is downfield shifted (see **Fig. VII 5c**) as witnessed for Zn_3Neclu_MT1 a metal ion coordination can be hypothesized. The [^{15}N,^{1}H] HSQC NMR spectra displays a second histidine pattern, which belongs to a minor differently metallated Zn^{II} Neclu_MT1 species, possibly a Zn_3Cys_8 metal cluster as will be proposed for the Cd_3Neclu_MT1 species (**Fig. VII 1**). Summarizing the considerations so far, we can conclude that the main metallated species can be described as a Zn_3Cys_8His metal cluster, characteristic for β-cluster of metallothioneins, despite the fact that these proteinous Zn^{II} cluster prototypes coordinate three Zn^{II} ions with nine cysteines only[180]. Both chiro-optical and magnetic induced chiro-optical properties of the Zn_3-form of Neclu_MT1 support the notion of a β-cluster assembly (**Fig. VII 4**) owing to the comparable shape, possessing a sinusoidal form with a positive band and 240 nm and a negative band at 225 nm(183). In contrast to EXAFS and NMR spectroscopy, which require low mM protein concentration, optical and chiro-optical spectroscopy can be applied to elucidate the concentration dependent metallation of Neclu_MT1 with Zn^{II} ions at low μM protein concentrations. The increase in ellipticity of the incident light when adding subsequent Zn^{II} equivalents is quantitative, while the shape of the CD spectra does not vary appreciably. This is the case for both low and high protein concentration (**Fig. VII 4e,f**). However, the absolute ellipticity at 240 nm is only half as pronounce for the 5 μM sample as for the 25 μM Neclu_MT1 sample, indicating a difference in metal cluster number or arrangement. In case of the high protein concentration the MCD band peaking at 230 nm increases steadily until three equivalents of Zn^{II}, suggesting that the cluster is either formed cooperatively or that each Zn^{II} equivalent, including the third coordinates to so-far free thiols/thiolates. In both cases a difference in metallation pathway relative to Cd^{II} is observed. In order to further elaborate the difference in metallation of low

and high Zn^{II} Neclu_MT1 concentration, thiolate titrations followed by UVvis spectroscopy have been performed (**Fig. VII 2**). From the absorption envelope at high and low protein concentration prepared at pH 7 as Zn_2- and Zn_3- forms significant differences in metallation are observed (**Fig. VII 2a**). Notably both Zn^{II}-forms at (5 μM) as well as the Zn_2-species at (25 μM) possess comparable extinction coefficient at 230 nm, assigned to the LMCT band of terminal Zn^{II}-S^- bonds. In contrast 25μM Zn_3Neclu_MT1 displays a significant higher ε_{230nm}. By deducing the absorption envelope of the respective Zn^{II} Neclu_MT1 forms at pH 7 from those at pH 11.2, the pH effect on absorption especially of the non-coordinated cysteines (S^{-1}) can be probed. A broad band centered around 280 nm may provide information on disulfide formation, while a sharp band peaking at 233 nm might refer to thiol to thiolate conversion. The difference in concentrations of Neclu_MT1 for both Zn_2- and Zn_3 species is assigned to disulfide formation (**Fig. VII 2b,c**). The appearance of a strong band at 233 nm for the Zn_2 species (25 μM) and Zn_3 species (5 μM) is attributed to the existence of free thiolates (**Fig. VII 2b,d**). In detail: for high protein concentration, we observe only an appreciable band at 233 nm not 280 nm, which vary in extinction coefficient by a factor of two (**Fig. VII 2b**). The difference between the 25 μM Zn_2- and the Zn_3Neclu_MT1 species arises at around pH 8.5 with the Zn_3-form stagnating at ε_{230nm} = 5500 M^{-1} cm^{-1} and the Zn_2-form jumping to ε_{230nm} = 11000 M^{-1} cm^{-1} (**Fig. VII 2c**). This behavior can be explained by the conversion of one (ε_{S^-} ~ 5000 M^{-1} cm^{-1}) non-coordinated thiol to a thiolate with a pK_A of 8.6. Moreover this implies that at two Zn^{II} equivalents not all cysteines are bonded and in agreement with apo Zn^{II} titration (see **Chapter VI**) rules out a strict cooperative cluster assembly (at two Zn^{II} equivalents 2.67 cysteines would be expected to be non-coordinating), more likely suggesting a stepwise Zn^{II} metallation of Neclu_MT1 as proposed for the Cd_3-form (see below). In case of low protein concentration the absorption envelope display at least three bands at 280 nm, 233 nm and 210 nm. For both Zn_2 and Zn_3 metallation the absorptivity at 280 nm jumps from ε_{280nm} = 600 M^{-1} cm^{-1} to 1800 M^{-1} cm^{-1} over a pH range of 8.25 to 9.5, indicative for disulfide bridge formation, which is not observable for the Zn_2- and Zn_3-form at high Neclu_MT1 concentration. The discrepancy between 5 μM and 25 μM protein concentration is further manifested in the absorption envelope at 233 nm. While at high protein concentration the Zn_2-form displays a jump in ε_{233nm} of 5000 M^{-1} cm^{-1} at pH 8.6, indicative for the transformation of one thiol to one thiolate, at low protein concentration this behavior is not evidenced for the Zn_2-form excluding the existence of free thiolates. However the Zn_3 species at 5 μM Neclu_MT1 evidences a steady pH dependent conversion of a thiol to a thiolate providing

evidence that not all cysteines are involved in bonding and moreover that they are not well accessible to oxidation (**Fig. VII 2c,d**). In the case of Zn_3-Neclu_MT1 at 25 μM protein concentration no increase at ε_{233nm} comparable to the Zn_2-form at 5 μM is observed, suggesting that all cysteines are involved in Zn^{II} coordination. Furthermore SEC data (data not shown) report multimer formation for Zn_3Neclu_MT1 species at 5 μM Neclu_MT1, while for high Neclu_MT1 concentration only the Zn_2-species forms some aggregates, which are all dimeric. Together with the EXAFS based observation of one nitrogen ligand (histidine) involved in Zn^{II} coordination of the Zn_2Neclu_MT1 species the following conclusion for the Zn^{II} Neclu_MT1 metallation may be drawn: **i)** there is a concentration dependent metallation and metal cluster formation; **ii)** at Neclu_MT1 concentration of 25 μM or higher a Zn_3Cys_8His metal cluster forms, putatively adapting the MT typical β-cluster conformation; **iii)** the cluster formation proceeds probably only moderately cooperatively during incorporation of the first two Zn^{II} equivalents most likely already forming a Zn_2Cys_6His metal cluster. With the third Zn^{II}-ion the cluster rearranges by coordinating the last two free cysteines and changing two terminal cysteines into two bridging; **iv)** at protein concentration of 5 μM or lower the Zn_3Cys_8His cluster can not form. More likely a Zn_2Cys_6His cluster forms, with different cysteines being involved in comparison to the intermediate Zn_2Cys_6His metal cluster evidenced at high protein concentration. The difference in Zn_2Cys_6His metal cluster connectivity may arise from transient dimerisation events, which trigger the Zn_3 cluster formation; **v)** the difference at low concentration between two and three Zn^{II} ions added may lie in the unspecific and Chelex®100 labile coordination of the third Zn^{II} ion to Neclu_MT1. Yet further experiments are needed to support these hypotheses.

VII 5 Conclusion

The metallothionein Neclu_MT1 was isolated from its natural habitat as a Cd^{II} binding protein[20]. This raised the question, whether an efficient Zn^{II} binding to Neclu_MT1 is even possible, despite the fact that Neclu_MT1 would be classified as Zn^{II} binding MT[6]. In consequence it remained doubtful whether this protein is "hijacked" by the more affinic metal ion Cd^{II} or whether it has been specifically designed to bind Cd^{II} for detoxification processes only. The later case seems more likely as studies suggest (see **Chapter VI**) that only Cd^{II} can induce Neclu_MT1 protein expression resulting in a Cd_3 protein species *in vitro*. This is in contrast to Zn^{II} coordination, where preliminary spectroscopic studies imply a concentration dependent metallation resulting at low concentration in a Zn_2-form and under higher concentration in a Zn_3-form (see **Chapter VI**). Being puzzled by these findings we investigated the metallation pathway and the resulting cluster architecture of the Zn^{II}- and the Cd^{II}-form, applying various types of spectroscopy. Distinct differences in Zn^{II} and Cd^{II} metallation are evidenced. The *C*-terminal histidine appears to play a major role moderately preferring Zn^{II} coordination to Cd^{II} association according to the HSAB concept. This is reflected in the metallation pathway. While the addition of two Zn^{II} equivalents to Neclu_MT1 leads to histidine coordination probably inducing a cluster formation, the first two Cd^{II} equivalents are exclusively bonded by cysteines largely resulting in two independent tetrahedral tetrathiolate binding sites. In case of Cd^{II} the addition of the third equivalent leads to a cluster formation, which dependening on the pH may either lead to a Cd_3Cys_8 metal site or a mix of a Cd_3Cys_8 and a Cd_3Cys_8His metal cluster. Both cluster arrangements are not reported in literature so far, rendering the proposed cluster topology speculative.

In case of Zn^{II} the incorporation of a third equivalent is concentration dependent. At Neclu_MT1 concentration of 5 μM or lower a third metal ion cannot be incorporated. Higher Neclu_MT1 concentration of 25 μM or more allow the formation of a Zn_3Cys_8His cluster, probably featuring an identical cluster topology as Cd_3Cys_8His. Previous studies suggest Neclu_MT1 expression levels in *H. lugdunensis* exposed to the metal ion concentration of the site of isolation to be less than 5 μM. This suggests that under physiological relevant conditions indeed only a fully loaded and probably fully functional Cd_3Neclu_MT1 species can be formed. The pH dependent Cd_3 cluster dualism might provide the first hint concerning the physiological involvement in Cd^{II} homeostasis, namely as Cd^{II} sensor and intracellular transporter possibly interacting with membrane embedded Cd^{II} transporter. Further

experiments both investigating the entire organism and the isolated protein are underway to shed more light on this fascinating protein and its noble task.

VII 6 Acknowledgements

This work was supported by the Swiss National Science Foundation (SNSF Professorship to E.F.).

References

[1] D. P. Jones, Y.-M. Go, C. L. Anderson, T. R. Ziegler, J. R. J. M. Kinkade, W. G. Kirlin, Cysteine/cystine couple is a newly recognized node in the circuitry for biologic redox signaling and control., *FASEB J.* **2004**, *18*, 1246-1248.

[2] M. Margoshes, B. L. Vallee, A cadmium protein from equine kidney cortex. *J Am Chem Soc* **1957**, *79*, 4813-4814.

[3] P.-A. Binz, J. H. R. Kägi, Metallothionein: Molecular evolution and classification, in *Metallothionein IV*, Eds. C. Klaassen, Birkhäuser Verlag, Basel, **1999**, pp. 7-13.

[4] E. Freisinger, Metallothioneins in plants. *Met. Ions Life Sci.* **2009**, *5*, 107-153.

[5] O. I. Leszczyszyn, R. Schmid, C. A. Blindauer, Toward a property/function relationship for metallothioneins: Histidine coordination and unusual cluster composition in a zinc-metallothionein from plants. *Proteins: Structure, Function, and Bioinformatics* **2007**, *68*, 922-935.

[6] Ò. Palacios, S. Atrian, M. Capdevila, Zn- and Cu-thioneins: a functional classification for metallothioneins?, *J. Biol. Inorg. Chem.* **2011**, *16*, 991-1009.

[7] C. A. Blindauer, M. D. Harrison, J. A. Parkinson, A. K. Robinson, J. S. Cavet, N. J. Robinson, P. J. Sadler, A metallothionein containing a zinc finger within a four-metal cluster protects a bacterium from zinc toxicity. *P Natl Acad Sci USA* **2001**, *98*, 9593-9598.

[8] E. A. Peroza, A. Al Kaabi, W. Meyer-Klaucke, G. Wellenreuther, E. Freisinger, The two distinctive metal ion binding domains of the wheat metallothionein E_c-1. *J. Inorg. Biochem.* **2009**, *103*, 342-353.

[9] E. A. Peroza, R. Schmucki, P. Güntert, E. Freisinger, O. Zerbe, The β_E-domain of the wheat E_c-1 metallothionein: A metal-binding domain with a distinctive structure. *J. Mol. Biol.* **2009**, *387*, 207-218.

[10] O. I. Leszczyszyn, C. A. Blindauer, Zinc transfer from the embryo-specific metallothionein E(C) from wheat: a case study., *Phys. Chem. Chem. Phys.* **2010**, *41*, 13408-13418.

[11] S. Zeitoun-Ghandour, J. Charnock, M. M. E. Hodson, O. I. Leszczyszyn, C. A. Blindauer, S. R. Stürzenbaum, The two *Caenorhabditis elegans* metallothioneins (CeMT-1 and CeMT2) discriminate between essential zinc and toxic cadmium., *FEBS Journal* **2010**, *11*, 2531-2542.

[12] E. Freisinger, Plant MTs - long neglected members of the metallothionein superfamily. *Dalton Trans.* **2008**, 6663-6675.

[13] L. Hanley-Bowdoin, B. G. Lane, A novel protein programmed by the mRNA conserved in dry wheat embryos. The principal site of cysteine incorporation during early germination. *Eur. J. Biochem.* **1983**, *135*, 9-15.

[14] B. G. Lane, R. Kajioka, T. D. Kennedy, The wheat-germ Ec protein is a zinc-containing metallothionein. *Biochem. Cell Biol.* **1987**, *65*, 1001-1005.

[15] I. Kawashima, T. D. Kennedy, M. Chino, B. G. Lane, Wheat E_c metallothionein genes. Like mammalian Zn^{2+} metallothionein genes, wheat Zn^{2+} metallothionein genes are conspicuously expressed during embryogenesis. *Eur. J. Biochem.* **1992**, *209*, 971-976.

[16] D. L. Laudencia-Chingcuanco, B. S. Stamova, F. M. You, G. R. Lazo, D. M. Beckles, O. D. Anderson, Transcriptional profiling of wheat caryopsis development using cDNA microarrays. *Plant Mol. Biol.* **2007**, *63*, 651-668.

[17] O. I. Leszczyszyn, C. R. J. White, C. A. Blindauer, The isolated Cys_2His_2 site in E_C metallothionein mediates metal-specific protein folding. *Mol. Biosyst.* **2010**, *6*, 1592-1603.

[18] W.-J. Guo, M. Meetam, P. Goldsbrough, Examining the specific contributions of individual arabidopsis metallothioneins to copper distribution and metal tolerance. *Plant Physiol.* **2008**, *146*, 1697-1706.

[19] Y. Ren, Y. Liu, H. Chen, G. Li, X. Zhang, J. Zhao, Type 4 metallothionein genes are involved in regulating Zn ion accumulation in late embryo and in controlling early seedling growth in Arabidopsis., *Plant Cell Environ.* **2012**, *35*, 770–789.

[20] G. Krauss, F. Bärlocher, P. Schreck, R. Wennrich, W. Glässer, G.-J. Krauss, Aquatic hyphomycetes occur in hyperpolluted waters in Central Germany. *Nova Hedwigia* **2001**, *72*, 419-428.

[21] G.-J. Krauss, M. Solé, G. Krauss, D. Schlosser, D. Wesenberg, F. Bärlocher, Fungi in freshwaters: ecology, physiology and biochemical potential. *FEMS Microbiol. Rev.* **2011**, *35*, 620-651.

[22] P. Jaeckel, G. Krauss, S. Menge, A. Schierhorn, P. Rücknagel, G.-J. Krauss, Cadmium induces a novel metallothionein and phytochelatin 2 in an aquatic fungus. *Biochem. Biophys. Res. Commun.* **2005**, *333*, 150-155.

[23] D. Meissner, smMT_NECLU - ein kleines Metallothionein aus dem aquatischen Hyphomyceten *Heliscus lugdunensis* – Physiologisch-biochemische Untersuchungen und Strukturanalyse., *MLU Halle-Wittenberg,* Dissertation, **2009**.

[24] B. Braha, H. Tintemann, G. Krauss, J. Ehrman, F. Bärlocher, G.-J. Krauss, Stress response in two strains of the aquatic hyphomycete *Heliscus lugdunensis* after exposure to cadmium and copper ions. *Biometals* **2007**, *20*, 93–105.

[25] K. Lerch, Copper metallothionein, a copper-binding protein from *Neurospora crassa*. *Nature* **1980**, *284*, 368-370.

[26] http://prosite.expasy.org/scanprosite, 2012

[27] C. F. Evans, D. R. Engelke, D. J. Thiele, ACE1 transcription factor produced in *Escherichia coli* binds multiple regions within yeast metallothionein upstream activation sequences., *Mol. Cell. Biol.* **1990**, *10*, 426-429.

[28] J. K. Hane, R. G. T. Lowe, P. S. Solomon, K.-C. Tan, C. L. Schoch, J. W. Spatafora, P. W. Crous, C. Kodira, B. W. Birren, J. E. Galagan, S. F. F. Torriani, B. C. McDonald, R. P. Olivera, Dothideomycete–plant interactions illuminated by genome sequencing and EST analysis of the wheat pathogen Stagonospora nodorum., *Plant Cell* **2007**, *19*, 3347–3368.

[29] C. Bouchet-Marquis, M. Pagratis, R. Kirmse, A. Hoenger, Metallothionein as a clonable highdensity marker for cryo-electron microscopy., *J. Struct. Biol.* **2012**, *177*, 119–127.

[30] B. A. Messerle, A. Schäffer, M. Vašák, J. H. R. Kägi, K. Wüthrich, Comparison of the Solution Conformations of Human $[Zn_7]$-Metallothionein-2 and $[Cd_7]$-Metallothionein-2 Using Nuclear-Magnetic-Resonance Spectroscopy. *J. Mol. Biol.* **1992**, *225*, 433-443.

[31] A. H. Robbins, D. E. McRee, M. Williamson, S. A. Collett, N. H. Xuong, W. F. Furey, B. C. Wang, C. D. Stout, Refined crystal structure of Cd, Zn metallothionein at 2.0 A resolution. *J. Mol. Biol.* **1991**, *221*, 1269-1293.

[32] B. Dolderer, Zur molekularen Architektur von Cu(I)-Thiolatzentren in Cu-Thioneinen., *Universität Tübingen,* Dissertation,**2004**.

[33] M. H. Frey, G. Wagner, M. Vašák, O. W. Sorensen, D. Neuhaus, E. Wörgötter, J. H. R. Kägi, R. R. Ernst, K. Wüthrich, Polypeptide-metal cluster connectivities in metallothionein 2 by novel ^{1}H-^{113}Cd heteronuclear two-dimensional NMR experiments. *J. Am. Chem. Soc.* **1985**, *107*, 6847-6851.

[34] J. D. Otvos, I. M. Armitage, Structure of the metal-clusters in rabbit liver metallothionein. *Proc. Natl. Acad. Sci.-Biol.* **1980**, *77*, 7094-7098.

[35] M. Vašák, Application of ^{113}Cd NMR to metallothioneins. *Biodegradation* **1998**, *9*, 501-512.

[36] M. F. Summers, ^{113}Cd NMR spectroscopy of coordination compounds and proteins. *Coord. Chem. Rev.* **1988**, *86*, 43-134.

[37] H. Li, H. Sun, NMR studies of metalloproteins, in *NMR of proteins and small biomolecules* Vol. 326, Eds. G. Zhu, Springer Verlag, Berlin, Heidelberg, **2012**, pp. 69-98.

[38] K. Wüthrich, *NMR of proteins and nucleic acids,* Wiley-Interscience, New York, **1986**.

[39] K. Wüthrich, Protein structure determination in solution by NMR spectroscopy., *J Biol Chem* **1990**, 22059–22062.

[40] J. Volk, T. Herrmann, K. Wüthrich, Automated sequence-specific protein NMR assignment using the memetic algorithm MATCH., *J. Biomol. NMR* **2008**, *41*, 127-138.

[41] T. Herrmann, P. Güntert, K. Wüthrich, Protein NMR structure determination with automated NOE-identification in the NOESY spectra using the new software ATNOS., *J. Biomol. NMR* **2002**, *24*, 171-189.

[42] T. Herrmann, P. Güntert, K. Wüthrich, Protein NMR structure determination with automated NOE assignment using the new software CANDID and the torsion angle dynamics algorithm DYANA. *J. Mol. Biol.* **2002**, *319*, 209-227.

[43] A. O. Pedersen, J. Jacobsen, Reactivity of the thiol-group in human and bovine albumin at pH 3-9, as measured by exchange with 2,2'-dithiodipyridine. *Eur. J. Biochem.* **1980**, *106*, 291-295.

[44] H. Willner, M. Vašák, J. H. R. Kägi, Cadmium-Thiolate Clusters in Metallothionein - Spectrophotometric and Spectropolarimetric Features. *Biochemistry-Us* **1987**, *26*, 6287-6292.

[45] M. Vašák, J. H. R. Kägi, H. A. Hill, Zinc(II), cadmium(II), and mercury(II) thiolate transitions in metallothionein. *Biochemistry-Us* **1981**, *20*, 2852-2856.

[46] M. Vašák, J. H. R. Kägi, B. Holmquist, B. L. Vallee, Spectral studies of cobalt(II)- and nickel(II)-metallothionein. *Biochemistry-Us* **1981**, *20*, 6659-6664.

[47] G. Meloni, P. Faller, M. Vašák, Redox silencing of copper in metal-linked neurodegenerative disorders - reaction of Zn_7metallothionein-3 with Cu^{2+} ions. *J Biol Chem* **2007**, *282*, 16068-16078.

[48] D. L. Pountney, C. J. Henehan, M. Vašák, Establishing isostructural metal substitution in metalloproteins using ^{1}H NMR, circular dichroism, and Fourier transform infrared spectroscopy., *Protein Sci.* **1995**, *8*, 1571-1576.

[49] A. Torreggiani, J. Domènech, A. Tinti, Structural modifications in metal complexes of a plant metallothionein caused by reductive radical stress: a Raman study. *J. Raman Spectrosc.* **2009**, *40*, 1687-1693.

[50] T. Elgren, D. E. Wilcox, A unique low frequency Raman band associated with metal binding to metallothionein., *Biochem. Biophys. Res. Commun.* **1989**, *163*, 1093-1099.

[51] S.-H. Hong, Q. Hao, W. Maret, Domain-specific fluorescence resonance energy transfer (FRET) sensors of metallothionein/thionein., *Prot. Eng. Des. Select.* **2005**, *18*, 255–263.

[52] D. L. Pountney, M. Vasák, Spectroscopic studies on metal distribution in Co(II)/Zn(II) mixed metal clusters in rabbit liver metallothionein-2., *Eur. J. Biochem.* **1992**, *209*, 335-341.

[53] K. E. R. Duncan, T. T. Ngu, J. Chan, M. T. Salgado, M. E. Merrifield, M. J. Stillman, Peptide folding, metal-binding mechanisms, and binding site structures in metallothioneins., *Exp. Biol. Med.* **2006**, *231*, 1488-1499.

[54] G. L. Öz, D. L. Pountney, I. M. Armitage, NMR spectroscopic studies of $I = {}^1/_2$ metal ions in biological systems. *Biochem. Cell Biol.* **1998**, *76*, 223-234.

[55] A. Prange, D. Schaumloffel, Hyphenated techniques for the characterisation and quantification of metallothionein isoforms., *Anal. Bioanal. Chem.* **2002**, *373*, 441-453.

[56] U. Heinz, L. Hemmingsen, M. Kiefer, H.-W. Adolph, Structural adaptability of zinc binding sites: different structures in partially, fully, and heavy-metal loaded states., *Chem. Eur. J.* **2009**, *15*, 7350 - 7358.

[57] M. Ryvolovaa, V. Adam, R. Kizek, Analysis of metallothionein by capillary electrophoresis., *J. Chromatogr. A* **2012**, *1226*, 31-42.

[58] M. Li, Y. S. Huang, U. S. Jeng, I.-J. Hsu, Y. C. S. Wu, Y. H. Lai, C. H. Su, J. F. Lee, Y. U. Wang, C.-C. Chang, Resonant X-Ray Scattering and Absorption for the Global and Local Structures of Cu-modified Metallothioneins in Solution., *Biophys. J.* **2009**, *197*, 609–617.

[59] M. Capdevila, R. Bofill, Ò. Palacios, S. Atrian, State-of-the-art of metallothioneins at the beginning of the 21st century., *Coord. Chem. Rev.* **2012**, *256*, 46-62.

[60] B. L. Vallee, Metallothionein: Historical review and perspectives, in *Metallothionein,* 1st ed., Eds. J. H. R. Kägi, M. Nordberg, Birkhäuser Verlag, Basel, **1979**, pp. 19-40.

[61] E. A. Peroza, E. Freisinger, Metal ion binding properties of *Triticum aestivum* E_c-1 metallothionein: Evidence supporting two separate metal-thiolate clusters. *J. Biol. Inorg. Chem.* **2007**, *12*, 377-391.

[62] W. Braun, M. Vašák, A. H. Robbins, C. D. Stout, G. Wagner, J. H. R. Kägi, K. Wüthrich, Comparison of the NMR solution structure and the X-ray crystal-structure of rat metallothionein-2. *P Natl Acad Sci USA* **1992**, *89*, 10124-10128.

[63] S. S. Narula, M. Brouwer, Y. Hua, I. M. Armitage, Three-dimensional solution structure of *Callinectes sapidus* metallothionein-1 determined by homonuclear and heteronuclear magnetic resonance spectroscopy. *Biochemistry-Us* **1995**, *34*, 620-631.

[64] R. Riek, B. Prêcheur, Y. Wang, E. A. Mackay, G. Wider, P. Güntert, A. Liu, J. H. R. Kägi, K. Wüthrich, NMR structure of the sea urchin (*Strongylocentrotus purpuratus*) metallothionein MTA. *J. Mol. Biol.* **1999**, *291*, 417-428.

[65] R. D. Palmiter, The elusive function of metallothioneins. *P Natl Acad Sci-Biol* **1998**, *95*, 8428-8430.

[66] P. Coyle, J. C. Philcox, L. C. Carey, A. M. Rofe, Metallothionein: The multipurpose protein. *Cell. Mol. Life Sci.* **2002**, *59*, 627-647.

[67] R. R. Finkelstein, S. S. L. Gampala, C. D. Rock, Abscisic acid signaling in seeds and seedlings. *Plant Cell* **2002**, *14*, S15-S45.

[68] E. Freisinger, Spectroscopic characterization of a fruit-specific metallothionein: *M. acuminata* MT3. *Inorg. Chim. Acta* **2007**, *360*, 369-380.

[69] M. Korbas, D. F. Marsa, W. Meyer-Klaucke, KEMP: A program script for automated biological x-ray absorption spectroscopy data reduction. *Rev Sci Instrum* **2006**, *77*, 1-5.

[70] G. Wellenreuther, V. Parthasarathy, W. Meyer-Klaucke, Towards a black-box for biological EXAFS data analysis. II. Automatic BioXAS refinement and analysis (ABRA). *J. Synchrotron Radiat.* **2010**, *17*, 25-35.

[71] N. Binsted, R. W. Strange, S. S. Hasnain, Constrained and restrained refinement in EXAFS data-analysis with curved wave theory. *Biochemistry-Us* **1992**, *31*, 12117-12125.

[72] L. Braunschweiler, R. R. Ernst, Coherence transfer by isotropic mixing - application to proton correlation spectroscopy. *J. Magn. Reson.* **1983**, *53*, 521-528.

[73] A. Bax, D. G. Davis, MLEV-17-based two-dimensional homonuclear magnetization transfer spectroscopy. *J. Magn. Reson.* **1985**, *65*, 355-360.

[74] A. Kumar, R. R. Ernst, K. Wüthrich, A two-dimensional nuclear overhauser enhancement (2D NOE) experiment for the elucidation of complete proton-proton cross-relaxation networks in biological macromolecules. *Biochem. Biophys. Res. Commun.* **1980**, *95*, 1-6.

[75] S. Macura, R. R. Ernst, Elucidation of cross relaxation in liquids by two-dimensional NMR-spectroscopy. *Mol. Phys.* **1980**, *41*, 95-117.

[76] G. Otting, Zero-quantum suppression in NOESY and experiments with a *z* filter. *J. Magn. Reson.* **1990**, *86*, 496-508.

[77] M. Rance, G. Bodenhausen, G. Wagner, K. Wüthrich, R. R. Ernst, A systematic approach to the suppression of *J* cross peaks in 2D exchange and 2D NOE spectroscopy. *J. Magn. Reson.* **1985**, *62*, 497-510.

[78] C. M. Palmer, M. L. Guerinot, Facing the challenges of Cu, Fe and Zn homeostasis in plants. *Nat Chem Biol* **2009**, *5*, 333-340.

[79] L. E. Kay, P. Keifer, T. Saarinen, Pure absorption gradient enhanced heteronuclear single quantum correlation spectroscopy with improved sensitivity. *J Am Chem Soc* **1992**, *114*, 10663-10665.

[80] C. Bartels, T. H. Xia, M. Billeter, P. Güntert, K. Wüthrich, The program XEASY for computer-supported NMR spectral analysis of biological macromolecules. *J. Biomol. NMR* **1995**, *6*, 1-10.

[81] R. L. J. Keller, *Computer aided resonance assignment tutorial,* CANTINA Verlag, Goldau, **2004**.

[82] P. Güntert, C. Mumenthaler, K. Wüthrich, Torsion angle dynamics for NMR structure calculation with the new program DYANA. *J. Mol. Biol.* **1997**, *273*, 283-298.

[83] P. Güntert, Automated NMR protein structure calculation. *Progr. Nucl. Magn. Reson. Spectrosc.* **2003**, *43*, 105-125.

[84] W. D. Cornell, P. Cieplak, C. I. Bayly, I. R. Gould, K. M. Merz, D. M. Ferguson, D. C. Spellmeyer, T. Fox, J. W. Caldwell, P. A. Kollman, A second generation force field for the simulation of proteins, nucleic acids, and organic molecules. *J Am Chem Soc* **1995**, *117*, 5179-5197.

[85] R. Koradi, M. Billeter, P. Güntert, Point-centered domain decomposition for parallel molecular dynamics simulation. *Comput. Phys. Commun.* **2000**, *124*, 139-147.

[86] P. Luginbühl, P. Güntert, M. Billeter, K. Wüthrich, The new program OPAL for molecular dynamics simulations and energy refinements of biological macromolecules. *J. Biomol. NMR* **1996**, *8*, 136-146.

[87] R. Koradi, M. Billeter, K. Wüthrich, MOLMOL: A program for display and analysis of macromolecular structures. *J. Mol. Graphics* **1996**, *14*, 51-55.

[88] W. Braun, G. Wagner, E. Wörgötter, M. Vašák, J. H. R. Kägi, K. Wüthrich, Polypeptide fold in the two metal clusters of metallothionein-2 by nuclear magnetic resonance in solution. *J. Mol. Biol.* **1986**, *187*, 125-129.

[89] J. D. Baleja, V. Thanabal, G. Wagner, Refined solution structure of the DNA-binding domain of GAL4 and use of $^{3}J(^{113}Cd,^{1}H)$ in structure determination. *J. Biomol. NMR* **1997**, *10*, 397-401.

[90] K. H. Gardner, S. F. Anderson, J. E. Coleman, Solution structure of the *Kluyveromyces lactis* LAC9 Cd_2Cys_6 DNA-binding domain. *Nat Struct Mol Biol* **1995**, *2*, 898-905.

[91] R. Marmorstein, S. Harrison, Crystal structure of a PPR1-DNA complex: DNA recognition by proteins containing a Zn2Cys6 binuclear cluster. *Genes Dev.* **1994**, *8*, 2504-2512.

[92] J. J. Lichty, J. L. Malecki, H. D. Agnew, D. J. Michelson-Horowitz, S. Tan, Comparison of affinity tags for protein purification., *Protein Express. Purif.* **2005**, *41*, 98-105.

[93] G. Q. Chen, J. E. Gouaux, Overexpression of bacterio-opsin in *Escherichia coli* as a watersoluble fusion to maltose binding protein: efficient regeneration of the fusion protein and selective cleavage with trypsin., *Protein* **1996**, *5*, 456-467.

[94] E. Hochuli, W. Bannwarth, H. Döbeli, R. Gentz, D. Stüber, Genetic Approach to Facilitate Purification of Recombinant Proteins with a Novel Metal Chelate Adsorbent., *Nature biotechnol.* **1988**, *6*, 1321-1325.

[95] T. G. Schmidt, A. Skerra, The Strep-tag system for one-step purification and high-affinity detection or capturing of proteins., *Nature Prot.* **2007**, *6*, 1528-1535.

[96] S. Chong, F. B. Mersha, D. G. Comb, M. E. Scott, D. Landry, L. M. Vence, F. B. Perler, J. Benner, R. B. Kucera, C. A. Hirvonen, J. J. Pelletier, H. Paulus, M.-Q. Xu, Single-column purification of free recombinant proteins using a self-cleavable affinity tag derived from a protein splicing element., *Gene* **1997**, *192*, 277-281.

[97] E. A. Peroza, E. Freisinger, Tris is a non-innocent buffer during intein-mediated protein cleavage. *Protein Expres. Purif.* **2008**, *57*, 217-225.

[98] A. Knappik, A. Plückthun, An improved affinity tag based on the FLAG peptide for the detection and purification of recombinant antibody fragments., *Biotechniques* **1994**, *17*, 754-761.

[99] D. B. Smith, K. S. Johnson, Single-step purification of polypeptides expressed in *Escherichia coli* as fusions with glutathione *S*-transferase., *Gene* **1988**, *67*, 31-40.

[100] L. G. Higgins, J. D. Hayes, Mechanisms of induction of cytosolic and microsomal glutathione transferase (GST) genes by xenobiotics and pro-inflammatory agents., *Drug Metab. Rev.* **2011**, *43*, 92-137.

[101] R. Morgenstern, J. Zhang, K. Johansson, Microsomal glutathione transferase 1: mechanism and functional roles., *Drug Metab. Rev.* **2011**, *43*, 300-306.

[102] B. A. Messerle, A. Schäffer, M. Vašák, J. H. R. Kägi, K. Wüthrich, Three-dimensional structure of human [$^{113}Cd_7$]metallothionein-2 in solution determined by nuclear magnetic resonance spectroscopy. *J. Mol. Biol.* **1990**, *214*, 765-779.

[103] A. Oakley, Glutathione transferases: a structural perspective., *Drug Metab. Rev.* **2011**, *43*, 138-151.

[104] I. Cummins, D. P. Dixon, S. Freitag-Pohl, M. Skipsey, R. Edwards, Multiple roles for plant glutathione transferases in xenobiotic detoxification., *Drug Metab. Rev.* **2011**, *43*, 266-280.

[105] A. Brymora, V. A. Valova, P. J. Robinson, Protein-protein interactions identified by pull-down experiments and mass spectrometry., *Curr. Protoc. Cell. Biol.* **2004**.

[106] J. Loebus, E. A. Peroza, N. Blüthgen, T. Fox, W. Meyer-Klaucke, O. Zerbe, E. Freisinger, Protein and metal cluster structure of the wheat metallothionein domain γ-E_c-1. The second part of the puzzle., *J. Biol. Inorg. Chem.* **2011**, *16*, 683-694.

[107] L. A. Basile, J. E. Coleman, Optical activity associated with the sulfur to metal charge transfer bands of Zn and Cd GAL4., *Protein* **1992**, *1*, 617-624.

[108] G. Otting, L. Orbons, K. Wüthrich, Suppression of zero-quantum coherence in NOESY and soft-NOESY., *J. Magn. Reson.* **1990**, *89*, 423-430.

[109] H. Yan, A. Saiani, A. F. Miller, Gelation of a model globular protein. *Macromol. Symp.* **2007**, *251*, 112-117.

[110] T. R. Chauncey, J. Westley, The catalytic mechanism of yeast thiosulfate reductase. *J. Biol. Chem.* **1983**, *258*, 15037-15045.

[111] A. M. Tommey, J. Shi, W. P. Lindsay, P. E. Urwin, N. J. Robinson, Expression of the pea gene PsMTA in E. coli Metal-binding properties of the expressed protein. *FEBS Lett.* **1991**, *292*, 48-52.

[112] K. Bilecen, U. H. Ozturk, A. D. Duru, T. Sutlu, M. V. Petoukhov, D. I. Svergun, M. H. J. Koch, U. O. Sezerman, I. Cakmak, Z. Sayers, Triticum durum metallothionein - Isolation of the gene and structural characterization of the protein using solution scattering and molecular modeling. *J Biol Chem* **2005**, *280*, 13701-13711.

[113] D. Walls, S. T. Loughran, Tagging Recombinant Proteins to Enhance Solubility and Aid Purification., *Proteins: Structure, Function, and Bioinformatics* **2011**, *681*.

[114] R. C. Stevens, Design of high-throughput methods of protein production for structural biology., *Structure* **2000**, *8*, 177-185.

[115] Y. Zhan, X. Song, G. W. Zhou, Structural analysis of regulatory protein domains using GST fusion proteins., *Gene* **2001**, *281*, 1-9.

[116] Y. H. Han, Y. H. Chung, T. Y. Kim, S. J. Hong, J. D. Choi, Y. J. Chung, Crystallization of Clonorchis sinensis 26 kDa glutathione S-transferase and its fusion proteins with peptides of different lengths. *Acta crystallogr. D* **2001**, *57*, 579-581.

[117] C. H. U. K. Liew, R. Gamsjaeger, R. E. Mansfield, J. P. Mackay, NMR spectroscopy as a tool for the rapid assessment of the conformation of GST-fusion proteins., *Protein* **2008**, *17*, 1630-1635.

[118] S. Banta, I. R. Wheeldon, M. Blenner, Protein engineering in the development of functional hydrogels. *Annu. Rev. Biomed. Eng.* **2010**, *12*, 167-186.

[119] K. Hayashi, C. Kojima, Efficient protein production method for NMR using soluble protein tags with cold shock expression vector., *J. Biomol. NMR* **2010**, *48*, 147-155.

[120] J. C. Rutherford, A. J. Bird, Metal-Responsive Transcription Factors That Regulate Iron, Zinc, and Copper Homeostasis in Eukaryotic Cells., *Eukaryot. Cell* **2004**, *3*, 1-13.

[121] W. Maret, Zinc coordination environments in proteins determine zinc functions., *J. Trace Elem. Med. Biol.* **2005**, *19*, 7-12.

[122] W. Maret, Y. Li, Coordination dynamics of zinc in proteins. *Chem. Rev.* **2009**, *109*, 4682-4707.

[123] P. A. Cobine, R. T. McKay, K. Zangger, C. T. Dameron, I. M. Armitage, Solution structure of Cu_6 metallothionein from the fungus *Neurospora crassa*. *Eur. J. Biochem.* **2004**, *271*, 4213-4221.

[124] S. Tottey, K. J. Waldron, S. J. Firbank, B. Reale, C. Bessant, K. Sato, T. R. Cheek, J. Gray, M. J. Banfield, C. Dennison, N. J. Robinson, Protein-folding location can regulate manganese-binding versus copper- or zinc-binding. *Nature* **2008**, *455*, 1138-1142.

[125] C. J. Henehan, D. L. Pountney, O. Zerbe, M. Vašák, Identification of cysteine ligands in metalloproteins using optical and NMR-spectroscopy - cadmium-substituted rubredoxin as a model $[Cd(CysS)_4]^{2-}$ center. *Protein Sci.* **1993**, *2*, 1756-1764.

[126] G. Ohanessian, D. Picot, G. Frison, Reactivity of polynuclear Zinc-thiolate sites., *Inter. J. Quant. Chem.* **2011**, *111*, 1239-1247.

[127] A. A. Jarzecki, Lead-poisoned zinc fingers: quantum mechanical exploration of structure, coordination, and electronic excitations., *Inorg. Chem.* **2007**, *46*, 7509-7521.

[128] E. Freisinger, M. Vasak, Cadmium in Metallothioneins., *Met. Ions Life Sci* **2013**, *11*, 339-371.

[129] J. McMaster, V. S. Oganesyan, Magnetic circular dichroism spectroscopy as a probe of the structures of the metal sites in metalloproteins., *Curr. Opin. Struct. Biol.* **2010**, *20*, 615–622.

[130] H. Willner, W. R. Bernard, J. H. R. Kägi, Synthesis, Structure and Properties of Metallothioneins, Phytochelatins, and Metal-Thiolate Complexes, in *Metallothioneins*, Eds. M. J. Stillman, C. F. Shaw III, K. T. Suzuki, VCH, New York, **1992**, pp. 128-143.

[131] H. Rupp, U. Weser, Circular Dichroism of Metallothioneins a Structrual Approach., *Biochim. Biophys. Acta* **1978**, *533*, 209-226.

[132] T. Simonson, N. Calimet, Cys(x)His(y)-Zn2+ interactions: thiol vs. thiolate coordination., *Proteins* **2002**, *49*, 37-48.

[133] L. Sanita di Topp, R. Gabbrielli, Response to cadmium in higher plants., *Environ. Exp. Bot.* **1999**, *41*, 105-130.

[134] J. P. Buchet, R. Lauwerys, H. Roels, L. Nick, L. Amery, Renal effects of cadmium body burden of the general population., *Lancet* **1990**, *336*, 699-702.

[135] J. M. Moulis, Cellular mechanisms of cadmium toxicity related to the homeostasis of essential metals., *Biometals* **2010**, *23*, 877-896.

[136] M. McLaughlin, D. R. Parker, J. M. Clarke, Metals and micronutrients – food safety issues., *Field Crop. Res* **1999**, *60*, 143-163.

[137] L. Järup, A. Akesson, Current status of cadmium as an environmental health problem., *Toxicol. Appl. Pharm.* **2009**, *238*, 201-208.

[138] N. Degraeve, Carcinogenic, teratogenic and mutagenic effects of cadmium., *Mutat. Res.* **1981**, *86*, 115-135.

[139] C. K. Jørgensen, Electron transfer spectra, in *Prog Inorg Chem*, Vol. 12, Eds. S. J. Lippard, John Wiley & Sons, Inc., **1970**, pp. 101-158.

[140] W. Maret, Zinc and Sulfur: A Critical Biological Partnership. *Biochemistry-Us* **2004**, *43*, 3301-3309.

[141] W. Maret, Zinc Coordination Environments in Proteins as Redox Sensors and Signal Transducers., *Antioxid. Redox. Sign.* **2006**, *8*, 1420-1441.

[142] G. Meloni, K. Zovo, J. Kazantseva, P. Palumaa, M. Vašák, Organization and assembly of metal-thiolate clusters in epithelium-specific metallothionein-4. *J Biol Chem* **2006**, *281*, 14588-14595.

[143] L. M. Utschig, J. W. Bryson, T. V. O'Hallaron, Mercury-199 NMR of the Metal Receptor Site in MerR and Its Protein-DNA Complex., *Science* **1995**, *268*, 380-384.

[144] G. M. Gadd, Tansley review No. 47: Interactions of fungi with toxic metals. *New Phytol.* **1993**, *124*, 25-60.

[145] J. Webster, Biology and ecology of aquatic hyphomycetes, in *The Fungal Community*, Eds. D. T. Wicklow, G. C. Carrol, Marcel Dekker, New York, **1981**, pp. 681-691.

[146] C. Gross, M. Kelleher, V. R. Iyer, P. O. Brown, D. R. Winge, Identification of the copper regulon in *Saccharomyces cerevisiae* by DNA microarrays. *J Biol Chem* **2000**, *275*, 32310–32316.

[147] S. Clemens, Evolution and function of phytochelatin synthases., *J. Plant Physiol.* **2006**, *163*, 319-332.

[148] D. Mendoza-Cózatl, H. Loza-Tavera, A. Hernández-Navarro, R. Moreno-Sánchez, Sulfur assimilation and glutathione metabolism under cadmium stress in yeast, protists and plants. *FEMS Microbiol. Rev.* **2005**, *29*, 653-671.

[149] C. A. Blindauer, O. I. Leszczyszyn Metallothioneins: unparalleled diversity in structures and functions for metal ion homeostasis and more *Nat. Prod. Rep.* **2010**, *27*, 720-741.

[150] M. Vašák, G. Meloni, Chemistry and biology of mammalian metallothioneins. *J. Biol. Inorg. Chem.* **2011**, *16*, 1067-1078.

[151] J. G. Wright, M. J. Natan, F. M. Macdonnell, D. M. Ralston, T. V. O'Halloran, Mercury(II) thiolate chemistry and the mechanism of the heavy-metal biosensor MerR. *Prog Inorg Chem* **1990**, *38*, 323-412.

[152] M. Osobova, V. Urban, P. L. Jedelsky, J. Borovicka, M. Gryndler, T. Ruml, P. Kotrba, Three metallothionein isoforms and sequestration of intracellular silver in the hyperaccumulator *Amanita strobiliformis*. *New Phytol.* **2011**, *190*, 916–926.

[153] O. I. Leszczyszyn, S. Zeitoun-Ghandour, S. R. Stürzenbaum, C. A. Blindauer, Tools for metal ion sorting: in vitro evidence for partitioning of zinc and cadmium in *C. elegans* metallothionein isoforms *Chem. Commun.* **2011**, *47*, 448-450.

[154] B. A. Krizek, D. L. Merkle, J. M. Berg, Ligand variation and metal ion binding specificity in zinc finger peptides. *Inorg. Chem.* **1993**, *32*, 937-940.

[155] K. R. Sridhar, G. Krauss, F. Bärlocher, R. Wennrich, G.-J. Krauss, Fungal diversity in heavy metal polluted waters in central Germany. *Fungal Divers.* **2000**, *5*, 119-129.

[156] M. G. Cherian, Induction of renal metallothionein synthesis by parenteral cadmium-thionein in rats. *Biochem. Pharmacol.* **1978**, *27*, 1163-1166.

[157] M. J. Bebianno, W. J. Langston, Metallothionein induction in *Mytilus edulis* exposed to cadmium. *Mar. Biol.* **1991**, *108*, 91-96.

[158] G. Santovito, P. Irato, E. Piccinni, Regulation of metallothionein (MT) in Tetrahymena: Induction of MT-mRNA and protein by cadmium exposure. *Eur. J. Protistol.* **2000**, *36*, 437-442.

[159] M. L. Sereno, R. S. Almeida, D. S. Nishimura, A. Figueira, Response of sugarcane to increasing concentrations of copper and cadmium and expression of metallothionein genes. *J. Plant Physiol.* **2007**, *164*, 1499-1515.

[160] L. J. Jiang, M. Vašák, B. L. Vallee, W. Maret, Zinc transfer potentials of the α- and β-clusters of metallothionein are affected by domain interactions in the whole molecule. *P Natl Acad Sci-Biol* **2000**, *97*, 2503-2508.

[161] P. K. Y. Pan, Z. F. Zheng, P. C. Lyu, P. C. Huang, Why reversing the sequence of the α domain of human metallothionein-2 does not change its metal-binding and folding characteristics. *Eur. J. Biochem.* **1999**, *266*, 33-39.

[162] T. R. Butt, E. J. Sternberg, J. A. Gorman, P. Clark, D. Hamer, M. Rosenberg, S. T. Crooke, Copper metallothionein of yeast, structure of the gene, and regulation of expression. *P Natl Acad Sci-Biol* **1984**, *81*, 3332-3336.

[163] D. R. Winge, K. B. Nielson, W. R. Gray, D. H. Hamer, Yeast metallothionein - Sequence and metal-binding properties. *J Biol Chem* **1985**, *260*, 4464-4470.

[164] M. Bellion, M. Courbot, C. Jacob, F. Guinet, D. Blaudez, M. Chalot, Metal induction of a *Paxillus involutus* metallothionein and its heterologous expression in *Hebeloma cylindrosporum*. *New Phytol.* **2007**, *174*, 151–158.

[165] R. D. Palmiter, Regulation of metallothionein genes by heavy metal appears to be mediated by a zinc-sensitive inhibitor that interacts with a constitutively active transcription factor, MTF-1. *P Natl Acad Sci-Biol* **1994**, *91*, 1219–1223.

[166] T. W. Lane, M. A. Saito, G. N. George, I. J. Pickering, R. C. Prince, F. M. M. Morel, A cadmium enzyme from a marine diatom. *Nature* **2005**, *435*, 42.

[167] C. A. Blindauer, M. T. Razi, D. J. Campopiano, P. J. Sadler, Histidine ligands in bacterial metallothionein enhance cluster stability. *J. Biol. Inorg. Chem.* **2007**, *12*, 393-405.

[168] X. H. Chen, M. H. Chu, D. P. Giedroc, Spectroscopic characterization of Co(II)-, Ni(II)-, and Cd(II)-substituted wild-type and non-native retroviral-type zinc finger peptides. *J. Biol. Inorg. Chem.* **2000**, *5*, 93-101.

[169] D. P. Giedroc, H. Qiu, R. Khan, G. C. King, K. Chen, Zinc(II) coordination domain mutants of T4 gene 32 protein. *Biochemistry-Us* **1992**, *31*, 765-774.

[170] J. L. Kosa, J. W. Michelsen, H. A. Louis, J. I. Olsen, D. R. Davis, M. C. Beckerle, D. R. Winge, Common metal ion coordination in LIM domain proteins. *Biochemistry-Us* **1994**, *33*, 468-477.

[171] W. J. Roberts, T. Pan, J. I. Elliott, J. E. Coleman, K. R. Williams, p10 single-stranded nucleic acid binding protein from murine leukemia virus binds metal ions via the peptide sequence Cys26-X2-Cys29-X4-His34-X4-Cys39. *Biochemistry-Us* **1989**, *28*, 10043-10047.

[172] T. L. South, B. Kim, M. F. Summers, ^{113}Cd NMR studies of a 1:1 Cd adduct with an 18-residue finger peptide from HIV-1 nucleic acid binding protein, p7. *J Am Chem Soc* **1989**, *111*, 395-396.

metal sensing. *Nature* **2009**, *416*, 823-830.

[174] E. Lombi, F. J. Zhao, S. P. McGrath, S. D. Young, G. A. Sacchi, Physiological evidence for a high-affinity cadmium transporter highly expressed in a Thlaspi caerulescens ecotype., *New Phyto.* **2001**, *149*, 53-60.

[175] S. Thomine, R. Wang, J. M. Ward, N. M. Crawford, J. I. Schroeder, Cadmium and iron transport by members of a plant metal transporter family in Arabidopsis with homology to Nramp genes., *P Natl Acad Sci USA* **2000**, *97*, 4991–4996.

[176] F. Thevenod, Catch me if you can! Novel aspects of cadmium transport in mammalian cells., *Biometals* **2010**, *23*, 857-875.

[177] O. K. Vatamaniuk, S. Mari, Y. Lu, P. A. Rea, AtPCS1, a phytochelatin synthase from Arabidopsis: isolation and in vitro reconstitution., *P Natl Acad Sci USA* **1999**, *96*, 7110–7115.

[178] C. Cobbett, P. Goldsbrough, Phytochelatins and metallothioneins: Roles in heavy metal detoxification and homeostasis. *Annu. Rev. Plant Biol.* **2002**, *53*, 159-182.

[179] S. Clemens, D. Persoh, Multi-tasking phytochelatin synthases., *Plant Sci.* **2009**, *177*, 266-271.

[180] A. Arseniev, P. Schultze, E. Wörgötter, W. Braun, G. Wagner, M. Vašák, J. H. R. Kägi, K. Wüthrich, Three-dimensional structure of rabbit liver [Cd7]metallothionein-2a in aqueous solution determined by nuclear magnetic resonance. *J. Mol. Biol.* **1988**, *201*, 637-657.

[181] G. Henkel, B. Krebs, Metallothioneins: Zinc, Cadmium, Mercury and Copper Thiolates and Selenolates Mimicking Protein Acive Site Features - Structural Aspects and Biological Implications. *Chem. Rev.* **2004**, *104*, 801-834.

[182] K. Kwon, C. Y. Cao, J. T. Stivers, A novel zinc snap motif conveys structural stability to 3-methyladenine DNA glycosylase I. *J Biol Chem* **2003**, *278*, 19442-19446.

[183] Jiang, CE MT., *University of Zurich,* Dissertation, **1996**.